UC San Diego

UC San Diego Electronic Theses and Dissertations

Title

Studies of depredating sperm whales (Physeter macrocephalus) off Sitka, AK, using videocameras, tags, and long-range passive acoustic tracking

Permalink

https://escholarship.org/uc/item/04g834md

Authors

Mathias, Delphine
Mathias, Delphine

Publication Date

2012

Peer reviewed|Thesis/dissertation

eScholarship.org Powered by the California Digital Library
University of California

UNIVERSITY OF CALIFORNIA, SAN DIEGO

Studies of depredating sperm whales (*Physeter macrocephalus*) off Sitka, AK, using videocameras, tags, and long-range passive acoustic tracking

A dissertation submitted in partial satisfaction of the
requirements for the degree Doctor of Philosophy
in
Oceanography

by

Delphine Mathias

Committee in charge:

Professor Aaron Thode, Chair
Professor Jay Barlow
Professor Gerald D'Spain
Professor William Hodgkiss
Professor Truong N'Guyen
Professor Jan Straley

2012

© 2012
Delphine Mathias,
All rights reserved.

The dissertation of Delphine Mathias is approved, and it is acceptable in quality and form for publication on microfilm:

_____

_____

_____

_____

_____

_____

Chair

University of California, San Diego

2012

For my parents Danièle and Jean-Pierre, and "l'amour de ma vie", Aurelien.

Dory: [about the humpback whale] Maybe he only speaks whale.

Dory: [slowly and deeply, imitating the whale] Mooo... Weeee neeeed...

Marlin: What are you doing? Are you sure you speak whale?

Dory: Maybe a different dialect. Mmmmooooooowaaaaah...

Marlin: Dory! This is not whale. You're speaking like, upset stomach.

Dory: Maybe I should try humpback.

Marlin: No, don't try humpback.

Dory: Woooooo! Woooooo!

Dory: Too much orca. Did it sound a little orca-ish to you?

Marlin: It doesn't sound orca. It sounds like nothing I've ever heard!

[after whale blows Marlin and Dory out]

Marlin: Thaaaannkkk Youuuu Sirrrrrrrrr.

Dory: Wow. I wish I could speak whale...

Finding Nemo, 2003

TABLE OF CONTENTS

Signature Page iii

Dedication iv

Epigraph v

Table of Contents vi

List of Figures xi

List of Tables xv

Acknowledgments xvi

Vita, Publications, and Presentations xix

Abstract xxi

Chapter I: Introduction 1
1 Sperm whale natural history and distribution 1
2 Sperm whale foraging and acoustic behavior 2
3 Sperm whale depredation on sablefish in the Gulf of Alaska 3
4 Southeast Alaska Sperm Whale Avoidance Project 6
5 Overview of thesis 7

Chapter II: Relationship between sperm whale (*Physeter macrocephalus*) click structure and size derived from videocamera images of a depredating whale (sperm whale prey acquisition) 11
1 Abstract 11
2 Introduction 12
3 Procedure 17
3.1 Video and audio recording equipment 17
3.2 Deployment procedure 17
3.3 Audio data Analysis 20
3.4 Video Analysis 22
4 Results 24
4.1 General description of the May 31st 2006 encounter 24
4.2 Acoustic Analysis 26
4.3 Body length estimation using visual and acoustic methods 32
5 Discussion 35
5.1 Relationship between IPI and anatomical structure 35

5.2 Unresolved questions . . . 37
6 Conclusion . . . 38
7 Acknowlegments . . . 38

Chapter III: Acoustic and diving behavior of sperm whales (*Physeter macrocephalus*) during natural and depredation foraging in the Gulf of Alaska . . . 40
1 Abstract . . . 40
2 Introduction . . . 41
2.1 Background on sperm whale foraging and acoustic behavior 41
2.2 Sperm whale depredation . . . 44
3 Materials and methods . . . 47
3.1 Equipment . . . 47
3.2 Deployments and visual observation protocols . . . 47
3.3 Dive profile analysis . . . 48
3.4 Acoustic data analysis . . . 49
3.5 Behavioral categories and hypothesis testing . . . 51
4 Results . . . 54
4.1 Summary of tag records . . . 54
4.2 Resting, natural foraging, and deep depredation behaviors from a tag deployed on 12 June 2009 . . . 55
4.3 Natural foraging behavior and shallow depredation from a tag deployed on 17 July 2007 . . . 57
4.4 Comparison of behavioral states across all tag records . . . 60
5 Discussion . . . 70
5.1 Is natural foraging behavior off Sitka similar to elsewhere in the world? . . . 70
5.2 Depredation vs. natural foraging behavior . . . 71
5.2.a Dive parameters during shallow depredation . . . 71
5.2.b Dive parameters during deep depredation . . . 71
5.2.c Acoustic parameters during shallow depredation . 72
5.2.d Acoustic parameters during deep depredation . . . 73
5.2.e Interpreting the meaning of silences after creaks . 74
5.3 Interpretation of deep vs. shallow depredation . . . 76
5.4 Interpretation of deep vs. shallow depredation . . . 78
5.5 Insight into potential depredation countermeasures . . . 81
6 Conclusion . . . 83
7 Acknowledgments . . . 84
8 Appendix 1: Body orientation analysis . . . 85
8.1 Equipment . . . 85
8.2 Angular definitions . . . 85
8.2.a Acceleration vector . . . 85
8.2.b Coordinate transformations . . . 87

8.2.c Pitch and roll . . . 89
8.2.d Angular displacement and angular velocity definitions . . . 90
8.3 Analyzing relationships between angular velocities, dive inflections, and creak events . . . 92
8.4 Hypothesis testing . . . 94
8.5 Results . . . 94
8.5.a Summary of tag records and behavioral categories 94
8.5.b 20 July 2007 : Natural foraging behavior . . . 95
8.5.c 12 June 2009 : Resting, natural foraging, and deep depredation behaviors . . . 98
8.5.d 17 July 2007 : Natural foraging behavior and shallow depredation . . . 102
8.5.e Comparison of behavioral states across all tag records . . . 102
8.6 Discussion . . . 107
8.7 Is natural foraging behavior off Sitka similar to elsewhere in the world? . . . 107
8.8 Depredation vs. natural foraging behavior . . . 108
9 Appendix 2: Comparison between theoretical and estimated fish consumption rates . . . 109
10 Appendix 3: Dive profile tag records . . . 111
10.1 2007 B-probe data . . . 111
10.1.a 17 July 2007 - GOA 08 . . . 112
10.1.b 18 July 2007 - GOA 97 . . . 113
10.1.c July 18th 2007 - GOA 33 . . . 114
10.1.d 20 July 2007 - GOA 26 . . . 116
10.1.e 20 July 2007 - GOA 97 . . . 117
10.1.f 20 July 2007 - GOA 47 . . . 118
10.1.g 20 July 2007 - GOA 08 . . . 120
10.1.h 20 July 2007 - GOA 26 . . . 122
10.2 2009 B-probe data . . . 123
10.2.a 12 June 2009 - GOA 47 . . . 123
10.2.b 14 June 2009 - GOA 104 . . . 124
10.2.c 21 June 2009 - GOA 105 . . . 125
10.3 2009 DST data . . . 126
10.3.a June 11th 2009 - No ID . . . 126
10.3.b June 13th 2009 - GOA 103 . . . 128
10.3.c 13 June 2009 - GOA 106 . . . 129
10.3.d 14 June 2009 - GOA 104 . . . 130
10.3.e 15 June 2009 - GOA 107 . . . 131
10.3.f June 15th 2009 - GOA 90 . . . 132
10.3.g June 21st 2009 - GOA 107 . . . 133

10.3.h June 21st 2009 - GOA 105 . . . 134
10.3.i June 29th 2009 - GOA 81 . . . 135
10.3.j 30 June 2009 - GOA 47 . . . 136
11 Acknowledgments . . . 138

Chapter IV: Changes in depredating sperm whale (*Physeter macrocephalus*) acoustic behavior during sound playbacks . . . 139
1 Abstract . . . 139
2 Introduction . . . 139
3 Materials and methods . . . 142
3.1 Equipment: playback device and bioacoustic tags . . . 142
3.2 Playback protocol . . . 143
3.3 Statistical analysis of tagging data . . . 144
4 Results and discussion . . . 145
4.1 Summary of deployments . . . 145
4.2 Statistical analysis of acoustic behavior . . . 150
4.3 Interpretation of playback results . . . 151
5 Conclusion . . . 153
6 Acknowlegments . . . 154

Chapter V: Depth and range tracking of sperm whales (*Physeter macrocephalus*) in the Gulf of Alaska using a two-element vertical array, satellite and bioacoustic tags . . . 155
1 Abstract . . . 155
2 Introduction . . . 156
2.1 Motivation for tracking sperm whales in the Gulf of Alaska 156
2.2 Sperm whale acoustic behavior . . . 157
2.3 Previous acoustic tracking research . . . 158
3 Data collection . . . 160
3.1 Vertical array deployment . . . 160
3.2 Satellite and bioacoustic tagging . . . 164
4 Localization methods . . . 170
4.1 Time synchronization . . . 170
4.2 Multipath pattern extraction when multiple whales are present . . . 171
4.2.a Multipath pattern extraction when bioacoustic sound data is available . . . 171
4.2.b Multipath pattern extraction when only satellite tag data is available . . . 177
4.2.c Computing arrival angles of ray paths . . . 181
4.3 Analytical formulas for sperm whale tracking at short ranges . . . 184

4.3.a Single hydrophone: multipath time arrivals 184
4.3.b Two hydrophones: multipath time arrivals and arrival angles 185
4.4 Using a ray-tracing numerical model for tracking 188
4.4.a Replica generation 188
4.4.b Producing an ambiguity surface using scoring . . . 192
4.4.c Producing an ambiguity surface using weighted mean-square error 193
5 Localization results 195
5.1 Depth and range tracking at ranges less than 2 km using analytical methods 195
5.2 Depth and range tracking at ranges greater than 2 km . . . 198
5.3 Click received level as a function of range 202
6 Discussion 208
6.1 Limits of the analytical approach 208
6.2 Nature of the acoustic propagation environment 208
6.3 Sources of localization error 214
6.3.a Inclination precision 214
6.3.b Environmental model 215
6.3.c Time of arrival measurement precision 215
6.3.d Angular measurement precision 215
6.3.e Sidelobes at long range 216
6.4 Comparison of ambiguity surface construction methods . . 216
6.5 Source level estimates 218
6.5.a Click source levels 218
6.5.b Creak click source levels 221
6.6 Limits of detection and tracking range 223
7 Conclusion 227
8 Acknowledgments 231

Chapter VI : Conclusion 232
1 Sperm whale sound production mechanism 233
2 Diving and acoustic behavior of depredating sperm whales 234
3 Effect of acoustic playbacks on sperm whale behavior 235
4 Passive acoustic tracking techniques 235
5 Insight into depredation countermeasures 237
6 Conclusion summary 240

Bibliography 241

LIST OF FIGURES

Figure I.1: Traditional evidence of depredation on black cod . . 4
Figure I.2: Schematic of a demersal longline 5
Figure I.3: Study Area off Sitka, Alaska 8

Figure II.1: Bent-horn model of sound production 14
Figure II.2: Schematic of camera deployment from fishing vessel 19
Figure II.3: Snapshots from the May 31st sperm whale encounter video 25
Figure II.4: Inter-Click Interval (ICI) for the May 31st camera sequence 27
Figure II.5: Stacked click structure of the May 31st sequence . . 29
Figure II.6: spectrogram of two types of clicks during May 31st sequence 30
Figure II.7: Stacked cepstra and averaged cepstrum of May 31st sequence 31
Figure II.8: Superimposition of the videocamera image with a pool calibration image 33
Figure II.9: Allometric relationships between body proportions of male sperm whales caught in the North Pacific . . . 34

Figure III.1: Local bathymetry off Sitka, AK 45
Figure III.2: Tag parameters of a whale displaying resting, natural foraging behavior and deep depredation behavior on 12 June 2009 56
Figure III.3: Tag parameters of a whale displaying natural foraging and shallow depredation behavior on 17 July 2007 . 59
Figure III.4: Boxplots of five dive parameter distributions 61
Figure III.5: Boxplots of five acoustic parameter distributions . . 62
Figure III.6: Boxplots of dive parameters only using tag records that display both natural and depredation behavior 65
Figure III.7: Boxplots of acoustic parameters only using tag records that display both natural and depredation behavior 66
Figure III.8: B-probe tag and reference axes 86
Figure III.9: Distribution of accelerometer magnitude 87
Figure III.10: Comparison of pitch and roll measurements between DST and B-probe 91
Figure III.11: Angular velocity plots of 20 July 2007 tag data, during natural foraging behavior 96

Figure III.12: Relative timing between dive inflections and creak events, during natural foraging behavior on 20 July 2007 tag data 97
Figure III.13: Angular velocity plots of 12 June 2009 tag data, during natural foraging behavior and deep-depredation, for *creak-only* events 99
Figure III.14: Angular velocity plots of 12 June 2009 tag data, during natural foraging behavior and deep-depredation, for *creak-pause* events 100
Figure III.15: Relative timing between dive inflections and creak events in 12 June 2009 tag data 101
Figure III.16: Angular velocity plots of 17 July 2007 tag data, during natural foraging behavior and shallow-depredation, for *creak-only* events 103
Figure III.17: Angular velocity plots of 17 July 2007 tag data, during natural foraging behavior and shallow-depredation, for *creak-pause* events 104
Figure III.18: Relative timing between dive inflections and creak events in 17 July 2007 tag data 105
Figure III.19: 17 July 2007 - GOA 08 112
Figure III.20: 18 July 2007 - GOA 97 113
Figure III.21: 18 July 2007 - GOA 33 115
Figure III.22: 20 July 2007 - GOA 26 116
Figure III.23: 20 July 2007 - GOA 97 117
Figure III.24: 20 July 2007 - GOA 47 119
Figure III.25: 20 July 2007 - GOA 08 121
Figure III.26: 20 July 2007 - GOA 26 122
Figure III.27: 12 June 2009 - GOA 47 123
Figure III.28: 14 June 2009 - GOA 104 124
Figure III.29: 21 June 2009 - GOA 105 125
Figure III.30: 11 June 2009 - No ID 127
Figure III.31: 13 June 2009 - GOA 103 128
Figure III.32: 13 June 2009 - GOA 106 129
Figure III.33: 14 June 2009 - GOA 104 130
Figure III.34: 15 June 2009 - GOA 107 131
Figure III.35: 15 June 2009 - GOA 90 132
Figure III.36: 21 June 2009 - GOA 107 133
Figure III.37: 21 June 2009 - GOA 105 134
Figure III.38: 29 June 2009 - GOA 81 135
Figure III.39: 30 June 2009 - GOA 47 137

Figure IV.1: Spectrogram of FM sweep playback signal 146
Figure IV.2: Spectrogram of FM sweep playback signal 147

Figure IV.3: Spectrogram of white noise playback signal 148
Figure IV.4: Spectrogram of killer whale playback signal 149
Figure IV.5: Creak-pause fraction for different types of sperm whale behavior 152

Figure V.1: Contour map of the study area 162
Figure V.2: Schematic of vertical array 163
Figure V.3: Sound speed profile 165
Figure V.4: Photo of depth-transmitting Mk10-A LIMPET satellite tag 166
Figure V.5: Photo of satellite tag and B-Probe tag 167
Figure V.6: Dive profile from B-probe tag 168
Figure V.7: Dive profile and range from the LIMPET satellite tag 169
Figure V.8: Time synchronization of two acoustic recorders . . . 172
Figure V.9: Spectrogram of acoustic data from B-probe and associated recording on VA 174
Figure V.10: Waterfall plot of stacked multipath arrival patterns between 19:01 and 19:04 on 15 August 2010. 175
Figure V.11: Spectrogram of direct path, surface-reflected path and bottom-reflected path recorded on the VA on 15 August 2010 at 19:01:30 178
Figure V.12: Tagged whale inter-click interval (ICI) 179
Figure V.13: Tagged whale multipaths labeled manually 180
Figure V.14: Tagged whale multipaths labeled manually 183
Figure V.15: Schematic for analytical method using a single hydrophone 185
Figure V.16: Schematic for analytical method using two hydrophones 187
Figure V.17: Sound speed profile used in propagation model BELLHOP 189
Figure V.18: Sound speed profile used in propagation model BELLHOP 191
Figure V.19: Modeled eigenrays between a whale at 500 m depth and a recorder at 300 m depth 191
Figure V.20: Depth estimates of tagged whale using analytical methods 196
Figure V.21: Range estimates of tagged whale using analytical methods 197
Figure V.22: Spectrogram of the ray path arrivals at various ranges 199
Figure V.23: Localization estimates of whale at 2 km range 200
Figure V.24: Localization estimates of whale at 5 km range 202
Figure V.25: Localization estimates of whale at 8 km range 203
Figure V.26: Localization estimates of whale at 22 km range . . . 204

Figure V.27: Localization estimates of whale at 35 km range . . . 205
Figure V.28: Received levels of clicks measured on the vertical array at various ranges 207
Figure V.29: Duration,maximum frequency and bandwidth of multipath arrivals at various ranges 211
Figure V.30: Transmission loss (TL) estimated up to 25 km range 213
Figure V.31: Estimated source levels 220
Figure V.32: Power spectral density during the 2-day experiment 225
Figure V.33: Ambient noise levels during the 2-day experiment . 226
Figure V.34: Detection and tracking range as a function of sea state 227
Figure V.35: Number of whales detected during the two-day deployment and associated range 230

LIST OF TABLES

Table II.1: Body length estimation for May 31st sequence: comparison between visual and acoustic data. 32

Table III.1: Dive statistics for 2007 and 2009 data 63
Table III.2: Acoustic statistics for 2007 and 2009 data 64
Table III.3: Dive statistics for 2007 and 2009 data using only tag records that display both natural and depredation behaviors 68
Table III.4: Acoustic statistics for 2007 and 2009 data using only tag records that display both natural and depredation behaviors 69
Table III.5: Angular velocity statistics for 2007 and 2009 data . 106
Table III.6: Angular velocity statistics for 2007 and 2009 data using only tag records that display both natural and depredation behaviors 107

Table IV.1: Signal categories used for playbacks 143
Table IV.2: Differences in tagged whale acoustic parameters between "haul-only" and "haul-playback" conditions 150

Table V.1: Sperm whale sightings 15-17 August 2010 during the vertical array deployment, near the Spencer Split. 170

ACKNOWLEDGMENTS

I wish to thank my advisor, Aaron Thode, for giving me the opportunity to pursue this thesis and explore the fascinating world of bioacoustic. Aaron's guidance challenged me as a scientist, from his lessons on efficient data analysis to conference talk advices. Aaron also allowed me to participate in many fieldworks: in Southeast Alaska to collect my thesis sperm whale data, in Laguna San Ignacio to collect grey whale data and in the Beaufort Sea to deploy bottom acoustic recorders.

My dissertation research would not have been possible without numerous collaborators. I would like to thank Jan Straley for obtaining the funding for some of this work and welcoming me to Sitka every summer. Jan shared insights and passion for the marine life, teached me how to become a field biologist, perform visual observations and interpret whale behavior. Many thanks to Lauren Wild for performing the visual observations, helping deploy, download and analyze acoustic data, and helping me go through "panic times". Thanks Jen Cederleaf for going through all the Photo-ID pictures with a smile. The tagging data has been collected thanks to the hard work of John Calambokidis and Greg Shorr from Cascadia Research Collective, and Russ Andrews from the Alaska SeaLife Center. I also would like to thank Rob Glatts for building the acoustic recorders.

My research would not have been possible without the collaboration of local fishermen. In particular I would like to thank Kendall Folkert for welcoming me on his longlining fishing vessel almost every summer and allowing us to transform the galley in an acoustic lab. Kendall always found a way to deploy our acoustic recorders in the best configuration possible. Kendall shared his incredible knowledge on sea conditions and whale depredation behavior with funny anecdotes.

Thanks to the rest of the Sitka Sound Science Center and Sitka community who were always supportive and interested in my research, made me feel at

home during my visits and made sure that I had fresh fish in my luggage for my way back home.

The support from the entire Scripps community contributed to my success as a graduate student and young scientist. A special thanks to Evelyn Doudera for helping with travel arrangements, equipment shipping and last minute trip changes. I also would like to thank Diana, Irina and Rob from the MPL computer help.

Thanks, of course, to my amazingly supportive friends and family. Thanks to my mom and dad for encouraging me to move to San Diego and believing in my passion for the ocean.

Finally, my deepest thanks go to my partner in any adventure, Aurelien, for sharing this journey with me and making it so much fun.

The research presented in this dissertation was made possible by funding provided by ALFA, the Department of Fish and Game, NOAA, NPRB, and the NPRB graduate student fellowship award.

Chapter 2, in part or in full, is a reprint of the material published in the Journal of acoustical society of America: Delphine Mathias, Aaron Thode, Jan Straley and Kendall Folkert, "Relationship between sperm whale (*Physeter macrocephalus*) click structure and size derived from videocamera images of a depredating whale (sperm whale prey acquisition)", J. Acoust. Soc. Am. **125**(5), 3444-3453 (2009). The dissertation author was the primary researcher and author of this material.

Chapter 3, in part, has been accepted for publication in the Journal of the Acoustical Society of America: Delphine Mathias, Aaron Thode, Jan Straley, Victoria O'Connell, John Calambokidis and Gregory S. Schorr, "Acoustic and foraging behavior of tagged sperm whales (*Physeter macrocephalus*) under natural and depredation foraging conditions in the Gulf of Alaska". The dissertation

author was the primary researcher and author of this material.

Chapter 5, in part, has been submitted for publication to J. Acoust. Soc. Am.: Delphine Mathias, Aaron Thode, Jan Straley, and Russel Andrews, "Acoustic tracking of sperm whales in the Gulf of Alaska using a two-element vertical array and tags". The dissertation author was the primary researcher and author of this material.

VITA

2005	Diplôme de l'ENSIETA, M.S. Oceanography ENSIETA, Brest, France
2005–2006	Research Engineer IFREMER Research Center, Brest, France
2006–2012	Research Assistant Scripps Institution of Oceanography, University of California, San Diego
2012	Ph.D., Oceanography Scripps Institution of Oceanography, University of California, San Diego.

PUBLICATIONS

D. Mathias, A. Thode, J. Straley, and R. Andrews, "Depth and range tracking of sperm whales (*Physeter macrocephalus*) in the Gulf of Alaska using a two-element vertical array, satellite and bioacoustic tags", Submitted, J. Acoust. Soc. Am.

D. Mathias, A. Thode, J. Straley, V. O'Connell, J. Calambokidis, and G.S. Schorr, "Acoustic and foraging behavior of tagged sperm whales (*Physeter macrocephalus*) under natural and depredation foraging conditions in the Gulf of Alaska", Accepted by J. Acoust. Soc. Am (2012).

D. Mathias, A. Thode,J. Straley, and K. Folkert, "Relationship between sperm whale (*Physeter macrocephalus*) click structure and size derived from videocamera images of a depredating whale (sperm whale prey acquisition)", J. Acoust. Soc. Am. **125**(5), 3444-3453 (2009).

D. Mathias, A. Thode, S. B. Blackwell, C. Green, "Computer-aided classification of bowhead whale call categories for mitigation monitoring", IEEE , Passive 2008: New Trends for Environmental Monitoring Using Passive Systems, 6 pp. (2008)

SELECTED PRESENTATIONS

"Depth and range tracking of sperm whales in the Gulf of Alaska using a two-element vertical array, satellite and bioacoustic tags", Delphine Mathias, Aaron Thode, Jan Straley, and Russel Andrews, Alaska Marine Science Symposium in Anchorage, 2012.

"Depth and range tracking of sperm whales in the Gulf of Alaska using a two-element vertical array, satellite and bioacoustic tags", Delphine Mathias, Aaron Thode, Jan Straley, and Russel Andrews, ASA Conference in San Diego, 2011.

"Depth and range tracking of sperm whales in the Gulf of Alaska using a two-element vertical array, satellite and bioacoustic tags", Delphine Mathias, Aaron Thode, Jan Straley, and Russel Andrews, DCL Workshop in Mt Hood, 2011.

"Acoustic and foraging behavior of tagged sperm whales (*Physeter macrocephalus*) under natural and depredation foraging conditions in the Gulf of Alaska", Delphine Mathias, Aaron Thode, Jan Straley, John Calambokidis, Gregory S. Schorr, and Bill Burgess, Invited talk at the ASA Conference in Seattle, 2011.

"Acoustic and foraging behavior of tagged sperm whales (*Physeter macrocephalus*) under natural and depredation foraging conditions in the Gulf of Alaska", Delphine Mathias, Aaron Thode, Jan Straley, Victoria O'Connell, John Calambokidis and Gregory S. Schorr, Alaska Marine Science Symposium in Anchorage, 2011.

"Automated detection of sperm whales (*Physeter macrocephalus*) creaks and association with depredation events", Delphine Mathias, Aaron Thode, Jan Straley, John Calambokidis, Gregory S. Schorr, and Bill Burgess, ASA Conference in Baltimore, 2010.

"Depth, orientation, and acoustics of sperm whales (*Physeter macrocephalus*) under natural and depredation foraging conditions in the Gulf of Alaska", Delphine Mathias, Aaron Thode, Jan Straley, John Calambokidis, Gregory S. Schorr, and Bill Burgess, Marine Mammal Conference in Quebec City, 2009.

"Depth, orientation, and acoustics of sperm whales (*Physeter macrocephalus*) under natural and depredation foraging conditions in the Gulf of Alaska", Delphine Mathias, Aaron Thode, Jan Straley, John Calambokidis, Gregory S. Schorr, Bill Burgess, Christopher Lunsford and O'Connell, Victoria, ASA Conference in Paris, 2008.

"Combined video and acoustic tracking analysis of sperm whale in close vicinity of a fishing longline", Delphine Mathias and Aaron Thode, 3rd International Workshop on Detection and Localization of Marine Mammals using Passive Acoustics, Boston, 2007.

ABSTRACT OF THE DISSERTATION

Studies of depredating sperm whales (*Physeter macrocephalus*) off Sitka, AK, using videocameras, tags, and long-range passive acoustic tracking

by

Delphine Mathias
Doctor of Philosophy in Oceanography
University of California, San Diego, 2012
Professor Aaron Thode, Chair

This dissertation uses videocameras, tags and acoustic recorders to investigate the diving and acoustic behavior of sperm whales in the Gulf of Alaska during natural and depredation foraging conditions. First, underwater videocamera footage of a sperm whale attacking a fishermans longline at 100 m depth was used to examine its acoustic behavior at close range and to estimate its size both acoustically and visually. Second, bioacoustic tagging data demonstrated that the same individuals displayed different acoustic behaviors during natural and depredation foraging states. Two broad categories of depredation, "shallow" and "deep," were also identified. These results suggest that passive acoustic monitoring at close ranges may yield useful metrics for quantifying depredation activity. Third, the behavioral reactions of depredating sperm whales to a variety of acoustic playbacks generated at relatively low source levels were investigated using bioacoustic tags. Finally, bioacoustic and satellite tag data were used to develop passive acoustic techniques for tracking sperm whales with a short-aperture two-element vertical array. When numeric sound propagation models were exploited, localization ranges up to 35 km were obtained. The tracking methods were also used to estimate the source levels of sperm whale "clicks" and "creaks", predict the maximum detection range of the signals as a function of sea state, and measure the drift of several whales away from a visual decoy.

Chapter I:

Introduction

I.1 Sperm whale natural history and distribution

The sperm whale is the largest of the toothed whales and is one of the most sexually dimorphic of all the whale species: mature males have an average length of 16 m and weight of 57 tons , while adult females are usually less than 12m and weight less than 24 tons (Rice *et al.*, 1989).

Sperm whales are distributed throughout the worlds oceans, and are mostly found near continental shelf margins, in waters deeper than 800 m. The distribution of sperm whales extends to all deep ice-free marine waters, from the equator to the edges of polar pack ice (Rice *et al.*, 1989). Although both sexes are found in tropical and temperate seas, only adult males travel into the higher latitudes towards colder waters. Currently, there is no precise estimate for the total number of sperm whales worldwide. Whitehead (2003) estimated the global population to be around 360,000 animals, based on extrapolations of visual data from a few areas. This number may correspond to a 68% decrease from pre-whaling estimates. The current population size and distribution of sperm whales in the Gulf of Alaska is unknown (Hill and Demaster, 1999), other than the fact that they have a year-round presence (Mellinger *et al.*, 2004). Commercial whaling for this species ended in 1988, with the implementation of a moratorium against whaling by the International Whaling Commission (IWC). The sperm whale is currently listed as

endangered throughout its range under the Endangered Species Conservation Act of 1969, and is also protected under the Marine Mammal Protection Act of 1972.

I.2 Sperm whale foraging and acoustic behavior

Sperm whales are deep and prolonged divers and can therefore exploit large portions of the water column, even in very deep areas. They feed on a wide variety of mesopelagic and bathypelagic prey, composed principally of squid, but also invertebrates and sh (Whitehead, 2003). Fish have been a natural part of their diet off Alaska, according to whaling records (Okutani *et al.*, 1964; Rice *et al.*, 1989; Sigler *et al.*, 2008). Lockyer (1981) estimated that this species consumes about 3.0-3.5% of its body weight per day.

During normal foraging behavior sperm whales alternate between deep (up to 2000 m) and long dives (45 minutes average) with average surface rest times of 15 minutes (Mullins *et al.*, 1988; Papastavrou *et al.*, 1989; Watkins *et al.*, 1993; Jaquet *et al.*, 2000; Wahlberg, 2002; Drouot, *et al.*, 2004; Watwood *et al.*, 2006).

Throughout most of their dives, sperm whales display consistent acoustic activity and produce 25-30 ms transient sounds called clicks (Goold *et al.*, 1995; Worthington and Schevill, 1957; Watkins and Schevill, 1977; Madsen *et al.*, 2002a; Wahlberg, 2002). Researchers have divided sperm whale sounds into a variety of categories, based on the timing between subsequent clicks in a sound sequence. This timing pattern, called the inter-click interval (ICI), has been used to classify clicks into usual clicks, slow clicks, creaks, and codas (Whitehead, 2003). Clicks are believed to serve a variety of functions, including echolocation and communication, depending on the click pattern. Usual clicks typically have an ICI of 0.5 s to 1.0 s, while creaks display a shorter ICI between 0.01s to 0.5 s (Madsen *et al.*, 2002a). ICI values within a given creak also tend to decrease with time, and orientation measurements from tagged animals have demonstrated that sudden changes in

orientation are associated with creak sounds (Miller *et al.*, 2004a; Watwood *et al.*, 2006). These observations, among others, suggest that creaks are used as an echolocation signal (Whitehead, 2003; Norris *et al.*, 1972, Whitehead *et al.*, 1991; Gordon *et al.*, 1987, Goold *et al.*, 1995; Jaquet *et al.*, 2001).

I.3 Sperm whale depredation on sablefish in the Gulf of Alaska

Sperm whales have learned how to depredate fishing gear (i.e., remove or damage fish from), particularly demersal longline operations (Figure I.1), in a number of locations around the globe. Longlining is a commercial fishing method that is used to catch groundfish, a generic name for fish that spend most of their lives near the ocean bottom, including halibut (*Hippoglossus stenolepsis*), sablefish ((*Anoplopoma fimbria*) and yelloweye rockfish ((*Sebastes ruberrimus*). Longlines are between one to three miles long and are laid along the ocean bottom, with baited hooks spaced at approximately 1.2 m intervals. Each end of the longline is weighted to sink to the ocean floor and is marked with a buoy on the surface for retrieving the line (Figure I.2). Fishermen leave the longline underwater for several hours or "soaking" overnight before hauling the line back onto the boat and harvesting the hooked fish.

Since 2002 reports of depredation have surfaced in Norway, Greenland, eastern Canada (Labrador and Newfoundland), Chile and the Falkland Islands. Sperm whales are the largest marine mammal known to depredate on human fishing activities, and these activities have received increasing coverage in the scientific literature (Ashford *et al.*, 96, Capdeville, Nolan *et al.*, 2000, Gonzalez *et al.*, 2001, Hill *et al.*, 1999, Hucke *et al.*, 2004, Purves *et al.*, 2004, Sigler *et al.*, 2008, Thode *et al.*, 2007). Worldwide, 15 species of odontocetes (toothed whales, dolphins and porpoises) have been implicated in the depredation of longline fisheries



Figure I.1: Traditional evidence of depredation on black cod.

and/or have become bycaught (Hamer *et al.*, 2011). Killer whales (*Orcinus orca*) most commonly participate in depredation in temperate and coastal waters at high latitudes, while false killer whales (*Pseudorca crassidens*) and pilot whales (*Globicephala* spp.) are the main species involved in tropical and offshore areas at lower latitudes.

Until the late 1980s the Southeast Alaska longline fishery was a derby-style fishery. Fisheries officials opened a certain portion of the coast for a set length of time as short as two weeks to harvest the years quota. Longline vessels then crowded together for the best areas, and crews scrambled to fish as much gear as they could to maximize their catch before the fishery closed. Vessels shed regardless of weather, and prices were often low because markets were flooded at the close of the fishery. In the late 1980s, the management of the halibut and sablefish fisheries converted into a quota system, where the annual quota is divided among license holders, and each holder may fish at almost any time of the year until his or her quota is met. The amount of harvested fish per year remains about

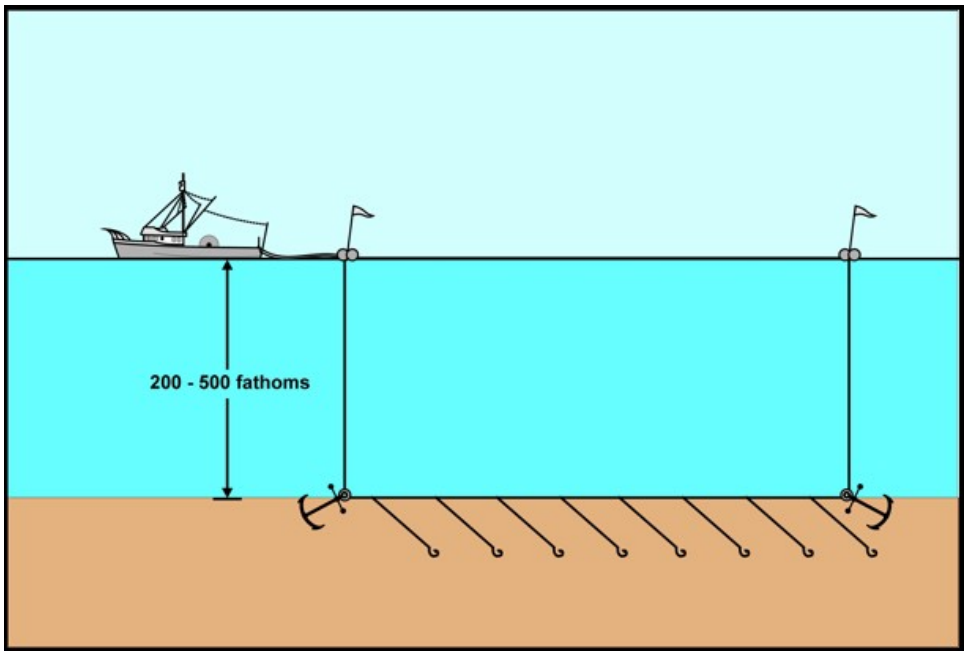

Figure I.2: A demersal longline extends about 3km horizontally on the ocean bottom, anchored on either end by vertical buoylines, which provide convenient locations to attach instruments.

the same as under the derby scheme, but the intensity of the fishing effort is now spread out over the year. This extended arrangement has probably led to increased interactions with sperm whales. Although there have been no official reports of sperm whale deaths or serious injuries from interactions with longline fishing gear in Alaska, fishermen and scientists are worried that depredation behavior may cause entanglements.

Sperm whale depredation on Alaskan longline sets is increasing during both the commercial longline sablefish fishery, and the sablefish survey conducted by the NOAA Alaska Fisheries Science Center (AFSC) Auke Bay Laboratories (ABL) sablefish survey for stock assessment research (Hanselman *et al.*, 2008, Sigler *et al.*, 2007). In 2008 evidence of sperm whale depredation occurred on approximately 90% of the sablefish survey hauls in the West Yakutat and Southeast Outside areas. However, the lack of quantitative data on the number of the depredation events per encounter makes developing a correction factor for the survey problematic. Quantifying depredation rates was cited as a specific concern in the 2009 Committee of Independent Experts review of the NOAA National Marine Fisheries Service (NMFS) Alaska Fisheries Science Center (AFSC) Auke Bay Laboratories (ABL) sablefish stock assessment (Amstrong *et al.*, 2009).

I.4 Southeast Alaska Sperm Whale Avoidance Project

In 2002 the Southeast Alaska Sperm Whale Avoidance Project (SEASWAP) was created to quantify the scale of sperm whale depredation in Southeast Alaska to recommend strategies to reduce depredation. A collaborative study between fishermen, scientists and federal management biologists, SEASWAP works with the coastal fishing fleet to collect various quantitative data on longline depredation, with the primary goal of refining the impact of depredation and

minimizing interactions.

Sablefish occur on the continental slope and most commercial longliners fish for this species in water depths between 400 and 1000 m. The continental shelf off the Kruzof and Baranof islands is very narrow; consequently, the SEASWAP study area off Sitka is relatively close to shore, within 12 to 20 miles (Figure I.3).

Since 2003 logbooks and cameras have been provided to fishermen to document the nature and extent of depredation. Photo-identication and biopsy studies were also conducted to provide an estimate of the number and gender of depredating whales. Under the leadership of Jan Straley and Victoria OConnell, SEASWAP built up a photo catalog of more than 100 individuals associated with fishing vessels. Genetic analysis determined that all the biopsied animals were males. In 2004 passive acoustic monitoring of sperm whale depredation began, and three types of instruments have been deployed since then in close vicinity to fishing longlines: moored autonomous recorder buoys, underwater video cameras and bioacoustic tags.

Thode *et al.* (2007) collected data suggesting that cavitation noise arising from the ships propeller is the best candidate for a distinctive acoustic cue that causes changes in the behavior of sperm whales in the area, which include the interruption of sperm whale acoustic activity, and the convergence and surfacing of animals around the vessel.

I.5 Overview of thesis

A primary goal of this thesis is assessing whether passive acoustic monitoring can both remotely measure depredation activity around longline vessels and provide an effective tool for rapidly evaluating the efficacy of potential depredation countermeasures. To that end this thesis uses passive acoustic data collected from videocameras, bioacoustic tags, and a vertical array to conduct applied research on the distinctive acoustic characteristics of depredation, and to conduct preliminary

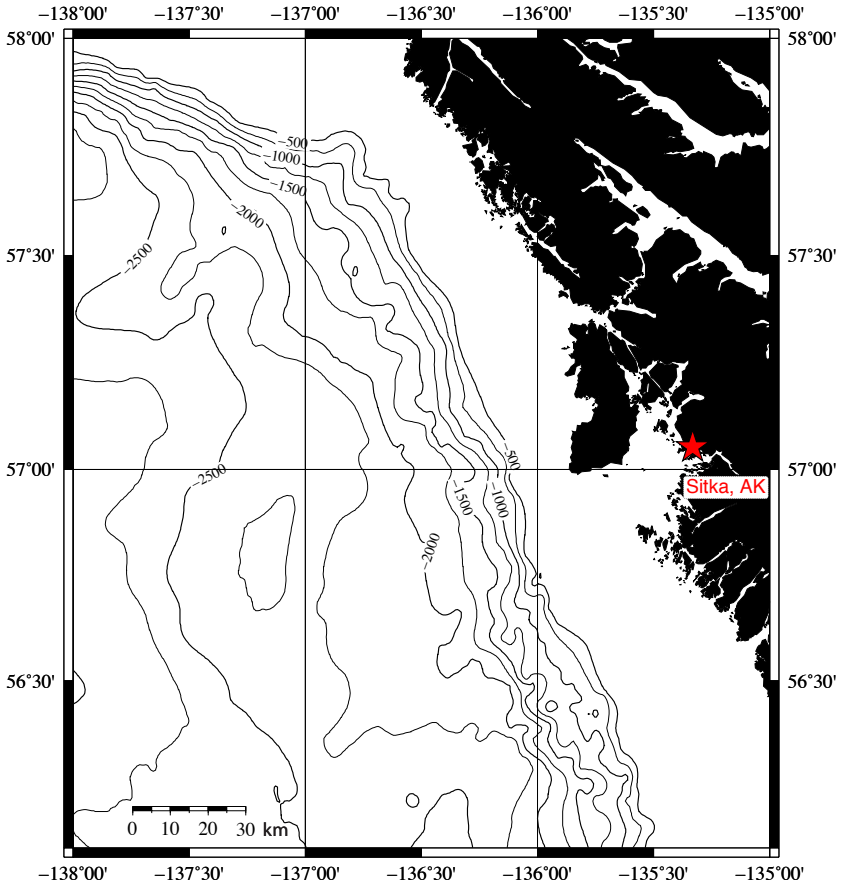

Figure I.3: Study Area off Sitka, AK.

testing of two methods to reduce depredation. Furthermore, this work has provided unique opportunities to conduct basic research into the sperm whale sound production mechanism and to develop a compact array deployments for long-range acoustic tracking.

Chapter 2 uses simultaneous acoustic and video recordings to study the acoustic behavior of a sperm whale depredating a fishing line in May 2006. The animals size is first estimated from the videocamera images, and then re-estimated by measuring the inter-pulse interval (IPI) of the acoustic clicks generated by the animal when depredating. While both visual and acoustic size estimates agrees on the overall length of the animal, the methods disagree on the size of the spermaceti organ, suggesting that current interpretations of how the sound production mechanism works may be incomplete.

In Chapter 3 bioacoustic tagging data is used to compare the acoustic and diving behavior of sperm whales during natural and depredation foraging. The chapter also investigates whether passive acoustic monitoring can quantify both sperm whale depredation attempt rates and (possibly) success rates, with the goal of improving the accuracy of fish abundance indices and reducing uncertainty in the sablefish stock assessment.

Chapter 4 investigates potential changes in depredating sperm whale acoustic behavior during sound playbacks. Bioacoustic recording tags were deployed simultaneously on depredating sperm whales. A two-sided Kolmogorov-Smirnov test found statistically significant differences in acoustic behavior between haul-only and haul-playback situations. Specifically, during haul-playbacks animals click and creak rates fell. However, the dive characteristics of the animals showed no significant differences.

Finally, Chapter 5 demonstrates how a two-element short-aperture vertical array can track sperm whales to at least 35 km range under sea state 3 conditions. Bioacoustic and satellite tag data are used to independently verify the localization estimates. The data are also used to model the mid-channel propaga-

tion environment, measure ambient noise levels, and estimate whale source levels and ultimate tracking range. Finally, the technique is used to measure the drift of several whales away from a decoy countermeasure.

Chapter II:
Relationship between sperm whale (*Physeter macrocephalus*) click structure and size derived from videocamera images of a depredating whale (sperm whale prey acquisition)

II.1 Abstract

Sperm whales have learned to depredate black cod (*Anoplopoma fimbria*) from longline deployments in the Gulf of Alaska. On May 31 2006, simultaneous acoustic and visual recordings were made of a depredation attempt by a sperm whale at 108 m depth. Because the whale was oriented perpendicularly to the camera as it contacted the longline at a known distance from the camera, the distance from the nose to the hinge of the jaw could be estimated. Allometric relationships obtained from whaling data and skeleton measurements could then be used to estimate both the spermaceti organ length and total length of the animal. An acoustic estimate of animal length was obtained by measuring the inter-pulse interval (IPI) of clicks detected from the animal, and using empirical formulas to convert this interval into a length estimate. Two distinct IPIs were extracted from the clicks, one yielding a length estimate that matches the visually-derived length to within experimental error. However, acoustic estimates of spermaceti organ size,

derived from standard sound production theories, are inconsistent with the visual estimates, and the derived size of the junk is smaller than that of the spermaceti organ, in contradiction with known anatomical relationships.

II.2 Introduction

The question of whether an organism's anatomical dimensions can be inferred from features of its acoustic signal has a long history in bioacoustics. The bulk of this research has focused on inferring the length of the mammalian vocal tract via formant analysis or other spectral measures (Peterson *et al.*, 1952; Fant *et al.*, 1960; Nearey, 1979; Lieberman, 1984; Fitch, 1997).

Attempts to derive a cetacean's body size from its acoustic signal structure face even greater challenges than terrestrial studies, due to the difficulty of obtaining independent and accurate measurements of animal dimensions in the wild. The most detailed theory linking a cetacean sound to an individual's anatomical dimensions concerns sperm whales (*Physeter macrocephalus*), which produce a 25-30 ms transient sound called a click. Researchers have divided sperm whale sounds into a variety of categories, based on the timing between subsequent clicks in a sound sequence. This timing pattern, called the inter-click interval (ICI), has been used to classify clicks into usual clicks, slow clicks, creaks, and codas (Whitehead, 2003). Clicks are believed to serve a variety of functions, including echolocation and communication, depending on the click pattern. Usual clicks typically have an ICI of 0.5 s to 1.0 s, while creaks display a shorter ICI between 0.2 s to 0.5 s (Gordon, 1987; Jaquet *et al.*, 2001; Watwood *et al.*, 2006). ICI values within a given creak also tend to decrease with time, and orientation measurements from tagged animals have demonstrated that sudden changes in orientation are associated with creak sounds (Miller *et al.*, 2004; Watwood *et al.*, 2006). These observations, among others, suggest that creaks are used as an echolocation signal (Norris and Harvey, 1972, Whitehead and Weilgart, 1991; Gordon, 1987, Goold and Jones,

1995; Jaquet *et al.*, 2001; Whitehead, 2003).

A click displays internal structure in the form of several local maxima, or "pulses," with the time interval between pulses within a click labeled the "inter-pulse interval" (IPI). Note that this quantity is different from the ICI defined earlier.

A 1972 paper by Norris and Harvey hypothesized that a click is initially generated at a pair of fatty tissues called the *museau de singe*, at the front of the animal′s nose. Under this hypothesis, most acoustic energy escapes the nose directly, while the remaining fraction propagates backwards through the spermaceti organ, gets reflected forward by the frontal air sac, and finally escapes into the water either via the anterior end of the spermaceti organ or the rostrum (Figure II.1).

Modifications to this model have been made by Mohl (Mohl *et al.*, 1981; Mohl, 2001; Mohl *et al.*, 03), and supported by Zimmer et al.(Zimmer *et al.*, 2005a; Zimmer *et al.*, 2005b). Under this "bent-horn" interpretation the initial omnidirectional pulse P_0 transmitted directly into the water is actually only a small portion of the sound generated at the museau de singe, whereas the bulk of the energy propagates backwards through the spermaceti organ and reflects off the frontal air sac. The largest component of this reflection is transmitted into the water via the junk, creating a highly directional main pulse P_1. Recent measurements (Zimmer *et al.*, 2005b) also indicate that a portion of the energy reflected from the frontal air sac (just over the skull) escapes directly into the water, creating a $P_{1/2}$ pulse that can be detected between the P_0 and P_1 pulse in recordings made off the longitudinal axis of the animal. Finally, under the revised theory a portion of the P_1 pulse energy propagates back into the junk and/or spermaceti organ, reflects off the frontal sac, and passes a second time through the junk into the water, creating a P_2 pulse. These propagation paths are illustrated in Figure II.1.

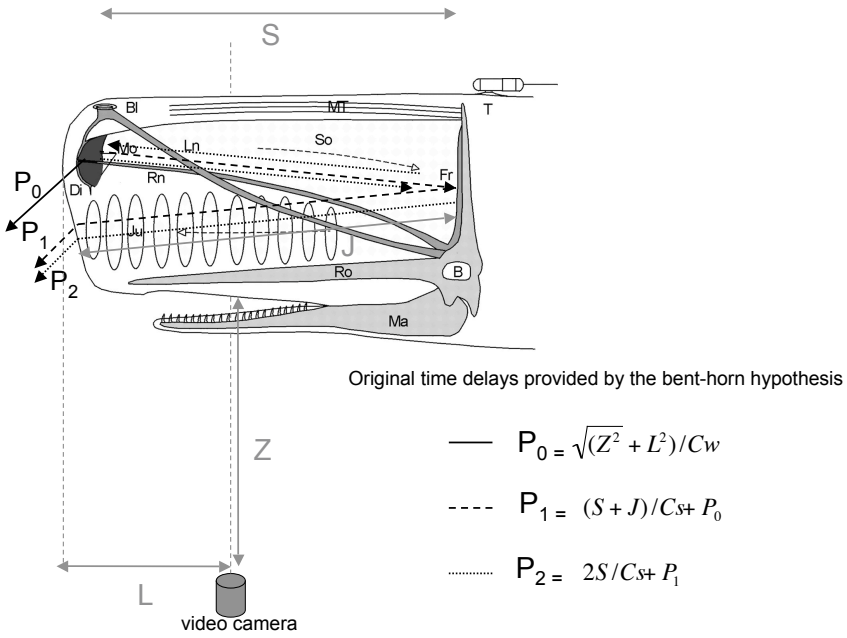

Figure II.1: Bent-horn model of sound production [adapted from Fig. 1 of Madsen *et al.* (2002a) and associated formulae for acoustic path lengths.

Anatomical labels: B: brain, Bl: blow hole, Di: distal air sac, Fr: frontal air sac, Ju: junk, Ln: left naris, Ma: mandible, Mo: monkey/phonics lips or *museau de singe*, MT muscle/tendon layer, Rn: right naris, Ro: rostrum, So: spermaceti organ.

Propagation path variables: S: length of the spermaceti organ, J: length of the junk, Z: distance between the video camera and the jaw of the animal, L: lateral distance between the nose and the video camera, Cw: sound speed in the water=1500 m/sec, Cs: sound speed in the spermaceti organ=1370 m/sec.

According to both the "Norris-Harvey" and "bent-horn" theories, the nominal IPI, or IPI between P_1 and P_2 (Teloni *et al.*, 2007), is proportional to the two-way acoustic travel time between the *museau de singe* and frontal sac, provided that the measurements are made either directly in front of or behind the animal, such that the aspect-dependent $P_{1/2}$ pulse merges with the P_0 or P_1 pulse. In 2005, Zimmer *et al.* showed that measurements made off the longitudinal axis yield off-axis "distortion," in the sense that the appearance of a $P_{1/2}$ pulse obfuscates the interpretation of the timing measurements.

A natural consequence of this hypothesis is that the nominal IPI could be used to estimate the length of the spermaceti organ or junk. Allometric relationships between nose size and body length (Nishiwaki, 1963) then suggest that the nominal IPI should be correlated with body length. Indeed, functional regressions between the nominal IPI and body length have been published (Clarke *et al.*, 1978; Gordon 1991; Rhinelander and Dawson, 2004). These polynomials were derived using analyzed IPIs from whales of independently measured length at the surface. However, no independent means of estimating the animal's spermaceti organ size were available.

Various automated methods have been explored for estimating the nominal IPI, but cepstral analysis (Bogert *et al.*, 1963) has been used in several published papers (Gordon, 1991; Goold and Jones, 1996, Teloni *et al.*, 2007), under the assumption that a click can be modeled as a convolution of a "source" and a "reflection" function. Teloni *et al.* (2007) showed that aspect-dependent features of the IPI estimates could be effectively removed by averaging a large number of cepstra derived from clicks recorded during an animal's foraging dive, during which the animal presumably presents a wide variety of orientations with respect to the recording hydrophone, thus permitting aspect-dependent features of the clicks to be averaged down and the nominal IPI to be enhanced.

This paper uses an unusual data set to directly compare visual estimates of the size of a sperm whale's head with acoustic estimates of its total length,

spermaceti organ length, and junk length. Under normal foraging conditions sperm whales typically dive to depths greater than 300 m (Clarke and Macleod, 1976, Wahlberg , 2002; Watkins *et al.*, 2002, Miller *et al.*, 2004; Watwood *et al.*, 2006), making it impossible to acquire video recordings of prey acquisition attempts. However, sperm whales have learned how to depredate fishing gear, particularly demersal longline operations, in a number of locations around the globe since 2002 (Rice, 1989, Ashford *et al.*, 1996, Capdeville, 1997, Nolan and Liddle, 2000, Gonzalez, 2001), including Norway, Greenland, eastern Canada (Labrador and Newfoundland), Chile and the Falkland Islands. It is the largest marine mammal known to depredate on human fishing activities, and these activities have received increasing coverage in the scientific literature (Ashford *et al.*, 1996; Capdeville, 1997, Hill *et al.*, 1999; Nolan and Liddle, 2000; Gonzalez, 2001, Hucke *et al.*, 2004; Purves *et al.*, 2004; Sigler *et al.*, 08; Thode *et al.*, 2007).

In 2003 the Southeast Alaska Sperm Whale Avoidance Project (SEASWAP) was established by scientists, managers and fishermen to characterize the severity of sperm whale depredation activity on black cod (*Anoplopoma fimbria*) off Sitka, Alaska. Passive acoustic measurements collected during SEASWAP discovered that the animals occasionally dove below the fishing vessels at depths less than 100 m, depths presumably shallow enough to permit visual observations of this activity. In 2006, videocameras were deployed for the first time to capture this behavior.

Section II.3 describes the video and acoustic recording equipment, discusses how the camera was deployed from a fishing vessel during an active longline haul, and then outlines the procedures used to derive visual and acoustic estimates of the size of an animal captured on camera. Section II.4 describes a specific depredation encounter recorded on May 31, 2006, during which the whale touches the fishing line at a known distance from an underwater videocamera lowered to 108 m depth. The visual and acoustic estimates of the animal's size are compared, and the timing between a particular set of pulses within a click yields an acoustic length

estimate that corresponds well with the visually-derived length estimate. The results confirm earlier studies that the IPI can be correlated with total body length, but finds inconsistencies in the visual and acoustic estimates of spermaceti organ size.

II.3 Procedure

II.3.1 Video and audio recording equipment

Visual data were collected by a Sony HVR-1AU videocamera, housed in a Gates Underwater Products HC1/A1U housing using a WP-25 lens port (80 degree field of view, 63.5 mm diameter lens). The data were recorded onto Sony PHDVM-63DM DigitalMaster tapes in DVCAM format, recording over 60 minutes of uncompressed audio and video per tape. The housing and camera port were depth-rated to 152 m (500 ft). The widest angle field of view was used for the recordings (minimum zoom).

The Gates housing also contained a Kobitone PN 252-LM049 Electret Condenser Microphone, recorded to an audio channel on the videotape simultaneously with the videostream. The official sensitivity range of the microphone was 20-12 kHz, with -162 dB re 1 V/uPa sensitivity. The data were sampled at 48 kHz.

II.3.2 Deployment procedure

All deployments took place from the F/V Cobra, a 59 ft fishing vessel mastered by one of the authors (Folkert), who also designed most of the camera deployment system (Figure II.2). A standard demersal longline is comprised of 200 m long lengths of 1/4 inch groundline called "skates," and at every meter along a skate a baited hook is attached by a small line called a "ganion," typically about 20 cm long. Under normal operations the longline is typically deployed by dropping a surface buoy over the side, deploying sufficient line to account for the

water depth and desired scope of the buoy, and then deploying a 30 kg anchor overboard. As the fishing vessel moves over the desired site, the baited longline pays out the back of the vessel. After a typical set has been cast (about 4-6 km long), a second anchor is deployed overboard, attached to a second surface buoy. After a 3-12 hour "soak," the upstream surface buoy is recovered, and the anchor line is passed over a "roller" mounted on the side of the vessel and through a hydraulically-operated pot-puller to haul the rope up and recover the fish. It is at this point that whales like to depredate the line, as fish are accessible throughout the water column.

The deployment technique was designed to avoid substantial changes in fishing procedures, which would have run into regulatory issues. Thus "blank" skates, marked at 50 m intervals, were inserted between every two baited skates, permitting a normal deployment and haul. During the recovery a blank skate would be hauled until the start of the next hooked skate began to emerge from the water. If whales were present, the camera assembly was activated, sealed, and attached to the start of the hooked skate, with the lens port oriented so that it would be facing the ocean surface. The camera was attached to the line so that two to six fish (already present on the line) would be visible above the camera. The distance of each fish from the camera and the length of each fish was recorded and noted. The assembly would then be lowered down into the water until tape marks on the line indicated the desired deployment depth had been reached by the camera (Figure II.2). The true deployment depth could be measured precisely by attaching a commercial dive computer to the line just underneath the camera. Thus the entire procedure minimized alterations to standard fishing procedures.

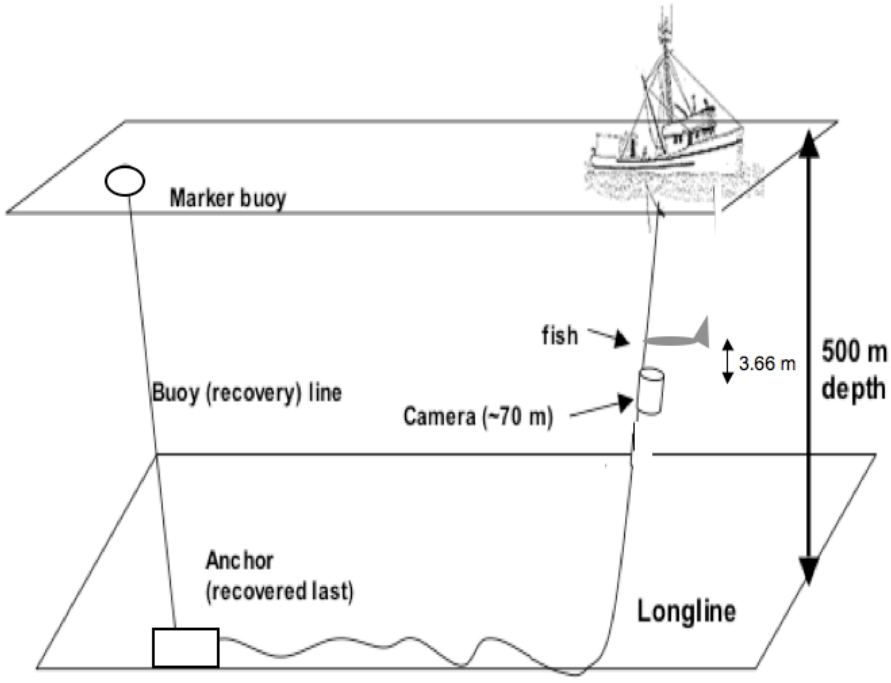

Figure II.2: Schematic of camera deployment from fishing vessel.

II.3.3 Audio data Analysis

Acoustic data from the camera were extracted from the video and stored as a 48 kHz 16-bit WAV file. A peak detector was used to locate echolocation clicks. For every local temporal maximum detected, a 30 ms click sample was extracted and saved, centered around the arrival time of the signal peak. This length of time window was chosen to avoid contamination by preceding or subsequent clicks.

The time difference between subsequent clicks was used to estimate the inter-click interval (ICI). By plotting ICI as a function of time, click detections that shared the same ICI "trajectory", and thus presumably belonging to the same whale, could be selected for further analysis, removing clicks generated by other whales in the vicinity.

Once the click samples from the camera sequence were isolated, the IPI was then extracted from each time sample using two different methods: an incoherent peak detection method, applied to the Hilbert transform of the signal; and via the signal cepstrum (Bogert *et al.*, 1963), which presumes that the click can be expressed as the convolution between a scattering/reflection function and an impulsive "excitation" function.

To obtain the first estimate of the click envelope, a Hilbert transform was applied to each click time series, and then the transforms were stacked on top of each other to permit a view of the click evolution. The time origin was defined as the arrival time of the most intense pulse within the click , which will be labeled as pulse 'B'. The envelopes were averaged over every 0.6 s of the recording to produce estimates evenly sampled in time. To determine pulse intervals, the local maxima in the [5-10] ms interval before and after pulse B were flagged, using methods nearly identical to the original peak detection method used to detect clicks in the data. These intra-pulse maxima were then labeled "A" and "C". (The conventional notation of "P_0","P_1", etc. used by the bent-horn hypothesis is avoided here in order to avoid a particular interpretation of the pulse structure). The precision in

the pulse estimate was typically 0.05 ms.

The second measurement method used cepstral analysis. Heuristically speaking, the cepstrum measures any periodic oscillation of the signal spectrum with respect to frequency, which can be interpreted in the time domain as the time delay between an original signal and its reflection. Thus for the case of a sperm whale click, the Norris-Harvey hypothesis and later modifications predict that the cepstrum, which is measured in units of time, should display a peak at the time corresponding to the two-way travel time between the *museau de singe* and the frontal sac (Gordon, 1991).

After band-pass filtering between 2 and 18 kHz, cepstral estimates were made over the entire 30 ms window, the -15 to 0 ms window, and the 0 to 15 ms window, in order to estimate separate IPI values for the A-B and B-C pulse intervals. Caution must be exercised when band-pass filtering a time series with an FIR filter before computing the signal cepstrum, since the application of the filter produces ripples in the output spectrum, which then produces an artificial peak in the cepstrum. It was found that by specifying a wide filter stopband of 1000 Hz, cepstral artifacts were restricted to 0-3 ms band in the cepstral output, outside the region of interest. Cepstral segments were then averaged over every 0.6 s of the recording (as with the Hilbert transform plots) to produce estimates evenly sampled in time.

Finally, the whale body length can be estimated from the IPI using the Gordon (1991) polynomial relating sperm whale body length and extracted IPI:

$$\textit{Total length (m)} = 4.833 + 1.453 * IPI(s) - 0.001 * IPI^2(s) \qquad \text{(II.1)}$$

Rhinelander and Dawson (2004) also derived a relationship between sperm whale size and IPI using photogrammetric length estimates, and measurements of the IPI for 12 individuals:

$$\textit{Total length (m)} = 17.120 - 2.189 * IPI(s) + 0.251 * IPI^2(s) \qquad \text{(II.2)}$$

Gordon used measurements from 11 individuals in the tropical Indian Ocean, while the Rhinelander *et al.* dataset contained 66 whales from Kaikoura (New Zealand). Gordon's regression contained only one individual longer than 12 m, while all individuals from Rhinelander's dataset were larger than 12 m, possibly explaining the large difference between the polynomial coefficients between Equations II.1 and II.2. Thus, Rhinelander's polynomial would be expected to be more suited for sperm whales living in the Gulf of Alaska, which are generally males greater than 12 m.

II.3.4 Video Analysis

The data set discussed here involves video images of a whale contacting a fishing line at a known distance of 3.66 m (12 feet) from the video camera, with its body oriented roughly perpendicular to the camera. The underexposed features of the whale were enhanced by performing a power law gray scale transformation ($\gamma = 0.5$). The animal was judged to be perpendicular to the camera plane when the teeth on the left side of the lower jaw lined up in such a way as to block the view of corresponding teeth in the right side of the jaw.

On shore the camera was attached to a rope and oriented so that when it was lowered to 3.66 m depth in a pool, the camera pointed toward the surface. A trellis of known size (1.22 m on a side) was slid on the surface across the camera's field of view to permit a conversion of pixel separation to physical distance.

The camera was further calibrated for image distortion using a printed checkboard pattern of 1.2 m width, 1m height, with 10 cm squares. The board was placed 3m from the camera, and was moved in many directions in order to get as many angular views as possible. Then 20 images were extracted and standard camera calibration procedures were used to extract the system's focal length, principal point and image distortion. The net result is a distortion model that maps the radial and tangential distortion of every pixel in the image. It was found

that pixels that lie within half the image width or height from the image center suffered less than 1% distortion, while pixels on the image borders experienced 4% distortion. The second estimate of distortion was made by placing the camera at 3.66 m water depth and measuring at the size variation of the treillis when moved across the camera's field of vision. In this case, it was found that the size of the treillis suffered less than 3% distortion when placed on the image border.

The combined scaling and distortion calibrations permitted three physical measurements to be extracted from the image: the distance between the tip of the snout to the point where the jaw hinges to the skull, or "gape angle" (SG), the distance between the tip of the nose to the start of the upper jaw (SJ) and the mean spacing between the animal's teeth (TS) . Ideally, the distance between the blowhole and the center of the eye should have been measured (BE), since this distance is a good estimate of the spermaceti organ length (Cranford, 1999), and thus the IPI estimate could be directly related to spermaceti organ size. However, due to the low level of ambient illumination the eye cannot be located in the silhouette.

Allometric relationships published in Nishiwaki (1963) relate the SG and the SJ to total body length, thus permitting an estimate of the size of the skull and the length of the whale, even if the entire animal is not visible in the video. Unfortunately, the SG measurement is not precise, because the actual location of the gape angle lies under the animal's skin, resulting in a possible error of 30-50 percent in animal size[1]. Thus an additional measurement was sought.

From the video it is possible to measure the distance between teeth along portions of the jaw, including the locations of the first 4 teeth near the tip of the jaw, and the rearmost 9 teeth. To determine whether an allometric relationship exists between total body length and mean tooth spacing, tooth measurements were obtained from three male sperm whale skeletons with original total body lengths 18.3, 11.9, and 14 m. Two skeletons were from beached animals stored

[1]as discussed with Ted Cranford in a personal communication on January 7th 2009.

by the Natural History Museum of Los Angeles County in Southern California, and thus originated from the Pacific Ocean, and the third was from the Nantucket Historical Association Whaling Museum in Nantucket, Massachusetts. The tooth separation varies with distance along the jaw, so the mean value of the spacing was computed using the teeth that correspond to the teeth visible in the image. The ratio between the total measured length and mean tooth spacing (MLTL) was then computed. A corresponding MLTL can be estimated from the image, using the TS measured from the image and the body length derived from the SJ and TS measurements, to determine whether the video MLTL lies within the ranges of the skeleton TLMLs.

II.4 Results

II.4.1 General description of the May 31st 2006 encounter

The first videotaped encounter of a depredating sperm whale took place on May 23rd 2006; however, the whale never contacted the rope, precluding a visual estimate of its body size. A second encounter was recorded on May 31, 2006, during one of the last attempts to obtain such a recording. The deployment depth of the camera was 108 m, and two black cod were present at distances of 3.66 m and 5.49 m (12 and 18 feet) from the camera respectively. The camera was activated at 10:25 local time, and by 10:45 had been lowered to the target depth. Significant sperm whale acoustic activity was recorded on the videotape from the moment the camera entered the water.

In this and all following sections, the relative timing of events will be expressed as seconds elapsed from 10:45:49, the time at which the acoustic activity from the animal initiated off camera. At 48 s (Figure II.3a), the jaw of a sperm whale appears and contacts the longline at an estimated distance of 1.8 meters from the camera. The animal then slides along the longline until its jaw lies adjacent

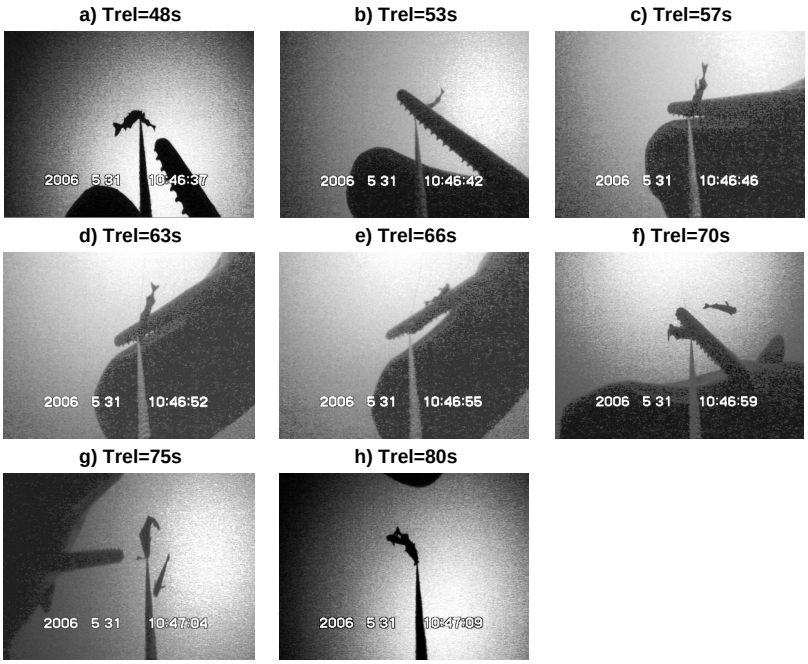

Figure II.3: Snapshots from the May 31st sperm whale encounter video, with the relative time in seconds counted from 10:45:59. Figures are labeled 'a' through 'h', starting from upper left, and moving left-to-right across columns. Figure 3f was used for the visual length estimate.

to the fish nearest the camera (3.66 m) at 53 s (Figure II.3b). The animal then seems to completely close its jaw around the longline at that point by 57 s (Figure II.3c), deflecting the rope a considerable amount. At 63 s (Figure II.3d) the animal performs a slight barrel roll, and the fish attached a distance of 5.49 m from the camera breaks off the longline and floats away. The fish immediately adjacent to the jaw does not detach. As the animal opens its jaw, it stops producing creak clicks and works itself free of the line between 66 s, 70 s and 75 s (Figure II.3e-g). Figure II.3f is the key image used in subsequent analysis; it is the moment when the whale's head is judged perpendicular to the camera. Once free, the animal and floating fish are seen on camera until 80 s, during which the whale seems to be orienting its head toward the loose fish. Unfortunately whatever happens next occurs after both the whale and fish float out of view.

II.4.2 Acoustic Analysis

The click detection procedure in Section II.3.3 generated 1723 click samples from the May 31st sequence over roughly 100 seconds. Figure II.4 displays the inter-click interval (ICI) between individual clicks, expressed in the relative time scale. The ICI was estimated simply by measuring the time interval between successive detections in the detection function. Note that the time between 30 s and 85 s corresponds to ICI values of under 50 ms, traditionally considered characteristic of "creak" activity (e.g. Miller *et al.*, 2004; Whitehead, 2003), and thus most of the sequence analyzed here involves high SNR creak clicks.

As an aside, note that even at times when the whale is biting down on the line, the animal still produces creak clicks, and these clicks indicate a minimum ICI of 30 msec, or about 33 per second, considerably lower than the maximum click rate of 90.9 click/s in other accounts (Jaquet *et al.*, 2001). The timing of these pulses is consistent with a two-way travel time from a target 22 m away, although the whale is clearly interested in targets just a couple of meters away. Thus Figure

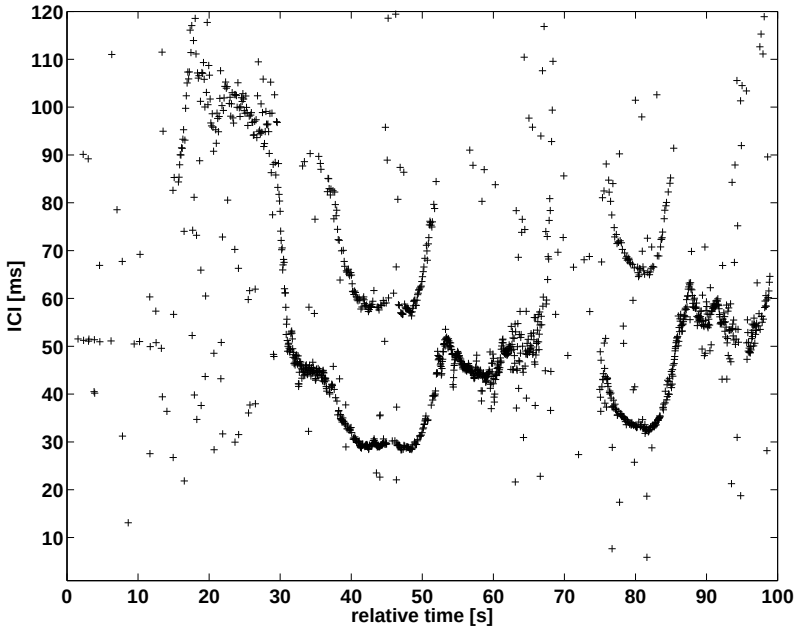

Figure II.4: Inter-Click Interval (ICI) for the May 31st camera sequence, with relative time referenced in seconds from 10:45:49.

II.4 suggests the whale may be reaching a physiological limit in its click production rate. The lack of a visible ICI between 68 and 75 sec corresponds to the time when the whale is working its jaw free of the line, and the ICI sequence reappears a fraction of a second after the jaw snaps free from the line. This correspondence between acoustic and visual events provides confidence that the clicks analyzed here were produced by the whale viewed on the camera. Figure II.4 was thus used to winnow clicks to those that fit this ICI pattern, and thus the on-camera whale, leaving 1178 clicks.

Figure II.5 displays the resulting stacked plot of the absolute values of the Hilbert transform of the filtered click time series for the May 31st sequence, following the procedure in Section II.3.3, with key events labeled using overlying letters that correspond to the images from Figure II.3. As previously discussed, each transform has been time-shifted so that the signal maximum (B pulse) aligns with the time origin.

One aspect of Figure II.5 that attracts instant attention is the sudden disappearance of either the A or B pulse from the train of clicks between 45 and 75 sec, which corresponds closely to the times that the depredating whale appears on-camera. In the rest of this discussion, click samples from within this time range are dubbed "ambiguous" clicks, because of the ambiguity in associating the missing pulse with either the P_0 or P_1 pulse of the bent-horn hypothesis. All other clicks outside this time range are dubbed "standard" clicks. Figure II.6 shows representative spectrograms of "ambiguous" and "standard" clicks. From this point on, the body length analysis uses only "standard" click samples.

As stated in Section II.3.3, two cepstra were computed from each "standard" click: one only containing the A and B pulses, and one only containing the B and C pulses. The individual click cepstra then needed to be averaged to produce a clear IPI peak, as was also found by Teloni *et al.* (2007). Cepstral averages over 5 sec and 10 sec time intervals were examined, but reliable cepstral estimates were only obtained by averaging all "standard" cepstra.

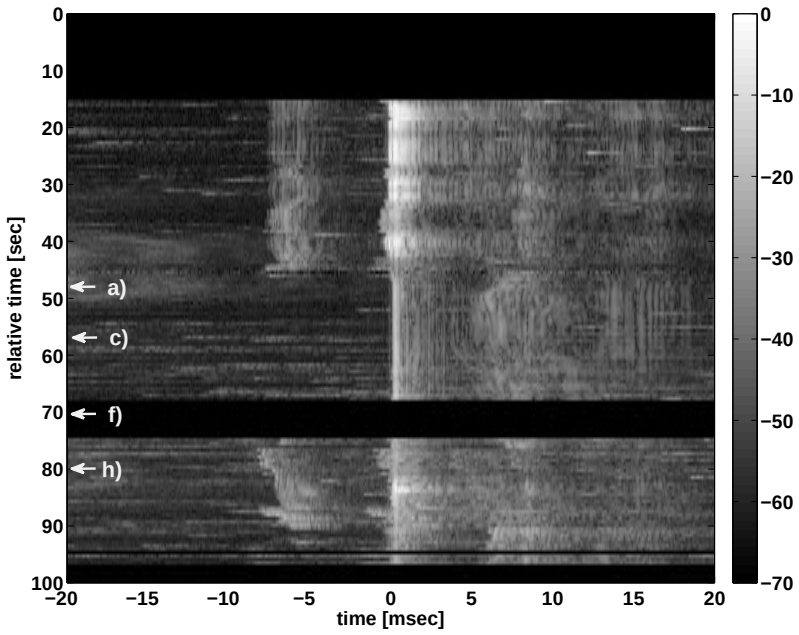

Figure II.5: Stacked click structure of the May 31st sequence, created by filtering each click sample between 2 and 18 kHz, applying the Hilbert transform, and averaging transforms in 0.6 second bins. Time on the y-axis is expressed relative to 10:45:49.

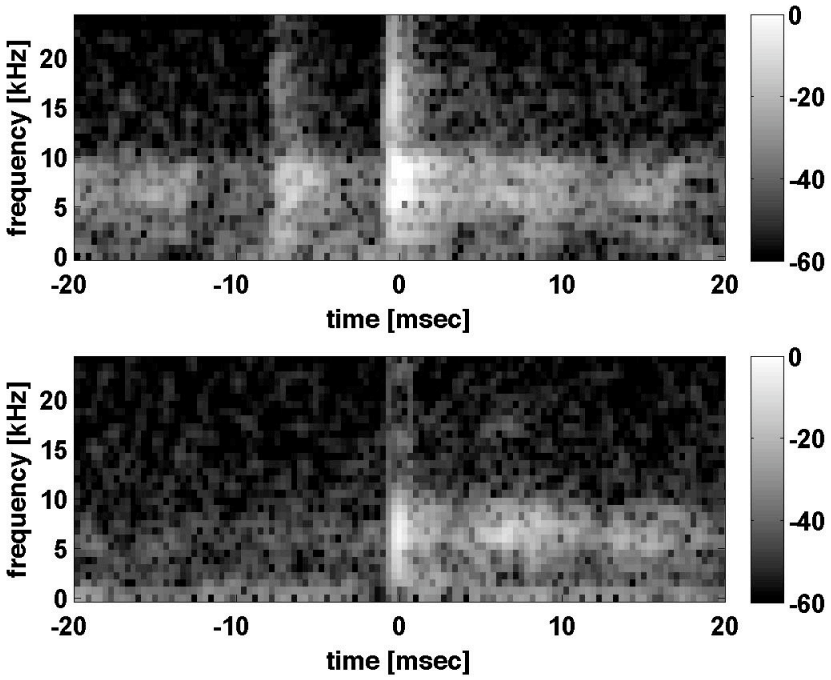

Figure II.6: Representative spectrogram of of (a) "standard click" (42 sec in Figure II.5), and (b) "ambiguous click" (55 sec in Figure II.5).

Figure II.7a displays the stacked cepstra generated from the entire click, Figure II.7b displays the average cepstrum using only the [A-B] portion of the standard clicks, and Figure II.7c displays the average cepstrum using only the [B-C] portion of the standard clicks. In Figure II.7b, a weak local maximum at 6.3 msec is discernable, while in Figure II.5c a strong local maximum at 8.15 msec is clearly visible.

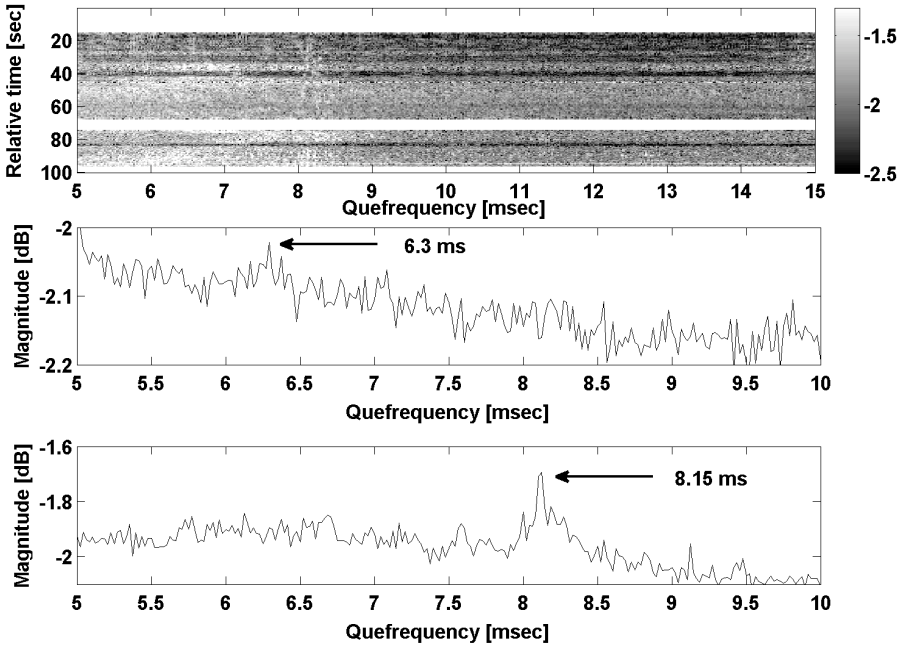

Figure II.7: a) Stacked cepstra of May 31st sequence,
computed over the set of "standard" clicks (0 to 48 sec in Figure II.5) ,
b) averaged cepstrum of the [A-B] portion of the standard click samples,
c)averaged cepstrum of the [B-C] portion of the standard click samples.

Table II.1 summarizes all IPI estimates extracted from the standard clicks, derived using both Hilbert transform and cepstral methods. Bootstrap methods were used to estimate the variance of the cepstral estimates, by randomly selecting 850 individual cepstra from the appropriate set of click types, averaging, and measuring the peak.

Table II.1: Body length estimation for May 31st sequence: comparison between visual and acoustic data.

			Acoustic measurements			
	IPI (msec)	*Body Length Eq. 1(m)*	*Body Length Eq. 2(m)*	*Anatomical dimension (m)*	*Body Length Fig.9(m)*	*Anatomical description*
B-C hilbert	7.6 (±0.9)	15.9 (±1.1)	15.1 (±1.0)	5.23 (±0.6)		spermaceti organ
B-C cepstral	8.1 (±0.2)	16.5 (±0.3)	15.8 (±0.3)	5.55 (±0.3)		spermaceti organ
A-B hilbert	6.4 (±0.8)	14.1 (±1.0)	13.4 (±1.1)	8.8 (±1.0)		spermaceti + junk
A-B cepstral	6.3 (±0.5)	13.9 (±0.5)	13.3 (±0.6)	8.6 (±0.6)		spermaceti + junk
			Video measurements			
SG est.				3.8 (±0.1)	15.2 (±0.3)	tip of snout to angle of gape
SJ est.				1.07 (±0.04)	15.25 (±0.06)	tip of snout to tip of lower jaw
BE est.				3.4 (±0.1)		blowhole to center of eye
Teeth est.				152 (±38)	15.2 (±0.3)	BL / mean teeth separation

II.4.3 Body length estimation using visual and acoustic methods

In Figure II.3f the entire whale's head is visible in the image, oriented perpendicularly with respect to the camera, from the tip of the nose to the point where the lower jaw meets the skull, or "gape angle". The point where the jaw touches the line is 3.66 meters from the camera.

Figure II.8 displays the superposition of Figure II.3f and an image from the pool calibration, from which the distance between the snout tip to gape angle (SG) is estimated as 3.8 (±0.1) m, and the distance between the snout tip to the lower jaw tip (SJ) is 1.07 (±0.04) m. These estimate uncertainties arise from both uncertainties in the exact location of the gape in the image, as well as distortion effects. To check how these measurements were affected by the specific image chosen, the measurements were repeated on two other video images extracted 0.5s before and after Figure II.3f, when the whale is not exactly perpendicular to the camera. The resulting estimates lie within 0.12 m of the results obtained from

Figure II.3f. The mean tooth separation is 0.100 (±0.02) m with a uncertainty of 0.005m on the measurements.



Figure II.8: Superimposition of the videocamera image (Figure II.3f) with a pool calibration image.

Figure II.9, derived using whaling data from Nishiwaki (1963), relates SG, SJ, and BE measurements as a function of total whale length. As mentioned above, the BE measurement provides an estimate of spermaceti organ length, and the SG measurement provides an upper bound on this organ's length . A 3.8 (±0.1) m SG length translates into a total body length estimate of 15.2 (± 0.3) m, while a 1.07 (±0.04) m SJ length translates into a total body length estimate of 15.25 (± 0.06) m. The resulting BE length estimate corresponds to a 3.4 (±0.1) m spermaceti organ.

As mentioned in Section II.3.4, the SG measurement may not be reliable, so the ratio between the derived body length and mean tooth separation was also

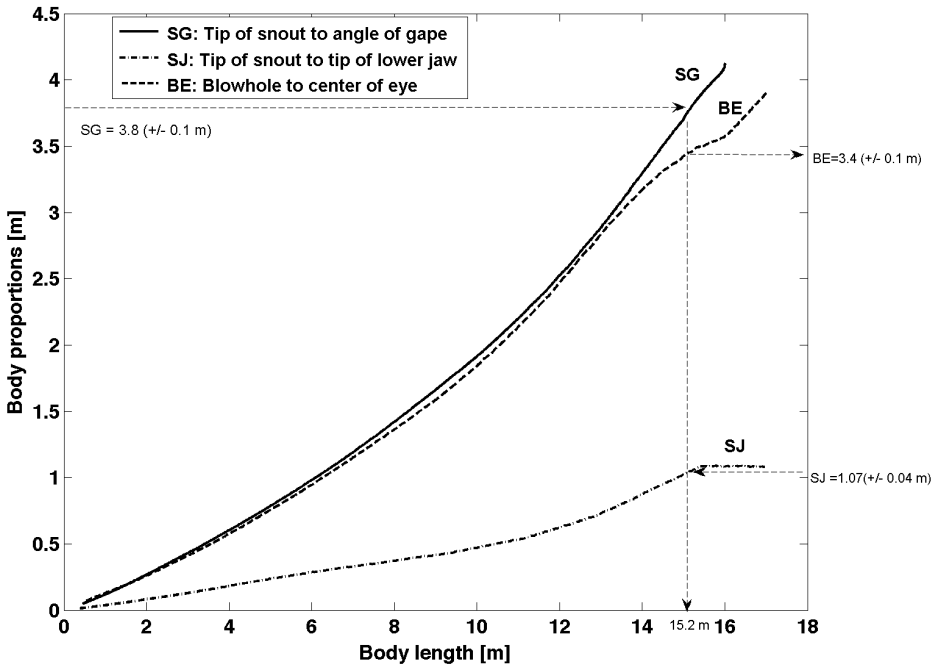

Figure II.9: Allometric relationships between body proportions of male sperm whales caught in the North Pacific [modified from Nishiwaki (1963)] Solid line: SG, distance from tip of snout to angle of gape; dot-dash line: SJ, distance from tip of snout to tip of lower jaw; dashed line: BE, distance from blowhole to center of eye. Both SG and SJ were measured directly from the image. The BE measurement is a proxy for spermaceti organ length.

calculated as a consistency check. This dimensionless ratio was 152 (±38) . The ratios extracted from the skeletons described in Section II.3.4 are 179 (±27) , 160 (±23) and 168 (±16). Thus the SJ and SG measurements yield virtually identical results for total length, and the teeth measurements produce the same length estimate to within experimental error. Thus concerns that the SG measurement would yield estimates that are 40-50 percent off the true value are alleviated.

Both the Gordon and the Rhinelander polynomials, (Equations II.1 and II.2), are combined with the two IPI estimates (Table II.1) to yield four acoustic estimates of the body length. The acoustic estimate obtained by applying the Rhinelander formula to the B-C measurements fits the visual estimate to within a meter, as would be expected from previous literature. An acoustic estimate of the spermaceti organ size can be derived, assuming that the B-C interval corresponds to the P_1- P_2 interval of the bent-horn hypothesis, which in turn represents the 2 way travel time within the spermaceti organ. An estimate of the junk size can then be derived by assuming the A-B interval corresponds to the P_0-P_1 interval, which yields the combined acoustic path length of the spermaceti organ and junk.

Table II.1 compares the derived body lengths for both the visual and acoustic methods (the latter using "standard" clicks only). A 8.1 msec B-C interval and 6.3 msec A-B interval yields respective spermaceti and junk lengths of 5.55 m and 3.1 m.

II.5 Discussion

II.5.1 Relationship between IPI and anatomical structure

Table II.1 shows that both the cepstral and Hilbert IPI estimation procedures produce similar results, in that they find that the A-B IPI is at least 1 msec shorter than the B-C interval. When this IPI difference is applied to either Eq. (II.1) or (II.2), the different IPI values yield a 2 m difference in whale length.

The body length computed from the B-C time interval, using the Rhinelander and Dawson polynomial (Eq. (II.2)), matches the body length estimated from the video (15.2 m) to within the 0.6 m experimental uncertainty, which indicates that the B-C "nominal" IPI (P_1- P_2 interval) must have dominated the IPI measurements used to derive the original polynomial fit. Equation (II.2) might be a better fit than Eq. (II.1) since all individuals from Rhinelander's dataset were larger than 12 m, whereas Gordon's regression contained only one individual longer than 12 m. Thus to this point, the observations are consistent with the bent-horn hypothesis.

However, the videocamera data raise some questions about the physical interpretation of the IPI in the animal. From the bent-horn hypothesis the P_1- P_2 interval represents the two-way travel time of a sound pulse inside the spermaceti organ; thus the acoustic measurements indicate a spermaceti organ on the order of 5.5 m (assuming a propagation speed of 1370 m/s (Goold and Jones, 1995; Goold and Jones, 1996). However, the visual estimate of the spermaceti organ length, using the BE measurement from the image, is only 3.4 m (Table II.1 and Figure II.9), which is only 60 percent of the acoustic estimate. One simple explanation for the discrepancy is that the BE measurement (from the blowhole to the center of the eye) is a biased estimate of spermaceti organ length. Whether that bias is so large to yield a factor of 2 error is unknown.

Another anatomical puzzle is that the 3.1 m length of the junk derived by Section II.4.3 is shorter than the 5.55 m spermaceti organ length, which is in contradiction with known anatomical relationships (Cranford, 1999). Were the *museau de singe* physically further from the camera than the acoustic exit point from the the junk, this discrepancy might be explained; however, the physical orientation of the whale relative to the camera indicates that the relative distance between the two expected acoustic exit points should not be a large effect.

In summary, the combined video/acoustic measurements suggest that the IPI of the sperm whale can be related to the total length of the animal, as has been demonstrated empirically elsewhere many times. However, the video observations

are inconsistent with standard interpretations of the propagation paths through the animal's head; namely, that the P_1- P_2 interval is a direct measure of the size of the spermaceti organ.

II.5.2 Unresolved questions

The data set shown in Figure II.5 shows some additional puzzling features that are worth mentioning briefly. The first is the lack of a so-called $P_{1/2}$ pulse, observed in detailed measurements elsewhere (Zimmer *et al.*, 2005b). The orientation of the animal captured by the videocamera would suggest a clear time separation between the P_0, $P_{1/2}$, and P_1 pulses, yet our results indicate no trace of this additional propagation path.

Even more puzzling is the temporal structure of the so-called "ambiguous" clicks, visible between the 48 and 80 second time window in Figure 5. Out of the two longline encounters captured by videocamera, this type of click structure only appears in the May 31st encounter. The ambiguous clicks are intriguing because they are produced when the whale is biting the line next to a fish, and have a highly variable inter-click interval Figure II.4). Why would a whale continue to creak or "buzz" while biting the line, when the presumed targets of interest are off-axis of the presumed sonar beam and actually behind the *museau de singe*?

Furthermore, the ambiguous clicks are missing a pulse, when compared with the "standard" clicks that are the focus of this study. However, a cepstral analysis of this click subset shows weak peaks at 6.37 and 8.1 msec, the same IPIs present in the standard clicks. A close visual inspection of the Hilbert transforms of Figure II.5 does seem to indicate weak local maxima arriving at about 6 and 8 msec after the arrival of the intense, temporally compact main pulse at 0 msec.

There a variety of explanations as to what could be happening, but given a sample size of one, such speculation is premature. Additional data will be needed to determine if these ambiguous clicks appear consistently during an actual depre-

dation event.

II.6 Conclusion

Video and audio recordings of a prey acquisition attempt from depredating sperm whales in the Gulf of Alaska have been processed to compare visual and acoustic methods for estimating animal size. The inter-pulse-interval (IPI) between the B and C pulses (interpreted as the P_1 and P_2 pulses in the bent-horn hypothesis) yields a size estimate that matches visual estimates to within experimental error, a result consistent with previous empirical studies. However, the video data also permit bounds to be placed on the size of the spermaceti organ of the animal, and those results suggest that the IPI might not be a direct measure of the size of this organ. Furthermore, the size of the junk derived from the acoustic data is smaller than the estimated size of the spermaceti organ, which is inconsistent with anatomical fact.

This paper has provided a glimpse of a possible new approach for investigating the biosonar of large marine mammals in the wild, that permits close-range measurements of the acoustic structure of the terminal "buzz" or "creak" of the animal, from both a broadside and on-axis orientation that lies within the main beam of the animal. These measurement locations are unavailable to bioacoustic tags, which can only measure sounds from orientations behind the animal. Only future work will tell whether close-range observations of depredating whales can yield sample sizes sufficient to draw additional conclusions about the biosonar properties of sperm whales, and whether echos from prey items might be identified.

II.7 Acknowlegments

The authors thank Marty, Tamantha and Jesse for allowing us to dedicate a portion of their black cod quota to the experiment. We also thank the video-

camera analysis efforts of Amanda Koltz, the feedback of Ted Cranford and two anonymous reviewers, whose comments have substantially improved the paper's quality and focus. This work was supported by Grant 7973-06 from the National Geographic Society and North Pacific Research Board grant 626. With regard to potential regulatory issues, the authors consulted consulted with the Permits, Conservation and Education Division, Office of Protected Resources, National Marine Fisheries Service (NMFS), which is processing the pending amendment to NMFS research permit 473-1700-02, to cover future camera work that may involve more substantial modifications of longlining fishing techniques. We also thank the Mammalogy Collections Manager Jim Dines and the Curator Dave Janiger from the Natural History Museum of Los Angeles County as well as the Collections Manager Tony Dumitru and teh Curator Ben Simons from the Nantucket Historical Association Whaling museum for their help with collecting the skeletons measurements.

Chapter 2, in part or in full, is a reprint of the material published in the Journal of acoustical society of America: Delphine Mathias, Aaron Thode, Jan Straley and Kendall Folkert, "Relationship between sperm whale (*Physeter macrocephalus*) click structure and size derived from videocamera images of a depredating whale (sperm whale prey acquisition)", J. Acoust. Soc. Am. **125**(5), 3444-3453 (2009). The dissertation author was the primary researcher and author of this material.

Chapter III:
Acoustic and diving behavior of sperm whales (*Physeter macrocephalus*) during natural and depredation foraging in the Gulf of Alaska

III.1 Abstract

Sperm whales have depredated black cod (*Anoplopoma fimbria*) from demersal longlines in the Gulf of Alaska for decades, but the behavior has recently spread in intensity and geographic coverage. Over a three-year period 11 bioacoustic tags were attached to adult sperm whales off Southeast Alaska during both natural and depredation foraging conditions. Measurements of the animals' dive profiles and their acoustic behavior under both behavioral modes were examined for statistically significant differences. Two rough categories of depredation are identified: deep and shallow. Deep depredating whales consistently surface within

500 m of a hauling fishing vessel and display significantly different acoustic behavior than naturally foraging whales, with shorter inter-click intervals, occasional bouts of high creak rates, and fewer dives without creaks. Shallow depredating whales conduct dives that are much shorter, shallower, and more acoustically active than both the natural and deep depredating behaviors, with median creak rates three times that of natural levels. These results suggest that depredation efforts might be measured remotely with passive acoustic monitoring at close ranges.

III.2 Introduction

III.2.1 Background on sperm whale foraging and acoustic behavior

Sperm whales (*Physeter macrocephalus*) are a cosmopolitan species distributed throughout the world's oceans (Whitehead, 2003; Barlow *et al.*, 2008; Berzin, 1971; Gosho *et al.*, 1984; Rice, 1989). While females and immature individuals generally reside at low latitudes, adult males also travel and forage at higher latitudes (Jaquet, 1996; Whitehead *et al.*, 1992; Teloni *et al.*, 2008). In the U.S., these whales are listed as an endangered species, but their current population in the North Pacific is unknown.

A deep-diving species, sperm whales regularly descend to depths greater than 400 m for periods ranging between 30 and 45 minutes, and rest at the surface for periods ranging between 5 and 10 minutes (Mullins *et al.*, 1988; Papastavrou *et al.*, 1989; Watkins *et al.*, 1993; Jaquet *et al.*, 2000; Wahlberg, 2002; Drouot, *et al.* 2004; Watwood *et al.*, 2006). The few data available from higher latitudes indicate shallower dive depths than what is measured in temperate or tropical latitudes (Whitehead *et al.*, 1992; Teloni *et al.*, 2008).

Sperm whales are vocally active underwater, and during a single dive an individual can generate thousands of impulsive sounds, called clicks (Goold *et al.*,

1995; Worthington and Schevill, 1957; Watkins and Schevill, 1977; Madsen *et al.*, 2002a; Wahlberg, 2002). Measurements in other regions of the world indicate that a whale typically falls silent about 10 to 15 minutes before it returns to the surface (Madsen *et al.*, 2002a; Douglas *et al.*, 2005; Watwood *et al.*, 2006), so by passively monitoring an animal's vocalizations, its dive cycle can be estimated. In the Gulf of Alaska (GOA), click sounds from sperm whales have been detected throughout the year on bottom-mounted recorders, revealing a year-long presence in the region (Mellinger *et al.*, 2004).

Another distinctive acoustic feature of sperm whales is the existence of "creak" (or "buzz") sounds, a sequence of pulses produced at a rate of 10 per second or faster (Madsen *et al.*, 2002a), and often characterized by a decrease in the pulse interval and (occasionally) amplitude over the five-to-ten second duration of the sound (Whitehead and Weilgart, 1990; Whitehead, 2003). Teloni *et al.* (2007) and Miller *et al.* (2004) reported creak rates close to 15 creaks per hour. Watwood *et al.* (2006) reported that 37 sperm whales in the Atlantic Ocean, the Gulf of Mexico and the Ligurian Sea made 22 ± 8.0 creaks per hour. Previous bioacoustic tagging work on sperm whales has shown that most creaks occur at foraging depths and are often associated with changes in the orientation of the animal (Miller *et al.*, 2004; Watwood *et al.*, 2006). Creaks are often followed by a few seconds of silence before the animal resumes "usual" clicking (Madsen *et al.*, 2002a), defined here as a creak-pause event.

There are several possible interpretations of creak-pause events. One is that these intervals are used to recycle air within the sound production system (Wahlberg *et al.*, 2002). Because creaks generally have lower received levels on hydrophones than usual clicks, it may also be possible that some clicks at the end of a creak become masked by noise, creating a false impression of silence. Another unproved hypothesis is that the silences are indicative of prey capture. Analogous signals observed in bats, dolphins, and beaked whales suggest that creaks are echolocation signals (Gordon, 1987; Madsen *et al.*, 2002a), and periods

of time where creaks are detected have been described as prey capture attempts (Miller *et al.*, 2004; Watwood *et al.*, 2006). Laboratory studies on bat echolocation have found that post-buzz pause durations were longer after successful captures (Acharya and Fenton, 1992; Britton and Jones, 1999; Surlykke *et al.*, 2003) than after unsuccessful attempts, but extending this conclusion to cetaceans is risky, as bats cannot produce sound when ingesting prey, while at least one cetacean species can (DeRuiter *et al.*, 2009). Miller *et al.* (2004) found that the majority of creaks produced by sperm whales in the Ligurian Sea and the Gulf of Mexico are followed by pauses of about 5 seconds. Beaked whales and porpoises often pause their echolocation for less than two seconds (Johnson *et al.*, 2004, DeRuiter *et al.*, 2009) and DeRuiter *et al.* (2009) found that porpoises ended creaks 0.8 s after prey capture, even though the animals are physiologically capable of echolocating and ingesting prey simultaneously. If this hypothesis is valid, then the presence of silences following creaks may permit the discrimination of successful prey capture attempts from unsuccessful ones on the basis of acoustic data obtained within a few kilometer range. Thus the duration of creaks, the rate at which they are produced, and the relative fraction of creaks that are followed by silence are all variables of interest in characterizing sperm whale acoustic dive behavior.

The diet of sperm whales generally consists of various cephalopod species, based on analyses of stomach contents (Okutani and Nemoto, 1964; Kawakami, 1980; Rice, 1989; Santos *et al.*, 2002; Whitehead, 2003; Evans and Hindell, 2004). However, in certain regions fish seem to comprise an unknown fraction of the diet as well (Roe, 1969; Berzin, 1971; Clarke and Macleod, 1976; Kawakami, 1980; Rice, 1989; Whitehead, 2003), including the eastern Gulf of Alaska (Okutani and Nemoto, 1964).

III.2.2 Sperm whale depredation

The question of the relative importance of fish to the sperm whale diet is a matter of practical concern, because sperm whales are known to take fish from fishing gear, a behavior known as "depredation". Although quantitative data are limited, sperm whale depredation appears to be increasing worldwide (Ashford *et al.*, 1996; Capdeville, 1997; Nolan and Liddle, 2000; Purves *et al.*, 2004). To date reports have been received from fishermen, engineers, fishery observers and biologists from Norway, Greenland, eastern Canada (Labrador and Newfoundland) and the Falkland Islands regarding interactions with sperm whales and bottlenose whales (Newfoundland only) in longline fisheries off these countries. Perez *et al.* (2006) estimated that marine mammal depredation on the combined longline fisheries in Alaska caused a loss of about 2.2 % of the total fishery groundfish catch during 1998-2004, based on visual evidence of torn or partial fish.

In the eastern Gulf of Alaska (GOA) a demersal longline fishery for sablefish (Anoplopoma fimbria) occurs about 8.5 months a year. Sablefish (also called blackcod and butterfish) reside on the continental slope, and most commercial longliners operate in water depths between 400 m and 1000 m. The continental shelf off Kruzof, Baranof and Chichagof islands, located near Sitka, AK, is very narrow; consequently, the sablefish grounds are within 12 miles of shore (Figure III.1). A domestic sablefish survey in the GOA looked at catch rates from 1999 to 2001 for all sets with sperm whales present; they compared sets with and without physical evidence of depredation and found a 5% lower catch rate in sets with depredation (Sigler, 2008).

In 2003 the Southeast Alaska Sperm Whale Avoidance Project (SEASWAP) was created to investigate this issue with the long-term goal of reducing depredation. A collaborative study between fishermen, scientists and managers, SEASWAP works with the coastal fishing fleet to collect various quantitative data on longline depredation. Using the shape of the flukes as a unique identifier,

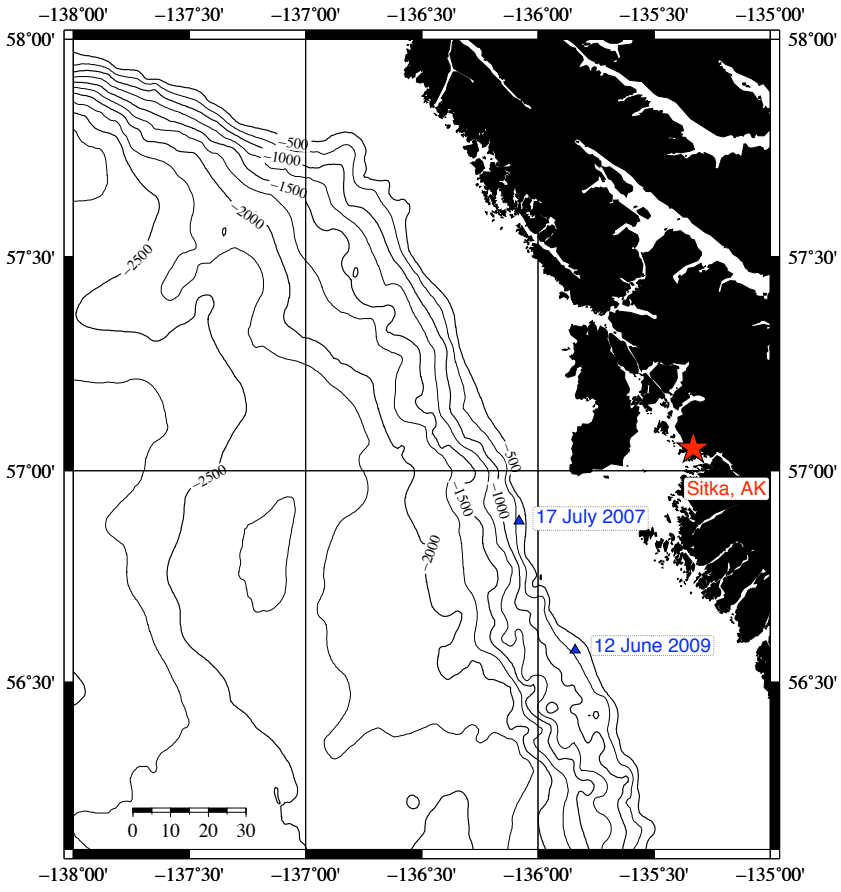

Figure III.1: Local bathymetry off Sitka, AK, marked with fishing haul positions for the two tagging examples discussed in detail in Sections III.4.2 and III.4.3. Water depths are shown in meters.

SEASWAP found that at least 106 individual sperm whales have been involved in depredation. Bayesian mark-recapture analyses estimate at least 123 ([94-174]; 95% credible interval) depredating whales in the GOA study area (Thode *et al.*, 2006). The most ambitious SEASWAP field effort deployed eleven bioacoustic tags on sperm whales in 2007 and 2009, under both natural and depredation conditions off the continental shelf of Sitka, AK. The archival tags logged acoustic, depth, and orientation data.

In this chapter these tag records are analyzed to address three issues. First, do natural foraging dives in Alaska differ from those measured from populations that rely primarily on cephalopods for their diet? Second, do acoustic behavioral parameters significantly change when the animals are depredating? To our knowledge few to no depredating marine mammals have ever been tagged before, and so the strategies employed by the animals are of interest, perhaps even suggesting mechanisms for reducing this behavior or its impact on the fishery. Finally, can passive acoustic monitoring be used to quantify depredation rates? Current methods rely on visual evidence at the surface, which is known to undercount depredation rates. A better "measuring stick" of depredation effort and/or success would be useful for evaluating the efficacy of future countermeasures.

The body orientation was also analyzed and the relationships between a given animal's depth profile, acoustic behavior and angular velocity are presented in Appendix 1. Estimates the fish consumption rates of the animal while depredating vs. foraging naturally are presented in Appendix 2. Appendix 3 displays the dive profile and associated acoustic behavior for all tags deployed in 2007 and 2009.

III.3 Materials and methods

III.3.1 Equipment

The acoustic behavior, dive profiles, and spatial orientation of sperm whales were investigated using digital acoustic B-probe sampling tags (Burgess *et al.*, 1998; Goldbogen *et al.*, 2006). Besides sampling acoustic data the B-probe contains a pressure sensor and a two-axis accelerometer (MXA2500GL, Memsic Inc., North Andover, MA 01845) with one axis parallel to the longitudinal axis of the probe. Data from the depth gauge and accelerometers are sampled at 1 Hz and stored within the tag. The acoustic signal was passed through a Linear Technologies LTC1164-6 switched-capacitor elliptic anti-aliasing filter before entering the analog-digital converter. The acoustic data analyzed in this paper were sampled at 4096 Hz, sufficient for detecting regular clicks and creaks.

III.3.2 Deployments and visual observation protocols

The SEASWAP tagging effort used a 16 foot RHIB, which mostly loitered in the vicinity of cooperating fishing vessels in order to spot tagging opportunities. The two fishing vessels discussed in this paper include a small commercial fishing vessel (F/V Cobra, 18 m), and a larger vessel (F/V Ocean Prowler, 38 m) performing the Southeast Alaska sablefish survey for the Alaska Department of Fish and Game (ADFG). No other fishing vessels were within 15 miles of either vessel during the tagging studies discussed here, as confirmed by both the RHIB visual observations and radar monitoring by the F/V Cobra.

The tag was deployed from the RHIB using a modified windsurfing mast. Photographs were taken of the relative orientation of the tag on the animal. Once tagged, a whale was identified and followed via both visual sighting and monitoring the tag radio beacon. Whenever possible further photographs of the tag placement were taken to note whether the relative orientation of the tag on the whale had

shifted over time. No significant shifting of tag position was ever observed.

The tagging team was active mostly in the early morning, with the goal of deploying tags on animals before the start of a fishing haul. Once a haul began the tagging boat drifted away from the fishing vessel to avoid unduly influencing animal behavior. The visual observers noted times and distances of surfacing animals relative to the vessel, recorded subsequent orientation and surface movements, and noted times of "fluke ups," indicative of the start of a foraging dive. Photos were taken of each individual surfacing within 500 m of the vessel. Individuals could be consistently identified by photo-ID when surfacing, due to the presence of distinctive profiles, scars, and coloring on all sides of the whale. Distances were estimated by a laser range-finder, when possible; otherwise, the range was marked as being greater than or less than 500 m range from the vessel. The presence of an animal within 500 m of a vessel was used to help classify whether a whale was in a depredation or natural foraging state, for reasons to be described in Section III.3.5.

III.3.3 Dive profile analysis

The pressure sensor data on the B-probe tags permitted recovery of dive profiles. The beginning and end of a given dive are defined as times when the animal's depth became deeper or shallower than 10 m. Within each dive, a set of dive "inflections" are defined as points where the vertical velocity of the whale (the time derivative of the pressure) changed sign, consistent with the definitions used in Miller *et al.* (2004). After an inflection is noted, an ensuing net vertical change of at least 10 m (approximately 2/3 of a typical body length) was required before a new inflection could be flagged.

The number of inflections logged during each dive was normalized by dividing the number of inflections in a dive by the total dive duration, yielding a rate of dive inflections per hour, or $\dot{Infl}$. The surface, bottom, and total dive

durations (T_s, T_b, T_d), as well as the maximum depth attained (D_{max}) were also extracted from each dive. The bottom time is measured from the end of the descent phase (the time when the pitch of the diving whale first rises above the horizontal plane) to the start of the ascent phase (the last point in time when the animal's pitch is below the horizontal plane), as defined in Miller *et al.* (2004).

III.3.4 Acoustic data analysis

Sperm whale "regular" clicks were automatically detected in the acoustic tag data by generating a series of 256 pt FFTs, overlapped 75%, and then integrating the power spectral density between 1200 and 1900 Hz. If a value exceeded a running-average estimate of background noise level by 20 dB, the presence of a click was flagged; otherwise, the information was used to update the running average. The output of this automated click detector was manually spot-checked to confirm that clicks produced by other nearby non-tagged whales were not incorporated into the results.

Detecting creaks was more difficult, because their signal-to-noise ratio (SNR) is generally much lower. Creak sounds are almost always preceded by a set of regular clicks with steadily decreasing inter-click intervals (ICI), which eventually transition into the creak. During a creak the ICI decreases from 0.2 s to 0.02 s (Goold *et al.*, 2005) and the creak amplitude decreases over time, with clicks at the end of a creak often 20 dB or more lower in level than at the beginning (Madsen *et al.*, 2002a).

Creak detection was semi-automated. The first step used automated click processing to note "gaps" in regular click trains, where a gap is defined as any pause between detected clicks between 5 and 60 s duration. Each gap was reviewed manually and aurally for the presence of a creak, and then categorized as a *silence*, *creak-only*, or *creak-pause* event. After a creak-only event, the whale began producing regular clicks within two seconds after the audible end of a creak,

while creak-pause events contained at least two seconds of silence between the end of an audible creak and the resumption of a click train.

Special efforts were made to ensure that no creaks were missed due to the relatively low acoustic sampling rate (4096 Hz) of the tag. Whenever a gap was first categorized as a *silence* but preceded by a decrease in the ICI of a regular click sequence, the sample was re-reviewed aurally and usually categorized as a *creak-only* or *creak-pause*. Of the silent gaps generated by the automated detector that were preceded by a decrease in the regular click ICI, only 2% provided no aural evidence of a creak on further examination, and were thus categorized as true silence. Therefore, a steady decrease in the ICI of usual clicks proved to be a reliable indicator of an upcoming creak event.

To address the possibility that extended pauses after creaks arose from noise masking weak creaks, the duration of each creak was also estimated. The start time of the creak was defined as the when the ICI dropped below 0.2 s, and the end time was defined as the start of a silent period of 2 s or longer duration.

Every tag record was decomposed into a set of dive profiles, with the beginning and end of each dive defined according to the criteria of the previous section. The following acoustic parameters were then extracted from each dive:

a) timing of first click (T_{Cl1}): the time difference in minutes between the start of a dive and when the first click is detected on the tag.

b) click rate ($\dot{Cl}$): the total number of clicks produced during a dive, divided by the total dive duration in seconds. Clicks associated with creaks were excluded from the analysis. While in principle heavy bouts of creaking could also reduce this value, in reality creak rates were never high enough to reduce the click rate.

c) mean Inter-Click-Interval ICI : the mean interval in seconds between successive clicks within the same click train. Creak clicks (with intervals less than 0.2 s) were excluded from this calculation. Note that ICI can differ from $\dot{Cl}$ if the whale is silent during substantial portions of the dive.

d) normalized creak-only ($\dot{Cr}$) and creak-pause ($\dot{CrP}$) rates: the number of a particular type of creak event produced during a dive, divided by the total dive duration in seconds.

e) fraction of creak-only (F_{Cr}) and creak-pause (F_{CrP}) events: the relative proportion of each creak event category for each dive.

III.3.5 Behavioral categories and hypothesis testing

The tag records were divided into four distinct behavioral categories, using the B-probe dive profile records, fluke photographs of tagged whales, and visual observations of sperm whale surface behavior. No acoustic or dive parameters (other than maximum dive depth) were used to assign a given dive to a category. The categories are defined as follows:

(1) *resting*: behaviors characterized by shallow drifting and minimal changes in body orientation, regardless of whether a fishing vessel is hauling;

(2) *natural foraging*: dives were conducted by animals at least 500 m from an actively hauling fishing vessel, or during times when the fishing vessel was not hauling gear.

The distribution of estimated ranges of surfacing animals (using a laser-range finder) generally clustered around 400 m or less, or at distances much greater than 500 m. A visual range of 500 m was thus chosen to demarcate the natural and depredation categories.

If a tagged whale was visually identified consistently surfacing within 500 m of a hauling fishing vessel, then the subsequent dive was assigned to one of the following two categories:

(3) *deep depredation*: maximum dive depths are greater than 200 m;

(4) *shallow depredation*: maximum dive depths are shallower than 200 m.

A potential objection to this categorization scheme is that fishing vessels and naturally foraging whales might exploit the same productive locations, and

thus these whales could randomly surface within 500 m of a hauling vessel. There is indeed evidence that depredation is more statistically likely to occur at more productive fishing spots (Straley, 2009); however, it is unlikely whales are surfacing close to the vessel by coincidence, for several reasons. First, experience has shown that sperm whales will generally not surface within 500 m of a fishing vessel before or after a haul, even if the vessel drifts for hours at the location of a fishing set. Just after a haul ends, a given whale will sometimes be sighted for one or two dives within 500 m of the vessel, but the range of the visual sightings always increases over time, unless the fishing vessel starts to maneuver or display other actions that may be associated with the beginning a of second haul.

Second, a hauling vessel generally travels 4-6 km laterally across the ocean floor when recovering longline gear, sometimes against the local current, but the same whales are consistently sighted within 500 m of the vessel during the entire haul. Thus the animals are diving in reference to the moving platform, and not in reference to some particular bathymetric feature, as might be expected were the whales simply exploiting a local hot spot of productivity.

Finally, the surface behavior of animals within 500 m of a hauling vessel is markedly different than that observed from a RHIB without a fishing vessel present. During a haul animals at the surface often orient their heads to point directly toward the vessel, often dipping their heads a slight amount underwater, while simultaneously generating bursts of clicks intense enough to be heard by a listener 1 m above the ocean surface. The cumulative impression left by these visual observations is that a whale consistently surfacing within 500 m of a hauling vessel should be assigned a different behavioral category than a whale surfacing during times when a haul is not occurring. The specific hypothesis examined in this paper is whether statistically significant differences in acoustic and diving behavior can be gleaned between categories initially defined by visual observations, vessel state, and maximum dive depth.

The distributions of the dive and acoustic parameters obtained for each

category are non-Gaussian, often highly skewed, and characterized by large tails that indicate relatively infrequent but significant events that could not be discounted as outliers. Thus a two-sided Kolmogorov-Smirnov (KS) test was used to evaluate the probability that two sample parameter distributions, obtained from different behavioral categories, could have been drawn from the same underlying cumulative probability distribution. The null hypothesis is that various parameters measured from both behavioral categories were drawn from the same underlying distribution. A Bonferroni correction is applied to account for the number of dependant or independent statistical tests performed (Bonferroni, 1936). As 10 parameters are tested for significant differences between behavioral categories, the p value for an individual test is reduced to $0.05/10 = 0.005$. Thus, KS p-values of less than 0.005 led to the rejection of the null hypothesis at the 5% significance level.

Two KS tests were performed for each parameter of interest. The first test used all dives assigned to a given category, regardless of what individual produced the dive. The second test attempted to account for potential differences in individual behavior by only using tag records that contained both natural and depredation behaviors. The test then divides natural foraging dives into two categories: those occurring on a tag record associated with deep depredation states, and those associated with shallow depredation states. No single tag record displayed both deep and shallow depredation states, so no ambiguity existed when assigning a dive to a category. The parameter distributions for shallow and deep depredating individuals are then compared with their associated natural foraging parameter distributions using the KS test. Differences in sample sizes between the categories are automatically incorporated into the two-sided KS test.

A potential objection to this method is that the data itself is used to define behavioral categories, so there could be a risk of correlation between the categories and the parameters tested for significant differences between them. However only the distance between the fishing boat and a whale is used to define the whale

state as natural behavior or depredation behavior. Only the maximum depth of the whale is used to separate deep depredation and shallow depredation behaviors. Then we test for potential differences in dive and acoustic parameters that have not been used to define the behavioral categories. Thus, even if there is a risk of correlated data, we believe that our approach reduces this risk.

III.4 Results

III.4.1 Summary of tag records

Acoustic tags were deployed on sperm whales during two field efforts in July 2007 and June 2009. In 2007 eight B-probes recorded a total of 79 hours of animal depth, orientation, and acoustic data. In 2009 three B-probes were deployed, generating 67 hours of animal depth, orientation, and acoustic data. Thus over the course of two field seasons, seven distinct animals were successfully tagged 11 times with functioning B-probes, and all were matched with a photo-identification catalog. Two individuals were tagged twice in 2007, and one individual was tagged in both 2007 and 2009. The mean, median, and mode of the tag deployment times were 9.8, 7.0, and 9.0 hours in 2007 and 22.3, 27.0, and 12.0 hours in 2009.

A given tag record from a long deployment could contain several different behavioral states, and in the next two subsections two such tag records are reviewed in detail, collectively illustrating the four states defined in Section III.3.5. Eight tag records had periods of natural foraging, documenting a total of 135 natural dives. Ten of the 11 whales tagged showed some degree of vessel association, in that the tagged animal consistently surfaced within 500 m of a hauling vessel. Seven of the 10 tagged whales seen surfacing close to a longline fishing vessel displayed deep depredation behaviors, while the other three displayed shallow depredation behaviors. A total of 52 deep depredation dives and 35 shallow depredation dives were documented. Whales displaying shallow depredation also conducted a total

of 64 natural dives, while the deep depredating whales also cumulatively displayed 66 natural dives. Three tags displayed 23 deep depredation dives with no natural foraging activity, and so these dives were excluded from the second K-S test. The statistical differences between the diving and acoustic parameters of the behavioral categories, excluding resting behavior, are presented in Section III.4.4.

III.4.2 Resting, natural foraging, and deep depredation behaviors from a tag deployed on 12 June 2009

This tag record is among the longest available, and covers two complete fishing hauls. The whale displaying this tag record had been following the F/V Cobra since 11 June 2009, before being tagged close to the vessel at 13:53 on 12 June 2009. Subsequently the first longline haul began at 14:00 and ended four hours later. The vessel began its second haul the following day (13 June) at 11:15, finishing at 14:30. Visual observers sighted three whales during the first haul and six whales during the second haul, all consistently surfacing within 400 m of the vessel. Figure III.2 displays the whale's dive profiles, along with each dives assigned behavioral category, inflection rate, click rate, mean ICI, and total creak rate (both with and without subsequent pauses). With the exception of the maximum dive depth, none of the data shown in Figure III.2 were used to assign a dive to a particular behavioral category. The start and end of the fishing hauls are indicated by the solid red and dotted green vertical lines, respectively. A magenta shaded area indicates that the tagged whale was sighted surfacing within 400 m of the fishing vessel for each shaded dive. The tag detached around 18:00 on 13 June.

At various times this whale displayed three of the four behavioral states defined in Section III.3.5. The labeled horizontal bars in Figure III.2 indicate each state:

(1) *resting* between 14:30 and 15:20 on 13 June, after completion of the

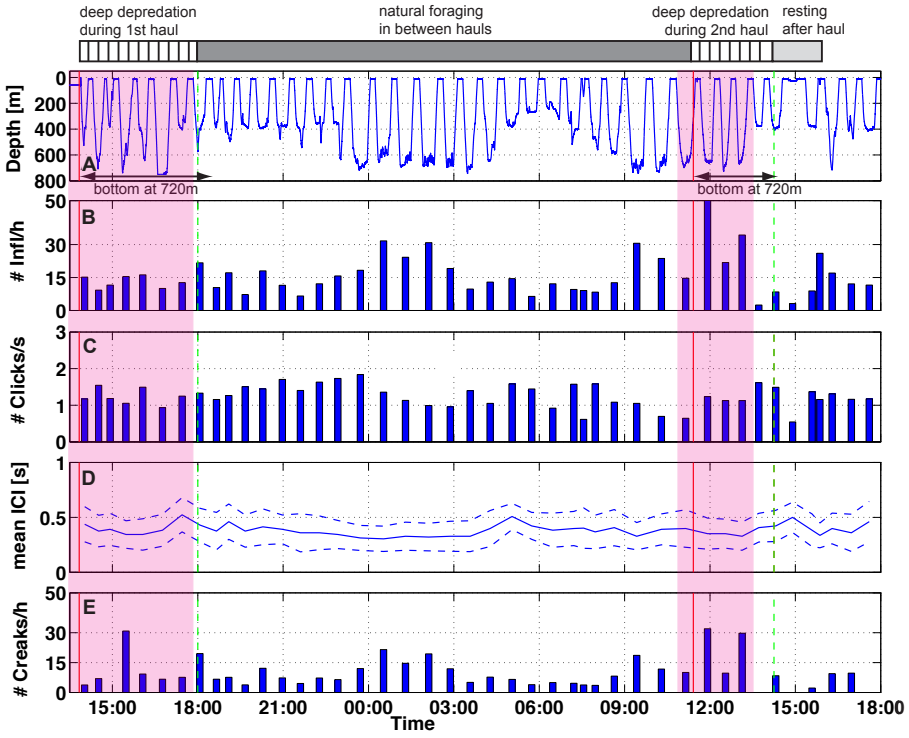

Figure III.2: Selected dive and acoustic parameters of a whale displaying resting, natural foraging behavior and deep depredation behavior on 12 June 2009: (a) dive profile; (b) normalized dive inflection rate per hour, $\dot{Infl}$, with each bar representing a distinct dive; (c) click rate per second, $\dot{Cl}$; (d) mean inter-click-interval ICI per dive, with dotted lines corresponding to one standard deviation; and (e) normalized creak rate per hour, combining *creak-only* and *creak-pause* events. The start and end times of the fishing hauls are indicated by the solid and dotted vertical lines, respectively. The shaded areas indicate when the tagged whale was visually sighted surfacing within 400m of the F/V Cobra for every dive.

second haul: the animal remains at less than 30 m depth, and its inflection rate, creak rate and click rate are at levels much lower than natural foraging conditions.

(2) *natural foraging* behavior between 18:00 on 12 June and 11:25 on 13 June, and between 15:20 and 18:00 on 13 June: the animal shows considerable variation in dive depth, with the dive profiles systematically shallowing and deepening between 250 and 750 m throughout the night and morning. The normalized creak rate also varies between 5 and 20 creaks/hr. During the natural foraging state 54% of creaks detected F_{CrP} were followed by distinctive pauses.

(3) deep depredation during both hauls: during the first haul, all depth and acoustic behaviors displayed by the animal lie within the range of normal foraging behavior, with the exception of a high creak rate of over 30 creaks/h for one dive. During this phase 43% of detected creaks were followed by distinctive pauses. During the second haul, the animal's depth range and usual click parameters also lay within normal bounds; however, the dive inflection rate is slightly greater than average, and the creak rate attains or exceeds 30 creaks/h through half the haul, then drops off to nothing for one dive. Only 30% of creaks were followed by distinctive pauses. The ICI seems similar during both natural and depredation states.

The water depth at both haul locations was 720 m, so the tagged whale sometimes dove all the way down to the ocean floor during deep depredation. The timing of dive inflections and timing of creaks is highly correlated, with a correlation coefficient of 0.78.

III.4.3 Natural foraging behavior and shallow depredation from a tag deployed on 17 July 2007

On 17 July 2007 a whale was tagged at 7:50, close to the F/V Ocean Prowler, which was deploying two longline sets at 690 m water depth. The vessel began hauling its first longline set at 10:00, ending at 12:50, and then began

hauling its second longline set at 13:30, ending at 18:00. A total of four whales surfaced within 500 m of the Prowler throughout both hauls, with the tagged whale consistently surfacing between 150 and 400 m astern of the Prowler during the hauls. After 17:30 the whale was sighted swimming away from the vessel, and by the end of the haul it was at least 2 km away.

Figure III.3 displays the whale's dive statistics in a format identical to that of Figure III.2. Between 7:50 and 10:00 the whale's dives became gradually shallower and less regular in terms of surface and dive durations. During both hauls, the whale performed shallow and irregular dives (120 $\pm$ 83 m). Between the end of the first haul and the start of the second, the whale made a 37 min dive down to 510 m. At 17:00, 30 minutes before the end of the second haul, the whale's dives became deeper and more regular in terms of surface and dive duration. From 18:00 until the tag released the whale alternated 28 min dives down to a median depth of 350 m with 11 min surface times.

During the shallow depredation state multiple dive parameters show significant differences from the other behavioral states. For example, during the haul depths are shallow (less than 200 m) compared to the remainder of the tag record (deeper than 300 m). During shallow depredation inflection rates are higher by a factor of two, click rates are six times higher, the mean ICI is smaller, and creak rates are 10 times higher. During shallow depredation 65% of all creaks were subsequently followed by silence (i.e. *creak-pause* events). Only three natural dives before and after the haul displayed creak sounds, with a creak-pause fraction of 47%, and click rates are very low, with minutes of time elapsing without the animal making a sound at depth. The timing of dive inflections and timing of creaks had a correlation coefficient of 0.71.

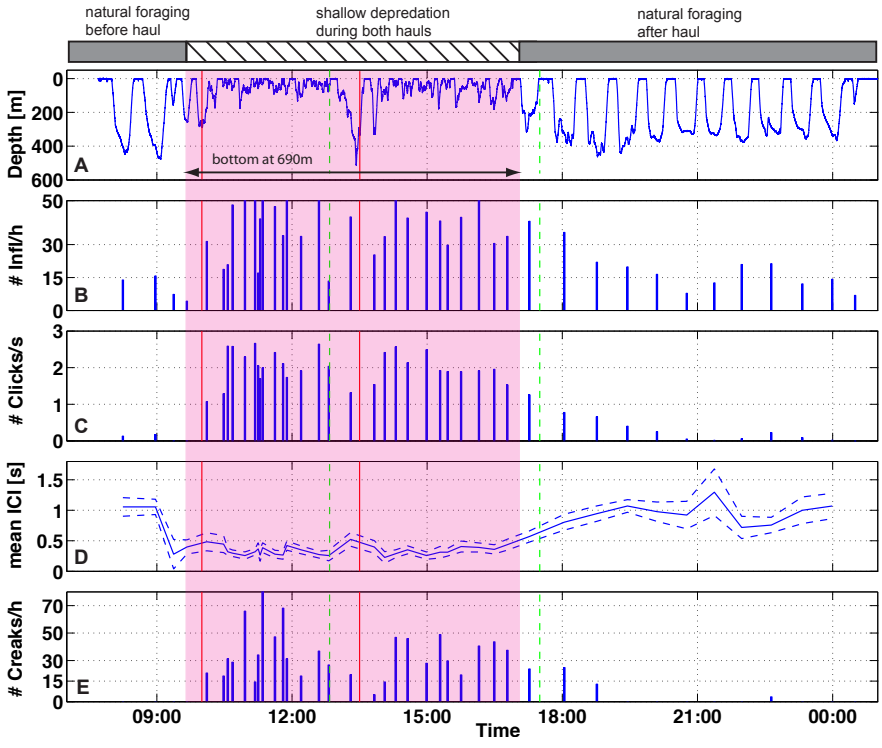

Figure III.3: Tag parameters of a whale displaying natural foraging and shallow depredation behavior on 17 July 2007, using the same format as Figure III.2. The shaded area indicates when the surfacing whale was visually sighted within 400 m of the F/V Prowler.

III.4.4 Comparison of behavioral states across all tag records

Figures III.4 and III.5 display the dive and acoustic parameter distributions compiled from all 11 tag records. Each figure contains five subplots, corresponding to the parameters defined in Sections III.3.3 and III.3.4. Each subplot shows three box plots corresponding to the natural foraging, deep depredation, and shallow depredation categories. Figure 5e also displays the creak-pause fractions measured by other biotagging studies in temperate latitudes (Miller *et al.*, 2004). Tables III.1 and III.2 summarize the mean and standard deviations of these distributions, along with the p values of the two-sample Kolmogorov-Smirnov (KS) non-parametric tests. p-values less than 0.005 are italicized.

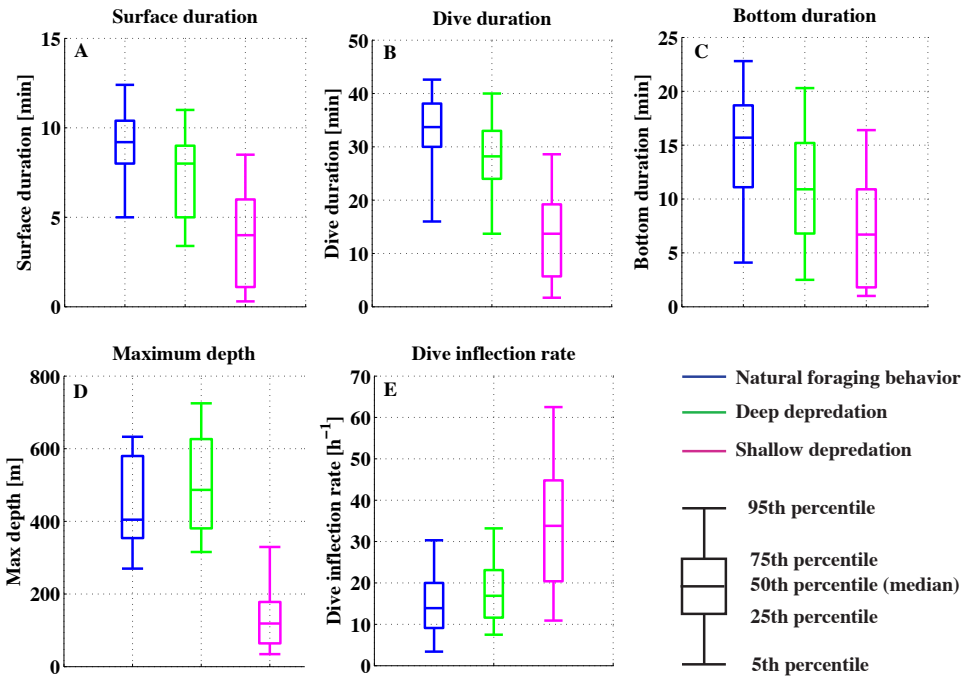

Figure III.4: Boxplots of five dive parameter distributions, obtained from all tag records, subdivided by behavioral state: (a) surface duration (min); (b) dive duration (min); (c) bottom duration (min); (d) maximum dive depth (m); and (e) normalized dive inflection rate per hour. These parameters are defined in Section III.3.3. The box plots show the 5th, 25th, 50th, 75th and 95th percentile values of the distributions.

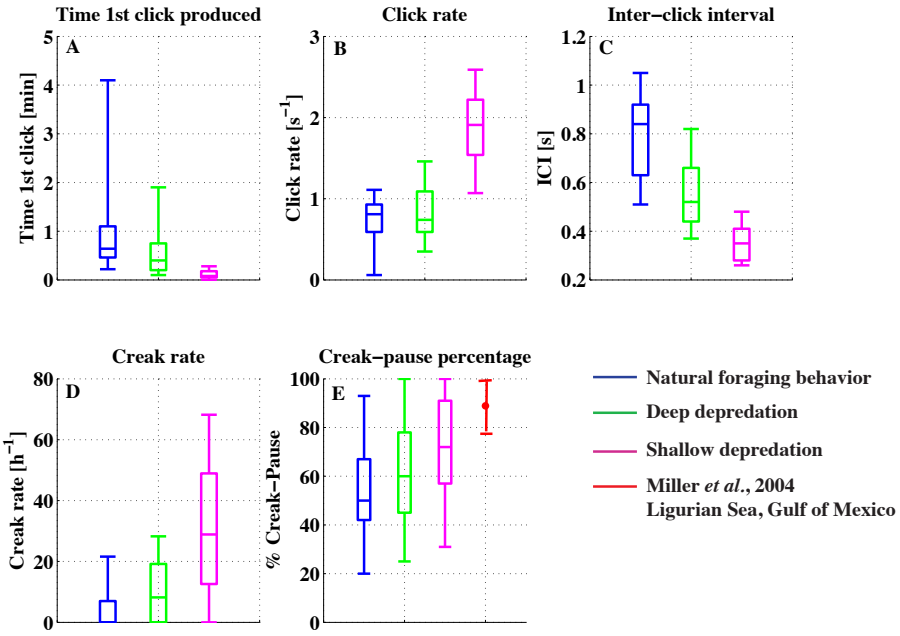

Figure III.5: Boxplots of five acoustic parameter distributions, obtained from all tag records, subdivided by behavioral state: (a) time of first click produced (min), relative to start of dive; (b) click rate per s; (c) inter-click interval (s); (d) normalized creak rate per hour (for all creak events); and (e) creak-pause percentage. These parameters are defined in Section III.3.4. The box plots show the 5th, 25th, 50th, 75th and 95th percentile values of the distributions.

Table III.1: Dive statistics for 2007 and 2009 data

	$\mathbf{D_{max}}$ (m)	$\mathbf{T_s}$ (min)	$\mathbf{T_d}$ (min)	$\mathbf{T_b}$ (min)	$\mathbf{\dot{Infl}}$ (h^{-1})	$\mathbf{N_d}$	$\mathbf{N_{tag}}$	$\mathbf{N_{ind}}$
Resting	31.7±3.5	6.1±0.6	15.9±2.3	7.1±1.6	5.0±1.8	10	3	3
Natural foraging	438.5±135.0	8.9±2.2	33.0±7.9	14.5±5.9	15.2±8.2	135	8	6
Deep depredation	487.2±160.4 *p=0.02*	7.4±2.4 *p<<0.005*	28.4±9.4 *p<<0.005*	11.7±6.2 *p<0.005*	19.1±10.8 *p=0.03*	52	7	5
Shallow depredation	145.1±108.2 *p<<0.005*	3.9±2.6 *p<<0.005*	13.8±8.9 *p<<0.005*	7.1±5.0 *p<<0.005*	35.1±16.9 *p<<0.005*	35	3	3

Values are means ± S.D. over the number of dives N_d considered.

N_{tag} corresponds to the number of tagged whales displaying each behavior

N_{ind} corresponds to the number of individuals whales displaying each behavior.

A p-value is the probability that the distribution is drawn from the same distribution as the natural foraging reference distribution.

Italic p-values indicate when the null-hypothesis that there is the same underlying distribution has been rejected (p<0.005).

Table III.2: Acoustic statistics for 2007 and 2009 data

	$\mathbf{T_{Cl1}}$ (min)	$\dot{\mathbf{Cl}}$ (s^{-1})	**ICI** (s)	$\dot{\mathbf{Cr}} + \dot{\mathbf{Cr}}\dot{\mathbf{P}}$ (h^{-1})	$\mathbf{F_{crP}}$(percent)
Resting	N/A	N/A	N/A	N/A	N/A
Natural foraging	0.9 ± 0.3	0.7 ± 0.2	0.8 ± 0.2	7.9 ± 4.6	48.4 ± 10.2
Deep depredation	0.5 ± 0.4 *p=0.03*	0.8 ± 0.3 0.08	0.4 ± 0.1 *p<<0.005*	11.3 ± 7.1 *p<0.005*	58.4 ± 13.0 p=0.08
Shallow depredation	0.1 ± 0.1 *p<0.005*	1.9 ± 0.4 *p<<0.005*	0.3 ± 0.1 *p<<0.005*	34.5 ± 15.2 *p<<0.005*	68.3 ± 16.4 *p=0.04*

Values are means ± S.D. over the number of dives considered.

A p-value is the probability that the distribution has been drawn from the same distribution as the natural foraging reference distribution.

Italic *p*-values indicate when the null-hypothesis that there is the same underlying distribution has been rejected (p<0.005).

Figures III.6 and III.7 use the same format as Figures III.4 and III.5, but here only data from tag records that display both natural and depredation behaviors are used. Two box plots for natural foraging behavior are now shown: one for dives preceding or following deep depredation, and one for dives preceding or following shallow depredation. The box plots thus show distributions drawn from the same pools of individuals, thus reducing potential individual variations in dive or acoustic behavior. Differences in sample sizes between the categories are automatically incorporated into the two-sided KS test.

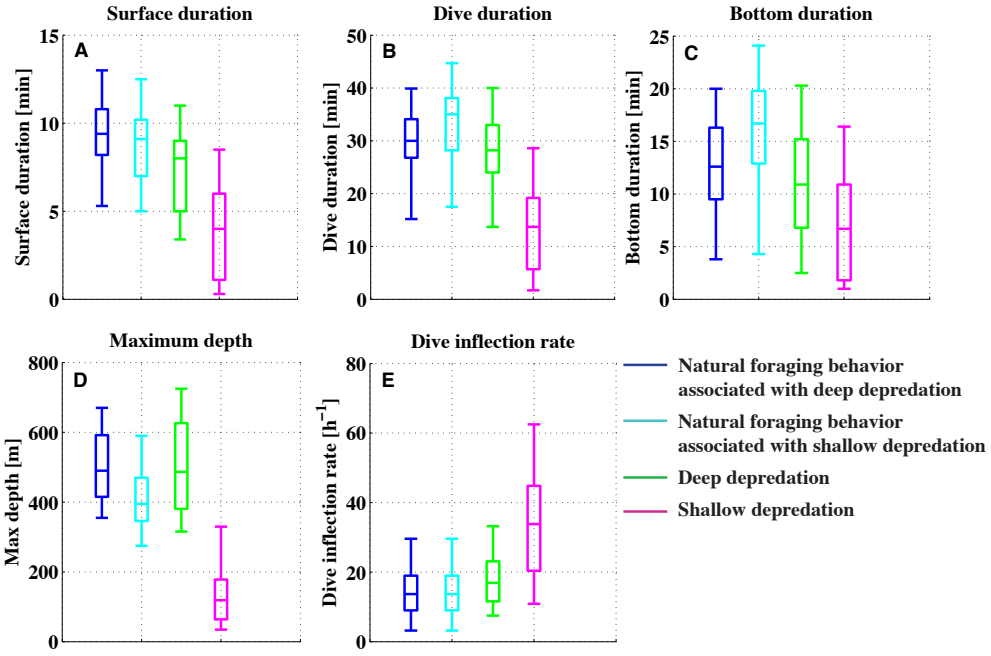

Figure III.6: Boxplots of same dive parameters shown in Figure III.4, but only using tag records that display both natural and depredation behavior. For each parameter, distributions are shown for deep and shallow depredation states, along with the distributions for the natural foraging states preceding/following a given depredation behavior. The box plots show the 5th, 25th, 50th, 75th and 95th percentile values of the distributions.

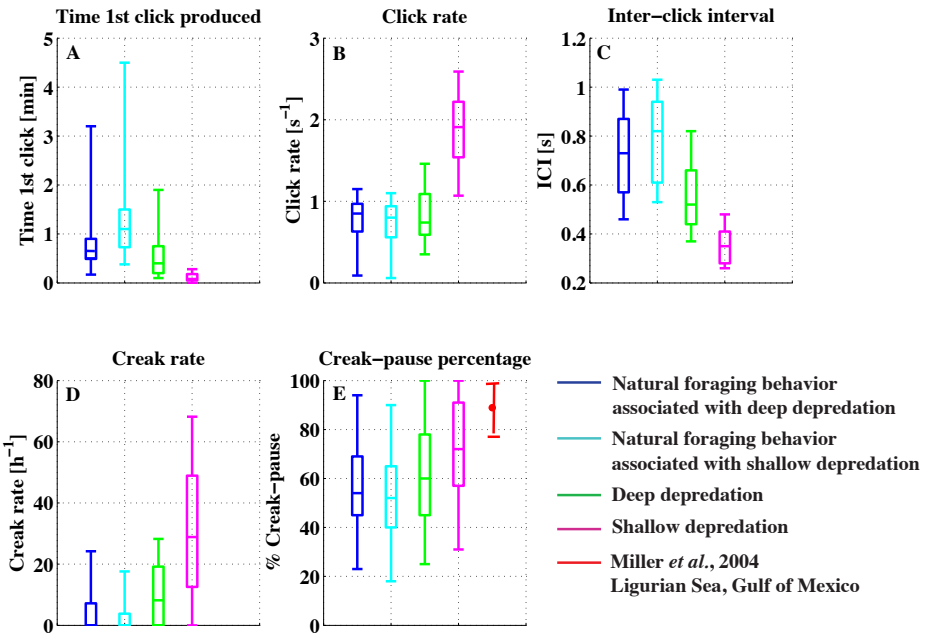

Figure III.7: Boxplots of same acoustic parameters shown in III.4, but only using tag records that display both natural
and depredation behavior. For each parameter, distributions are shown for deep and shallow depredation states, along with the distributions for the natural foraging states preceding/following a given depredation behavior. The box plots show the 5th, 25th, 50th, 75th and 95th percentile values of the distributions.

Tables III.3 and III.4 display the results of the K-S analysis on the distributions shown in Figures III.6 and III.7, with the p-values indicating the result of comparing a particular depredation category with natural foraging dives preceding or following that type of depredation.

Miller *et al.* reported that while foraging at depth, 22 sperm whales from the Ligurian Sea and the Gulf of Mexico made 12.5 ± 4.0 dive inflections per hour, and a mean of 32% of all creaks were produced within 10 s of a dive inflection. The sperm whales in this study made 15.2 ± 8.2 dive inflections per hour (Figure III.4e), and consistent relationships were also found between the timing of dive inflections and creak events: 85% of creaks started within 30 s of a dive inflection, and 56% started within 10 s of a dive inflection. Three of the 11 tagged whales displayed a total of 10 resting dives, all of them being head-down drift-dives. The durations of those resting dives (15.9 ± 2.3 min) and the depths at which they occurred (31.7 ± 3.5 m) are consistent with those reported in Miller *et al.* (2008). Thus dive parameters from naturally foraging sperm whales in the eastern Gulf of Alaska are within the bounds measured at other regions around the world.

However, two significant differences in natural acoustic behavior were found. First, 50% of dives werent associated with any creaks (Figure 5d), which is higher than what Teloni *et al.* (2007) reported (15%). Second, the relative proportion of creak-pause events (F_{CrP} is 48.4% ± 10.2 in Figure III.4e, which is considerably lower than the only other published description of this fraction (88.9% ± 13.5), in Miller *et al.* (2004). The potential relevance of these differences is examined in Section III.5.2.c.

Table III.3: Dive statistics for 2007 and 2009 data using only tag records that display both natural and depredation behaviors

	$\mathbf{D_{max}}$ (m)	$\mathbf{T_s}$ (min)	$\mathbf{T_d}$ (min)	$\mathbf{T_b}$ (min)	$\mathbf{\dot{N}fl}$ (h^{-1})	$\mathbf{N_d}$	$\mathbf{N_{tag}}$	$\mathbf{N_{ind}}$
Resting	31.7 ± 3.5	6.1 ± 0.6	15.9 ± 2.3	7.1 ± 1.6	5.0 ± 1.8	10	3	3
Natural foraging associated with deep depredation	481.6 ± 152.7	9.2 ± 2.5	30.0 ± 7.7	12.6 ± 5.0	15.6 ± 7.0	66	4	2
Natural foraging associated with shallow depredation	417.4 ± 119.3	8.9 ± 2.0	35.0 ± 8.1	16.7 ± 8.3	14.8 ± 9.3	64	3	3
Deep depredation	487.2 ± 160.4 *p=0.04*	7.4 ± 2.4 *p<0.005*	28.4 ± 9.4 *p<0.005*	11.7 ± 6.2 *p=0.04*	19.1 ± 10.8 p=0.05	29	4	2
Shallow depredation	145.1 ± 108.2 *p<<0.005*	3.9 ± 2.6 *p<<0.005*	13.8 ± 8.9 *p<<0.005*	7.1 ± 5.0 *p<<0.005*	35.1 ± 16.9 *p<<0.005*	35	3	3

Values are means ± S.D. over the number of dives N_d considered.

N_{tag} corresponds to the number of tagged whales displaying each behavior

N_{ind} corresponds to the number of individuals whales displaying each behavior.

A p-value is the probability that the distribution is drawn from the same distribution as the natural foraging reference distribution.

Italic p-values indicate when the null-hypothesis that there is the same underlying distribution has been rejected (p<0.005).

Table III.4: Acoustic statistics for 2007 and 2009 data using only tag records that display both natural and depredation behaviors

	$\mathbf{T_{Cl1}}$ (min)	$\dot{\mathbf{Cl}}$ (s^{-1})	**ICI** (s)	$\dot{\mathbf{Cr}}$ (h^{-1})	$\mathbf{F_{crP}}$ (percent)
Resting	N/A	N/A	N/A	N/A	N/A
Natural foraging associated with deep depredation	0.6 ± 0.2	0.8 ± 0.2	0.6 ± 0.2	8.7 ± 4.9	53.9 ± 9.3
Natural foraging associated with shallow depredation	1.2 ± 0.3	0.7 ± 0.3	0.8 ± 0.1	6.3 ± 3.5	46.7 ± 7.0
Deep depredation	0.5 ± 0.4 *p<0.005*	0.8 ± 0.3 0.2	0.4 ± 0.1 *p<<0.005*	11.3 ± 7.1 *p<<0.005*	58.4 ± 13.0 p=0.07
Shallow depredation	0.1 ± 0.1 *p<0.005*	1.9 ± 0.4 *p<<0.005*	0.3 ± 0.1 *p<<0.005*	34.5 ± 15.2 *p<<0.005*	68.3 ± 16.4 *p=0.04*

Values are means ± S.D. over the number of dives considered.

A p-value is the probability that the distribution has been drawn from the same distribution as the natural foraging reference distribution.

Italic *p*-values indicate when the null-hypothesis that there is the same underlying distribution has been rejected (p<0.005).

III.5 Discussion

III.5.1 Is natural foraging behavior off Sitka similar to elsewhere in the world?

A distinctive feature of sperm whale behavior is the depths of their foraging dives. Although aspects of the diving, acoustic and body motion behavior of male sperm whales have been studied at both low (Gordon *et al.*, 1987; Whitehead *et al.*, 1991; Watwood *et al.*, 2006) and high latitudes (Mullins *et al.* ,1988; Whitehead *et al.*, 1992; Jaquet *et al.*, 2000; Madsen *et al.*, 2002a; Douglas *et al.* 2005; Teloni *et al.*, 2008), no data have been published for the Gulf of Alaska area. A question that arises is whether dive and acoustic parameters of the Alaskan whales under natural foraging conditions are consistent with measurements obtained elsewhere. Male sperm whales in this study dove to mean maximum depths of 438 m (Table III.1) when displaying natural foraging behavior, with maximum dive depths of around 800 m. Thus most dives did not descend to the ocean floor, and the observed dive and surface durations (Figure III.4a-b) are similar to the ones reported in another high-latitude study (Teloni *et al.*, 2008). That same study also reported natural dives shallower than 200 m off Norway, but there has been no indication that sperm whales in this study naturally perform such shallow dives. Off Sitka naturally foraging male sperm whales spent 85% of their total dive time emitting usual clicks, generally starting within 1 min of the descent phase and stopping early during the ascent phase. The mean depths of their first creaks were shallower (80 m) than the mean depths of the last creaks (300 m), suggesting that the whales weren't searching for prey items during the ascent phase. These results are similar to what has been reported in other studies (Madsen *et al.*, 2002a; Douglas *et al.*, 2005; Watwood *et al.*, 2006). The click and creak rates, as well as the ICI values, reported in Figure III.5b-d lie within the ranges reported by Miller *et al.* (2004) at low latitudes and by Teloni *et al.* (2007) off Norway.

III.5.2 Depredation vs. natural foraging behavior

III.5.2.a Dive parameters during shallow depredation

Three of the ten tagged whales seen surfacing close to a hauling longline fishing vessel had dives assigned to the shallow depredation category. Figures III.4 and III.6 demonstrate how this category is substantially different from the other categories across all dive parameters. The maximum dive depths of animals during this state were generally much shallower than those of naturally foraging whales (Figure III.4d). The surface, dive and bottom durations were also much shorter than the corresponding natural durations in Figures III.4a-c and III.6a-c. The contrast in bottom duration time is particularly striking in that tagged whales displaying shallow depredation generally conducted longer natural dives, when compared with the natural bottom time distribution for deep depredating animals (Figure III.6c, second box plot). Finally, dive inflection rates were twice as high during shallow depredation than during natural situations. Given the strong visual contrasts in the dive parameter distributions in Figures III.4 and III.6, it is not surprising that the K-S tests yield highly significant p-values for all dive parameters (Tables III.1 and III.3).

III.5.2.b Dive parameters during deep depredation

The seven other tagged whales seen surfacing consistently next to a fishing vessel were assigned to the deep depredation category. The differences between deep depredation and natural behavior were subtler than for shallow depredation. Deep-depredating whales had shorter surface, dive, and bottom durations when compared to the complete distribution of natural foraging samples (Figure III.4a-c); however, when the natural foraging dive samples were restricted to tag records displaying deep depredation only, the differences became much smaller, except for the surface duration (Figure III.6a). The K-S tests of the distributions in Figure III.6 (Tables III.1 and III.3) still showed statistically significant differences for

surface and dive durations.

At first glance Figure III.4d suggests that depredation dives were slightly deeper than natural foraging dives; for example, 40% of deep-depredation dives exceeded 600 m vs. only 15% of all natural foraging dives. But when the natural dive samples were restricted to those conducted by deep depredating whales only (Figure III.6d), one found little visible difference between the maximum dive depths, and the p-value for that analysis was not significant ($p = 0.04$). The dive inflection rate distribution varied little between natural foraging and deep depredation and was not statistically significant.

Interestingly, two of the ten depredating whales also performed either one or two resting dives, just before or after a series of shallow or deep depredating dives. Those resting dives thus happened in the middle of the day, while resting dives observed during natural foraging behavior usually happened during the night. This suggests that depredating dives might be more energy consuming than normal foraging dives, that depredating animals become satiated and can rest before resuming natural feeding, and/or that whales might rest while waiting for the start of a haul.

III.5.2.c Acoustic parameters during shallow depredation

Shallow depredating animals were very active acoustically, when compared with natural foraging behavior (Figures III.5 and III.7, Tables III.2 and III.4). They continuously produced usual clicks, even when resting at the surface, and they began clicking almost immediately after starting a dive (Figures III.5a and III.7a). Their median click rate was nearly double over that displayed by naturally foraging dives; the reason for this difference is that the inter-click interval during shallow depredation was much smaller; over 75% of clicks during this behavior had an ICI less than 0.4, an interval never observed during natural behavior. Similar patterns arose for creak production rates; the median creak rate of 30 creaks/hr during shallow depredation was more than three times higher than

natural creak rates. The spread in creak rate values was also very high during shallow depredation: the 25 and 75th percentiles lie between 10 and 50 creaks per hour, respectively, while the spread was much narrower for natural dives. There was much less dramatic change in the median percentage of creak-pause events during shallow depredation; however, Figure III.5e shows that 75% of dives had creak-pause percentages exceeding 58%, while only 40% of natural foraging dives exceeded this fraction. Figure III.7e shows that this difference persisted even when the natural foraging dives were restricted to individuals that also display shallow depredation. However, the large spread in the creak-pause percentage distributions under both behavioral conditions resulted in a non-significant p-value from the K-S test ($p = 0.04$), the only acoustic parameter for shallow depredation not to differ significantly from natural behavior.

Shallow depredation dives showed another interesting acoustic effect, in that both click and the creak rates are generally lower during natural foraging dives that occurred after a haul is completed (e.g. Figure III.3). One possible interpretation of this result is that whales become satiated or tired after shallow depredation.

III.5.2.d Acoustic parameters during deep depredation

The acoustic behavior of deep depredating whales showed significant differences from natural foraging behavior as well. One noticeable behavioral shift was that deep depredating whales displayed significantly shorter ICIs (median 0.5 s) vs. a median value of 0.75 s for the same individuals during natural dives (Figure III.7c) and a median value of 0.85 s for all natural foraging dives from all individuals. The K-S test confirmed that a shift in the ICI distribution was the most significant effect (lowest p-value). Surprisingly, the average click rate of deep depredating whales did not change significantly, despite the noticeable shift in ICI levels. In other words, during a dive, deep depredating animals were silent for longer periods of time than under natural conditions. Deep depredating whales

also began clicking sooner than naturally-foraging whales after they started a dive (Figures III.5a and III.7a), but the shift was not as dramatic as what was found for shallow depredation.

Also interesting is the fact that deep depredating whales had higher creak rates than under natural situations (Figures III.5d and III.7d), and both K-S tests showed highly significant differences between the two (Figure III.7d). The differences arose from two factors. First, most deep depredation dives had creak rates similar to those found under normal conditions, but occasionally very high creak rates were generated during a dive (e.g. Figure III.2e), and these relatively infrequent situations cannot be dismissed as statistical outliers. Second, a large number of natural foraging dives contained no creaks (50%) vs. only (25%) for deep-depredation dives, which led to a significant difference between the two distributions.

While the creak rates of deep depredating whales increased significantly, their percentage of *creak-pause* events did not differ significantly ($p = 0.08$) when compared with natural conditions. This same pattern also appeared with shallow depredation.

III.5.2.e Interpreting the meaning of silences after creaks

Figures III.5d and III.5e showed that the creak-pause percentage is much lower in the Gulf of Alaska than measured in more temperate locations, as discussed at the end of Section III.5.1. There were also much larger numbers of dives in the Gulf of Alaska that display no creaks at all.

One interpretation of creak-pause events is that they are indicative of a successful prey capture, as opposed to just a prey capture attempt. Figures III.5d and III.5e could thus be interpreted as showing that Alaskan whales generally had lower prey acquisition success rates than whales in the Gulf of Mexico or Ligurian Sea; i.e. the Alaskan whales required more creaks per capture. The fact that Alaskan whales include fish as a natural part of their diet provides one

potential explanation for this difference. Figure III.5e also suggests that shallow depredation required fewer creaks per prey acquisition, although the change was not statistically significant. When Figure III.5e is compared to the creak rate distributions in Figure III.5d, one gets the impression that during both types of depredation a whale may get many more prey opportunities (as shown by higher creak rates), but with only slightly higher capture rates (as shown by the small change in percentage of creak-pause events).

There are several possible alternative interpretations of what a pause following a creak means, including air recycling (Wahlberg *et al.*, 2002) and a simple inability to detect weak creaks on the tag. As discussed in Section III.3.4 it is unlikely that the low acoustic sampling rate of the tag was missing creak events, because creak events were almost always preceded by an easily-detectable decrease in usual click ICI. The argument that a pause after a creak is primarily due to air recycling seems inconsistent with the observation that *creak-pause* events in this study were much lower than observed in Miller *et al.* (2004). Furthermore, if air-recycling were the primary reason why pauses after clicks exist, one would expect that shallow depredation dives would yield relatively fewer pauses after creaks; after all, shallow depredation dives are nearly five times shallower on average that a natural dive, and thus the available air volume inside the animal is five times larger. Instead, one finds that the relative creak-pause fraction increases slightly during shallower dives.

A third interpretation for a creak-pause event is simply that the received level of a weak creak becomes too low to be detected, and becomes buried in noise. This interpretation is not consistent with what is heard aurally; a creak sound usually transitions to a lower ICI before stopping completely, and this slowdown is detectable during most creak-pause situations. Furthermore, no significant difference in creak duration was detected between creak-only (16 ± 7 s) and creak-pause (19 ± 9 s) events. If creak-pause events were actually weak creaks that become masked, then one would expect the duration of the audible portion of the creak to

be shorter during creak-pause situations.

In summary, the interpretation of creak-pause fraction that is most consistent with our analysis is that the fraction is a measure of relative capture success. Our results indicate that depredating whales have many more opportunities to acquire prey, but have to expend as much effort per target as under natural foraging conditions. Both creak rate and creak-pause fraction might provide useful proxies for measuring depredation attempts and depredation capture rates, provided that the proper passive acoustic configurations are used, and the ranges of the instruments from the activity are not too great.

III.5.3 Interpretation of deep vs. shallow depredation

Figures III.5d and III.5e showed that the creak-pause percentage is much lower in the Gulf of Alaska than measured in more temperate locations, as discussed at the end of Section III.5.1. There were also much larger numbers of dives in the Gulf of Alaska that display no creaks at all.

One interpretation of creak-pause events is that they are indicative of a successful prey capture, as opposed to just a prey capture attempt. Figures III.5d and III.5e could thus be interpreted as showing that Alaskan whales generally had lower prey acquisition success rates than whales in the Gulf of Mexico or Ligurian Sea; i.e. the Alaskan whales required more creaks per capture. The fact that Alaskan whales include fish as a natural part of their diet provides one potential explanation for this difference. Figure 5e also suggests that shallow depredation required fewer creaks per prey acquisition, although the change was not statistically significant. When Figure III.5e is compared to the creak rate distributions in Figure III.5d, one gets the impression that during both types of depredation a whale may get many more prey opportunities (as shown by higher creak rates), but with only slightly higher capture rates (as shown by the small change in percentage of creak-pause events).

There are several possible alternative interpretations of what a pause following a creak means, including air recycling (Wahlberg *et al.*, 2002) and a simple inability to detect weak creaks on the tag. As discussed in Section III.3.4 it is unlikely that the low acoustic sampling rate of the tag was missing creak events, because creak events were almost always preceded by an easily-detectable decrease in usual click ICI. The argument that a pause after a creak is primarily due to air recycling seems inconsistent with the observation that creak-pause events in this study were much lower than observed in Miller *et al.* (2004). Furthermore, if air-recycling were the primary reason why pauses after clicks exist, one would expect that shallow depredation dives would yield relatively fewer pauses after creaks; after all, shallow depredation dives are nearly five times shallower on average that a natural dive, and thus the available air volume inside the animal is five times larger. Instead, one finds that the relative creak-pause fraction increases slightly during shallower dives.

A third interpretation for a creak-pause event is simply that the received level of a weak creak becomes too low to be detected, and becomes buried in noise. This interpretation is not consistent with what is heard aurallya creak sound usually transitions to a lower ICI before stopping completely, and this slowdown is detectable during most creak-pause situations. Furthermore, no significant difference in creak duration was detected between creak-only (16 ± 7 s) and creak-pause (19 ± 9 s) events. If creak-pause events were actually weak creaks that become masked, then one would expect the duration of the audible portion of the creak to be shorter during creak-pause situations.

In summary, the interpretation of creak-pause fraction that is most consistent with our analysis is that the fraction is a measure of relative capture success. Our results indicate that depredating whales have many more opportunities to acquire prey, but have to expend as much effort per target as under natural foraging conditions. Both creak rate and creak-pause fraction might provide useful proxies for measuring depredation attempts and depredation capture rates, provided

that the proper passive acoustic configurations are used, and the ranges of the instruments from the activity are not too great.

III.5.4 Interpretation of deep vs. shallow depredation

While the cumulative distributions of most parameters during deep depredation were shown to be statistically different from those derived from natural behavior, the differences between mean and median values are slight, with substantial overlap in standard deviation. In other words, even though the animals clearly associate themselves with hauling fishing vessels, many aspects of their acoustic and dive behavior remain similar to natural behavior. The most prominent exceptions are much shorter ICIs and higher creak rates displayed during deep depredation. What could the animals be doing around the fishing vessels? Our favored interpretation is that numerous black cod are being shaken loose from the longline, or "spun off", during the haul to the surface. A recent study by Sigler *et al.* (2008) used timers triggered to individual longline hooks to discover that up to one-third of the hooks triggered on the ocean floor had no fish when recovered on the surface. Some fish may have struck the bait and not been hooked, or may have escaped when hooked on the bottom, but hooks can also tear from the relatively soft mouths of the cod as they are being hauled to the surface. Underwater video of sperm whales approaching longlines shows one case of a whale approaching the line after a fish had spun loose (Mathias *et al.*, 2009).

These spun-off fish would make easy targets for sperm whales, which naturally consume such prey, and thus could feed in a natural manner. As the fish are free-swimming, the foraging success rate (as represented by the creak-pause percentage in Figures III.5e and III.7e would remain similar to natural levels, but whales have more opportunities to target fish in the mid-water column, thus explaining the generally higher creak rates per dive (Figures III.5d and III.7d). If most fish happen to spin off relatively close to the ocean floor, then the whales

would still have to dive deep to reap the rewards, explaining why the maximum dive depths are relatively unchanged. The low ICI suggests the animals are using their sonar to monitor something at close range. For example, ICI rates have been associated with the two-way travel time of sound to the ocean floor (Thode, 2002) or to a feeding patch midway in the water column (Zimmer, 2003). Making the same assumption, our best guess for the existence of a median ICI of 0.5 s for deep depredating whales is that they are monitoring a target 300-400 m away, such as the longline and/or hauling vessel, perhaps to coordinate their dive location at depth. Additional data is therefore needed to determine exactly what sperm whales are doing during this so-called "deep depredation" behavior.

While deep depredation seems superficially very similar to natural behavior, shallow depredation differs from natural behavior in almost every parameter measured. Short, shallow dives with high creak rates indicate that the animal is not waiting long for feeding opportunities, so spun-off fish are unlikely to be the sole source of opportunity for this behavior. An underwater video showing a whale biting a longline at shallow depths suggests that sperm whales attack the line directly under a shallow depredation state. This video also demonstrated that the animals still actively creak while biting the longline, even under good visual conditions (Mathias *et al.*, 2009).

Another interesting aspect of the shallow depredation state is that the animals behavior does not quite revert to normal once the haul is completed. For example, the whale tagged on 17 July 2007, shown in detail in Figure III.3, shows the most extreme deviations from natural behavior during vessel hauls, but also displays intriguing behavior long after the haul is completed. After depredating the whale returned to dive depths down of about 400 m, similar to natural foraging depths in this region. However, the acoustic record from the tag reveals that the whale had little to no acoustic activity: the whale produced almost no creaks, and occasionally even no usual clicks; periods of complete silence of up to several minutes at depth were common. This behavior lasted for at least six hours (until

the tag released) and suggests that the whale didn't forage for a long period of time after depredating for several hours. The animal may be transiting to a new location; however, it is unclear why the whale continues to dive to such deep depths. No orcas or other predators were observed by the tagging RHIB during daylight hours. In general, Figure 7d indicates that animal tag records associated with shallow depredation also tend to be associated with lower levels of acoustic activity during the "natural foraging" sections in the rest of the record. One possible implication is that animals need to forage less after a profitable round of shallow depredation.

Why do two distinct types of depredation behavior exist? Two possible explanations include conspecific competition, and individual preference, neither of which can be rejected based on the current available data. Up to seven sperm whales have been documented depredating a single line simultaneously, and one might argue that the more whales present, the more "aggressive" the depredation behavior might become as animals compete over the haul, driving them to forage deeper along the longline. The tag records may also simply be revealing that each individual has a unique approach to depredation, arising from different levels of motivation, experience or preference. The fact that no individual displays both deep- and shallow-depredation behavior lends weight to this latter interpretation.

We speculate that animals displaying deep depredation could be either transient migrating animals, or other animals with little experience with longlining vessels. They would be unwilling to approach the line directly, but are attracted to the fish spun-off from the line, which can be consumed using foraging techniques they naturally use. Over time, as an individual becomes more experienced, it would monitor the line more closely, capturing more spin-off opportunities, thus increasing its creak rate while still maintaining most of its natural foraging movements. If most fish spin off near the bottom, the animal will still need to maintain a deep dive profile. The shallow depredation stage would then correspond with experienced (perhaps local) animals that would risk biting the line directly, per-

mitting shallower dives and thus less effort. Therefore, the observed depredation states could reflect different stages in the evolution of depredating behavior among animals, with spin-off fish providing a convenient "entry-level" opportunity. If this speculation is correct, photo-ID records of whales displaying shallow depredation should match animals that have been observed depredating multiple times, while photo-ID records from deep-depredating animals should have a shorter, more recent depredating history.

III.5.5 Insight into potential depredation countermeasures

Sperm whales display at least two different types of behavior when depredating, and this factor must be considered when developing countermeasures, since one does not want to reduce one type of depredation, only to increase the incidence of another type. Therefore a combination of countermeasures might be necessary to target both shallow and deep depredation.

The results of this study have several practical implications when considering ways depredation could be reduced. First, both shallow and deep depredation behaviors are characterized by increased acoustic activity by the animal, a result that suggests that passive acoustic monitoring could remotely identify depredation behavior. Measuring creak rates could indicate the number of depredation attempts per unit time occurring in the vicinity of the longline, provided that the acoustic monitoring gear is not too distant from the hauling site. Our detection range estimate for sperm whale creaks, based on empirical measurements, suggests creak detection ranges between 3.3 and 10 km, depending on sea state and animal orientation. Measuring the fraction of creaks that are associated with pauses may also provide a measure of depredation *success* per unit time, although this interpretation remains speculative. These observations are important because current methods of flagging depredation rates (visual evidence of depredation on fishes) underestimate true depredation activity levels. Thus, the identification of accurate

acoustic metrics for depredation attempts/success may provide a crucial step in evaluating depredation countermeasures over reasonable time scales.

The second implication is that if spin-off fish provide a convenient entry for whales to learn depredation, then one of the simplest long-term ways to discourage depredation would be to discover gear modifications that reduce the odds of accidentally spinning off a fish, once it is caught.

The acoustic results presented here can also help predict the distances whales are willing to swim to depredate vessels, which then provides a third implication: that the manner in which a vessel sets gear may be more important than anything the vessel does when hauling gear. We arrive at this conclusion by first assuming that the number of creaks detected per unit time is closely related to the number of prey consumed per unit time. This assumption can be checked by using estimates of average male sperm whale lengths in the North Pacific Ocean (Oshumi and Masak, 1977; Kasuya *et al.*, 1991), empirical relationships between length and weight (Omura, 1950; Lockyer, 1976) and estimates of energetic needs (Sergeant, 1969; Kleiber, 1975; Clarke, 1980; Lockyer, 1981). We estimate that male sperm whales in this study would require 132 ± 70 fish a day for sustenance. Naturally foraging whales produce an average of three to eight creaks per hour in this area, or 50 to 144 creaks per day. The creak rates measured are thus consistent with the estimated energetic intake rates of sperm whales. The uncertainties in the estimates are too large to permit us to determine whether creak-pause events only are related to caloric intake.

If the measured creak rates truly translate into foraging intakes, then the results presented here indicate that shallow depredating whales can attain three to four times greater calorie intakes per unit time than during natural conditions. A three-hour fishing haul would thus provide the equivalent of nine to 12 hours of natural foraging effort by a whale. Figure III.3 may provide some support for this idea (see Section III.4.3): after being very active for six hours next to a fishing vessel hauling two longlines, the tagged whale has reduced acoustic activity for at

least six hours. These tagging results imply that whales should be willing to swim up to six hours, or up to 30 nautical miles, toward a location where gear is being set. However, once a haul begins, it would only make energetic sense for a whale to swim up to two hours in order to depredate for one hour. Thus, fishing vessels have a large incentive to explore techniques for reducing their acoustic signature when setting gear, and for departing an area once gear is set. Reducing the acoustic signature when hauling will not be as effective in reducing the encounter rate. Furthermore, if vessels can deploy some sort of decoy that can delay the response of a whale to a true haul by even an hour, the incentive to depredate would be substantially reduced.

III.6 Conclusion

Over two field seasons 11 bioacoustic tags have been deployed on seven distinct whales, permitting observations of the animals' dive profiles and acoustic behavior during natural and depredation foraging conditions.

No single depredation strategy has been observed; instead, two behavioral states that deviate from natural conditions can be identified: deep and shallow depredation. Deep depredating whales display behavior relatively similar to natural foraging dives, but they produce higher creak rates and significantly lower inter-click intervals, and begin clicking sooner after starting a dive. Shallow depredation differs from natural foraging behavior in almost every way: irregular dive and surface durations, many dive inflections, and intense acoustic activity (even at the surface). Creak rates three to four times (even seven times) greater than natural foraging rates have been observed during shallow depredation behaviors, along with slightly higher percentages of creak-pause events. Additional experiments are needed to help determine whether differences in depredation behavior arise from conspecific competition and/or individual preference based on experience.

The identification of a useful "measuring stick" for depredation success is

a crucial problem in identifying ways of reducing depredation. This study suggests that passive acoustic monitoring could remotely detect prey capture attempts, provided that an appropriate configuration of acoustic hydrophones is deployed sufficiently close to the depredation activity. Preliminary measurements made from several autonomous hydrophones deployed around commercial hauling activities found that creaks could be detected at 3.3 km range under sea state 2 conditions, with an SNR sufficient to permit possible detection out to 10 km range in similar conditions.

Potential depredation countermeasures suggested by this study include modifying gear to reduce spin-off fish rates, reducing noise generated when setting gear, not loitering around deployed gear, and setting decoy buoys to delay the response of whales to hauling activity by around one hour.

III.7 Acknowledgments

The authors thank Bill Burgess of Greeneridge Sciences and Joe Olson of Cetacean Research Technologies for providing the tags, flotation and attachment systems. Erin Oleson of the Scripps Whale Acoustic Lab gave us useful advice on tag deployments on sperm whales. We also thank Jen Cedarleaf, Melania Guerra and Lauren Wild for their help during data collection. Visual identifications of sperm whales was possible thanks to Jen Cedarleaf and Lauren Wild of the University of Alaska, SE whale research lab. Jay Barlow provided advice on statistical analysis, and Bill Hodgkiss provided advice on the manuscript. The authors thank Torry O'Connel for comments to improve the discussion on depredation strategies. This work was supported by the North Pacific Research Board, a National Geographic Exploration grant, and the Joint Industry Project of the Oil and Gas Producers Association.

III.8 Appendix 1: Body orientation analysis

III.8.1 Equipment

The spatial orientation of sperm whales were investigated using both high-resolution digital acoustic sampling tags "B-probe" (Greeneridge Sciences, Burgess et at. 1998) and a Data Storage Tag (DST) comp-tilt (Star-Oddi). The characteristics of the "B-probe" are described in Section III.3.1. The DST comp-tilt tag, with dimensions of 46 by 15 mm, measures temperature, depth, and compass heading with respect to magnetic north, as well as local acceleration along three orthogonal axes. While the sampling rate of these data can be adjusted, in this paper the tag data were digitally recorded once every 10 s. The DST tag data were used mostly to check the data quality of the B-probe data. The DST tag was small compared with the B-probe assembly, and so was simply taped onto the syntactic float, which had sufficient buoyancy to lift the entire assembly to the surface when detached from the whale. Once on the surface, the tag assembly could be detected and located using the radio beacon.

III.8.2 Angular definitions

III.8.2.a Acceleration vector

Figure III.8 displays the reference frames discussed here. The "whale reference frame" is defined such that the positive x-axis points toward the rostrum of the animal, while the positive z-axis is aligned with the local gravitational acceleration. The "tag reference frame" defines the axes relative to the inertial frame of the instruments.

Both the B-probe and DST tag provide measurements of gravitational acceleration along at least two orthogonal axes, and so an acceleration vector a can be defined with components (a'_x,a'_y,a'_z), expressed in units of gals (1 gal =9.8 m/s^2) in the tag reference frame. Each raw measurement $a_{i,raw}$ obtained from the

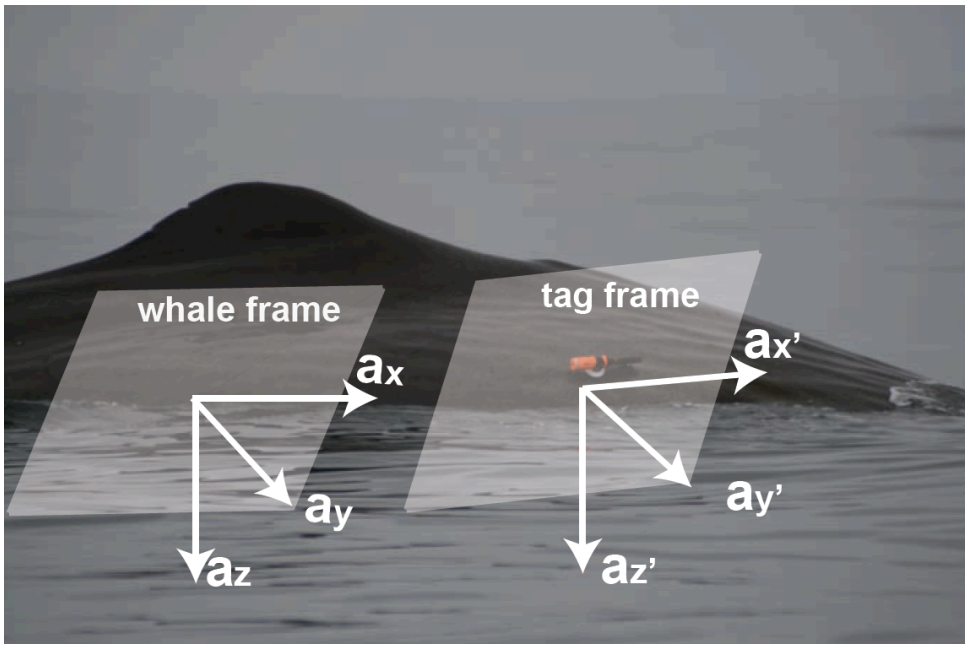

Figure III.8: Picture of B-probe tag with associated reference axes (primed), along with whale reference axes (unprimed)

tag was normalized into gals by measuring the full-scale maximum value $a^*_{i,raw}$ output from a tag along each axis, after correcting for bias, and then computing $a'_i = a_{i,raw}/|a^*_{i,raw}|$.

The DST tag measures all three components of a every 10 seconds, while the B-probe only measures two components, but sampled every second. However, if one assumes that the magnitude of a is dominated by the static gravitational acceleration, and not by accelerations from the animal's motion or wave action slapping on the tag at the surface, then the three components are not independent, and the third component of a on the B-probe can be derived from the other two. To test the robustness of this assumption, Figure III.9 displays the distribution of $|a|$ from all DST records collected in 2009, covering 229 hours of data. Two distributions are displayed: those derived from time spent at the surface, and those derived from all other times. Both distributions show that 95% of the samples yield $|a|$ within 2.5% of 1 gal, consistent with a previous detailed analysis of the dynamics

of tagged sperm whales, which found that the animals' acceleration was generally less than 0.01 m/s^2 (Miller *et al.*, 2004b). Thus the assumption that $|a| \sim |1|$ gal is generally valid, and the third vector component of a on the B-probe can be safely estimated, allowing higher-resolution time measurements of the animals' motion.

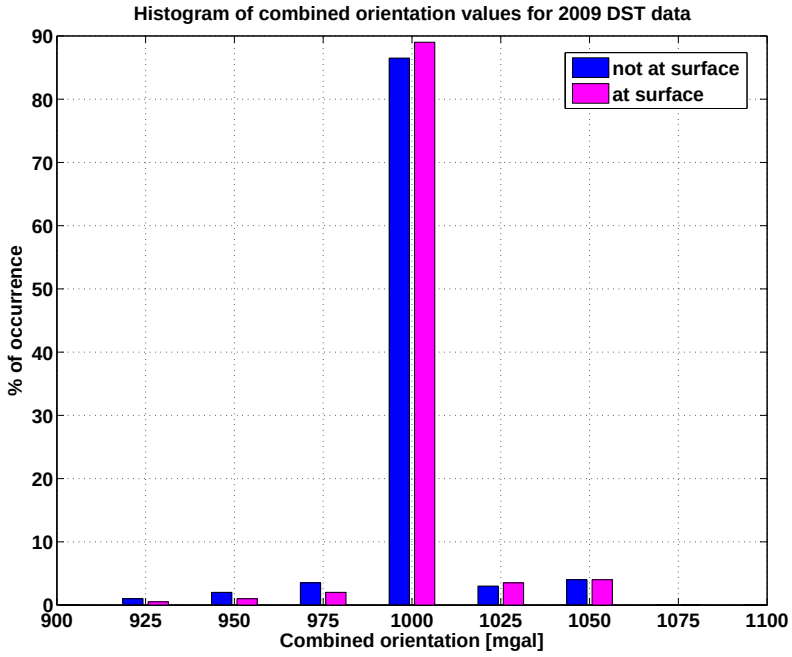

Figure III.9: Distribution of accelerometer magnitude $|a|$ for all (10) DST tag records deployed in 2009, covering 229 hours of data. Magenta: times when whale is surfacing; blue: all times below 10 m depth.

III.8.2.b Coordinate transformations

During most deployments the major axes of the tag assembly are slightly misaligned with the whale's reference frame. Thus the coordinates of the acceleration measured in the tag frame (a'_x,a'_y,a'_z) must be transformed into the whale-centered coordinate system (a_x,a_y,a_z) displayed in Figure III.8.

Using the angular definitions and matrix notation of Johnson *et al.* (2003)

if the pitch, roll, and heading of the tag with respect to the whale frame are θ_t, ψ_t, and ϕ_t, then the relationship between a and a' is as follows:

$$\mathbf{a} = (\mathbf{H^T P^T R^T})\mathbf{a'} \tag{III.1}$$

where

$$\mathbf{H^T} = \begin{pmatrix} \cos(\phi_t) & -\sin(\phi_t) & 0 \\ \sin(\phi_t) & \cos(\phi_t) & 0 \\ 0 & 0 & 1 \end{pmatrix}$$

$$\mathbf{P^T} = \begin{pmatrix} \cos(\theta_t) & 0 & -\sin(\theta_t) \\ 0 & 1 & 0 \\ \sin(\theta_t) & 0 & \cos(\theta_t) \end{pmatrix}$$

$$\mathbf{R^T} = \begin{pmatrix} 1 & 0 & 0 \\ 0 & \cos(\psi_t) & -\sin(\psi_t) \\ 0 & \sin(\psi_t) & \cos(\psi_t) \end{pmatrix}$$

Estimates for all three correction angles were made during times when a tagged animal was surfacing to breathe, as per previous tagging studies (Johnson *et al.*, 2003, Miller *et al.*, 2004a). From Figure III.9 the magnitude of a specific accelerometer measurement a'_0 taken at these times is 1 gal, and assuming that the z-axis of the whale frame is aligned with the gravitational acceleration, Equation (III.1) becomes

$$\begin{pmatrix} 0 \\ 0 \\ 1 \end{pmatrix} = (\mathbf{H^T P^T R^T})\mathbf{a'_0} = (\mathbf{P^T R^T})\mathbf{a'_0} \tag{III.2}$$

The second equality arises from the definition for $\mathbf{H^T}$, which indicates that the x and y-elements of a'_0 must be zero after the first two rotations for the equation to be solved. Stated another way, data from the accelerometer alone

are insufficient to determine the heading of the tag relative to the whale. Solving Equation (III.2) yields

$$\theta_t = \arcsin(a'_{x,0}) \tag{III.3}$$

$$\psi_t = \arctan(\frac{a'_{y,0}}{a'_{z,0}}) \tag{III.4}$$

Finally, photographs of a tagged animal while surfacing were used to estimate ϕ_t. Specifically, a yaw angle was estimated, γ_t, that would rotate the a'_x axis into the a_x axis aligned with the whale. Substituting $a' = [\mathbf{1\ 0\ 0}]^{\mathbf{T}}$ into Equation (III.1) and using the relationship $\hat{a_x} \bullet \hat{a'_x} = \cos(\gamma_t)$ one obtains:

$$\cos(\phi_t) = \frac{\cos(\gamma_t)}{\cos(\theta_t)} \tag{III.5}$$

In general, a large majority of tag deployments were nearly parallel with the tagged whale's longitudinal axis, and Equation III.5 was used infrequently.

III.8.2.c Pitch and roll

If only acceleration data are available to estimate the sperm whale's orientation, and not heading information, a yaw motion of the animal cannot be distinguished from a roll, and so only the animal's pitch (θ) and roll (ψ) can be derived from a:

$$\theta(t) = \arcsin(a_x(t)) \tag{III.6}$$

$$\psi(t) = \arctan(\frac{a_y(t)}{a_z(t)}) \tag{III.7}$$

Alternatively one can use the formula used in Goldboggen *et al.* (2006), which links the roll directly to a_x and a_y without requiring estimation of a_z :

$$\psi(t) = [\frac{1}{1 - (\frac{a_x(t)}{a_x^*})}] \quad [cos(asin(\frac{a_x(t)}{a_x^*}))]^2 \quad [asin(\frac{a_y(t)}{a_y^*})] \tag{III.8}$$

Figure III.10 shows a comparison between data from a DST tag, using Equations (III.6) and (III.7), and data from a B-probe deployed simultaneously, using Equations (III.6), (III.7) and (III.8). The results indicate that Eq(III.8) is generally valid, but tends to underestimate roll values.

III.8.2.d Angular displacement and angular velocity definitions

In this paper a "combined angular displacement" η_{all} is defined as the angular change in the direction of the acceleration vector over a fixed time interval δt. Thus if the acceleration at two distinct times is $[a_x(t), a_y(t), a_z(t)]$ and $[a_x(t+\delta t), a_y(t+\delta t), a_z(t+\delta t)]$ then η_{all} is defined by :

$$\cos(\eta_{all}(t)) = \frac{a_x(t)a_x(t+\delta t) + a_y(t)a_y(t+\delta t) + a_z(t)a_z(t+\delta t)}{|a(t)||a(t+\delta t)|} \tag{III.9}$$

A "combined angular velocity" Ω_{all} is defined as a combined angular displacement per second :

$$\Omega_{all}(t) = \frac{\eta_{all}}{\delta t} \tag{III.10}$$

Two additional angular displacements and velocities can be defined in terms of pitch and roll :

$$\eta_{pitch}(t) = |\theta(t+\delta t) - \theta(t)| \quad ; \quad \Omega_{pitch}(t) = \frac{\eta_{pitch}}{\delta t} \tag{III.11}$$

$$\eta_{roll}(t) = |\psi(t+\delta t) - \psi(t)| \quad ; \quad \Omega_{roll}(t) = \frac{\eta_{roll}}{\delta t} \tag{III.12}$$

The three angular displacements are not independent; any one can be derived from the other two. The combined velocity is a useful quantity to estimate in that its values are independent of a particular coordinate reference frame. In

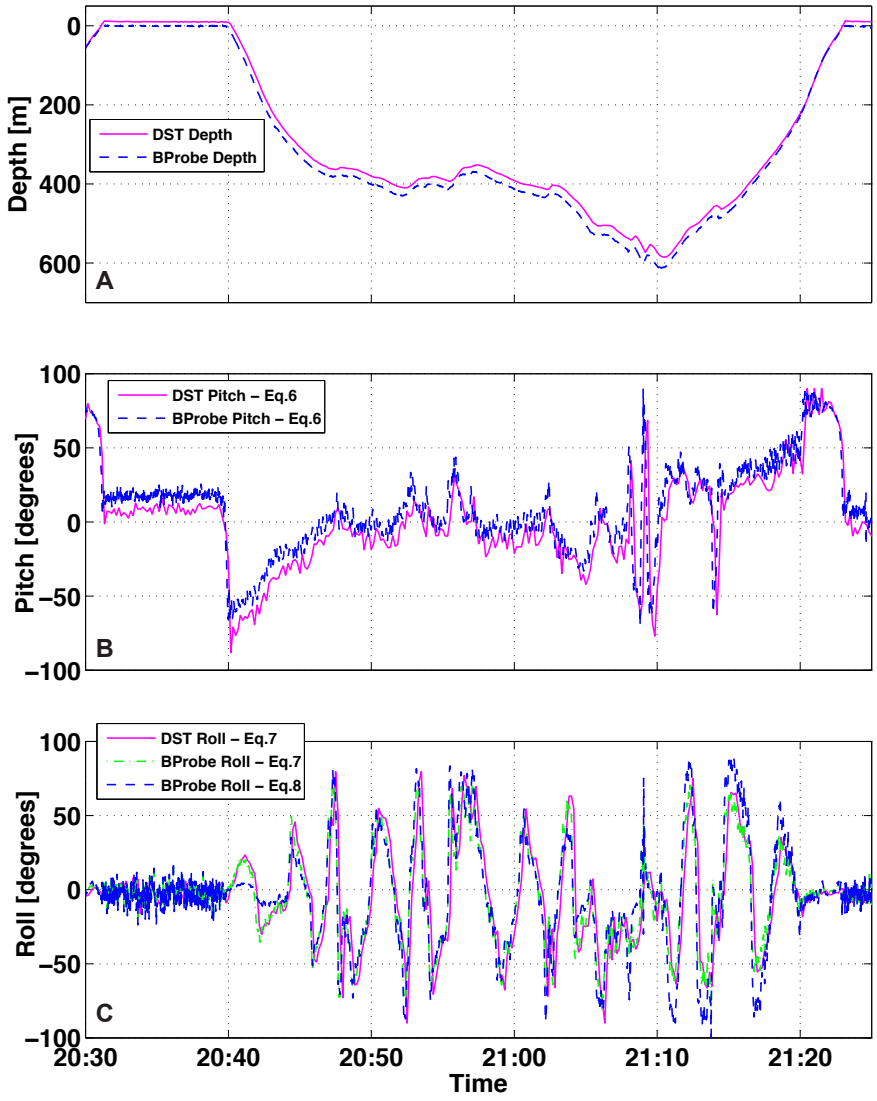

Figure III.10: Comparison of pitch and roll measurements between DST (solid magenta lines) and B-probe (dotted blue lines and dashed-dotted green line) when both tags were deployed simultaneously on 21 June 2009 : (a) dive profile; (b) pitch; (c) roll. For the B-probe data, the pitch was computed using Equation (III.6); the roll was computed using both Equation (III.7) and Equation (III.8).

the following analyses angular displacements are estimated over 3 s increments, shifting the measurement window by 1 s for subsequent estimates. The angular displacements and thus the angular velocities will always be non-zero because the tag readings fluctuate randomly around the presumed steady-state value. Low-pass filtering the time series to reduce fluctuations was not practical, because the timescale of interest for an animal's rotation was on the order of ten seconds or less.

III.8.3 Analyzing relationships between angular velocities, dive inflections, and creak events

The relationships between a given animal's depth profile, acoustic behavior, and angular velocity were examined by creating "velocity plots" that display the details of the animal's motion during certain key times (e.g. Figure III.11). Possible key times include times during which the animal generates creaks, or times when the animal produces a dive inflection. A review of all tag records found that 81% of creak events occurred within 30 s of a dive inflection. The remaining 19% of creaks, not associated with dive inflections, occur during descent and ascent, with 90% of them being *creak-only* events. However, no precise relationship was found between the timing of the whale's angular motions and the start of creak within a 30 s time window. By contrast, consistent relationships were always found between angular rotations and dive inflections. It is hardly surprising that a relationship exists between pitch velocity and dive inflections–after all, a change in pitch is needed to generate changes in depth–but consistent relationships between roll and inflection were found as well. Thus in the following sections the velocity plots will be generated with respect to dive inflection times.

To generate a velocity plot, each tag record is first decomposed into a sequence of dives, with the beginning and end of each dive defined according to the criteria of Section III.3.3. Then, for each dive, the angular velocities of pitch, roll,

and combined angle [Equations (III.10) through (III.12)] are computed starting 30 s before the start of every dive inflection, and recomputed every second, using a sliding 3 s window, until 30 s after the inflection, generating an "angular velocity time series" (AVTS). The complete set of AVTS curves from the tag record are then grouped according to behavioral state, as well as whatever type of creak event was detected within a given velocity time series window. For every group the mean and standard deviation of the velocities at every second are then computed. By plotting the mean values as a line and the bounds of the standard deviations as vertical bars, a final velocity plot is created, summarizing the angular motion of the animal over multiple types of creak events.

Dive inflections not associated with creak events are used to generate "control plots" during subsequent discussion, under the assumption that these angular motions are unrelated to prey capture events. Because the number of dive inflections not associated with any creak events is generally much larger than the number of dive inflections associated with creaks, the control plots are generated using a random subsample of dive inflections not associated with creaks, such that the sample size used is the same as the one used for dive inflections associated with creaks. A "deviation" is defined as the difference between a control plot and any other velocity plot.

For every velocity plot the following parameters are extracted:

a) time of maximum roll deviation (T_{dev}): relative time of the maximum deviation in roll velocity in seconds;

b) maximum pitch deviation (P_{dev}): value of the maximum pitch velocity deviation in °/s;

c) maximum roll deviation (R_{dev}): value of the maximum roll velocity deviation in °/s;

d) maximum combined deviation (C_{dev}): value of the maximum combined velocity deviation in °/s.

III.8.4 Hypothesis testing

A two-sided Kolmogorov-Smirnov (KS) test (Section III.3.5) was used to evaluate the probability that two orientation parameter distributions, obtained from different behavioral categories, could have been drawn from the same cumulative probability distribution. The null hypothesis is that various parameters measured from both behavioral categories were drawn from the same underlying distribution. KS p-values less than 0.05 led to rejection of the null hypothesis.

III.8.5 Results

III.8.5.a Summary of tag records and behavioral categories

Acoustic tags were deployed on sperm whales during two field seasons: July 2007 and June 2009. In 2007 a total of 8 B-probes recorded successfully, producing a total of 79 hours of animal depth, orientation, and acoustic data. No DST tags were deployed that year. In 2009 a total of 3 B-probe/DST assemblies were deployed, generating 67 hours of animal depth, orientation, and acoustic data. Thus, over the course of two field seasons, seven distinct animals were successfully tagged 11 times with functioning B-probes, and all were identified using photo-identification. Two individuals were tagged twice in 2007, and one individual was tagged in both 2007 and 2009. The mean, median, and mode of the tag deployment times in 2007 were 9.8, 7.0, and 19.0 hours; the corresponding numbers for 2009 were 22.3, 27.0, and 12.0 hours. Additional DST tag dive data are available, but are not used in this analysis.

The behavioral categories are defined in Section III.3.5.

A given tag record could contain several different behavioral states, and in the next subsection the orientation analysis three such tag records are reviewed in detail, collectively illustrating the four behavioral states shown by the 11 sperm whale tag records. Section III.8.5.e summarizes the statistical differences in the angular velocity profiles between the behavioral categories, excluding sleep.

The other tag records are also described in detail in Appendix 3.

III.8.5.b 20 July 2007 : Natural foraging behavior

Figure III.11 displays the tag record velocity plots for the pitch, roll, and combined angular velocities during natural foraging conditions (after 18:00), computed according to the procedures outlined in Section III.8.3. Each subplot displays three velocity plots; the solid and solid-dotted lines indicate periods associated with *creak-only* and *creak-pause* events only, while the dashed lines are "control plots," with associated dive inflections not associated with creaks. The control plots are relatively constant over time, and show the "noise floor" of the tag accelerometer.

Deviations between the control curve values and velocity plots associated with creaks are visible for all angles in Figure III.11, starting between 10 to 15 s before the dive inflections. The maximum deviations occur 5 s before the dive inflections, and the deviations generally disappear by 10 s after the dive inflections. The maximum pitch and roll deviations during *creak-only* events (2.6 °/s and 5.6 °/s) are more substantial than the deviations during *creak-pause* events (1.1 °/s and 3.0 °). For this tag record, all deviations are smaller for *creak-pause* events than for *creak-only* events. The bulk statistics in Table III.5 statistics show that this tag record is unusual; typically the *creak-pause* events are associated with greater roll velocities.

The relative timing between the start of both types of creak events and dive inflections (as defined in Section III.8.3) are shown in Figure III.12. The distribution of relative times is quite broad, but most creak events occur before the dive inflection (mode -10 to -15 s), corresponding well to the times of the maximum angular velocity rates and deviations.

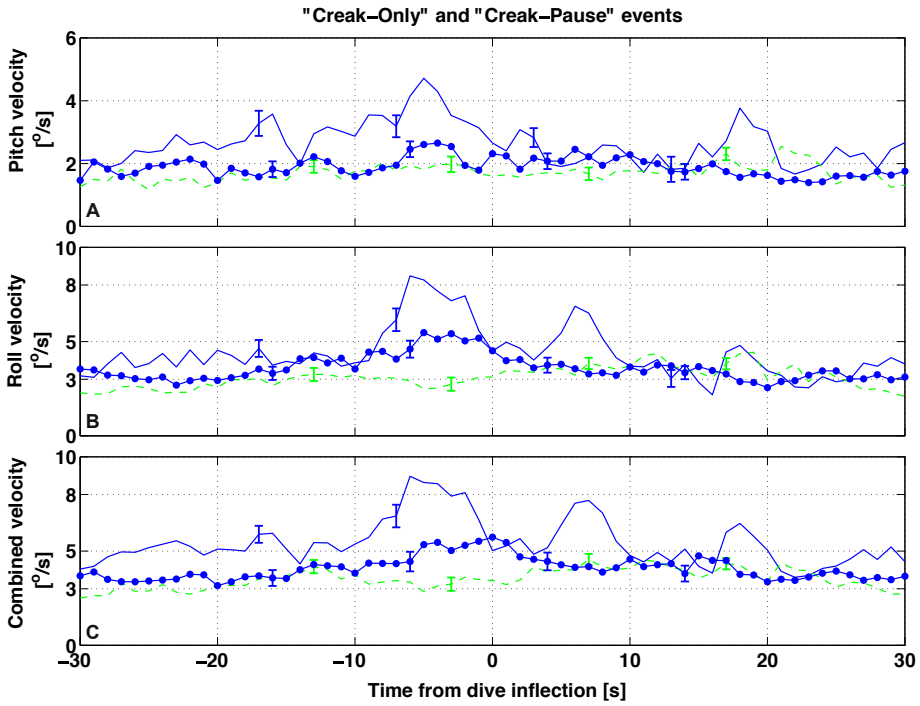

Figure III.11: Angular velocity plots of 20 July 2007 tag data, during natural foraging behavior. The values are computed by computing the angular change over a 3 s sliding window, as described in Section III.8.3. Lines and vertical bars show the mean and standard deviation of each angular velocity time series. Solid blue: *creak-only* events; solid-dotted blue: *creak-pause* events. Dashed green: control periods (defined in Section III.8.3). (a) pitch velocity Ω_{pitch} ; b) roll Ω_{roll} velocity; c) combined velocity Ω_{all}.

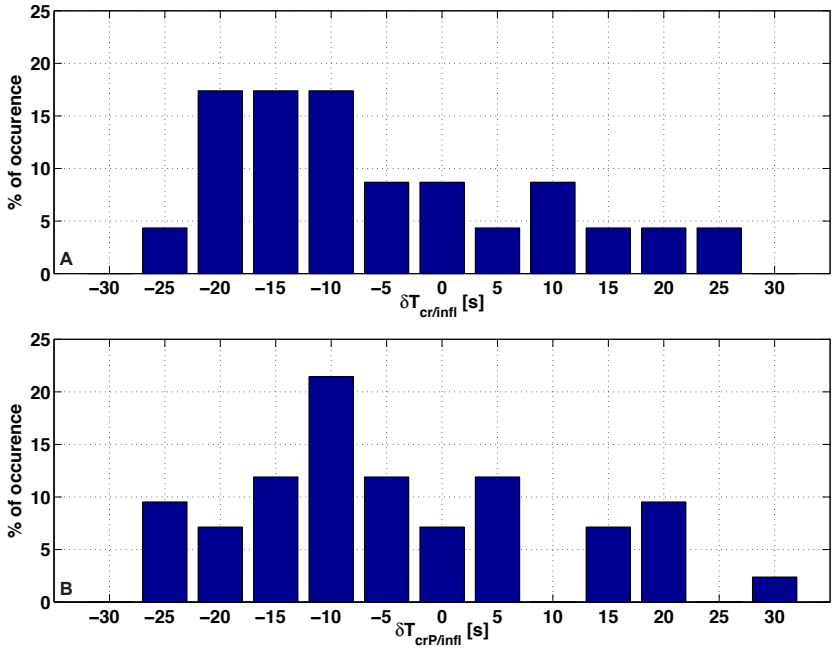

Figure III.12: Relative timing between dive inflections and creak events, during natural foraging behavior on 20 July 2007 tag data. (a) *creak-only* events $\delta T_{cr/infl}$; (b) *creak-pause* events $\delta T_{crP/infl}$.

III.8.5.c 12 June 2009 : Resting, natural foraging, and deep depredation behaviors

Figure III.13 displays the tag record velocity plots associated with *creak-only* events, separated by behavioral state. Plots show angular velocities associated with *natural foraging behavior* and *deep depredation* states during both hauls, along with control periods. Deviations from the control curve are visible for all angles and for all behavioral states, with the maximum deviations occurring between 5 s and 10 s before the dive inflection.

The maximum pitch deviation is similar between natural foraging behavior and deep depredation during the first haul (8.5 $^{\circ}s/$) but smaller during the second haul (3.3 $^{\circ}/s$). The maximum roll deviation is consistently larger during natural foraging behavior (12.9 $^{\circ}/s$) than during the vessel hauls (8.6 $^{\circ}/s$ and 7.0 $^{\circ}/s$). The combined velocity is also larger during natural foraging behavior than during both vessel hauls.

Figure III.14 is similar to Figure III.13, except that dive inflections associated with *creak-pause* events are shown. As before, deviations from the control curve are visible for all angles and behavioral states. The maximum pitch deviation is similar between natural foraging behavior (9.0 $^{\circ}/s$), and deep depredation during both hauls (8.1 $^{\circ}/s$ and 7.0 $^{\circ}/s$), and displays similar timing (5.9 s before the dive inflection). The maximum roll deviation is greater for natural foraging behavior (9.8 $^{\circ}/s$) than for deep depredation during second haul (6.7 $^{\circ}/s$). The roll deviation is very variable for deep depredation during the first haul, so that no clear maximum roll deviation can be identified.

During natural foraging behavior, *creak-only* events are associated with higher angular velocities than *creak-pause* events, a result similar to Section III.8.5.b. During the second fishing haul, the *creak-pause* angular velocities are much greater than the *creak-only* velocities. More whales were surfacing close to the fishing boat during the second haul.

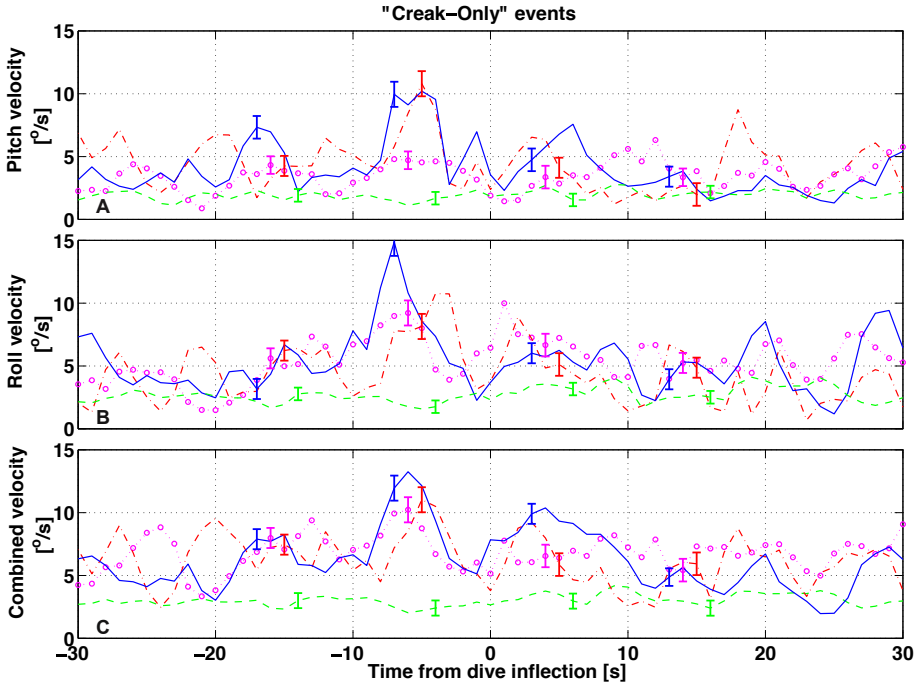

Figure III.13: Angular velocity plots of 12 June 2009 tag data during natural foraging behavior and deep-depredation, for *creak-only* events, computed in a manner identical to Figure III.11. The lines and associated vertical bars show the mean and standard deviation of the ensembled angular velocity time series. Solid blue: natural foraging behavior; dashed-dotted red: first fishing haul; solid-dotted magneta: second fishing haul; dashed green: control periods (defined in Section III.8.3) not associated with creak sounds.

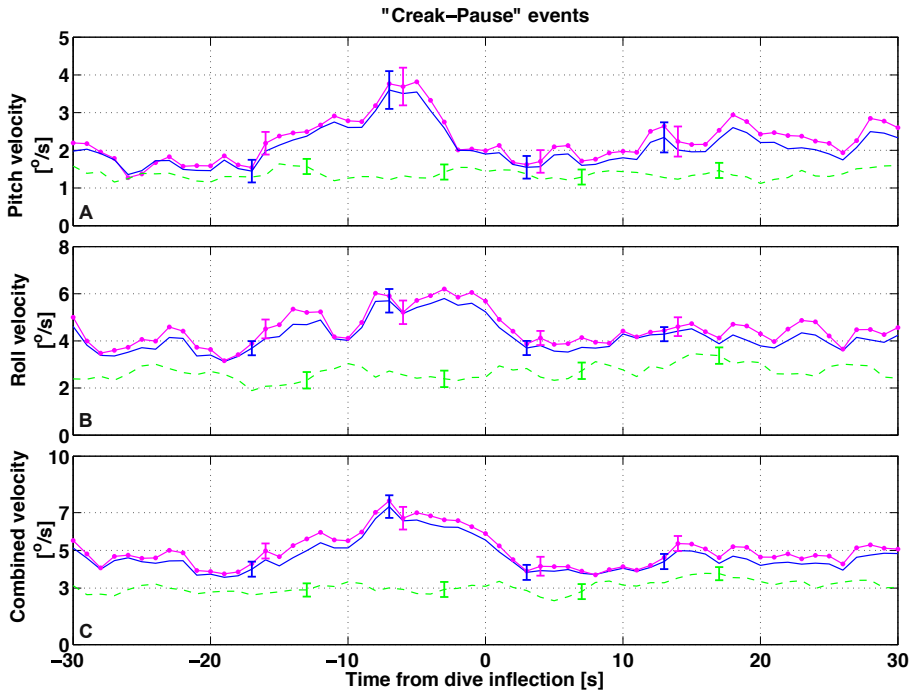

Figure III.14: Same as Figure III.13, but the lines show mean and standard deviations of angular velocity time series associated with *creak-pause* events.

The relative timing between the start (as defined in Section III.8.3) of both types of creak events and dive inflections are shown in Figure III.15, with all categories grouped together. The distribution of relative times is quite broad, but most creak events occur before the dive inflection (mode -5 to -10 s), corresponding well to the maximum deviation times visible in the velocity plots. The distributions are similar to the natural foraging relationships shown in Figure III.12.

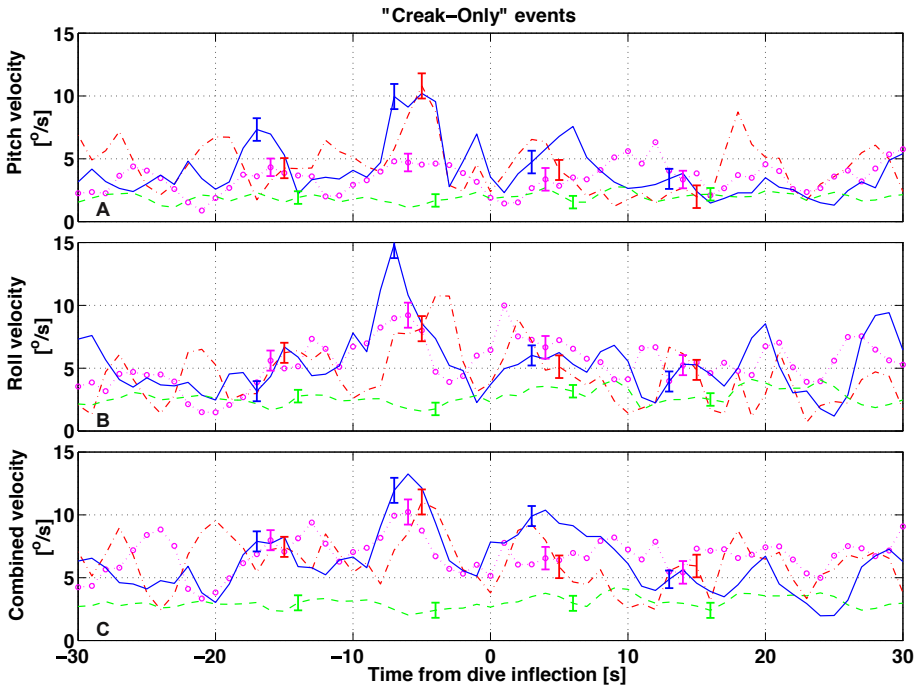

Figure III.15: Relative timing between dive inflections and creak events in 12 June 2009 tag data. (a) *creak-only* events $\delta T_{cr/infl}$; (b) *creak-pause* events $\delta T_{crP/infl}$.

III.8.5.d 17 July 2007 : Natural foraging behavior and shallow depredation

Figures III.16 and III.17 display the tag record velocity plots for the pitch, roll, and combined angular velocities for the two behavioral states, with the former figure displaying *creak-only* inflections, and the latter *creak-pause* inflections. Deviations from the control curve values are visible for all angles and both behaviors for both creak types, at times beginning 15 to 20 s before the dive inflections, with maximum deviations attained between 0 and 10 s before the dive inflections. However, the velocity plots associated with natural foraging behavior are more variable for *creak-only* events.

For *creak-only* events (Figure III.16), the maximum pitch and roll deviations are larger for shallow depredation(2.7 $^\circ/s$ for both angles) than for natural foraging behavior (1.4 $^\circ/s$ and 2.4 $^\circ/s$). By contrast, for *creak-pause* events (Figure III.17), the angular velocities are strikingly similar for both behavioral states at all angles. The maximum pitch deviation (2.8 $^\circ/s$) occurs 7 s before the dive inflection and the maximum roll deviation (3.8 $^\circ/s$) occurs 8 s before the dive inflection.

The relative timing between the start (as defined in Section III.8.3) of both types of creak events and dive inflections are shown in Figure III.18. The distribution of relative times is quite broad, but most creak events occur 10 to 15 s before the dive inflection, corresponding well to the maximum deviation times observed for all angles.

III.8.5.e Comparison of behavioral states across all tag records

Table III.5 summarizes angular velocity statistics compiled from all 11 tag records. Each row corresponds to a behavioral category defined in Section III.3.5. Kolmogorov-Smirnov(KS) two-sample, non-parametric tests are used to

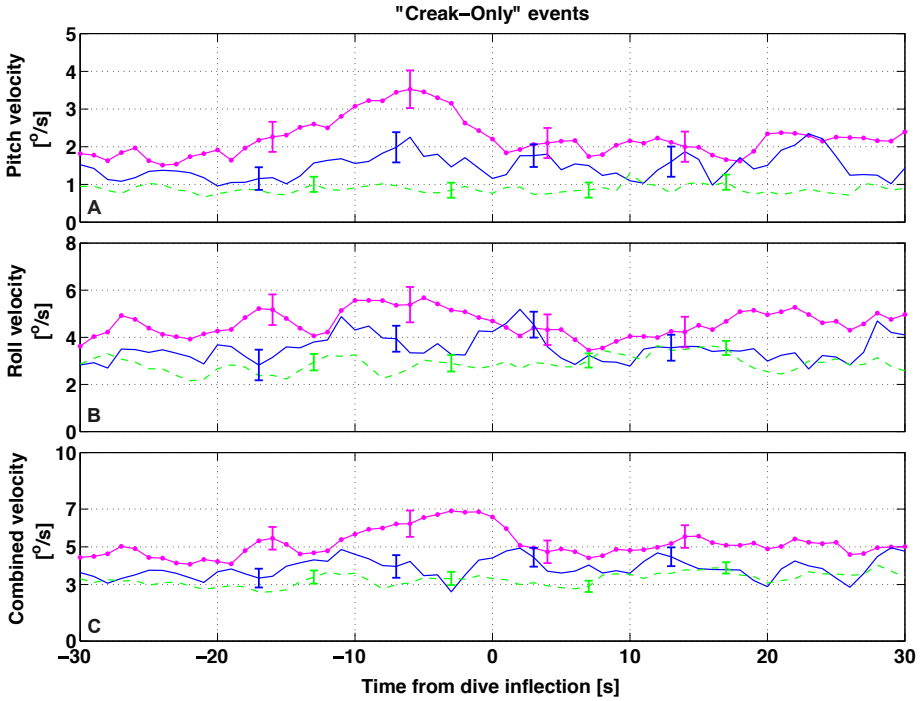

Figure III.16: Angular velocity plots of 17 July 2007 tag data during natural foraging behavior and shallow-depredation, for *creak-only* events, computed in a manner identical to Figure III.11. Solid blue: natural foraging behavior; solid-dotted magneta: shallow-depredation behavior; dashed green: control periods (defined in Section III.8.3) not associated with creak sounds.

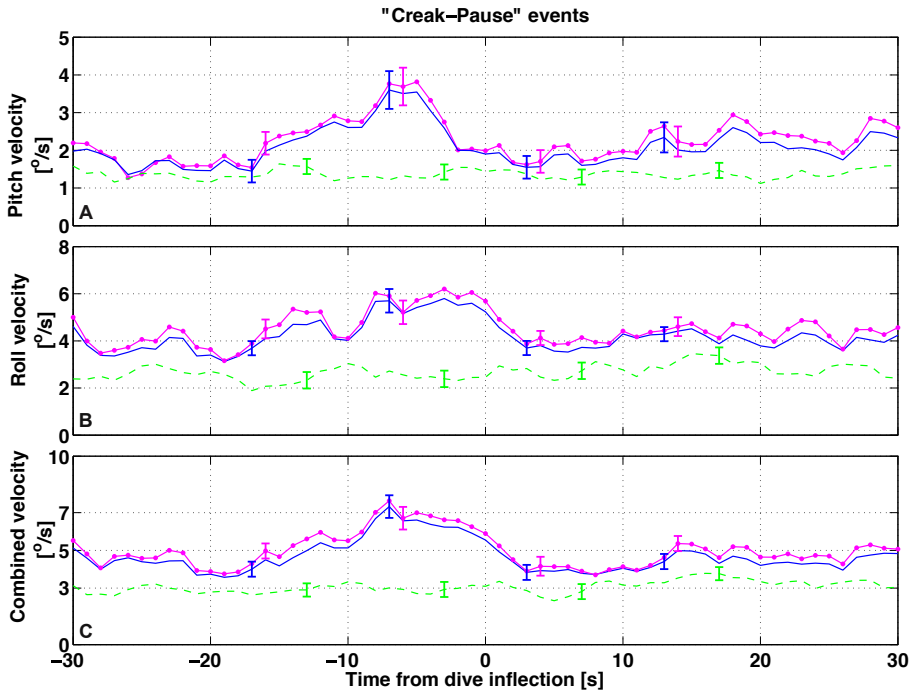

Figure III.17: Same as Figure III.16, but displaying angular velocities associated with *creak-pause* events.Creak Excursion.

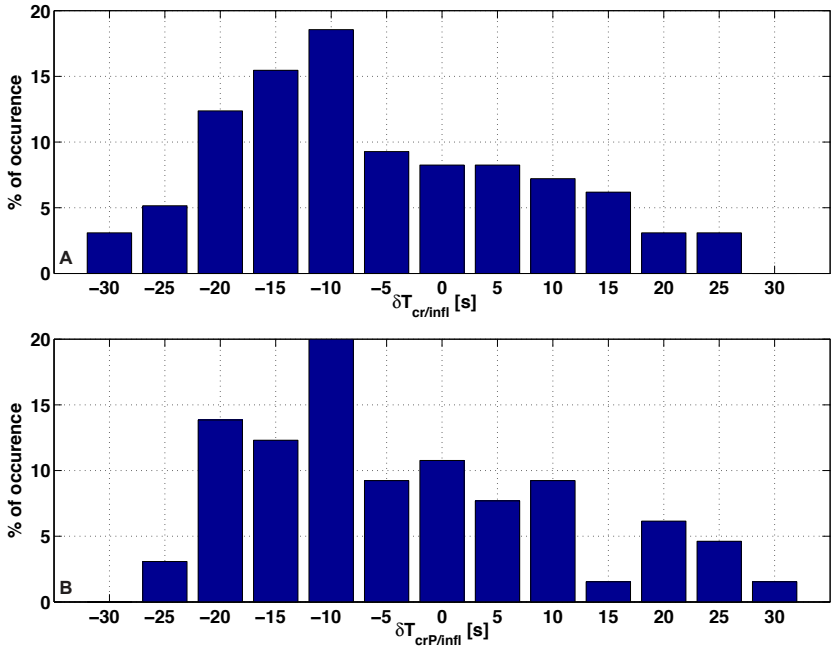

Figure III.18: Relative timing between dive inflections and creak events in 17 July 2007 tag data. (a) *creak-only* events $\delta T_{cr/infl}$; (b) *creak-pause* events $\delta T_{crP/infl}$.

assess whether the cumulative distribution of a given parameter during shallow or deep depredation is significantly different from the same parameter distribution derived for the natural behavioral state. The KS test captures differences in means, medians, and variances in the distributions. The KS two-sample test is also applied to angular velocity parameter distributions associated with the two different creak events, both within and between behavioral states. The corresponding p-values are displayed in the tables, with italicized values indicating test results that attain statistical significance, defined here as p values less than or equal to 0.05.

Table III.5: Angular velocity statistics for 2007 and 2009 data

	$\mathbf{T_{dev}}$ (s)	$\mathbf{P_{dev}}$ ($^o/s$)	R_{dev} ($^o/s$)	C_{Dev} ($^o/s$)
Resting	N/A	N/A	N/A	N/A
Natural foraging	6.3±1.1/6.1±1.2 p=0.06	5.5±0.7/5.3±0.8 p=0.07	5.5±0.5/7.8±0.7 *p=5.4*×10^{-3}	5.6±0.3/7.9±0.7 *p=6.2*×10^{-4}
Deep depredation	5.9±0.9/5.0 ±0.9 *p=0.02* p=0.1/p=0.08	6.1±0.6/6.6±0.4 p=0.06 *p=0.05/p=0.02*	7.5±0.7/8.3±0.5 *p=0.05* *p=2.9*×10^{-3}/p=0.06	7.6±0.4/8.3±0.6 p=0.06 *p=0.04*/p=0.07
Shallow depredation	8.0±1.0/7.2 ±1.3 *p=0.03* *p=5.3*×10^{-5}/*p=2.2*×10^{-3}	5.0±0.4/5.6±0.5 p=0.06 p=0.20/p=0.27	4.7±0.3/7.5±0.5 *p=3.5*×10^{-6} *p=0.01*/p=0.08	4.9±0.2/7.7±0.5 *p=5.0*×10^{-6} *p=0.05*/p=0.11

Values are means ± S.D. for *creak-only* / means ± S.D. for *creak-pause*

Underneath, the single p-value is the probability that the distributions for *creak-only* and *creak-pause* have been from the same distribution. On the third line, a p-value is the probability that the distribution has been drawn from the same distribution as the natural foraging reference distribution. Italic p-values indicate when the null-hypothesis that there is the same underlying distribution has been rejected (p<0.05).

Table III.6 is similar to Table III.5 respectively but the natural foraging dives have been divided in two categories: natural foraging dives associated with a whale performing deep depredation and natural foraging dives associated with a whale performing shallow depredation. The parameters for shallow and deep depredation dives are then compared to the associated natural foraging dives using KS test described above. This is done to verify wether individual behavior is a significant factor in the results.

Table III.6: Angular velocity statistics for 2007 and 2009 data using only tag records that display both natural and depredation behaviors

	$\mathbf{T_{dev}}$ (s)	P_{dev} ($^o/s$)	R_{dev} ($^o/s$)	C_{Dev} ($^o/s$)
Resting	N/A	N/A	N/A	N/A
Nat. for. ass. with deep dep.	6.1±1.0/5.8±1.1 p=0.06	5.4±0.7/5.2±0.7 p=0.07	5.3±0.5/7.5±0.6 *p=3.1*×10^{-3}	5.4±0.3/7.5±0.5 *p=2.8*×10^{-4}
Nat. for. ass. with shallow dep.	6.5±1.1/6.3±1.2 p=0.07	5.7±0.5/5.6±0.6 p=0.08	5.7±0.5/8.0±0.6 *p=6.3*×10^{-3}	5.7±0.3/7.9±0.6 *p=7.5*×10^{-4}
Deep depredation	5.9±0.9/5.0 ±0.9 *p=0.02* p=0.09/p=0.07	6.1±0.6/6.6±0.4 p=0.06 *p=0.05*/*p=0.02*	7.5±0.7/8.3±0.5 *p=0.05* *p=3.6*×10^{-3}/p=0.06	7.6±0.4/8.3±0.6 p=0.06 *p=0.04*/p=0.06
Shallow depredation	8.0±1.0/7.2 ±1.3 *p=0.03* *p=9.1*×10^{-5}/*p=5.8*×10^{-3}	5.0±0.4/5.6±0.5 p=0.06 p=0.12/p=0.19	4.7±0.3/7.5±0.5 *p=3.5*×10^{-6} *p=0.01*/p=0.07	4.9±0.2/7.7±0.5 *p=5.0*×10^{-6} *p=0.04*/p=0.08

Values are means ± S.D. for *creak-only* / means ± S.D. for *creak-pause*

Underneath, the single p-value is the probability that the distributions for *creak-only* and *creak-pause* have been from the same distribution. On the third line, a p-value is the probability that the distribution has been drawn from the same distribution as the natural foraging reference distribution. Italic p-values indicate when the null-hypothesis that there is the same underlying distribution has been rejected ($p<0.05$).

III.8.6 Discussion

III.8.7 Is natural foraging behavior off Sitka similar to elsewhere in the world?

In the Miller *et al.* (2004) study the authors reported that while foraging at depth, 22 sperm whales from the Ligurian Sea and the Gulf of Mexico made 12.5 (± 4.0) dive inflections per hour, and a mean of 32% of all creaks were produced within 10 s of a dive inflection. Their study also reveals a peak of 8.7 (±0.5) $^\circ/s$ in roll velocity centered on the end of creaks. The sperm whales in this study made 15.2 (± 8.2) dive inflections per hour, and consistent relationships were also found between the timing of dive inflections and creak events : 85% of creaks started within 30 s of a dive inflection. This study also found a peak in pitch, roll and combined angle velocities occurring about 6 s before dive inflections associated with a creak event.

An interesting aspect of this study, compared with previous published

literature on sperm whale foraging, is that we divide creak events into two categories, and find there are significant differences between how the animal rolls during these creak events. Table III.5 shows that the animals' roll velocities are significantly different between *creak-pause* and *creak-only* events during natural behavior ($p = 5.4 * 10^{-3}$), and that the mean roll velocities are larger for *creak-pause* events, a relationship that is also visible during the natural behavioral state on 17 July 2007,but not on 20 July 2009 and 2 June 2009. The results of the bulk statistical analysis indicate that roll rates are generally higher when associated with what we interpret to be successful captures. Over 90% of creaks not associated with dive inflections are *creak-only* events, and most occur when the whale is first descending. Finally, the energetics estimation in Appendix 2 suggests that making the assumption that *creak-pause* events are feeding events is not incompatible with sperm whale food requirements.

III.8.8 Depredation vs. natural foraging behavior

Animals in the deep depredation state also display a larger dive inflection rate (p=0.03): 40% of the values are higher than 20 inflections/h. The pitch and roll velocity distributions in this state are significantly different from their corresponding natural distributions for all creak events (expect for *creak-pause* roll rates, which just miss the 5% p-value. The mean values for both angular rates are greater than the natural rates, but the standard deviations are large.

The angular motions of animals in the shallow depredation state also show significant differences from natural behavior, although there are some surprises. The time between the maximum angular deviation and a dive inflection is much greater for shallow depredation than the other two behavioral states, but the mean angular deviations (Table III.5) of shallow-depredating whales are lower than those from the deep-depredating sample, although the roll deviations still show statistically significant differences from natural distributions for *creak-only*

events. An interesting result is that angular deviations associated with *creak-pause* events, or "foraging successes", are not significantly statistically different from angular motion during *creak-pause* events under natural foraging conditions, even when significant differences exist between behavioral states for creak-only events. Stated another way, there seem to be many ways to fail in acquiring prey, but successful prey captures share similar angular deviations across all behavioral categories.

III.9 Appendix 2: Comparison between theoretical and estimated fish consumption rates

Current methods of depredation estimation involve visual counts of bitten or partial fish remains hauled to the surface, a procedure that is known to undercount the activity (Thode *et al.*, 2008), as a videorecording exists, showing a whale removing a fish completely off a longline (Mathias *et al.*, 2009). One goal of the SEASWAP project is to determine whether passive acoustics can refine estimates of depredation rates by counting the number of creaks made by an animal during a dive. There are several obstacles that need to be addressed for acoustics to become a viable "measuring stick" for depredation, such as ensuring reliable detections of creak sounds if one is made by an animal, which is a function of the receiver range and depth, background noise conditions, and perhaps whale orientation. Another obstacle, addressed here, is whether *creak-pause* events alone indicate prey capture, or whether *creak-only* events can indicate capture success as well. The tag data analyzed here presumably detected every creak type made by a tagged animal, which permits a rough calculation as to whether the various creak rates generated by sperm whales align with rough expectations of the caloric requirements of the animals. These calculations may also provide some insight into the energy budget of the animal while depredating vs. foraging naturally.

The analysis begins by estimating the body mass of a whale, using the formula developped by Lockyer (1976) that uses Omura (1950) whaling data for mature male sperm whales:

$$W = (6.648 \times 10^{-3}) * L^{3.18} \quad \text{(III.13)}$$

where W is the weight in metric tons and L is the length of the whale in meters. Given an average size of 15 m of a male sperm whale in the Gulf of Alaska (Oshumi *et al.*, 1977; Kasuya *et al.*, 1991), Equation III.13 leads to an average weight of 36 metric tons.

Dietary requirements for large whales are usually expressed as a percentage of the animal weight per day, ranging from 2.0 to 3.5% for sperm whales (Sergeant *et al.*, 1969; Kleiber *et al.*, 1975, Clarke *et al.*, 1980; Lockyer *et al.*, 1981). Several factors contribute to this wide range (Santos *et al.*, 2001). It is believed that smaller individuals have higher energy requirements per unit body weight than larger ones. All prey categories do not have the same calorific content. A sperm whale feeding on high calorie preys such as sablefish would need to consume a smaller amount of food than if feeding on cephalopods which are lower in calorific content (Lockyer *et al.*, 1991). Thus, between 720 kg and 1260 kg of prey are needed to completely supply the dietary requirements of a mature sperm whale in the GOA. According to catch data in the GOA, an average commercially-caught black cod measures about 70 cm and weighs about 5 to 10 kg. Thus, if feeding exclusively on black cod, a sperm whale would need to eat between 70 and 250 fish a day to fulfill its metabolic requirement. If sperm whale lengths are assumed to vary by 10%, and propagating uncertainties in all the numbers, the daily requirement of a sperm whale is 132 ± 70 fish a day.

During the natural foraging state, the tag data indicate that sperm whales were actively foraging around 75% of the time, excluding surface intervals and resting periods, a result similar to worldwide estimates (Whitehead *et al.*, 2003). Though there was variability across dives and individuals, the average creak rate

per dive was 7.9 ± 4.6 creaks/h, of which around half were *creak-pause* events. (Miller's rate was 12 creaks/h for an animal feeding on squid, higher than the rates derived here, which would be expected if an animal has to consume more squid mass to satisfy same feeding requirement). Thus, the number of *creak-pause* events produced daily by a whale displaying natural foraging behavior can be estimated at around 70 ± 40 creaks per day, if every creak is associated with foraging success. Thus the creak rates measured are not inconsistent with the estimated energetic intake rates of sperm whales, but the spread of both estimates is such that almost any value of the *creak-pause* fraction can be chosen. These energy calculations will be used in the next section to estimate the energetic advantages whales gain from depredation.

III.10 Appendix 3: Dive profile tag records

III.10.1 2007 B-probe data

The figures in this section display the whale's dive profile, along with the dive inflection rates, click rates, mean ICI, and creak rates (both with and without subsequent silent intervals). The beginning of a fishing haul is indicated by a solid red line while the end of the fishing haul is indicated by a dotted green line.

In 2007, 1 whale was tagged on 17 July, 2 whales were tagged on 18 July and 5 whales were tagged on 20 July. Three individuals were tagged twice.

The general situation (fishing vessel presence, number of whales in the area) for each day is described below. If available, the identification number of the tagged whale in the Gulf of Alaska (GOA) catalog is indicated.

III.10.1.a 17 July 2007 - GOA 08

This tag record was discussed in detail in Section III.4.3 as it is our most dramatic example of shallow depredation.

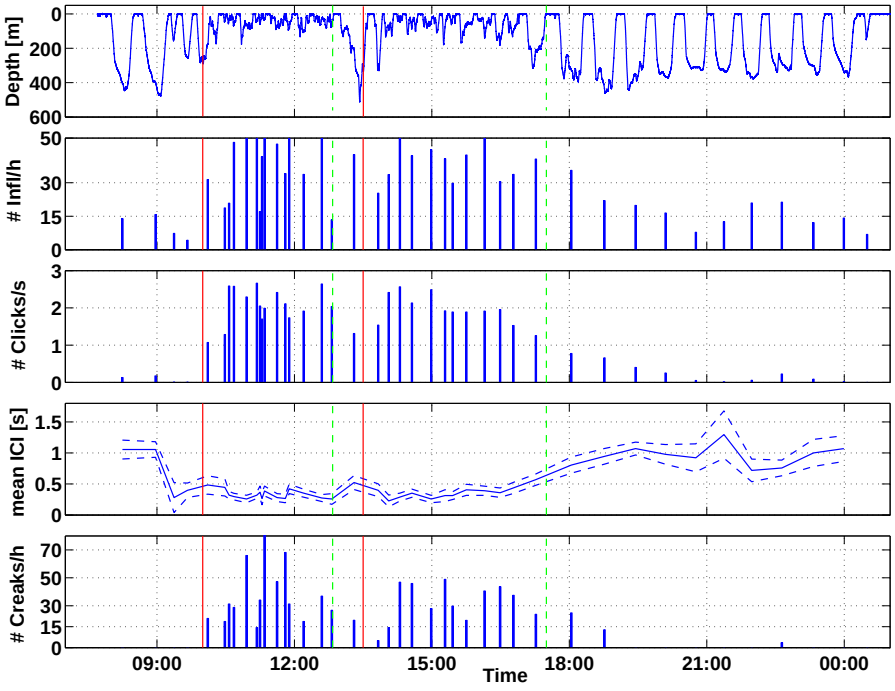

Figure III.19: 17 July 2007 - GOA 08

III.10.1.b 18 July 2007 - GOA 97

On 18 July 2007, the first whale was tagged at 12:00, close to the F/V Ocean Prowler, which was deploying a longline sets at 800 m water depth. The vessel began hauling its first longline set at 13:00, ending at 18:00. A total of four whales surfaced within 500 m of the Ocean Prowler during the haul (two of them were tagged). The tag fell off at 16:00, midway through the haul but visual observations indicate that the tagged whale was surfacing between 100 m and 600 m during the whole duration of the fishing haul.

The whale deepened gradually its dives. Between 12:00 and 13:00, just before the start of the haul, the whale spent most of his time shallower than 250 m depth and did some very large dive inflections. After the haul started, the whale deepened its dive and its last three dives were deeper than 550 m. Except for the last few dives, the dive inflection and creak rates were high.

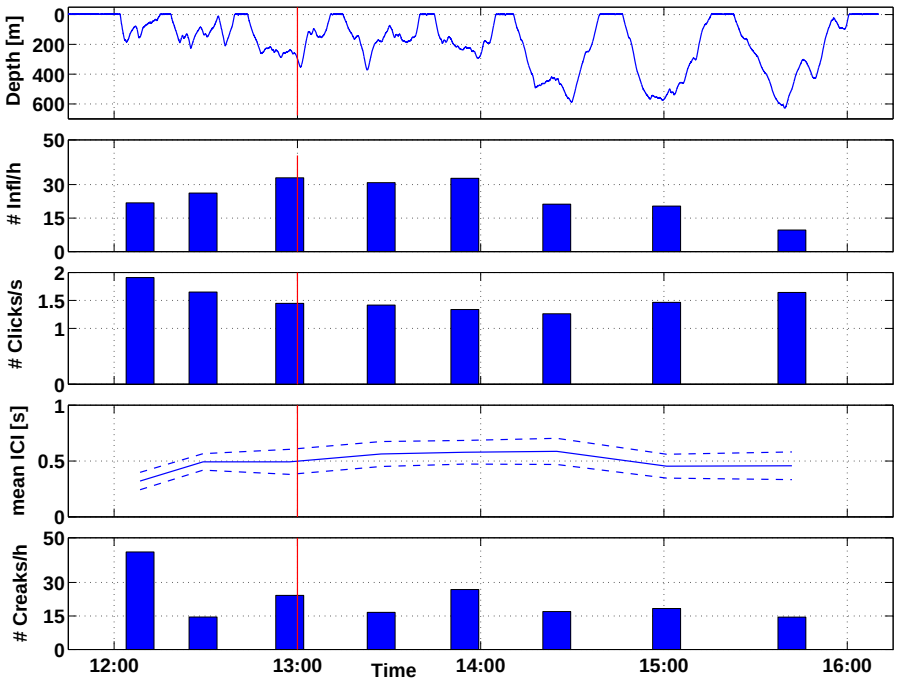

Figure III.20: 18 July 2007 - GOA 97

III.10.1.c July 18th 2007 - GOA 33

On 18 July 2007, a second whale was tagged at 13:00, close to the F/V Ocean Prowler, which had deployed a longline set at 800 m water depth. The vessel began hauling its longline set at 13:00 and ended at 18:00. A total of four whales surfaced within 500 m of the F/V Ocean Prowler during the haul, with the tagged whale surfacing between 100 m and 700 m away until 5pm. He swam away afterwards. and at 5:30pm, the whale was already 1nmi away and the tag fell off at 18:15, just after the end of the haul.

The whale performed two short and shallow ($<$ 200 m) dives just after the start of the haul and then did four deep and long dives ($>$ 400 m). During those deeper dives, the whale seemed to "work its way up the line". The dive inflection rate was higher than the reported "normal" rate. Also, the whale had an high acoustic activity with as much as 60 creaks/h and a low ICI (0.5 s). The bottom depth was 800m indicating that at that point the whale was diving all the way down to the bottom. His last dive, corresponding to the time he left the fishing area, was shallower with smaller dive inflection and creak rates.

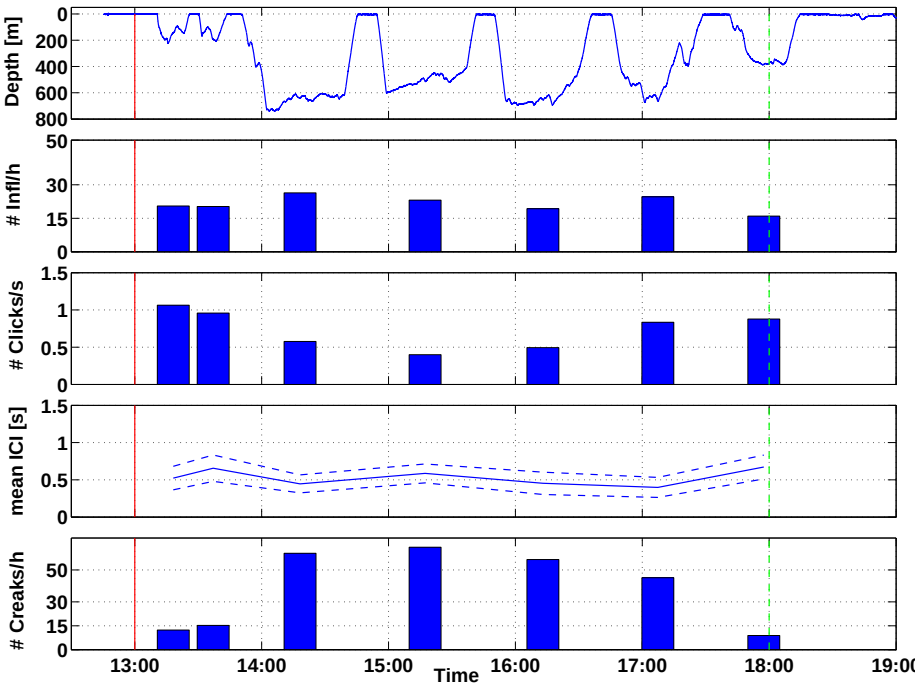

Figure III.21: 18 July 2007 - GOA 33

III.10.1.d 20 July 2007 - GOA 26

On 20 July 2007, the first whale was tagged at 11:15, close to the F/V Cobra which started hauling his longline at 12:00. Five whales total were surfacing close to the Cobra at that point but the tagged whale moved away at 13:00pm and the tag fell off at 13:45.

Only four dives were recorded by the tag. Except for the first dive, all the dives were about 40 min long. The average dive depth was 400 m and the dive inflection, click and creak rates fall within the "normal" range. The ICI is relatively stable (between 0.6 s and 0.9 s).

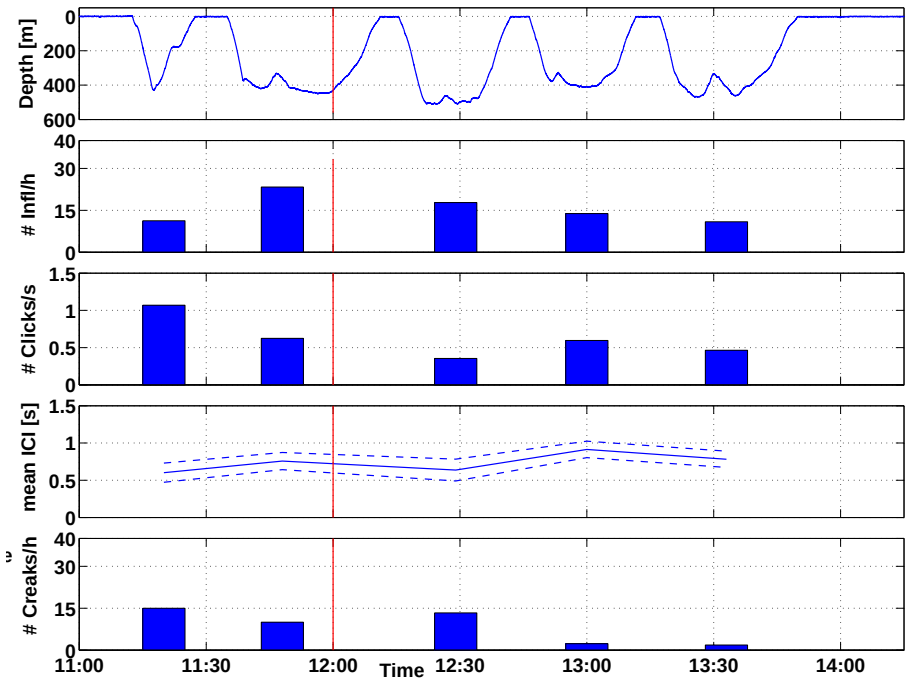

Figure III.22: 20 July 2007 - GOA 26

III.10.1.e 20 July 2007 - GOA 97

On 20 July 2007, a second whale was tagged at 11:50, close to the F/V Cobra which started hauling his longline at 12:00. Five whales total were surfacing close to the Cobra (< 500 m) but the tagged whale moved away at 12:30pm and was 2.5km away at 1pm. The tag fell off at 13:45.

Only four dives were recorded by the tag. The first dive corresponds to the start of the haul. The whale dove down to 375 m and did some very large dive inflections on the way up. The second dive was really short and shallow (a few minutes at 30 m depth). As the whale left the area, it performed two dives that were longer (40 min) and deeper (450 m).

Except for the second dive (very short and shallow), the dive inflection, click and creak rates fall within the "normal" range and the ICI is relatively stable (between 0.6 s and 0.7 s).

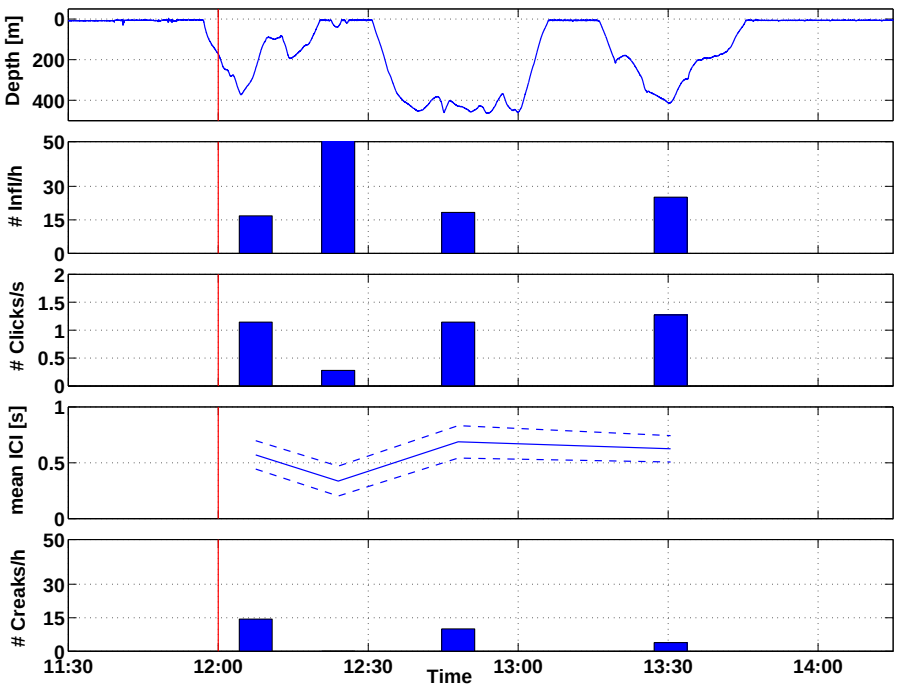

Figure III.23: 20 July 2007 - GOA 97

III.10.1.f 20 July 2007 - GOA 47

On 20 July 2007, a third whale was tagged at 12:40, close to the F/V Cobra, which started hauling a longline set deployed at 600 m depth at 12:00. The haul ended at 18:00 and a total of 5 whales were surfacing close to the Cobra (<500m) at the start of the haul but only three were present between 15:00 and 18:00. The tagged whale surfaced 400 m to 500 m away during the whole record. The tag came off at 19:30, just after the end of the haul.

During the whole duration of the tagged record, the whale performed regular dives, spending 40 min a depth and resting 10 min at the surface. The whale was diving down to an average depth of 500 m but three of his dives were down to the bottom at 600 m

The dive inflection, click and creak rates fall are slightly higher than the "normal" values during the haul. After the end of the haul, the dive inflection and creak rates are really small and the ICI is higher, suggesting that the whale's body and acoustic activity is decreasing.

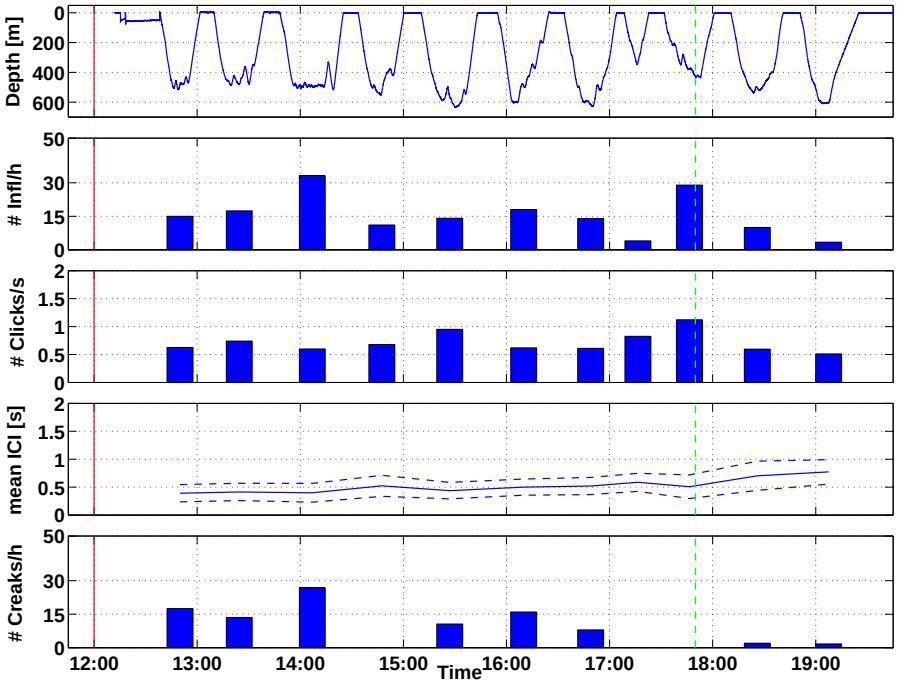

Figure III.24: 20 July 2007 - GOA 47

III.10.1.g 20 July 2007 - GOA 08

On 20 July 2007, a fourth whale was tagged at 15:00, close to the F/V Cobra, which was hauling a longline set deployed at 600 m depth. The haul ended at 18:00 and a total of 3 whales were surfacing close to the Cobra (<500 m) between 15:00 and 18:00. The tag came off at 10:00 on 21 July, just as another longline haul was starting.

During the whole duration of the tag record, the whale performed very regular dives, spending 40 min a depth and resting 10 min at the surface. The whale was diving down to an average depth of 350 m until 05:00 on 21 July and then to 200 m until the start of the haul. The last recorded dive of the whale was deeper (475 m) and corresponded to the start of the haul.

The dive inflection rate and the creak are well correlated throughout the tag record, There is an increase in both rates around 21:00 on 20 July and after 05:00 on 21 July as the whale shallowed its dives before the start of the haul. The click rate and ICI stayed relatively stable throughout the tag record.

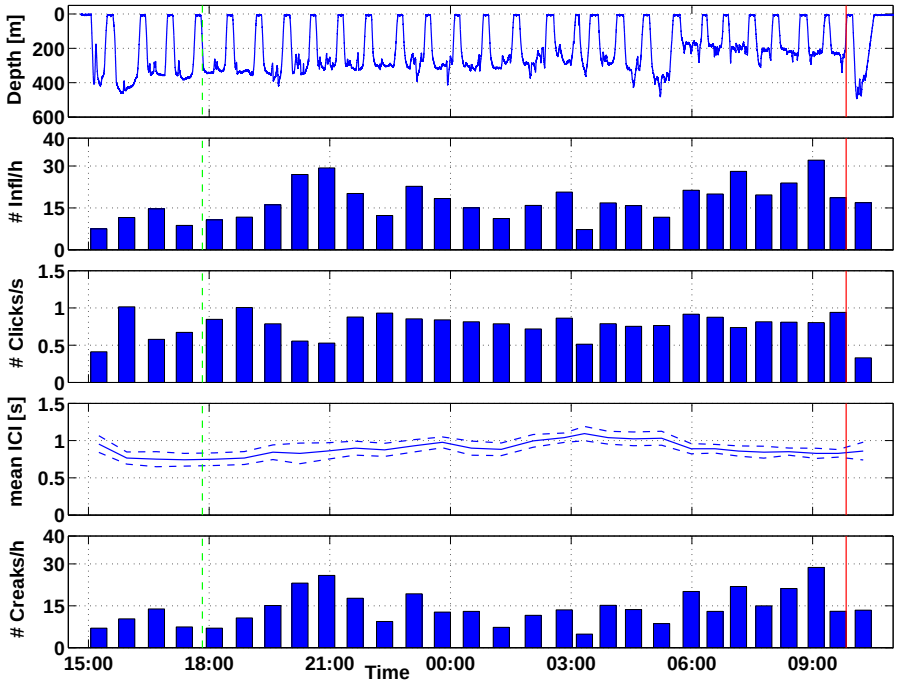

Figure III.25: 20 July 2007 - GOA 08

III.10.1.h 20 July 2007 - GOA 26

On 20 July 2007 a whale was tagged at 15:04, within 300 m of the Cobra during a haul, in the vicinity of two other whales near the vessel. After the haul ended at 18:00, visual observers noted the whale's departure from the vessel, so the animal conducted natural foraging behaviors until the tag released the following morning at 09:50.

A short period of the shallow depredation state is visible at the end of the haul, between 16:00 and 18:00. After the haul's conclusion, the animal typically spends about 40 min at a median depth of 350 m, punctuated by 10 min rests at the surface. The water depth at the whale's location was 800 m at 18:00, so the whale was only diving down to mid-water depth when he left the area.

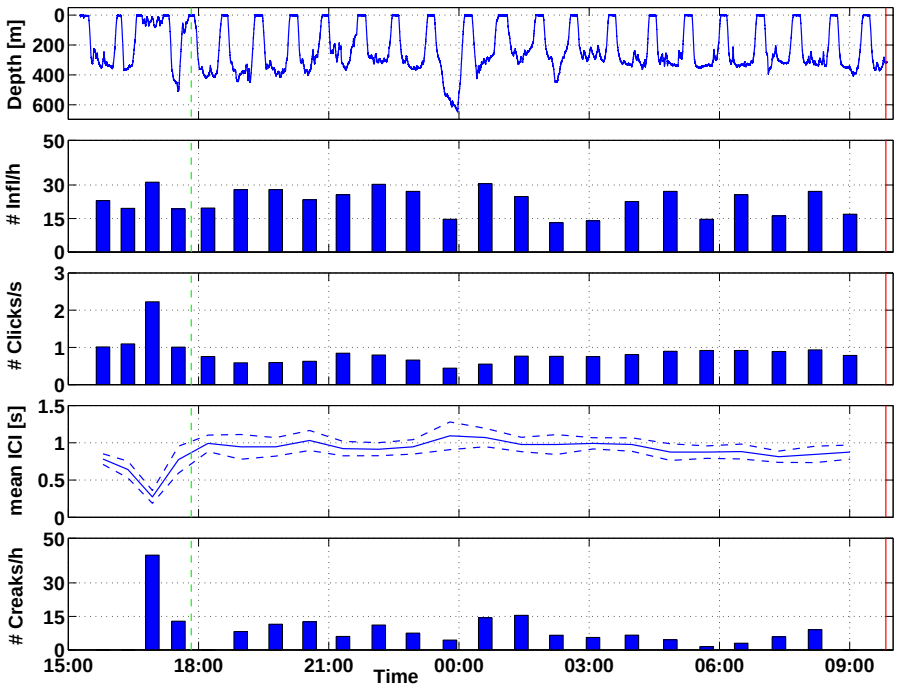

Figure III.26: 20 July 2007 - GOA 26

III.10.2 2009 B-probe data

The figures in this section summarizes the tag records using the same format as before.

Three functioning B-probes were deployed in 2009, on three different days and individuals.

All of the tagging activity happened in close vinicity of the F/V Cobra.

III.10.2.a 12 June 2009 - GOA 47

This tag record was discussed in detail in Section III.4.2 as it is our longest example of deep depredation. Indeed the tag records covers two fishing hauls.

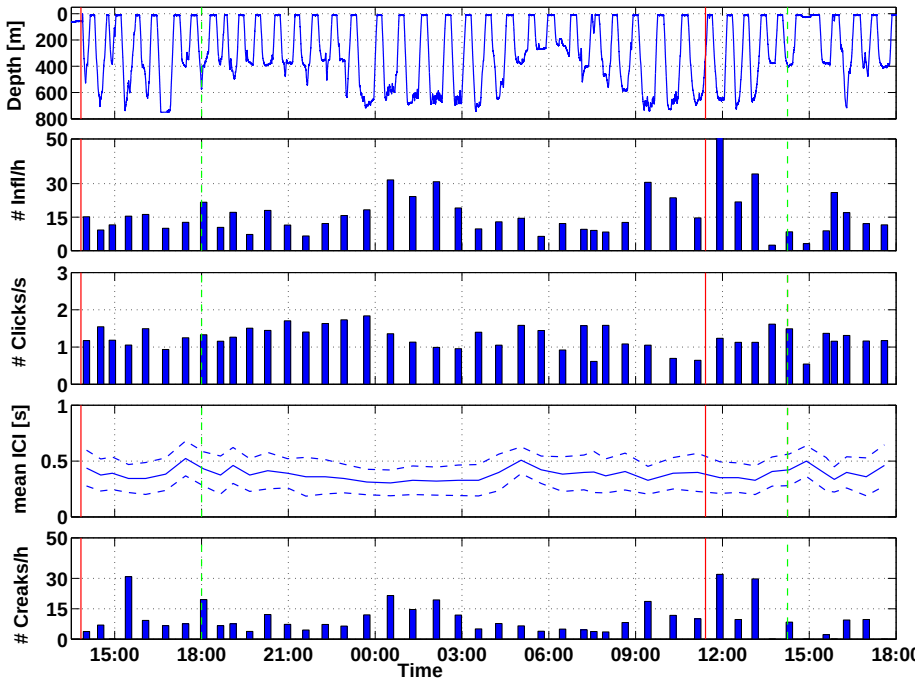

Figure III.27: 12 June 2009 - GOA 47

III.10.2.b 14 June 2009 - GOA 104

On 14 June 2009, a whale was tagged with a B-Probe/DST assembly at 13:30, midway through a fishing haul. The haul ended at 15:00 and the B-Probe stopped recording just after midnight. However the DST recorded until the tag came off on 15 June at 11:00 (cf. Section III.10.3.d). During the haul, the tagged whale and two other whales were surfacing close to the Cobra (<500 m). At 18:30 the whale was still very close to the boat (100 m), even though the haul was done. The dives that occurred during the haul were quite deep (between 450 m and 600 m) and the whale produced many creaks during its first dive. After the haul, most of the dives were down to around 400 m and the dive inflection rate and acoustic activity were normal.

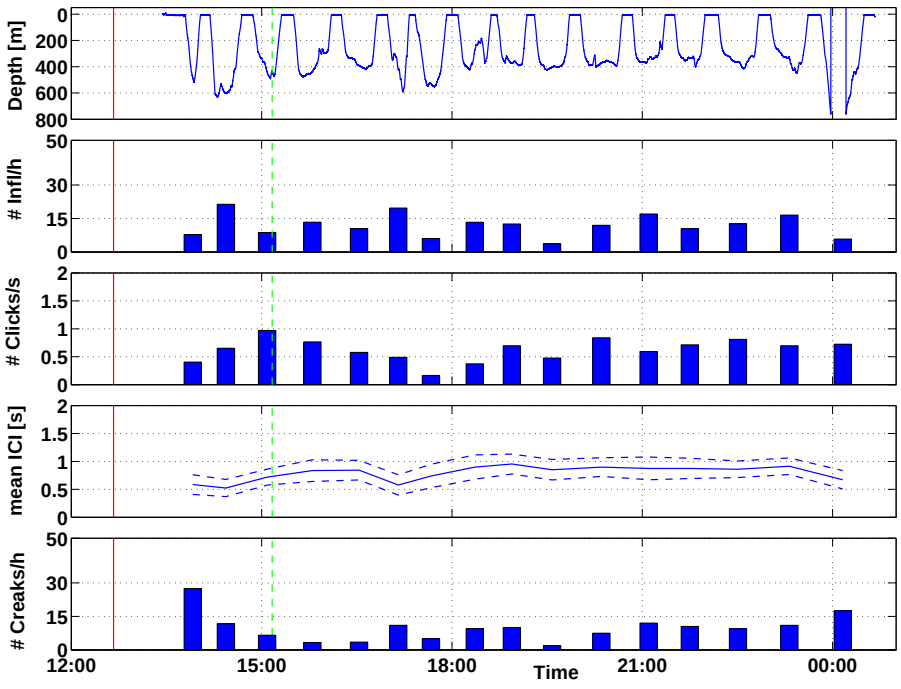

Figure III.28: 14 June 2009 - GOA 104

III.10.2.c 21 June 2009 - GOA 105

On 21 June 2009, a whale was tagged with a B-Probe/DST at 13:00. The Cobra started hauling his longline at 17:00 and ended at 19:30. During the whole duration of the haul, between three and four whales were surfacing close (100 m - 400 m). The tagged whale was more than 500 m away before the start of the haul but moved closer when the haul started and was surfacing very close (100 m - 200 m) during the fishing haul. Before the start of the haul, the whale performed regular deep dives (between 400 m and 700 m) and its dive inflection rate and acoustic activity were normal. When the haul began, the whale started to do some shallow and very irregular dives, associated with high inflection rate and acoustic activity. As soon as the haul ended, the whale went back to performing regular deep dives with normal dive inflection rate and acoustic activity. The whale performed some sleep dives from 07:00 to 09:00 on 21 June.

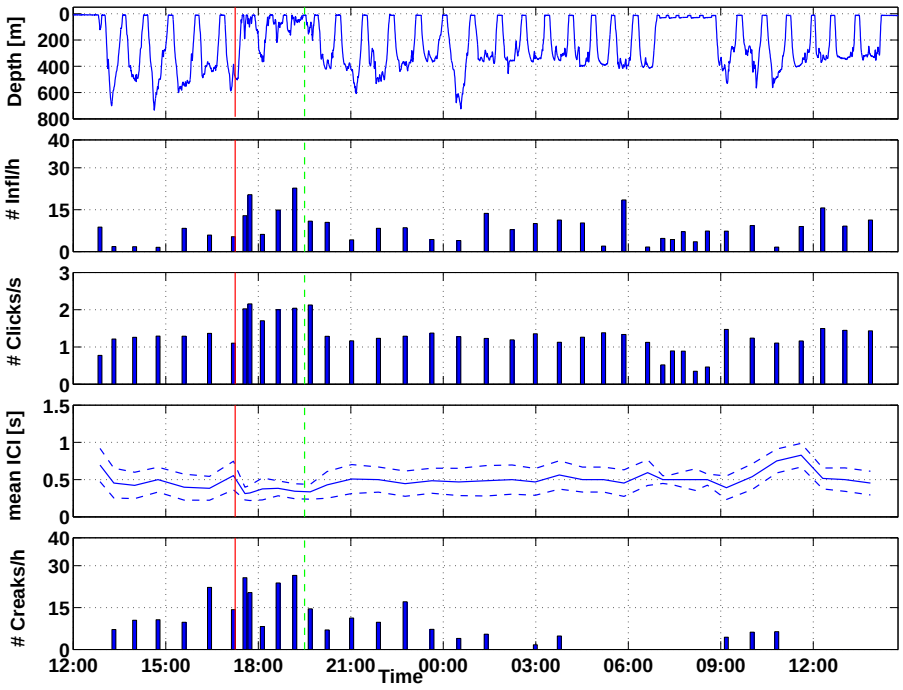

Figure III.29: 21 June 2009 - GOA 105

III.10.3 2009 DST data

DST data only provides pressure and orientation data. Thus, the figures in this section only display the whale's dive profile, along with the dive inflection rates.

Ten DST tags were deployed in 2009. Among them, 2 were coupled with a functioning B-probe and one whale was tagged on two different days. Thus, a total of nine different individuals have been tagged in 2009.

All of the tagging activity happened in close vinicity of the F/V Cobra.

III.10.3.a June 11th 2009 - No ID

On 11 june 2009, a whale was tagged at 14:00 when a fishing haul started. Three whales were around the vessel during the soak and the haul. The tagged whale was about 300 m away during both the soak and the haul.

A second haul happened during the tag duration, between 08:00 and 11:00 on 12 June 2009. Three whales were around the vessel during the soak and the haul. The tagged whale was about 259 m away during both the soak and the haul.

During the first haul, the whale performed deep dives of varying length. The deepest dive corresponded to an higher dive inflection rate. Between the two hauls, the whale mostly performed regular dives down to 300 m - 400 m. The whale made some sleep dives between 02:00 and 06:00 on 12 June but resumed to dives down to at least 400 m two hours before the start of the second haul. During the first dive of the haul, the whale gradually works its way up on the ascent. This dive shape has been observed for other individuals during fishing hauls as well.

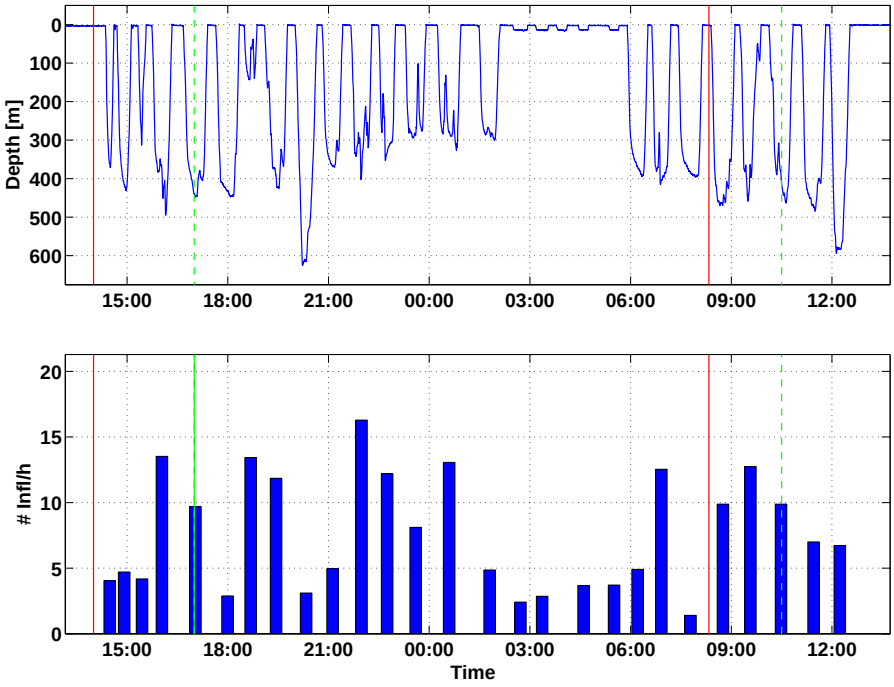

Figure III.30: 11 June 2009 - No ID

III.10.3.b June 13th 2009 - GOA 103

On 13 june 2009, a whale was tagged at 09:10 during the soak. The tag came off just before the start of the haul. Four whales were around the vessel (< 800 m) during the soak and between five and six during the haul. Among them, between four and six were surfacing less than 500 m away during the haul. The tag came off just before the start of the haul but visual observations indicate that the tagged whale was 200m away at the start of the haul and within 500 m of the vessel during the haul.

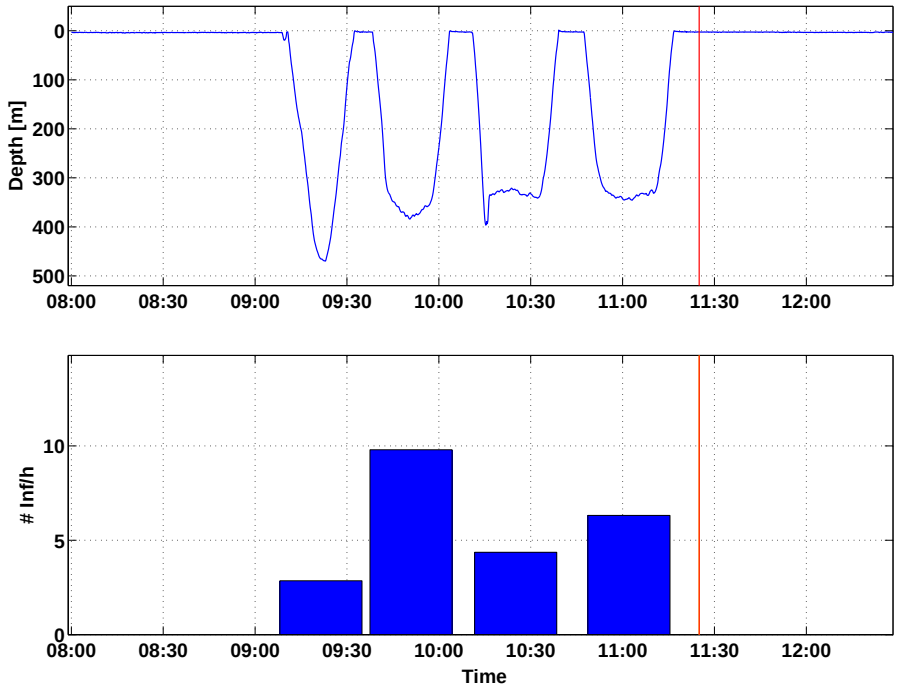

Figure III.31: 13 June 2009 - GOA 103

III.10.3.c 13 June 2009 - GOA 106

On 13 June 2009, a whale was tagged one hour into a fishing haul. Four whales were around the vessel (< 800 m) during the soak and between five and six during the haul. Among them, between four and six were surfacing less than 500 m away during the haul. The tagged whale was one of them. Just after being tagged, the whale performed two short and shallow dives (< 150 m) associated with a very high dive inflection rate (> 25 inflections / hr). This happened midway through the fishing haul. Afterwards, for the remaining of the fishing haul and the tag record, the whale performed regular deep dives associated with normal dive inflection rate. Most of the dives occurred around 300 m depth but the whale occasionally went deeper (500 m). The dive inflection rate stayed in the normal range throughout the tag record.

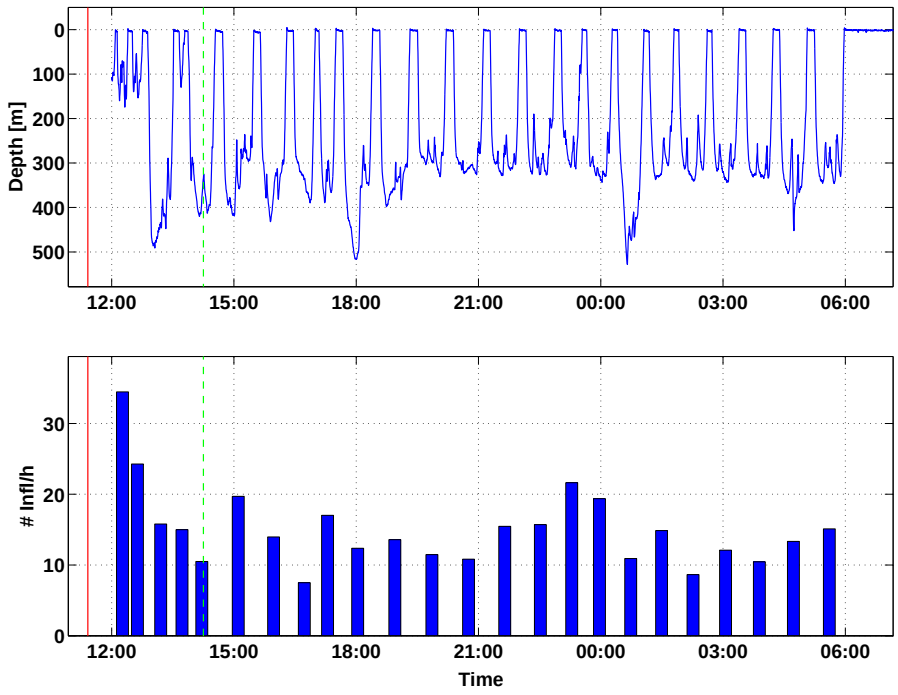

Figure III.32: 13 June 2009 - GOA 106

III.10.3.d 14 June 2009 - GOA 104

On 14 June 2009, a whale was tagged one hour into a fishing haul. Three whales were close to the vessel until 14:30. Two whales joined afterwards. The tagged whale was between 100 m and 500 m during the whole duration of the haul and stayed close to the vessel for a few hours after the end of the haul. The whale performed regular deep dives during the tag duration. Most of the dives were down to 400 m but the whale did a few deeper dives (600 m - 800 m). Two of those deep dives happened just before and after a period of sleep dives (between 00:30 and 02:00 on 15 June).

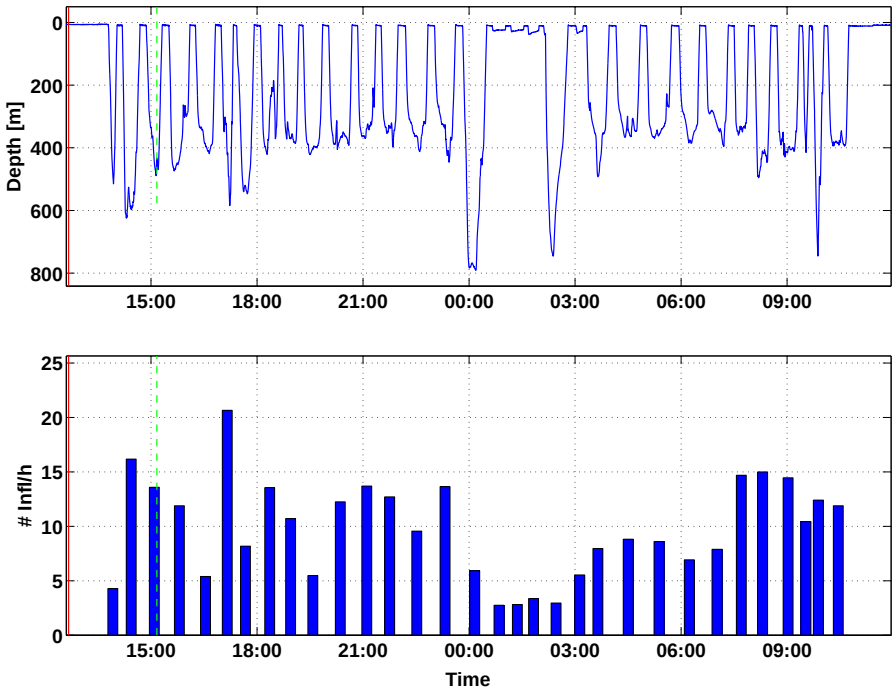

Figure III.33: 14 June 2009 - GOA 104

III.10.3.e 15 June 2009 - GOA 107

On 15 June 2009, a whale was tagged one hour prior to a fishing haul. Three whales were close to the vessel during both the soak and the haul. The tagged whale was 200 m away during the soak and between 150 m and 400 m during the haul. During the soak and the haul, the whale performed deep dives (> 500 m) associated with a high inflection rate. After the haul, the whale lowered its dive inflection rate and performed regular dives at 300 m until the tag came off on 16 June 2009 at 14:45. The whale displayed a sleeping behavior between 04:00 and 08:00 on 16 June 2009.

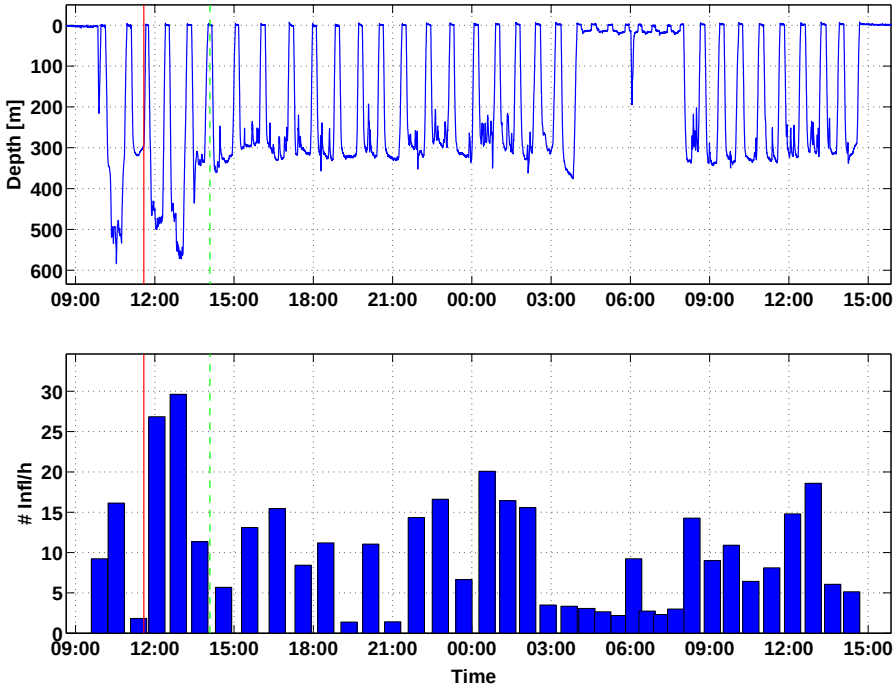

Figure III.34: 15 June 2009 - GOA 107

III.10.3.f June 15th 2009 - GOA 90

On 15 June 2009, a whale was tagged at 15:30, one hour before the end of a haul. Three whales were close to the vessel until 14:30. Two whales joined afterwards. On 16 June 2009, another fishing haul happened between 11:00 and 14:00 and three whales were in the area during both the soak and the haul. The tagged whale was 400 m away during both hauls. From the start of the tag record until the beginning of the haul on 15 June, the whale did some regular dives mostly between 250 and 400m, with some occasional deeper dives. The whale displayed a sleeping behavior between 23:00 and 3:00 followed by its deepest dives of the tag record ($>$ 500m). During the haul on June 16, the whale deepened its dives and its dive inflection rate was high. When the haul ended, the whale resumed to dives mostly between 200 m and 350 m with a normal dive inflection rate.

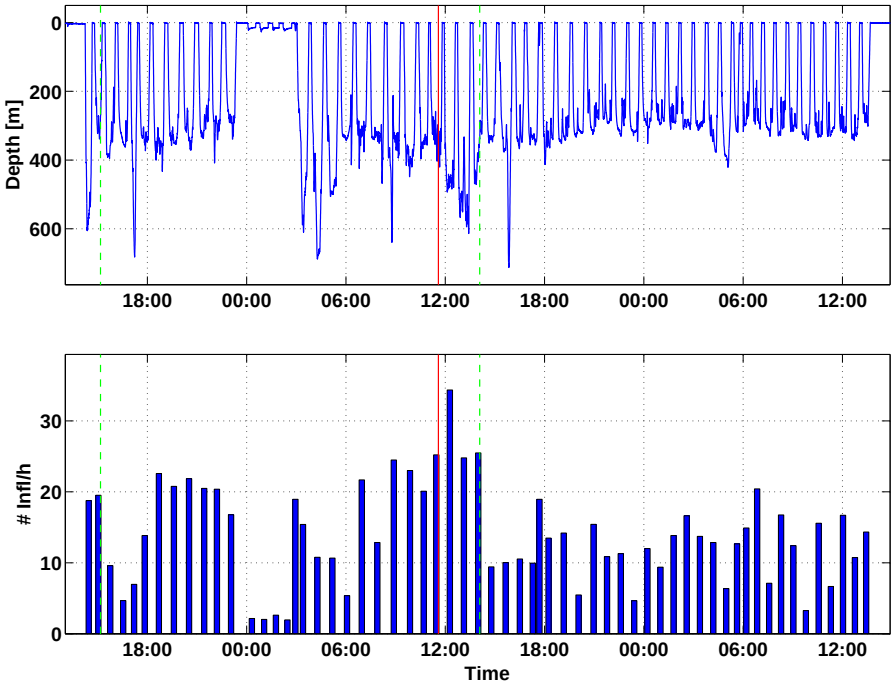

Figure III.35: 15 June 2009 - GOA 90

III.10.3.g June 21st 2009 - GOA 107

On 21 june 2009, a whale was tagged at 12:15 and a fishing haul occurred between 17:00 and 20:30. Three whales were around the vessel during the soak (<800m) and close (<500m) to vessel during the haul. The tagged whale was 500 m away during soak (between noon and 5pm), and 100 m - 300 m during the haul. During the whole duration of the tag record, the whale mostly performed dives between 300 m and 600 m. The dive inflection rate was significantly higher during the first two dives of the fishing haul and lower afterwards. Indeed after these high inflections dives, the whale performed a few very flat dives and then resumed to regular dives.

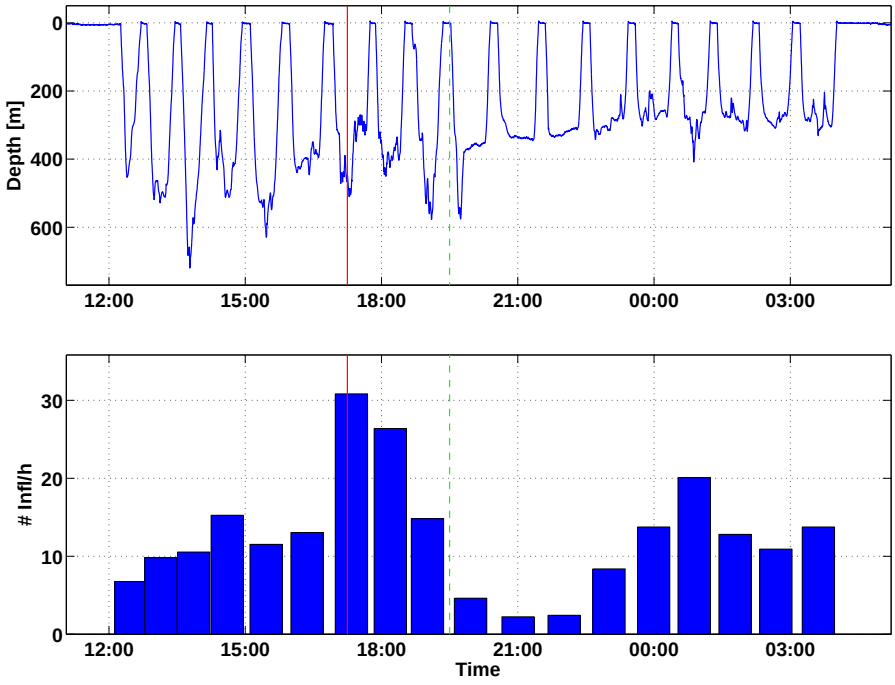

Figure III.36: 21 June 2009 - GOA 107

III.10.3.h June 21st 2009 - GOA 105

On 21 June 2009, a whale was tagged with a B-Probe/DST at 13:00. The Cobra started hauling his longline at 17:00 and ended at 19:30. During the whole duration of the haul, between three and four whales were surfacing close (100 m - 400 m). The tagged whale was more than 500 m away before the start of the haul but moved closer when the haul started was surfacing very close (100 m - 200 m) during the fishing haul. Before the start of the haul, the whale performed regular deep dives (between 400 m and 700 m) and its dive inflection rate and acoustic activity were normal. When the haul began, the whale started to do some shallow and very irregular dives, associated with high inflection rate and acoustic activity. As soon as the haul ends, the whale goes back to regular deep dives with normal dive inflection rate and acoustic activity. The whale performed some sleep dives from 07:00 to 09:00 on 21 June.

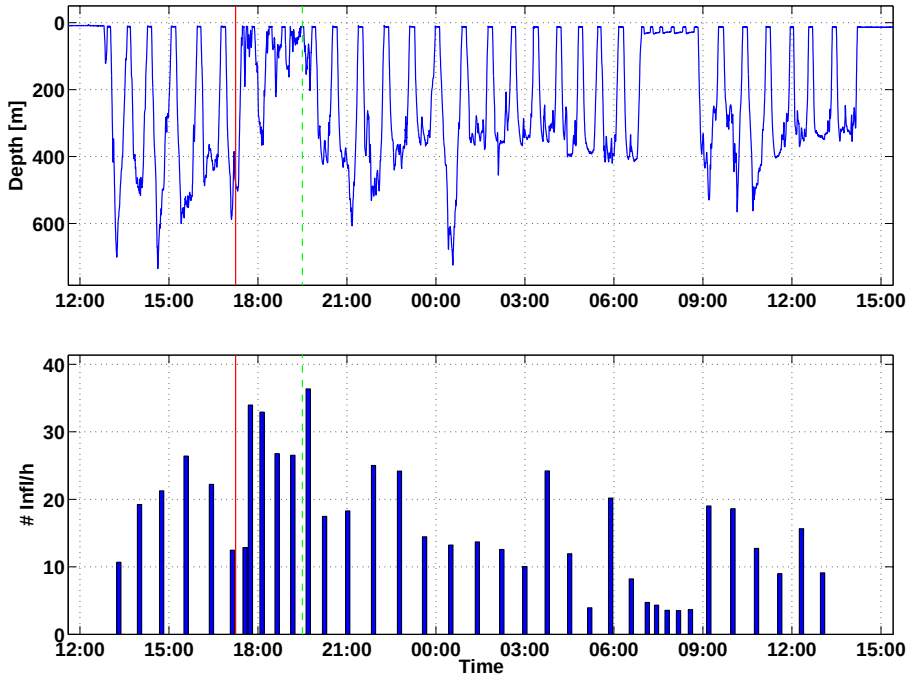

Figure III.37: 21 June 2009 - GOA 105

III.10.3.i June 29th 2009 - GOA 81

On 29 june 2009, a whale was tagged close to the Cobra during a longline deployment. The whale stayed in the area until the following day. Two whales were close to teh vessel during the soak and the haul and both of them were tagged. Between 18:00 on 29 June and 09:00 on 30 June, the whale mostly performed regular foraging dives, with the depth varying between 250 m and 550 m. The whale did only one long sleep dive around 05:00 on 30 June. As soon as the haul started at 09:15 , the whale changed dramatically its diving behavior and performed some very irregular dives associated with high dive inflection rate. When the haul ended at 10:30, the whale deepened its dives and lowered its dive inflection rate. The tag came off as a second haul was about to start.

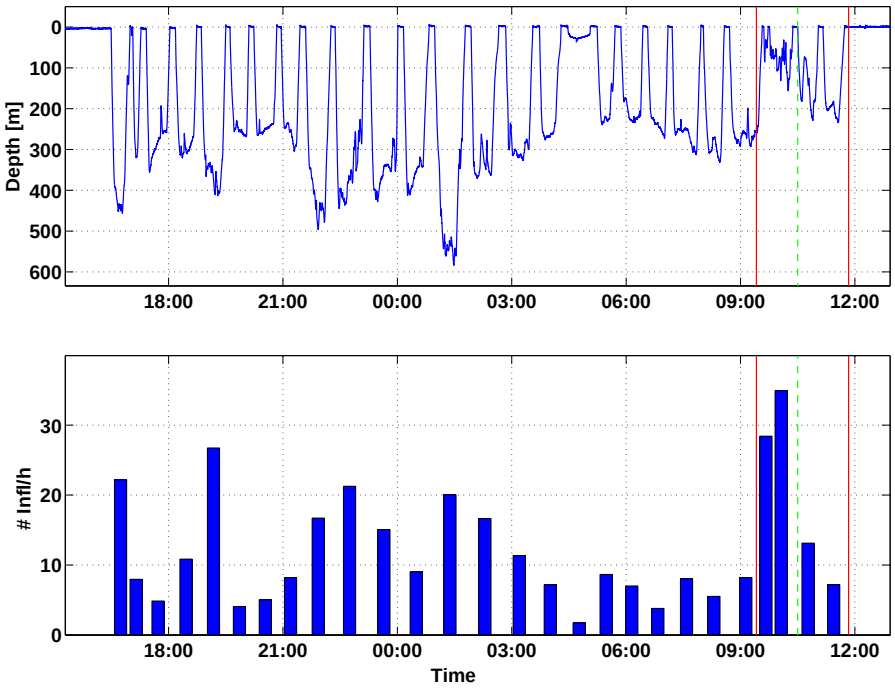

Figure III.38: 29 June 2009 - GOA 81

III.10.3.j 30 June 2009 - GOA 47

On 30 June 2009 a whale was tagged at 09:00 just as a fishing haul was starting. This haul ended at 10:30 and a second haul happened between 12:00 and 14:00. Two whales were close during both soaks and hauls, both of them were tagged. This tagged whale joined at the end of the first soak. The whale stayed in the fishing area after the second haul was done on 30 June and was present when the Cobra hauled his longline on 1 July. The tag came off just before the end of that haul. During the first haul of 30 June, the whale performed some shallow dives (< 200 m) associated with a high dive inflection rate. The dives were deeper and the dive inflection rate smaller between the 2 hauls but the dive inflection rate increased during the second haul. Just after the end of the second haul, the whale displayed a sleeping behavior for a few hours at mid-day. Sperm whales usually display sleeping behavior at night. This suggests that the whale behavior during the hauls required some rest. This could be a sign of successful feeding when depredating. Between 16:00 on 30 June and 09:00 on 1 July, the whale performed natural foraging dives between 350 m and 700 m. The dive inflection rate was high during some of the dives, maybe indicating feeding dives. Before the start of the haul on 1 July, the whale displayed sleeping behavior for three hours. He was within 800m of the vessel and resumed to deep dives with an extremely high dive inflection rate (> 45 inflections / hr) just when the haul started. This could mean that the whale knew that the haul would start soon and thus wanted to get some rest before a period of intense diving, acoustic and maybe feeding activities.

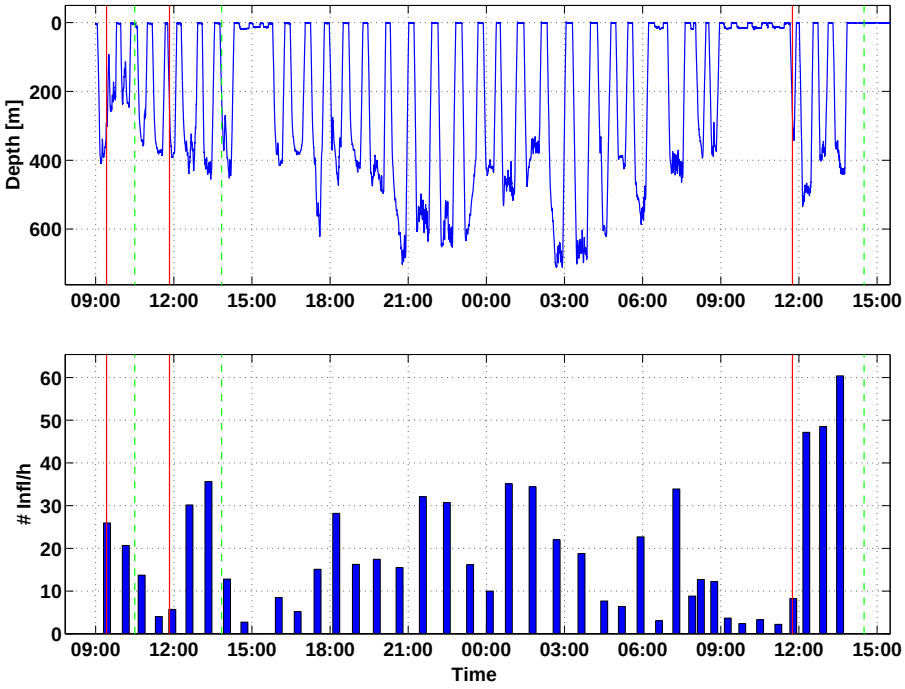

Figure III.39: 30 June 2009 - GOA 47

III.11 Acknowledgments

Chapter 3, in part, has been accepted for publication in the Journal of the Acoustical Society of America: Delphine Mathias, Aaron Thode, Jan Straley, Victoria O'Connell, John Calambokidis and Gregory S. Schorr, "Acoustic and foraging behavior of tagged sperm whales (*Physeter macrocephalus*) under natural and depredation foraging conditions in the Gulf of Alaska". The dissertation author was the primary researcher and author of this material.

Chapter IV:
Changes in depredating sperm whale (*Physeter macrocephalus*) acoustic behavior during sound playbacks

IV.1 Abstract

In 2009 acoustic playbacks were conducted during longline fishing hauls off southeastern Alaska. A variety of sounds were broadcast at source levels between 140 and 160 dB re 1uPa at 1 m rms. Bioacoustic recording tags were deployed simultaneously on depredating sperm whales. Sample sizes were too small to examine sounds individuals, but a two-sided Kolmogorov-Smirnov test found statistically significant differences in acoustic behavior between haul-only and haul-playback situations for all sounds pooled. Specifically, during haul-playbacks animals click and creak rates fell. The relative fraction of creaks followed by short pauses, interpreted here as a measure of relative foraging success, also decreased during playbacks, down to fractions displayed by non-depredating animals.

IV.2 Introduction

Sperm whales, designated an endangered species in the U.S., are distributed throughout the worlds oceans (Whitehead, 2003) and present year-around

in the Gulf of Alaska (GOA) (Mellinger *et al.*, 2004). The exact composition of a sperm whales diet is a question that has attained a practical importance in Alaska, as sperm whales remove fish from longline fishing gear, a behavior known as depredation.

Sperm whale depredation has increased in frequency, severity and geographic extent over the past decade. A domestic sablefish survey in the GOA looked at catch rates from 1999 to 2001 for all sets with sperm whales present, compared boats with and without physical evidence of depredation and found a 5% lower catch rate in boats with depredation (Sigler, 2008). However, video-camera observations (Mathias *et al.*, 2009) have shown that whales can depredate longlines without leaving behind any fish remains, so analyses of depredation impact based only on physical evidence observed at the surface can only provide a lower bound on true depredation rates.

The reception and production of sound is an important aspect of sperm whale behavior, as they use sound for echolocation, orientation and communication (Whitehead, 2003). For example, Thode *et al.* (2007) found evidence that cavitation noise arising from the ships propeller is the best candidate for a distinctive acoustic cue that attracts sperm whale to fishing boats in the GOA. A distinctive sperm whale sound is the creak, a sequence of clicks produced at a rate of 10 per second or faster (Madsen *et al.*, 2002a), and often characterized by a decrease in the click interval over the five-to-ten second duration of the sound (Whitehead and Weilgart, 1990; Whitehead, 2003). Bioacoustic tagging work on sperm whales has shown that most creaks occur at foraging depth and are often associated with changes in the orientation of the animal (Miller *et al.*, 2004; Watwood *et al.*, 2006). Previous research on bat echolocation has speculated that creaks followed by a pause in clicking, or creak-pause events, are indicative of prey capture success (Acharya and Fenton, 1992; Britton and Jones, 1999), as opposed to creak-only events, during which a creak is immediately followed by a series of regular clicks, and thus indicative of an aborted prey capture attempt. For sperm

whales the fraction of total creak sounds that are creak-pause events has been quantified in one study (Miller *et al.*, 2004), who found that 88.9 % (±13.5 %) of creaks produced by whales in the Gulf of Mexico and Ligurian Sea are followed by a pause in clicking of 4.8 s (±2.4 s). In this manuscript this creak-pause fraction will be dubbed the "success fraction".

Over the past four years the Southeast Alaska Sperm Whale Avoidance Project (SEASWAP) has used underwater video, bioacoustic tags and autonomous acoustic recorders to demonstrate that sperm whales make creak sounds when acquiring fish from longlines and that measurements of the acoustic success fraction may help distinguish depredation attempts from depredation captures (Mathias *et al.*, 2012). Mathias *et al.* (2012) also delineated two rough categories of depredation: deep and shallow. Animals exhibiting deep depredation display dive depths and durations similar to those displayed by other local animals foraging naturally, but are occasionally more acoustically active. During shallow depredation animals dive to relatively shallow depths, have short dive durations, and are much more active acoustically than under natural local conditions (Mathias *et al.*, 2012).

In 2009 SEASWAP conducted sound playback studies for the first time off a commercial fishing vessel in Southeast (SE) Alaska, to determine whether nearby tagged sperm whales demonstrated any changes in dive profile, orientation, or acoustic behavior in response to a variety of sounds, as part of a long-term goal to explore whether acoustic deterrents can practically reduce longline depredation by sperm whales. Acoustic playback experiments have been conducted on marine mammals for at least 40 years; an excellent review of 46 playback studies on marine mammals prior to 2006 is given in (Deecke, 2006), with a more selective review of playbacks in the context of controlled exposure experiments given in (Tyack, 2009). A few studies have sought to determine sounds that would deter animals from depredating fishing gear (Fish and Vania, 1971; Shaughnessy *et al.*, 1981). Specific types of signals used in these studies include narrowband pulses (Carlstrom *et al.*, 2002; Johnston, 2002; Morton and Symonds, 2002), tonals (Kastelein *et al.*,

2001; Nowacek *et al.*, 2004; Kastelein *et al.*, 2006a; Kastelein *et al.*, 2006b), FM sweeps (Nowacek *et al.*, 2004), or various types of killer whale sounds (Cummings and Thompson, 1971; Fish and Vania, 1971; Shaughnessy *et al.*, 1981; Deecke *et al.*, 2002).

IV.3 Materials and methods

IV.3.1 Equipment: playback device and bioacoustic tags

For the experiment an autonomous playback device was built that stood 1.2 m high and had 30 kg lb dry weight. The device could store up to 4 Gb of playback data, sampled at 125 kHz, and would broadcast the signal between a frequency bandwidth of 2-50 kHz, using a ITC-4004A transducer for components between 2 and 10 kHz, an ITC-1001 for components between 10 and 35 kHz, and an ITC-1032 for components between 35 and 50 kHz. The entire device was encased in a steel cage to protect all components from collisions with fishing gear and the fishing vessels hull.

Six different categories of signals were broadcast into the water: continuous white noise, FM sweeps, white noise bursts, sperm whale creaks and selections of orca transient calls (Deecke *et al.*, 2005). For most signal types, four different instances of each type were selected for playback, in order to compensate for pseudo-replication and habituation concerns(Kroodsma, 1990; Deecke, 2006). For example, four different instances of FM sweeps were used, each with different start and end frequencies and durations. Table IV.1 summarizes the playback categories and the range of variation of their appropriate parameters used to derive specific instances for playback.

The acoustic behavior, dive profiles, and spatial orientation of sperm whales in response to the playbacks were investigated using high-resolution digital archival acoustic sampling tags, or B-probes (Burgess *et al.*, 1998), which sampled

depth and 2-D acceleration at 1 Hz, and acoustic data at 4096 Hz. The tagging procedures are described in Chapter III (Mathias *et al.*, 2012).

During every fishing haul and playback session at least three autonomous passive acoustic recorders were deployed on anchorline fishing gear, at depths between 200 and 500 m, about 2 km from the midpoint of the fishing deployment. The recorders sampled acoustic data at 50 kHz. These instruments were used to independently estimate the playback source levels and the transmission loss characteristics of the environment.

Table IV.1: Signal categories used for playbacks, along with parameter ranges used to construct specific instances.

Signal	Instances	Source	Variable parameters	Parameter ranges
Continuous white noise	1	Synthesized		
FM sweeps	4	Synthesized	Start and end frequency, Duration	0.5-3 kHz (start) 8-15 kHz (end) 1-4 s (duration)
White noise bursts	4	Synthesized	Pulse duration, Pulse interval	8-15 msec 0.05-0.2 sec
Sperm whale creaks	1	Longline video camera data Mathias *et al.* 2009	None	None
Orca transient calls : continuous sequence	4	Volker Deecke St Andrews University	Start time in file	3:30, 10:40 19:40, 23:20 min into file
Orca transient calls : cherry-picked calls	5	Volker Deecke St Andrews University	Five high SNR calls randomly concanated	None

IV.3.2 Playback protocol

When directed by the skipper, the autonomous playback device was deployed by the fishing crew off the port bow of the fishing vessel at a depth of approximately 10 m. Each signal was played back with 125 kHz sampling rate, midway through a fishing haul. A monitoring HTI-96min hydrophone was placed two meters above the playback devices cage. The vessels 25 kHz echo-sounder was active at all times when outside the harbor, including during all playbacks, as was typical during all fishing hauls.

Once activated the playback device would remain silent for five minutes,

then would select a signal category to play. A 20% probability existed of selecting a zero category, which contained a single instance of a digital file with no signal. If a different category had been selected, a particular instance of that category would be randomly chosen. The selection would then be played back for 2 min at -20 dB below the maximum attainable source level (MAO) of 160 dB re 1uPa rms at 1 m, then after a certain pause time (1 min) the same instance would be replayed for 2 min at -10 dB below MAO and finally at MAO. This set of three playbacks is defined here as a playback set. After a playback set had been completed, an extended pause time (5 min) would elapse before the cycle repeated, with a new signal category possibly being selected. All playback sets conducted during one haul comprised a playback session. A total of 48 playback sets were conducted over 10 playback sessions, but only the 3 playback sessions that involved functioning tags are analyzed here.

IV.3.3 Statistical analysis of tagging data

The tagging data were processed to distill parameters about the dive, acoustic, and orientation behavior of sperm whales during fishing hauls with and without acoustic playbacks, or haul-playback and haul-only conditions. The mechanics of the data analysis are described in further detail in Mathias *et al.* (2011). The following five acoustic parameters were extracted from each dive : (a) timing of 1st click (T_{Cl1}); (b) click rate ($\dot{Cl}$); (c) mean inter-click-interval (ICI); (d) creak-only ($\dot{Cr}$) and creak-pause($\dot{CrP}$) rates; and (e) creak success fraction (F_{CrP}). All rates are normalized in terms of events per hour, regardless of the duration of the dive.

The distributions of the acoustic parameters obtained for each category are non-Gaussian, often highly-skewed, and characterized by large tails that indicate relatively infrequent but significant events that could not be discounted as outliers. Thus a two-sided Kolmogorov-Smirnov (KS) test was used to evaluate

the probability that two sample parameter distributions, obtained from different haul situations, could have been drawn from the same underlying cumulative probability distribution. The null hypothesis is that various parameters measured from haul-only and haul-playback situations were drawn from the same underlying distribution. A Bonferroni correction is applied to account for the number of dependant or independent statistical tests performed (Bonferroni, 1936). As 5 parameters are tested for significant differences between behavioral categories, the p value for an individual test is reduced to $0.05/5 = 0.01$. Thus, KS p-values of less than 0.01 led to the rejection of the null hypothesis at the 5% significance level. The same statistical test was applied in Chapter III (Mathias *et al.*, 2012) to determine statistically significant differences between natural and depredation behaviors of sperm whales.

IV.4 Results and discussion

IV.4.1 Summary of deployments

A total of ten playback sessions were conducted during hauls between 12 June and 2 July , 2009. Three playback sessions occurred when no tagged whales were present. Eleven B-probe tags were deployed, but only 3 B-probes recorded acoustic data for any length of time (12 June, 13 June, and 21 June). The duration of the successful B-probe tag records was quite long, however, with mean, median, and mode durations of 22.3, 27.0, and 12.0 hours. Dive and orientation profiles, along with acoustic data, were obtained from B-probes during four playback sessions (two on June 12, one on June 13, and one on June 21), yielding a total of eight dives during hauls without playbacks, and seven dives during playbacks. The dive profiles of all tagged animals during playbacks were consistent with deep depredation behavior, and not shallow depredation.

Figures IV.1 and IV.2 show an example of one instance of FM sweeps

being played during a time when a tagged whale was nearby. Figure IV.1 displays the signal recorded 2 m away from the playback projector by the monitoring hydrophone. Instantaneous source levels of the FM sweeps are determined to be 156 dB re 1uPa rms at 1 m. Figure IV.2 illustrates the same signal as detected by an autonomous recorder mounted on a fishing anchorline 1.3 km away from the playback device. Figure IV.3 and Figure IV.4 respectively show examples of white noise and killer whale sounds played when a tagged whale was nearby.

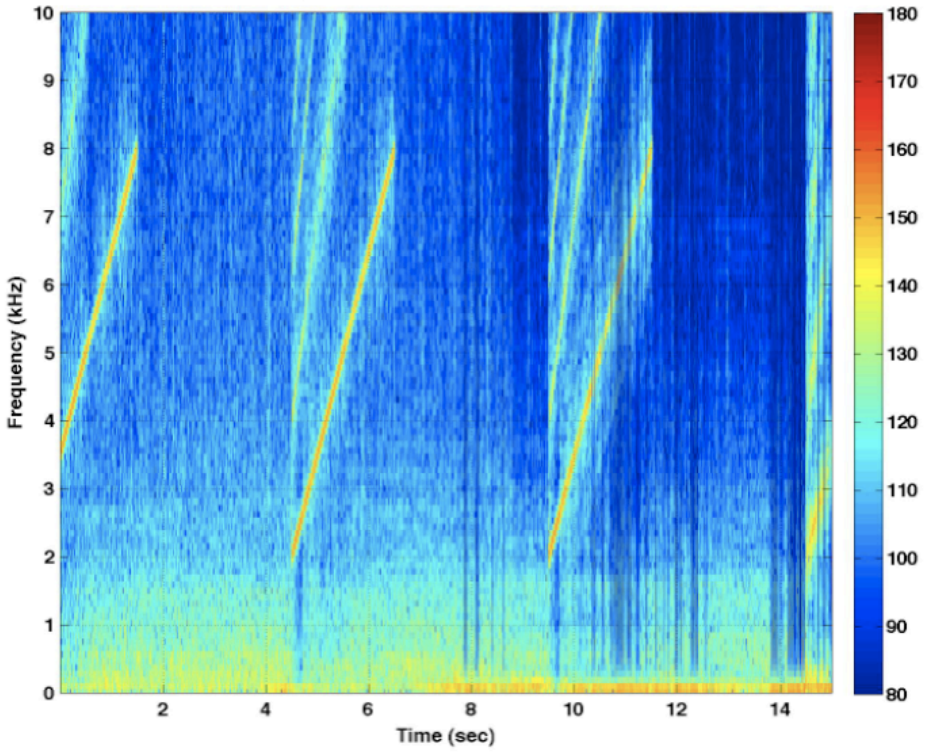

Figure IV.1: Instance of FM sweep played at 19:09:00, 21 June 2009 at 15 m depth, measured at 2 m range. The estimated instantaneous source level is 156 dB rms re 1uPa rms at 1m.

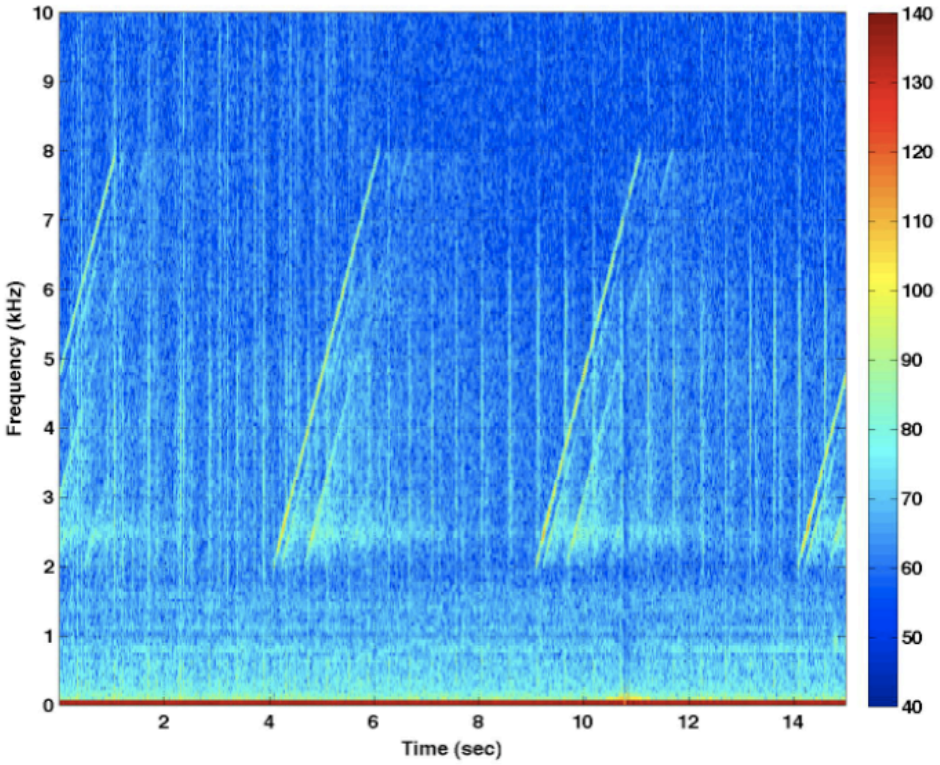

Figure IV.2: Same signal as Figure IV.1, received at 1.3 km at 250 m depth on an autonomous recorder. Multipath arrivals are also apparent, and sperm whale clicks are visible as vertical lines. At this range the received level of the playback is around 100 dB re 1uPa rms, consistent with the source level derived from Figure IV.1.

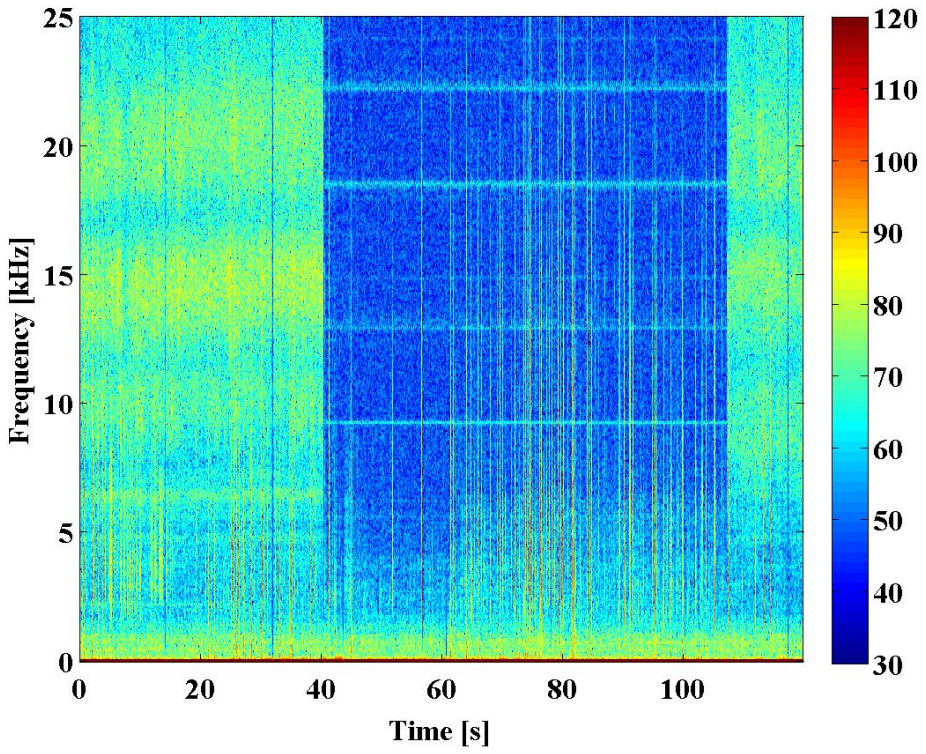

Figure IV.3: Instance of white noise played.

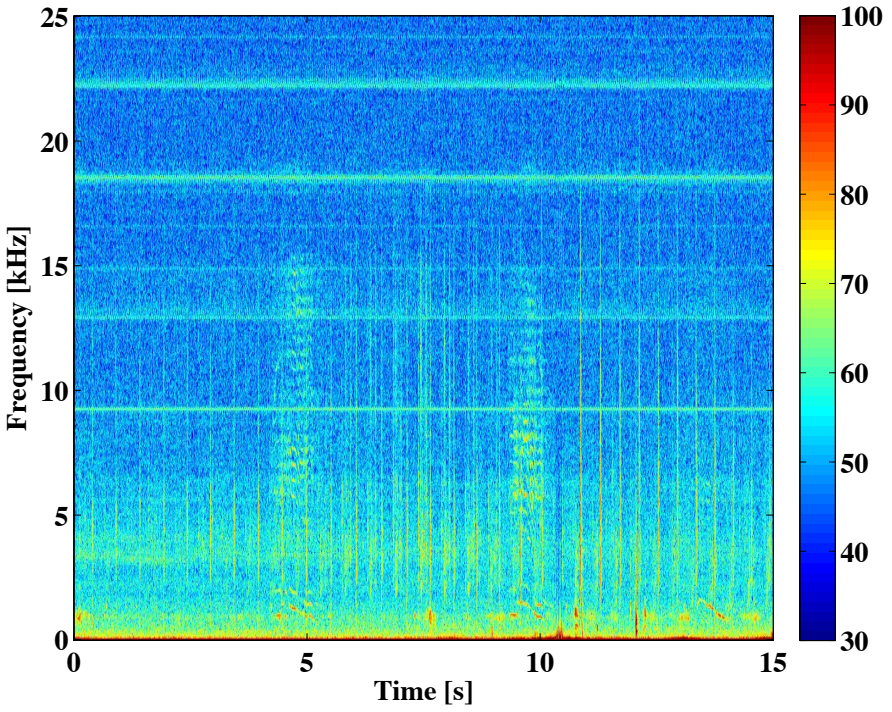

Figure IV.4: Instance of killer whale calls played.

IV.4.2 Statistical analysis of acoustic behavior

No statistically significant differences in dive profiles or orientation behavior were found for haul-only and haul-playback conditions; however, differences in acoustic behavior were identified.

Table IV.2 summarizes the mean and standard deviations of the five acoustic parameters measured during haul-only and haul-playback conditions. Due to small sample sizes the playback trials were not subdivided by playback signal category. The p-values of the two-sided K-S test are also displayed, with values below the 5% level italicized.

Table IV.2: Differences in tagged whale acoustic parameters between haul-only and haul-playback conditions. Nd: Number of distinct dives used in analysis; $Ntag$: Number of B-probe tag deployments available; $Nind$: Number of individual animals available; T_{Cl1}: Time of first usual click, relative to the start of a dive; $\dot{Cl}$: click rate averaged over entire dive; ICI: inter-click interval; $\dot{Cr} + \dot{CrP}$: combined normalized creak and creak-pause rates; F_{CrP}: the success fraction, or the fraction of creak events that are followed by short pauses, potentially indicative of prey capture. The p-value shows the probability that the haul-playback distribution is drawn from the same cumulative empirical distribution as the haul-only distribution, using the two-sided K-S statistical test. Bold-italic p-values indicate the rejection of the null-hypothesis of a common underlying distribution ($p < 0.01$).

	$T_{Cl1}(min)$	$\dot{Cl}$ (s^{-1})	$ICI(s)$	$\dot{Cr} + \dot{CrP}$ (h^{-1})	F_{CrP} (%)	Nd	Ntag	Nind
Haul-only	0.3 ± 0.1	1.1 ± 0.3	0.4 ± 0.1	20.1 ± 6.2	62.7 ± 8.1	8	3	3
Haul-playback	0.4 ± 0.1 p=0.21	0.8 ± 0.2 p=0.04	0.5 ± 0.1 p=0.11	12.2 ± 4.0 ***p=0.01***	45.1± 6.9 ***p=8.7e^{-3}***	7	3	3

The acoustic tags recorded during only four playback sessions. Despite this small sample size the K-S test rejects the null hypothesis for three acoustic parameters: the long-term average click rate, the total creak rate, and the success fraction. In essence, during playback sperm whales make fewer creaks, and their success fraction F_{CrP} falls.

Figure IV.5 illustrates the distributions of the success fraction for the haul-only and haul-playback conditions. As mentioned previously, all playbacks were conducted on whales displaying deep depredation. Also shown is the success fraction distribution obtained from locally tagged animals displaying both natural foraging behavior and shallow depredation (Chapter III). Finally, Figure IV.5 displays the distribution of the success fraction reported by Miller *et al.* (2004) for tagged sperm whales in lower-latitude regions.

Figure IV.5 shows how the natural success fraction of the SE Alaskan whales was considerably lower than natural success fractions elsewhere, if a short pause following a creak is interpreted as being indicative of a successful prey capture. Stated another way, the Alaskan whales require more creaks per capture. However, when depredating the success fraction of the Alaskan whales increases, with larger effects visible during shallow depredation, but with significant effects still visible for deep depredation. Finally, during the playbacks the animals success fraction returned to those of non-depredating (natural foraging) animals in SE Alaska.

IV.4.3 Interpretation of playback results

Under haul-playback conditions the relative amount of time the animals spent creaking decreased. Intriguingly, the success fraction also decreased. The results suggest that while the playbacks did not deter the animals from approaching the fishing gear, they potentially decreased the efficacy of the animals in removing fish. Unfortunately, the sample sizes of the playbacks are too small to determine whether a particular type of playback (FM sweep, orca, etc.) was primarily responsible for the observed changes.

A weakness of the experimental protocol was that the playbacks were always conducted during the latter portion of the haul; perhaps sperm whale acoustic behavior naturally tapers off toward the end of a haul, even if playbacks are

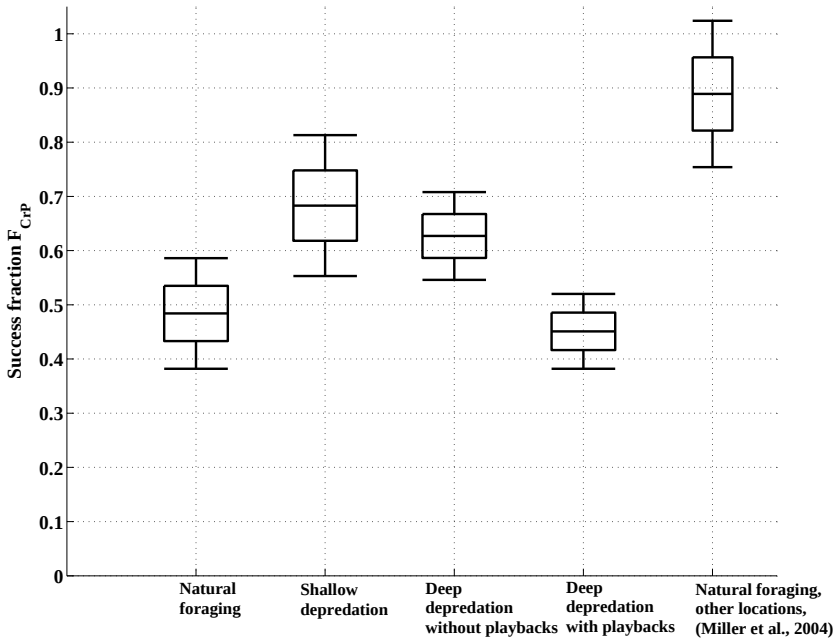

Figure IV.5: Box plot of success fraction F_{CrP} for different types of sperm whale behavior. The band near the middle of the box is the 50th percentile (the median) and the ends of the whiskers represent the standard deviation above and below the mean of the data. Natural foraging behavior is measured when no fishing haul is being conducted. Shallow depredation and Deep depredation without playbacks are behaviors measured during haul-only events, and Deep depredation with playbacks measures acoustic behavior during haul-playback events. No playbacks occurred when animals were displaying shallow depredation behavior. The last column shows the success fraction derived from tag data collected from naturally foraging whales in the Gulf of Mexico and Ligurian Sea, presented in Miller *et al.*, 2004. See Chapter III for further details on natural foraging and shallow depredation measurements in Southeast Alaska.

not conducted. To check this possibility the acoustic dive behavior of two deep-depredating whales during hauls without playbacks (randomly selected from 2007) were reviewed, to determine whether the success fraction decreased near the end of a haul. The first whale had six depredation dives during the haul, with success fractions of 0.67, 0.70, 0.78, 0.80, 0.75, and 0.85; the five depredation dives of the second whale had success fractions of 0.86, 0.70, 0.63, 0.89, and 0.67. Therefore, little evidence exists that the success fraction of depredating animals gradually decreases as a haul progresses.

IV.5 Conclusion

The behavioral reactions of depredating sperm whales to a variety of acoustic playbacks generated at relatively low source levels were investigated using bio-acoustic tags. No significant changes in dive depths or durations were found; however, a two-sided Kolmogorov-Smirnov test found statistically significant differences between haul-only and haul-playback situations, in terms of the acoustic behavior of the animals. The sample size for playbacks was not large enough to determine which particular signal category was responsible for the observed differences.

The study, if taken in isolation, does not provide strong evidence that acoustic deterrent devices are effective in reducing depredation; the number of playbacks and test subjects are too small, and the time interval over which the playbacks were conducted was too short to account for long-term issues like habituation. The primary value of these results is that they provide additional evidence that the so-called success fraction F_{CrP} may provide a useful acoustic metric for measuring depredation success, along with the number of depredation attempts. At present, relying on visual evidence to estimate depredation rates is inaccurate, time-consuming, and slow, making it difficult to judge the effectiveness of depredation countermeasures over reasonable and cost-effective time scales. If the success

fraction were demonstrated to be an accurate remote measure of relative foraging success, then the ability to evaluate depredation countermeasures would be substantially enhanced.

IV.6 Acknowlegments

The International Association of Oil and Gas Producers Joint Industry Project (JIP) supported this work under grant JIP 22 06/01. The North Pacific Research Board (NPRB) also provided support under Project Number 918. The authors thank Russell Tait, Jennifer Miksis-Olds and other members of the JIP project support group for comments to improve the manuscript. Tagging and playback work was conducted under NOAA Office of Protected Resources National Marine Fisheries Permit 473-1700-2.

Chapter V:
Depth and range tracking of sperm whales (*Physeter macrocephalus*) in the Gulf of Alaska using a two-element vertical array, satellite and bioacoustic tags

V.1 Abstract

This chapter demonstrates the tracking performance of a simple two-element vertical array, deployed between 15-17 August 2010 on the continental slope off Southeast Alaska in 1200 m water depth. The instruments were attached to a longline fishing buoyline at 300 m depth, close to the sound-speed minimum of the deep-water profile. The buoyline also served as a depredation decoy, attracting seven sperm whales to the area throughout the two-day deployment. One animal was tagged with both a LIMPET satellite and bioacoustic B-probe tag, thus recording dive depth, surface position, and sounds produced by the animal. This data was used as an independent check of various passive acoustic schemes for tracking the whale in depth and range, using both analytic and numeric sound propagation models. All approaches used the relative arrival times and elevation angles of multiple ray paths. Analytical methods can be used to track sperm whales up to 2 km range, and numerical methods yield accurate estimates up to

at least 35 km range. The tracking system was used to estimate the source level of sperm whale clicks and creaks, predict the maximum detection range of the signals as a function of sea state, and measure the drift of several whales away from the decoy over time.

V.2 Introduction

V.2.1 Motivation for tracking sperm whales in the Gulf of Alaska

Sperm whales (Physeter macrocephalus) have learned how to remove black cod from deep-water longline gear in the Eastern Gulf Of Alaska (EGOA), and this activity has increased in frequency, severity and geographic extent over the past decade (Hanselman *et al.*, 2009; Sigler *et al.*, 2008). In 2002 the Southeast Alaska Sperm Whale Avoidance Project (SEASWAP) was created to quantify the scale of sperm whale depredation in the EGOA to recommend strategies to reduce depredation. Passive acoustic monitoring and bioacoustic tagging became important tools for studying sperm whale behavior during natural and depredation foraging behaviors (Thode *et al.*, 2007; Mathias *et al.*, 2012). One key aspect of the study has been determining what acoustic cues alert the animals to fishing activity, and over what distance these cues are detectable above background noise levels. Preliminary work found that whales identify fishing hauls by the cavitation sounds generated by the engagement/disengagement of the vessels' propellers during hauling (Thode *et al.*, 2007). However, determining the ranges over which whales respond to these cues is more problematic.

Tracking whales acoustically around fishing vessels would establish ranges over which the animals respond to fishing activity, and would allow observations of their diving and acoustic behavior upon their arrival. Unfortunately, standard methods for tracking sperm whales using passive acoustics are impractical to use

under most practical fishing scenarios, as these methods require the deployment of multiple hydrophones separated by hundreds to thousands of meters, a process that absorbs prohibitive amounts of time. Similar problems arise when studying depredation of other marine mammal species.

In this chapter I present a passive acoustic tracking method that requires only a single deployment of two hydrophones, attached to the fishing gear itself. The hydrophones, arranged as a vertical array, exploit the depth-dependant sound speed profile of the cold-water region to detect multipath propagation of sperm whale sounds and thus establish range and depth estimates. Section V.2.2 reviews sperm whale acoustic behavior and previous published work on long-range tracking, and Section V.3 describes the circumstances behind the 2010 vertical array experiment, including tag deployments. Section V.4 reviews the tracking theory and introduces the practical problems encountered when processing real data, and Section V.5 shows how the 2010 deployment was able to track whales out to 35 km. Finally, Section V.6 provides simple analytic formulas for the measured transmission loss, discusses the sensitivity of the methods to various uncertainties, and estimates the apparent source levels of sperm whale sounds at long ranges, as well as the ultimate detection and tracking range of the system as a function of sea state. The Conclusion discusses how to improve the localization performance further.

V.2.2 Sperm whale acoustic behavior

Sperm whales were one of the first cetaceans to be identified using passive acoustics (Worthington and Schevill, 1957). Sperm whales are among the most acoustically active cetaceans and produce impulsive sounds called clicks when diving. Clicks have inter-click intervals (ICIs) of 0.5-2 s (Goold and Jones, 1995; Jaquet *et al.* 2001), durations of about 10-20 ms (Goold and Jones, 1995), and significant power spectral densities between 100 Hz to above 20 kHz (Watkins *et*

al., 1993; Zimmer *et al.*, 2005b). Sperm whales display a powerful forward directed beam (Mohl *et al.*, 2000; Madsen *et al.*, 2002a,b), and Mhl *et al.* (2000) reported click source levels up to 223 dB re 1 uPa (rms) along the main axis of this beam.

A deep-diving species, sperm whales regularly descend to depths greater than 400 m, for periods ranging between 30 and 45 minutes, and rest at the surface for intervals ranging between 5 and 10 minutes. They typically start emitting clicks within 2 min of starting a descent and fall silent during most of the ascent (Wahlberg *et al.*, 2002; Madsen *et al.*, 2002a; Drouot *et al.*, 2004; Douglas *et al.*, 2005; Watwood *et al.*, 2006).

V.2.3 Previous acoustic tracking research

The frequent acoustic activity of sperm whales, combined with the high broadband intensity of their sounds, makes them ideal candidates for passive acoustic localization. Clicks can be heard on hydrophones several kilometers from a vocalizing sperm whale (Leaper *et al.*, 1992; Norris *et al.*, 1996; Mellinger *et al.*, 2003; Barlow and Taylor, 2005). Multipath arrivals (direct, reflected and refracted paths) can often be differentiated in time, expanding tracking capabilities further (Nosal *et al.*, 2006; Tiemann *et al.*, 2006).

Passive acoustic methods for detecting and localizing sperm whales have existed for decades and have become standard tools for researching their behavior and abundance. A common technique for tracking the position of sperm whales is known as hyperbolic fixing and exploits the time differences of arrival of a sperm whale click heard on two spatially separated acoustic receivers (Clark 1980; Clark *et al.*, 1986; Mitchell, 1995; Stafford *et al.*, 1998; Janik *et al.*, 2000; Spiesberger, 2001; Nielson et al, 2006). If a homogenous sound speed is assumed throughout the medium, then a hyperboloid defines the possible source locations. If the two hydrophones are towed behind a vessel, the resulting hyperbola effectively defines a relative bearing to the animal, subject to a left/right ambiguity (Gordon, 1987;

Whitehead, 2003; Barlow *et al.*, 2005; Thode *et al.*, 2010).

A third and fourth receiver spaced hundreds to thousands of meters away from the other hydrophones allows additional hyperboloids to be defined, and the intersection of these curves provides range and depth information, in addition to relative direction (Spiesberger, 2004).

Multipath reflections from the ocean bottom and surface arrive at the receiver at different times and can be treated as data obtained by "virtual" receivers above the ocean surface, and incorporated into the solution to improve the accuracy of estimated source positions, or to reduce the number of hydrophones required for a solution (Whitney, 1968; McDonald *et al.*, 1995; Mouy *et al.*, 2011). Thode *et al.* (2004) used a two-hydrophone wide-aperture towed array and multipath arrivals for obtaining low-resolution dive tracks of multiple sperm whales.

The most recently published tracking techniques use numerical acoustic propagation models to account for both ray-refraction and multipath effects generated by realistic depth-dependant sound speed profiles. Measurements of multipath arrival times are compared with modeled arrival times to create an ambiguity surface. Tiemann *et al.* (2006) demonstrated a three-dimensional localization method for tracking sperm whales using only one acoustic sensor, along with a model of the azimuthally-dependent bathymetry surrounding the sensor. Nosal *et al.* (2006) developed a model-based method for exploiting relative arrival time differences between direct and surface-reflected clicks to track a sperm whale in three dimensions, using recordings from five widely-spaced bottom-mounted hydrophones at a U.S. naval test range, where the elements were separated by 7.5 km.

In this chapter, data from a two-element vertical acoustic array is used to demonstrate that sperm whale long-range tracking can be performed with a single compact deployment, without knowledge of the regional bottom bathymetry. The results are independently confirmed by comparing the method's range and depth estimates with location and depth information provided from a tagged sperm

whale. The whale was originally tagged within a few hundred meters of the array, and then over two days traveled 80 km away under fixed weather conditions, providing an ideal scenario for observing and understanding the performance of the system with tracking range.

The analysis proceeds in several stages. First, close-range sounds from the tagged animal, recorded on one element of the vertical array, were used to obtain relative arrival times of direct, surface-reflected, and bottom-reflected paths on a single hydrophone. Analytical equations derived from rectilinear assumptions (Thode *et al.*, 2004) were then used to solve for the animal's range and depth. Second, the vertical array data was used to estimate vertical arrival angles of the direct and surface-reflected paths to determine whether range and depth localization could occur without the use of bottom multipath, and thus without knowledge of bottom bathymetry. Both analyses estimated the ranges at which the analytic solutions begin to break down. Finally, at larger ranges the analytic formulas were replaced with an acoustic propagation model to account for a realistic sound speed profile and its accompanying ray refraction effects. The addition of a numerical propagation model adds several layers of complexity, including the need to obtain accurate sound speed profile data, choosing appropriate run parameters for the model (including grid mesh sizes), and developing appropriate methods for comparing model predictions with measured data.

V.3 Data collection

V.3.1 Vertical array deployment

Between 15 and 17 August 2010, the F/V Northwest Explorer deployed a two- element vertical array in 1200 m water depth at the Spencer Spit (57.8115 N, -137.4043 W), an underwater feature roughly 60 km west of Yakobi Island, on the southeast Alaskan continental slope (Figure V.1). The array was comprised of two

acoustic recorders, each using a Persistor CF2 data acquisition system, attached at 300 m depth to a longline buoyline, separated by 10 m vertically (Figure V.2). The recorders used HTI-96min hydrophones (High-Tech Inc.) with a sensitivity of 172 dB re 1uPa/V. After an analog voltage amplification of 26 (28 dB gain) the data were written to a 2.5 V A/D converter. Thus the system could record peak-to-peak impulses of 153 dB re 1uPa (pp) without clipping. The Persistor system would log data to a 4 Gb flash memory card for 10 hours, then stop sampling for 2 hours to transfer the data to a hard disk. Onset's HOBO Pendant G data loggers were taped inside each recorder to monitor the system's vertical inclination by measuring the 3-dimensional angular displacement every minute. Two Sonotronics acoustic pingers were attached 1 m above each unit. Every 30 s each pinger emitted a 10 ms pulse at 10 kHz, which was used to time synchronize the acoustic data (Section V.4.1). A Seabird SBE39 was deployed between the acoustic recorders, providing pressure and temperature measurements every minute. During deployment and recovery the SBE39 also provided a temperature profile of the water column to 300 m depth. Furthermore, the pressure data helped assess the gross vertical stability of the array deployment, and the temperature data helped assess the environmental stability over the two days of the deployment, since large temperature changes would affect the sound speed profile and thus the sound propagation in the area. A 30 kg lead cannonball was placed below all instruments to keep the system as vertical as possible throughout the deployment. This instrumental configuration was easy to attach and deploy using standard longline fishing techniques.

Prior to the vertical array deployment, the Seabird SBE39 was attached about 3 m above a 30 kg anchor and cast into the water, where it measured the temperature and pressure every second down to 475 m depth. The Mackenzie equation (1981) was used to derive the sound speed in sea-water as a function of temperature, salinity and depth. The salinity was assumed to be 32.4 psu at all depths based on the World Ocean Atlas (Antonov *et al.*, 2010), and the temperature was assumed constant below 475 m. Figure V.3 displays the resulting sound

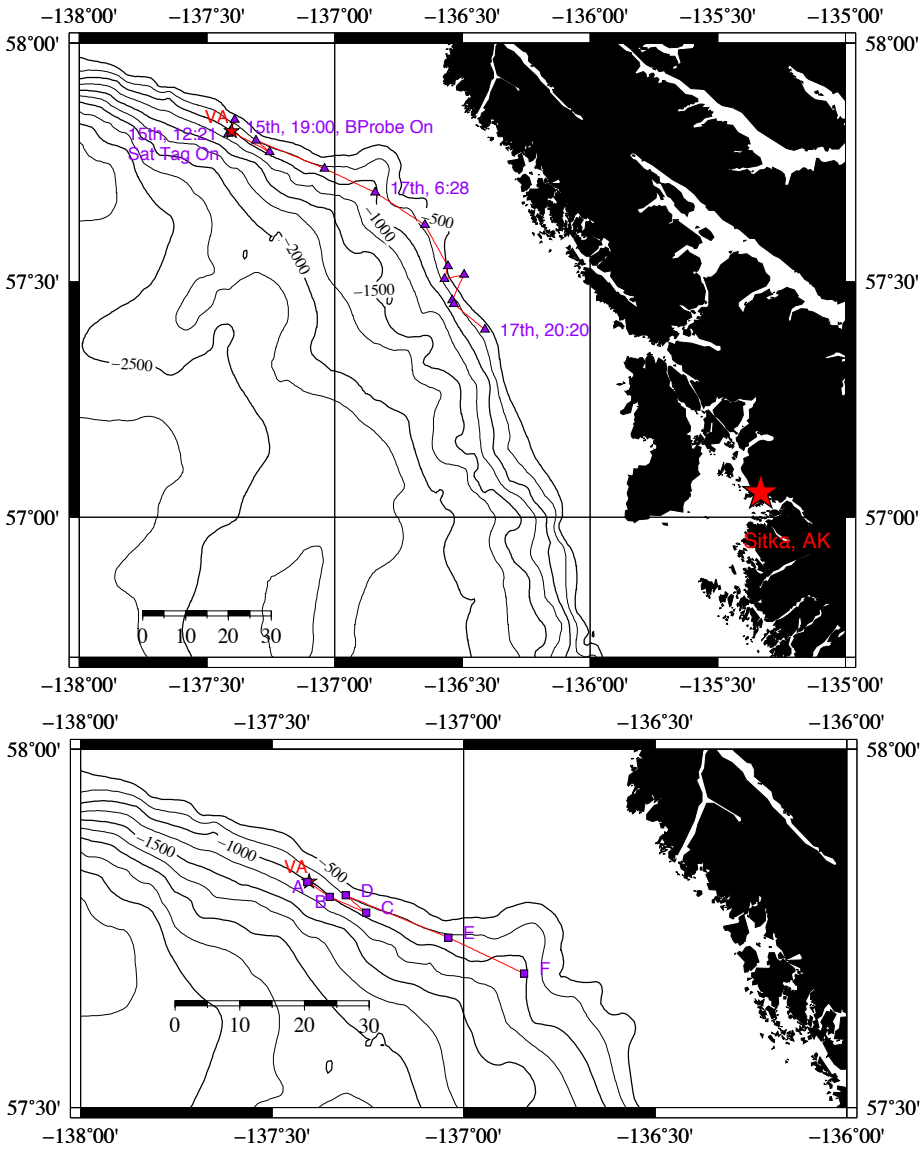

Figure V.1: Top panel: Contour map (depth in meters) of the study area. The location of Sitka and the vertical array deployment are marked with stars. The vertical array deployment occurred at 57.8160 N and 137.4037 W. The whale was tagged 1.4 km away from the vertical array on 15 August 2010 at 12:21 and was 80 km away on 17 August 2010 at 20:20. The satellite locations of the tagged whale during the vertical array deployment are marked with triangles. The precision of the satellite positions is 1 km. Bottom panel: Acoustic localizations at 300mm (A), 2 km (B), 5 km (D), 8 km (C), 22 km (E) and 35 km (F) range from the vertical array are marked with squares.

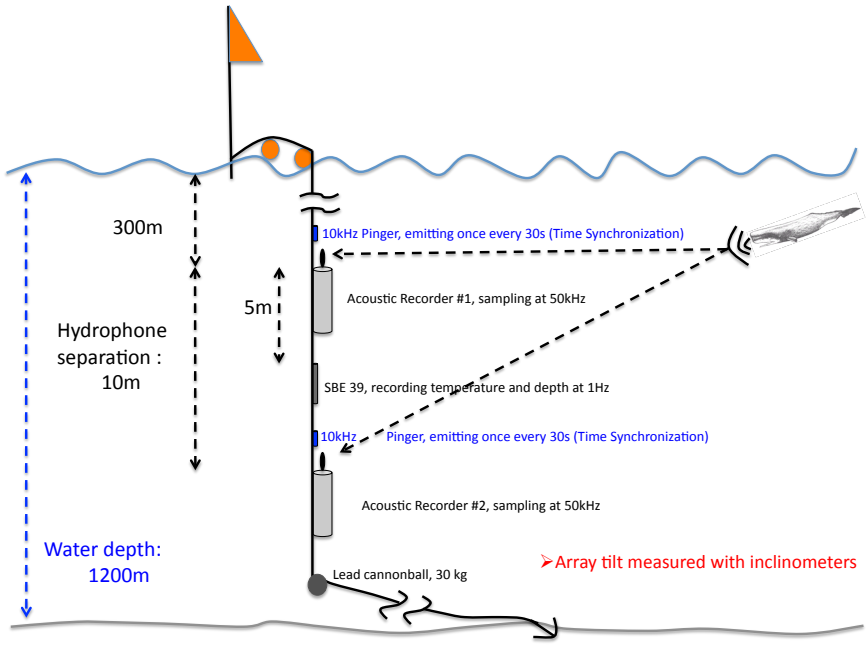

Figure V.2: Schematic of vertical array deployed on 15 August 2010 at 12:00 and recovered on 17 August 2010 at 8:45.

speed profile and reveals that the local sound speed minimum lies close to 300 m. This depth was selected for the subsequent array deployment, in the anticipation that some of the sound generated by the deep-diving animals would refract toward the sound speed channel with minimum surface or bottom interactions, thus minimizing its transmission loss and thus increasing the potential detection range. The fact that sperm whales often forage at 300-600 m depth even raised the possibility that sounds could become "trapped" in the channel for considerable distances. A second cast was made at the end of the experiment (3 days later) and revealed a very similar sound-speed profile. The average sound speed variation between the two casts was less than 0.1 m/s.

V.3.2 Satellite and bioacoustic tagging

During the same trip that deployed the array, newly developed tags in the Low Impact Minimally Percutaneous External electronics Transmitter (LIMPET) configuration were also deployed several times from a small boat launched by the F/V Northwest Explorer (Figure V.4) (Andrews *et al.*, 2008). The tags are based on the Wildlife Computers Mk10-A processor, which is able to log and transmit detailed information on diving behavior. The tags were programmed to transmit a time series of depth measurements every 2.5 minutes (with a depth resolution of 0.5 m); however, for every dive they also transmit more accurate data on the maximum dive depth (1-2% resolution), dive duration, overall dive profile shape, and post-dive surface interval, provided that enough surface time is available for transmitting the data via the Argos-system. Geographic locations of tags were determined by Service Argos (CLS America) using the Doppler shift created by the satellite passing overhead. For a high-quality "hit" the location accuracy was within 1 km. The tags have enough battery capacity for approximately 30 on days, so they were programmed to transmit every day for the first 20 days after attachment, and then the duty cycle was decreased to one transmission day every 3

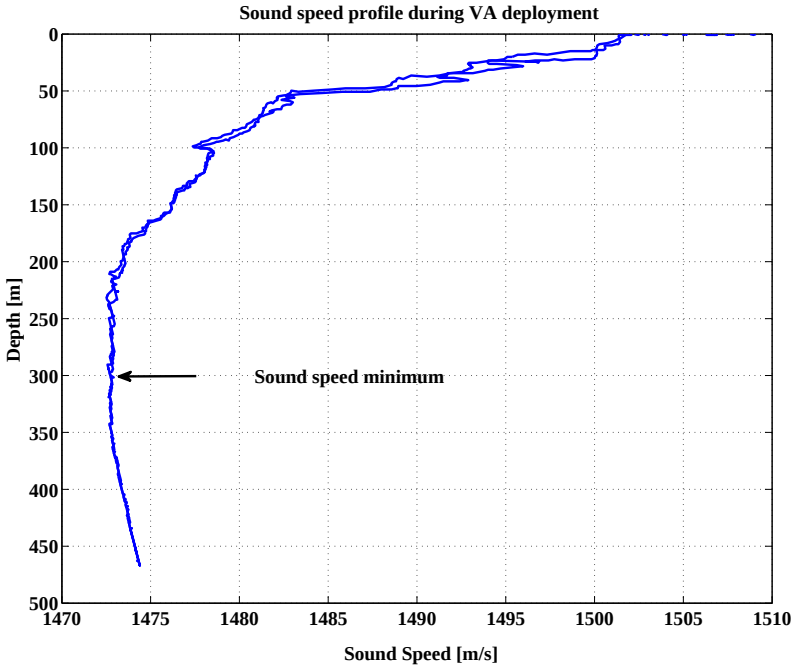

Figure V.3: Sound speed profile derived from a temperature-depth downcast and upcast taken before the vertical array deployment. The Mackenzie equation (1981) was used to derive the sound speed in sea-water as a function of temperature, salinity and depth, where the salinity was assumed to a uniform 32.4 psu over depth based on historical databases (Section V.3.1)

days over the next 30 days, and then once every 10 days thereafter. The LIMPET Mk10-A tags were deployed between 6 to 10 m from a whale using a pneumatic rifle and rely for attachment on two barbed titanium darts that penetrate around 6.5 cm into the dorsal ridge. Positioning a tag there aids radio transmission by lifting the tag as high away from the seawater groundplane as possible during surfacing.



Figure V.4: Depth-transmitting Mk10-A LIMPET satellite tag (Andrews *et al.*, 2008) with titanium attachment darts. (Photo courtesy of Russ Andrews)

A high-resolution digital bioacoustic B-probe sampling tag (Burgess *et al.*, 1998; Goldbogen *et al.*, 2006; Oleson *et al.*, 2007) was also deployed during the experiment (Figure V.5), once concurrently with a LIMPET tag. Besides sampling acoustic data, the B-probe contains a pressure sensor and a two-axis accelerometer (MXA2500GL, Memsic Inc., North Andover, MA 01845) with one axis parallel to the longitudinal axis of the probe. Data from the depth gauge and accelerometers are sampled at 1 Hz and stored within the tag. The tag was attached to the animal via two suction cups (manufactured by Canadian Tire Inc.), and deployed using a modified 4 m telescoping boat hook. After a certain length of time the passive

suction cups work their way loose from the animal, and a syntatic foam float (designed by Cetacean Research Technology, Seattle WA) on the tag assembly assures the system floats to the surface, where a radio beacon permits it to be detected and recovered using a directional Yagi antenna (Oleson *et al.*, 2007). The acoustic tag data analyzed in this paper were sampled at 4096 Hz, sufficient for detecting sperm whale regular clicks and creaks (Mathias *et al.* 2012).



Figure V.5: Satellite tag and B-Probe tag (Burgess *et al.*, 1998) deployed on the same sperm whale. Photo by SEASWAP in 2009; deployment courtesy of Cascadia Research Collective.

At 12:21 on 15 August 2010 a whale was tagged with a LIMPET satellite tag 1.4 km away from the vertical array, and was later tagged at 19:00 with a B-probe suction cup tag 300 m away from the vertical array. The B-probe stayed on the whale for 2.5 hours and provided high resolution acoustic, depth and orientation data for three full dives. Figure V.6 displays the whales dive profile recorded by the B-probe during those three dives, with the lower-resolution LIMPET tag data overlain on top. The LIMPET satellite tag continued to transmit location and

depth data until 30 August 2010, when it was 1000 km away to the South from the original tagging site. Figure V.7 displays the whale's dive profile and range provided by the satellite tag data during the vertical array experiment (15-17 August 2010).

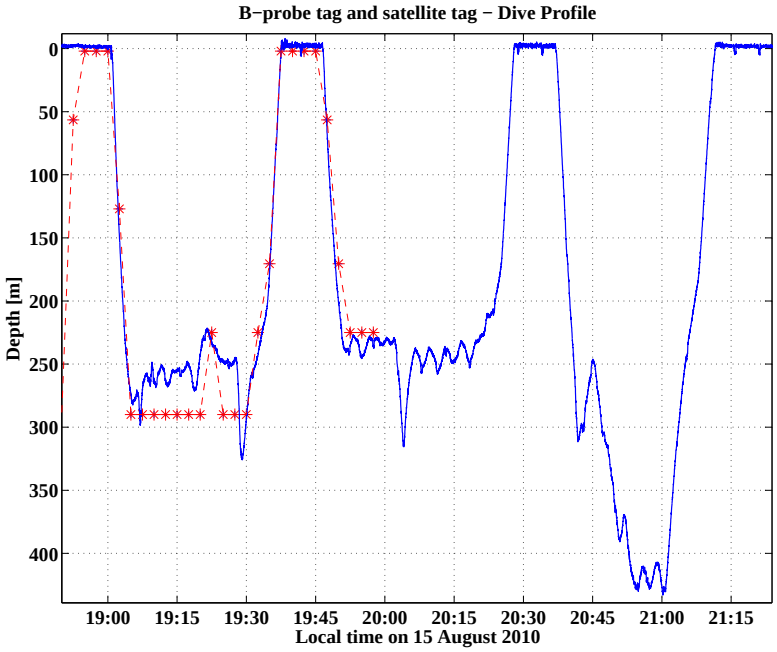

Figure V.6: Dive profile from B-probe tag (full blue line) deployed on 15 August 2010 at 19:00. The tag recorded three 40-minute dives. The satellite tag dive profile (only available until 20:00) is overlaid with a dashed red line. The satellite tag didnt provide data between 20:00 and 22:00 on 15 August.

Sperm whales were photographed for individual identification and compared with the Gulf of Alaska catalog of sperm whales. At least seven different sperm whales were sighted close to the vertical array during the two-day experiment (Table V.1). All whales had been seen previously in the EGOA. No longliners were present in the region, and the vertical array served as a decoy to attract and keep sperm whales in the area. The whale tagged with both a B-probe and a

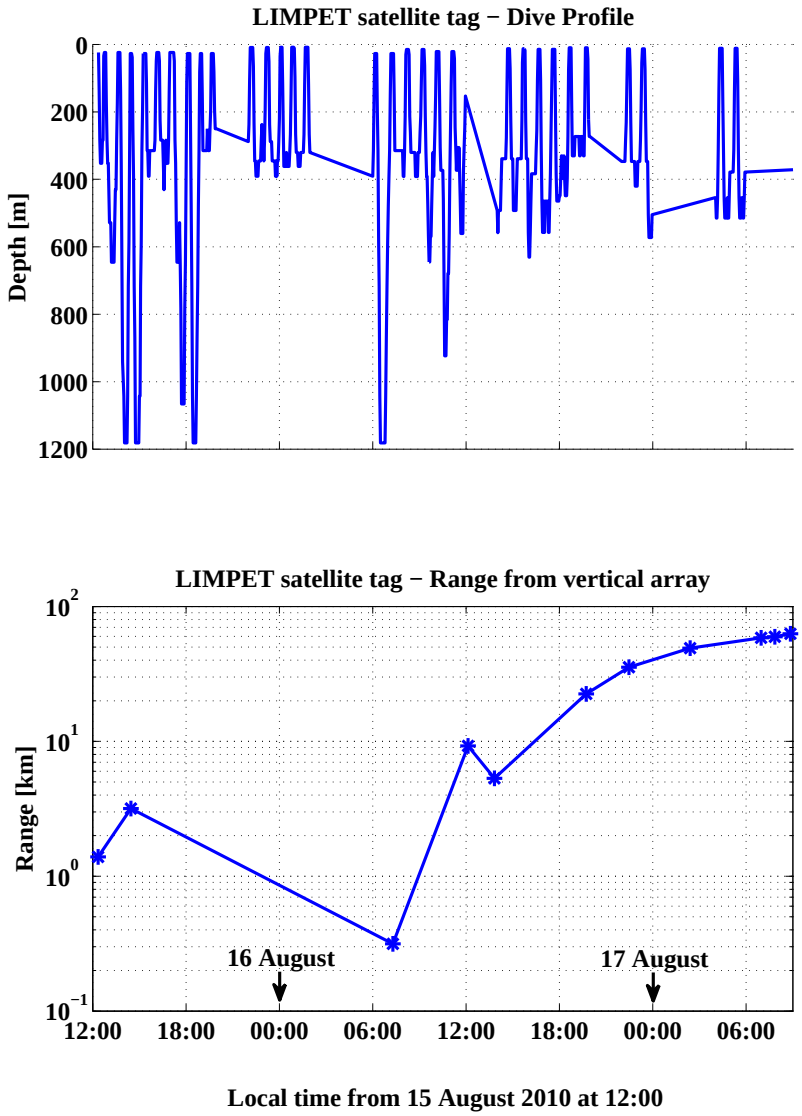

Figure V.7: Top panel: Dive profile from the LIMPET satellite tag. Bottom panel: Range of whale from vertical array, using ARGOS locations transmitted from the LIMPET tag.

satellite tag was recognized as GOA 025 and had been sighted in 2003 and 2004 close to fishing vessels in the Sitka fishing area. This whale will be referred as the tagged whale in the text.

Table V.1: Sperm whale sightings 15-17 August 2010 during the vertical array deployment, near the Spencer Split.

Whale ID	15 August 2010	16 August 2010	17 August 2010
GOA011	X		
GOA042	X	X	
GOA050	X	X	
GOA025	X		
GOA023	X	X	
GOA091	X		
GOA027		X	

V.4 Localization methods

The techniques presented in this section will be illustrated using data collected by the vertical array and the B-probe at the start of the first dive after the B-probe was attached, on 15 August 2010 between 19:01:00 and 19:04:00.

V.4.1 Time synchronization

Time synchronization of the two acoustic recorders (Unit 5, or top unit, and Unit 7, or bottom unit) is required in order to accurately measure the relative differences in click arrival times between the two units. The data needs to be synchronized to within a millisecond or less for optimum performance. Two acoustic pingers, each emitting a 10 ms pulse at 10 kHz every 30 seconds, were attached 1m above the top unit and 1 m above the bottom unit. The clock offset between the two acoustic recorders was obtained using only one pinger, while the second pinger was used to confirm the 10 m separation between the instruments.

A pulse time series from the top pinger was cross-correlated between both acoustic units to yield a relative time delay, after filtering both time series between

9.5 kHz and 10.5 kHz (Figure V.8). Since the pinger was 1 m away from the top unit and 11 m away from the bottom unit, the true relative travel time was known, and the necessary clock offset could thus be estimated. This time-synchronization operation was performed every 5 minutes throughout the two-day deployment. The initial offset between the top unit and the bottom unit was 0.419 s, and the resulting clock drift was determined to be linear at 0.026 s/hr (or 0.624 s/day).

V.4.2 Multipath pattern extraction when multiple whales are present

In this chapter the primary method for localizing a sperm whale requires measuring the relative arrival times of click multipath on and between the two acoustic units. The presence of multiple clicking whales complicates the task, especially whenever the whale of interest is not the closest (loudest) one. Two different techniques were used to extract the tagged whale click trains and multipath arrivals from a given array hydrophone, depending on whether bioacoustic probe data from the tagged whale was available.

V.4.2.a Multipath pattern extraction when bioacoustic sound data is available

Sperm whale clicks were automatically detected in the bioacoustic tag data by generating a series of 256 pt Fast Fourier Transforms (FFTs) (0.064 s window), overlapped 75%, and then integrating the power spectral density between 1200 and 1900 Hz. If a value exceeded a running-average estimate of background noise level by 20 dB, the presence of a click from the tagged animal was flagged; otherwise, the information was used to update the running average, which equalized over 15 s. This 20 dB threshold was selected to exclude click sounds from nearby non-tagged whales; the output of the automated click detector was manually spot-checked to confirm that clicks not produced by the tagged animal were not logged

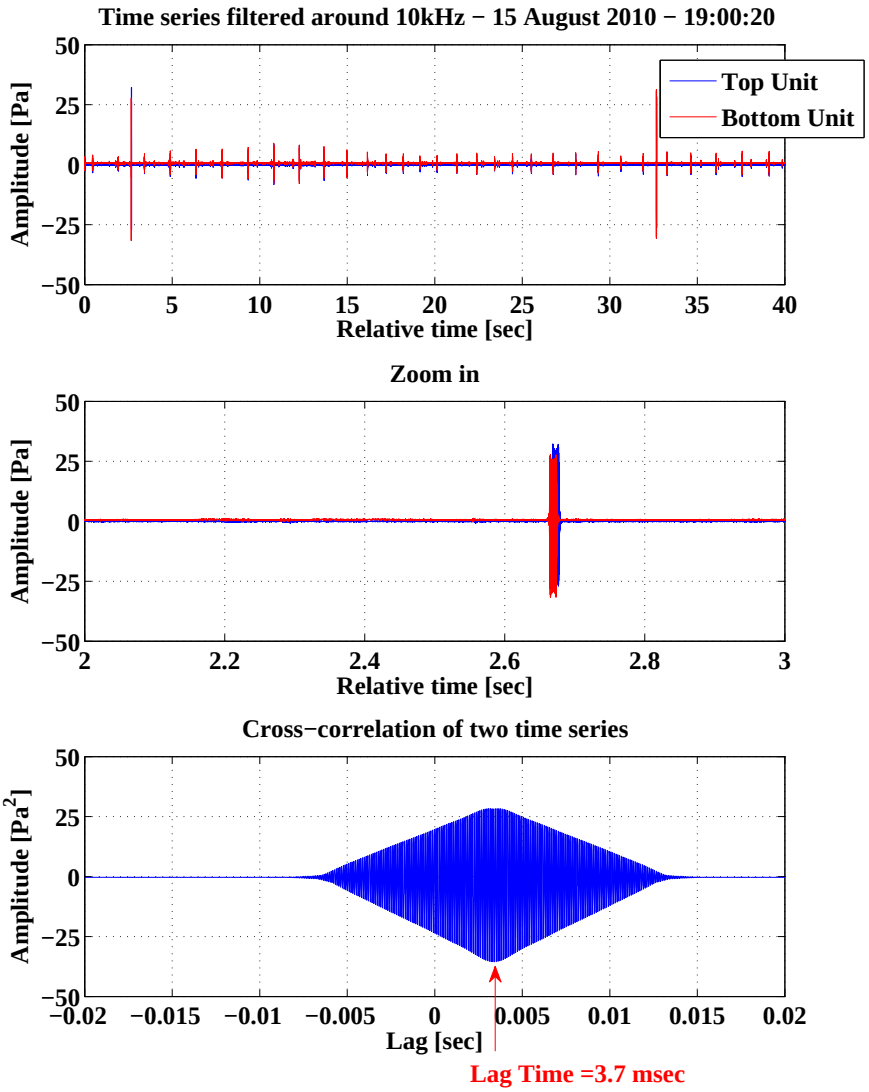

Figure V.8: Time synchronization of two acoustic recorders. The recorder time series are filtered between 9.5 kHz and 10.5 kHz on both units. Top and middle panels show both time series, and bottom panel shows the cross-correlation function between the series. The large-amplitude signals at 2.6 s and 33 s are pinger signals; other impulsive sounds are sperm whale clicks.

as detections. Similarly, all sperm whale clicks and associated multipath arrivals were detected on one hydrophone of the vertical array acoustic data by generating a series of 512 pt FFTs (0.0102 s window), overlapped 75%, and then integrating the power spectral density between 5000 and 9000 Hz. This frequency range excluded vessel noise (below 4 kHz) and pinger pulses (10 kHz). The detection threshold on the array data was set to 5 dB.

Since multiple sperm whales were present in the area and vocalizing simultaneously, the tagging data was used to flag the tagged whale click trains and multipath arrivals in the vertical array acoustic data. The B-probe depth and acoustic data were used to determine when the tagged whale began a dive, and when a sequence of its clicks began and ended. These events were then used to manually identify the first and last direct and surface-reflected path arrival times of the tagged whale click train on the vertical array hydrophone, using a MATLAB graphical user interface. Figure V.9 displays a spectrogram of 30 s of data recorded by both the B-probe tag and the top vertical array unit as the tagged whale started descending during its first dive after being tagged. Flagging the first clicks at the start of a dive is particularly straightforward, as the first surface-reflected path is merged with the direct path at the start of the dive, creating a distinctive pattern on a waterfall plot of a given click sequence (Figure V.10). As the whale descends, the relative time arrival difference between those two paths gradually grows, until they can be visually separated on a 1024 pt FFT spectrogram (50 kHz sampling rate) when the whale is around 50 m depth.

For a given first (direct-path) pulse arrival, the normalized autocorrelation was performed between the filtered 10 msec pulse waveform and the following 2 seconds of data on the same hydrophone:

$$R(\Delta t) = \frac{\sum_{t=1}^{n} x_t \; x_{t+\Delta t}}{\sqrt{\sum_{t=1}^{n} x_t^2 \quad \sum_{t=1}^{n} x_{t+\Delta t}^2}} \tag{V.1}$$

where n is the number of samples in the waveform, x_t is the amplitude of the

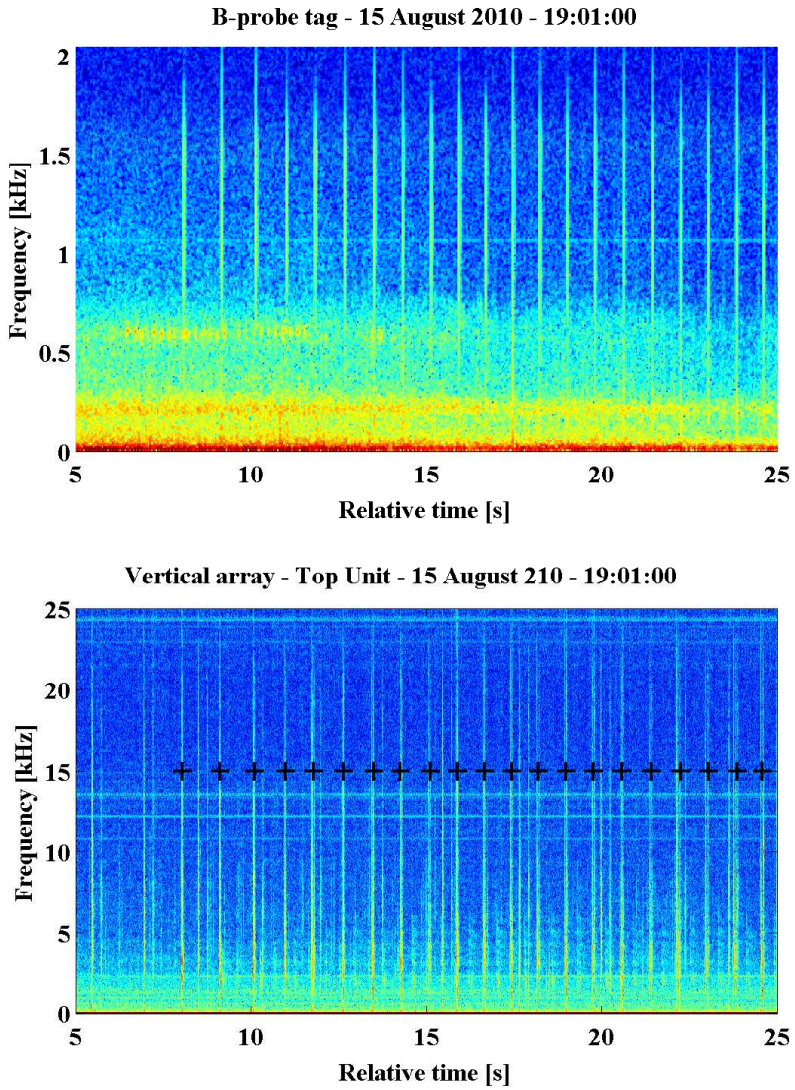

Figure V.9: Spectrogram of acoustic data from B-probe (top panel) and associated recording on top recorder of vertical array (bottom panel). The tagged whale has just begun a dive and starts a click train at 19:01:05.

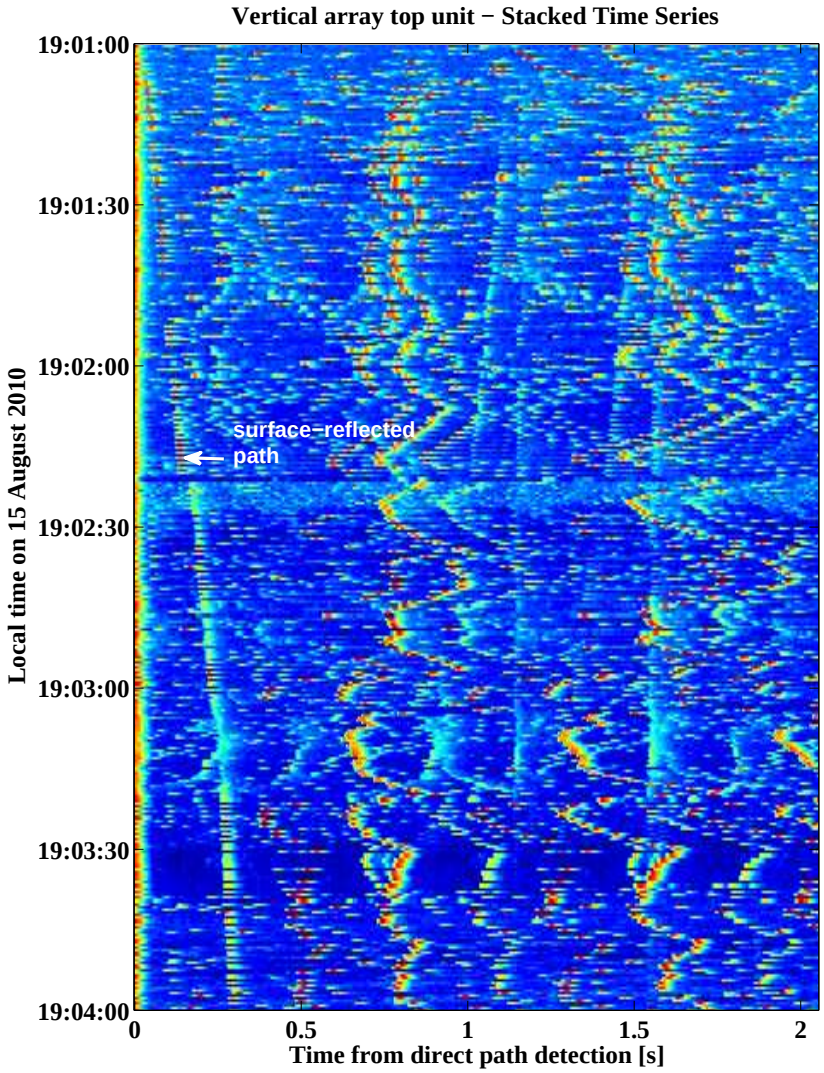

Figure V.10: Waterfall plot of the corresponding stacked multipath arrival patterns on the top acoustic recorder of the vertical array between 19:01 and 19:04 on 15 August 2010. The surface-reflected path (indicated by a white arrow) is merged with the direct path at the start of the dive, but as the whale gets deeper, the relative time arrival difference between those two paths gradually grows, until they can be visually separated on the stacked waterfall plot.

waveform at time t , and $x_{t+\Delta t}$ is the amplitude of the waveform at time lag $t+\Delta t$. If x and y are of different lengths, the shortest waveform is zero-padded. Equation (V.1) might technically be considered a normalized cross-correlation, as one signal segment is substantially longer than the other, with no time overlap between the two. However, in this chapter the term "autocorrelation" will continue to be used, as the two signals are derived from the same time series, even though Eq. (V.1) does not follow the formal definition of the autocorrelation. All correlations discussed from this point are implicitly assumed to be normalized, such that the maximum possible output for perfect correlation is 1.0.

The largest peak in the absolute value of the autocorrelation output was selected as the next tagged whale direct path arrival if Eq. (V.1) exceeds 0.5 at that time. The second largest peak amplitude of this function was selected as the surface-reflected path, and other peaks above 0.1 indicated other potential multipath arrivals.

This process was repeated using the most recent direct path waveform until the click train ended, so that no peak in the autocorrelation output exceeds the threshold. Once all the direct path arrivals had been flagged, the multipath arrivals were extracted using a manual waterfall plot analysis based on the hypothesis that multipath arrivals change only gradually over time (Tiemann *et al.*, 2006). More specifically, the direct-path arrivals were stacked in a waterfall plot and consistent relative arrivals were manually flagged (e.g. Figure V.10). The same relative arrival needed to occur at least 5 times within a 10 click sequence (tolerance of 5 ms) to be flagged as a tagged whale multipath arrival. This was done using the entire click sequence and associated multipath. The whole process was repeated on the bottom vertical array data stream. For every direct path arrival detected on both array hydrophones, the relative arrival times of all potential multipaths was saved.

The autocorrelation between the tagged whale's direct-path click and another whale's direct path click never exceeded 0.15 (Figure V.11). So if other

whale sounds were present, they would have only flagged as potential multipath arrivals and thus subsequently excluded by the waterfall plot analysis.

To confirm that the final extracted times arose from the tagged whale, the inter-click interval (ICI) sequence of the tagged sperm whale was extracted from the B-probe click detection times and compared with the ICI of the direct path arrivals estimated from the array (Figure V.12).

This procedure thus extracted the tagged whale direct path and associated multipath arrivals on both array hydrophones for the whole three-dive duration of the B-probe tag data. Section V.4.2.c discusses how these arrivals were matched between array hydrophones.

V.4.2.b Multipath pattern extraction when only satellite tag data is available

The bioacoustic tag released after three dive cycles, so as the tagged whale swam further away from the vertical array, the exact click pattern of the animal was no longer available. Thus, a slight alteration was required in the previously-described technique.

The satellite tag data provided the start time of most of the dives (when the connection between the tag and the Argos-system was successful), and a sperm whale usually starts clicking within two minutes of the start of a dive, so the satellite tag data could provide pretty good estimates when to expect a new click train to appear in the array data. By stacking the time series of all detected clicks as a waterfall plot (Figure V.10), it became possible to identify the click train of a whale that has just started vocalizing while starting its descent from the surface. The surface-reflected path is merged with the direct path near the surface, but the relative arrival time differences between those two paths gradually grows as the whale gets deeper, until the two paths can be visually separated, creating a distinctive pattern in the waterfall plot. Once the surface-reflected path becomes visually distinct from the direct path, all multipath arrivals were then manually

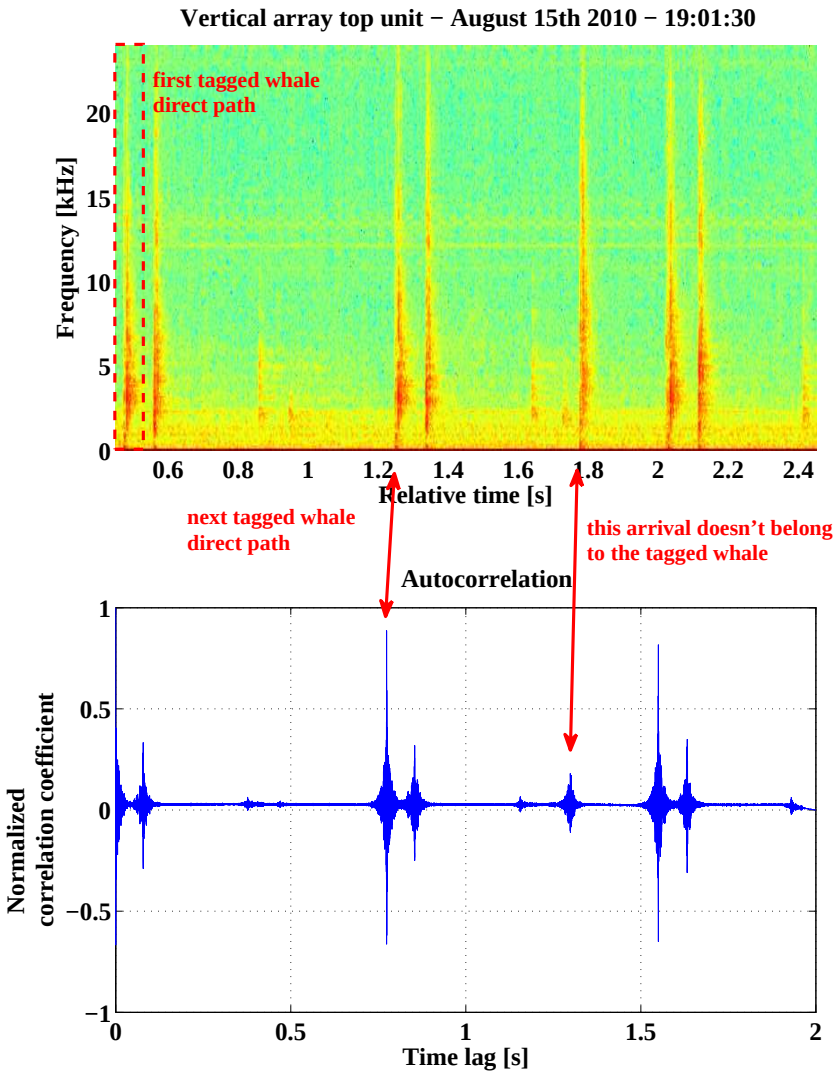

Figure V.11: Top panel: Spectrogram of direct path, surface-reflected path and bottom-reflected path recorded on 15 August 2010 at 19:01:30 on vertical array top hydrophone. Bottom panel: Normalized autocorrelation (Eq. (V.1)) between first 0.1 s of data (first tagged whale direct path) and the remaining 2 s of data shown in the top panel.

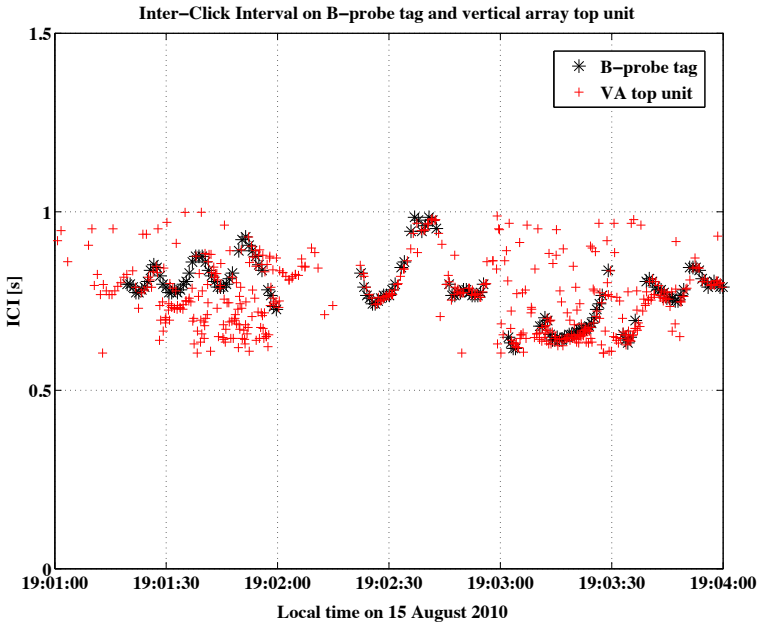

Figure V.12: Tagged whale inter-click interval (ICI) derived from B-probe and associated vertical array (VA) top unit between 19:01 and 19:04 on 15 August 2010.

extracted by plotting 10 s of the filtered time series (Figure V.13), starting from the time when the surface-reflected path becomes distinguishable from the direct path. This permitted consistent multipath arrival patterns to be extracted from the tagged whale.

At very long ranges (>20 km), the click signal-to-noise ratio is so low that the automated incoherent energy detector (Section V.4.2.a) fails. However, a manual inspection of the spectrograms allowed the start of a new click train to be noted, and the multipath arrival times to be manually extracted. At the end of this process, the tagged whale direct path and associated multipath arrivals have been extracted on both array hydrophones during a 10 s window, selected a few minutes after the satellite tag reported the start of a dive.

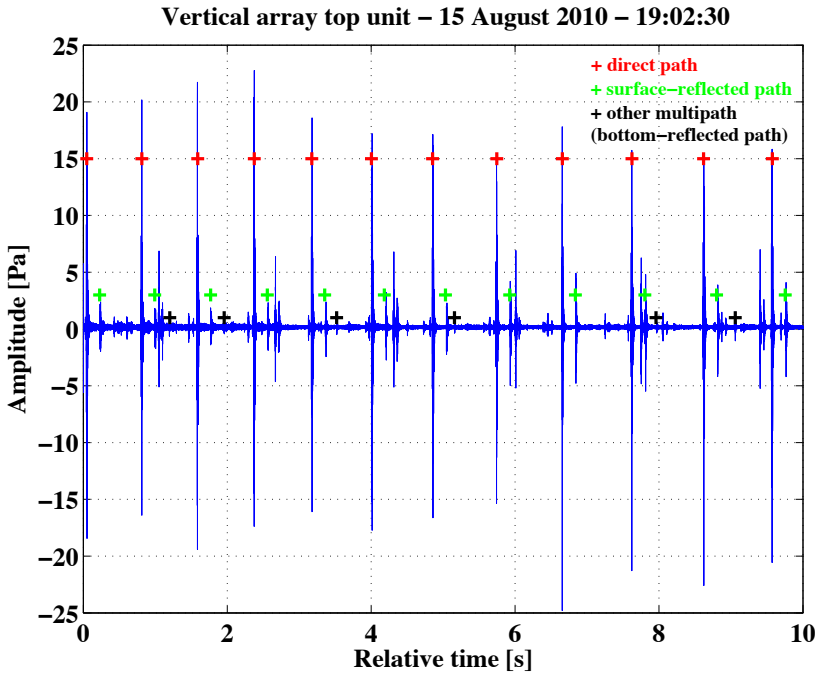

Figure V.13: Filtered time series recorded on vertical array top recorder on 15 August 2010, with tagged whale multipaths labeled manually.

V.4.2.c Computing arrival angles of ray paths

Once all ray paths from a click were flagged on the top array hydrophone, matching arrival times needed to be found on the bottom hydrophone. For each click's first ray path arrival, a short time series segment was extracted, starting 0.2 s before the arrival and ending 0.2 s after the arrival. This segment was then cross-correlated with 2 seconds of data from the bottom hydrophone time series, starting 1 s before the first path arrival time on the top hydrophone (Figure V.14). The largest peak in the resulting normalized cross-correlation output corresponds to the relative arrival time of the arrival on the top hydrophone. Because the relative arrival times of additional paths on the bottom hydrophone have already been computed, the relative arrival times of all ray paths between the hydrophones phones are then readily obtained. The relative arrival time difference of a given ray arrival in seconds, $TDOA_{multipath}$, translates into a vertical arrival angle $\alpha_{multipath}$ (in radians) if the element separation is known:

$$\alpha_{multipath} = asin\left(\frac{c_{water}\ TDOA_{multipath}}{D} \right) , \tag{V.2}$$

where c_{water} is the sound speed, set to 1470 m/s, and D is the hydrophone separation in m, set to 10 m. A 0 deg arrival angle corresponds to a horizontal path, and a positive angle corresponds to a path arriving from the surface. The expected angular resolution of an array θ (in radians) at broadside is a function of array aperture and frequency (Johnson and Dudgeon, 1993):

$$\theta = 1.22\ \frac{\lambda}{D} , \tag{V.3}$$

where λ is the wavelength of the source in m, and D is the hydrophone separation in m, set to 10 m. The expected angular resolution is thus 0.7 deg at 15 kHz, a frequency component usually detected at shorter ranges. At larger ranges the higher frequency components get stripped from the signal, yielding a typical frequency of 6 kHz, which provides a lower resolution of 1.7 deg.

In the example provided in Figure V.14, both tagged whale ray paths arrived first at the top hydrophone, indicating that the whale was shallower than the vertical array. The first (direct) path arrived 4 ms earlier on the top hydrophone, which corresponds to a vertical angle of 54 deg. The different relative arrival times of the second ray path on both hydrophones, relative to the direct path on each phone, can then be recast as a vertical arrival angle for the second path.

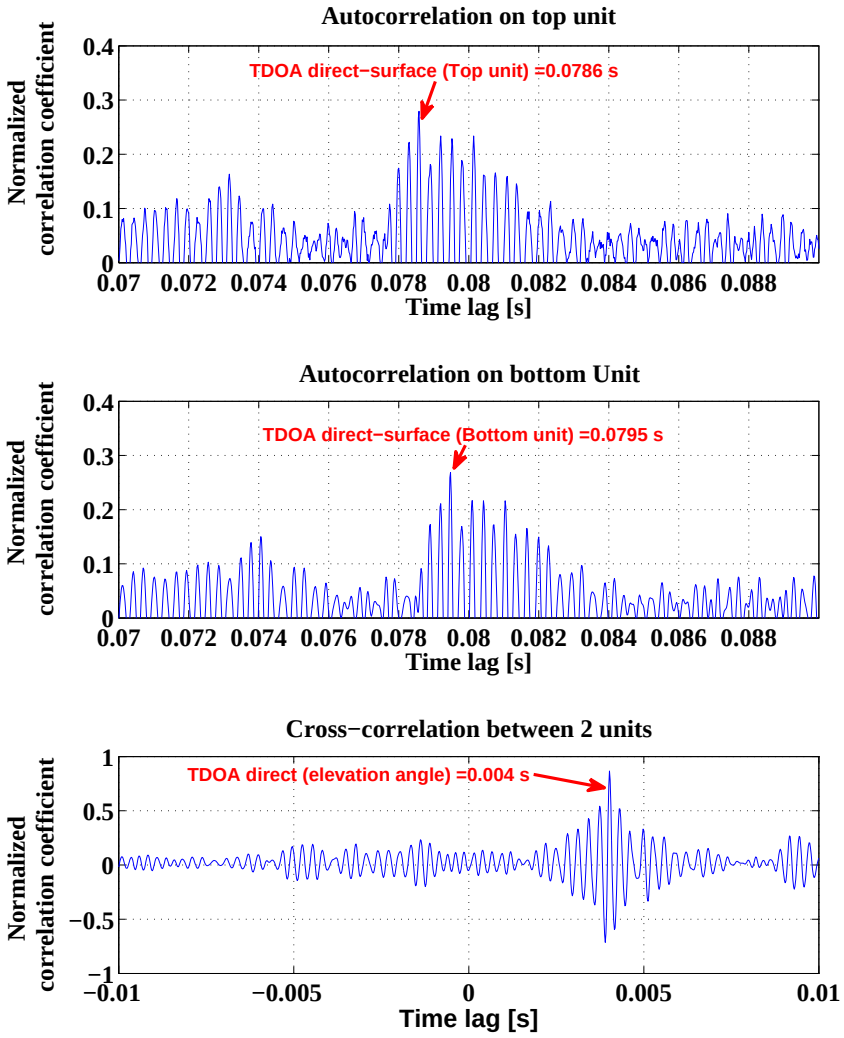

Figure V.14: Top panel and middle panel: autocorrelation of time series recorded on the vertical array on 15 August 2010 at 19:01:30 for estimation of multipath time difference of arrival (TDOA). Bottom panel: cross-correlation of direct path time series for estimation of vertical elevation angle. The normalized correlation coefficient is defined in Eq. (V.1).

V.4.3 Analytical formulas for sperm whale tracking at short ranges

At ranges close to the vertical array, the acoustic multipath arrives at steep angles, and thus does not refract much through the water column. For this reason at short ranges the acoustic propagation (ray) paths can often be assumed to be straight lines, and analytic formulas can be used to derive the whale's location. Section V.5.1 discusses at what ranges ray-refraction effects cannot be neglected.

V.4.3.a Single hydrophone: multipath time arrivals

At very close ranges (less than 2 km) the surface-reflected path and bottom-reflected path from a click can be isolated in time from the direct path received on one hydrophone, and the whales depth Z_w and range R_w from a single hydrophone can be determined (Thode *et al.*, 2002):

$$P_{bd} = c_{water}\ dt_{db}\ ,$$
$$P_{sd} = c_{water}\ dt_{ds}\ ,$$
$$P_d = 4H\ (H - z_a)\ -\ {P_{bd}}^2\ +\ {P_{sd}}^2\ \left(1 - \tfrac{H}{Z_a}\right)\ ,$$
$$P_d = 0.5\ \frac{P_d}{P_{bd}\ +\ P_{sd}\ \left(\frac{H}{Z_a} - 1\right)}\ ,$$

$$Z_w = 0.25\ P_{sd}\ \left(\frac{2P_d\ +\ P_{sd}}{z_a}\right)\ , \tag{V.4}$$

$$R_w = \sqrt{{P_d}^2\ -\ (Z_w - z_a)^2}\ , \tag{V.5}$$

where dt_{db} is the time difference of arrival in seconds between the direct path and the bottom-reflected path,dt_{ds} is the time difference of arrival in seconds between the direct path and the surface-reflected path, c_{water} is the 1470 m/s sound speed, H is the 1200 m water depth, and z_a is the 300 m hydrophone depth.

Figure V.15 illustrates the problem geometry. The autocorrelation technique defined in Section V.4.2.a was used to determine the relative time arrival

differences between the direct path and the surface and bottom-reflected paths. The relative difference in time arrivals between the direct path and the surface and bottom-reflected paths are the largest peaks of the positive lag autocorrelation function (Eq. (V.1), Figure V.14).

At short tracking ranges this technique was a useful "sanity check" to confirm that the acoustic data were being processed correctly when more complex methods were applied.

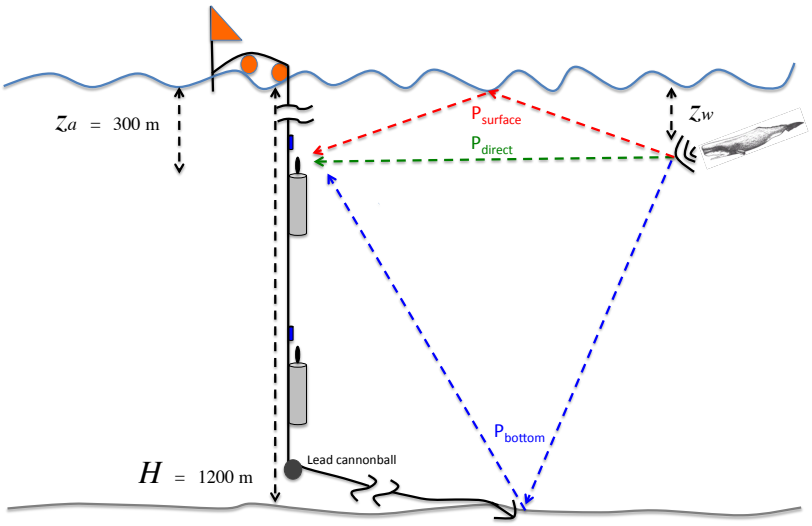

Figure V.15: Schematic illustrating analytical method for estimating depth and range of a sperm whale using a single hydrophone (Section V.4.3.a, Eqs. (V.4-V.5)).

V.4.3.b Two hydrophones: multipath time arrivals and arrival angles

While the presence of bottom-reflected multipath permits depth and range tracking with a single hydrophone, the technique only works over short ranges and requires considerable knowledge of the regional bathymetry. If two hydrophones are available, the requirement of a third propagation path (e.g. bottom-reflected path) can be eliminated; only a second (e.g. surface-reflected) path is

required. Stated another way, whenever a surface reflection from a click can be detected on two hydrophones and can be isolated in time from the first ray path, then the whales depth Z_w and range R_w can be determined without knowing the bottom depth (Thode *et al.*, 2002):

$$Z_w = \frac{c\ t_{ds,2}\ (2t_{d,2} + t_{ds,2})}{4z_{a,2}}\ , \tag{V.6}$$

$$R_w = {P_d}^2\ -\ (z_w - z_a)^2\ , \tag{V.7}$$

$$\text{with } P_d = \frac{c_{water}\ (t_{ds,1} - S\ (dt_{ds,1} + 2dt_{dd}))}{2\ (S-1)}\ ,\ S = \frac{dt_{ds,2}\ z_{a,1}}{dt_{ds,1}\ z_{a,2}}\ ,\ t_{d,2} = \frac{P_{d,2}}{c_{water}}\ ,$$

where $dt_{ds,1}$ is the time difference of arrival between the direct and surface-reflected paths on the top hydrophone, $dt_{ds,2}$ is same quantity measured on the bottom hydrophone, dt_{dd} is the time difference of arrival of the direct path between both hydrophones, c_{water} is the sound speed set to 1470 m/s, $z_{a,1}$ is the top hydrophone depth set to 300 m, and $z_{a,2}$ is the bottom hydrophone depth set to 310 m.

Figure V.16 illustrates the problem geometry. The relative difference in arrival times between the direct and surface- reflected paths was estimated by computing the autocorrelation of each time series, as discussed in Section V.4.2.a. The arrival angle of the direct path was estimated by computing the cross-correlation between the direct path time series recorded by the two acoustic units, as discussed in Section V.4.2.c. Figure V.14 provides an example where the tagged whale direct and surface-reflected paths arrived first at the top hydrophone, indicating that the whale was shallower than the vertical array. By plugging the measured relative difference in time arrivals into the analytical formulas (Eq. (V.6) and Eq. (V.7)), the whale was estimated to be at 68 m depth and 190 m range. The B-probe data indicated that the animal was indeed at 65 m depth at this time.

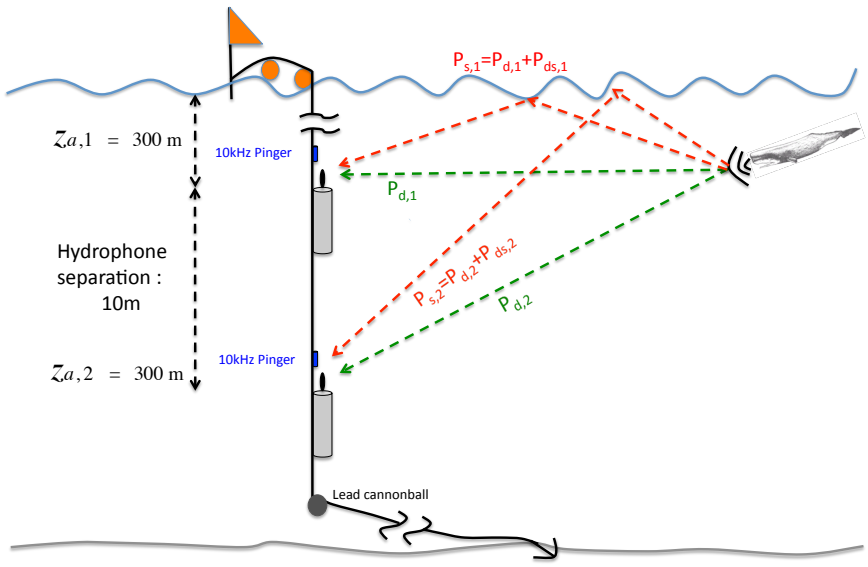

Figure V.16: Schematic illustrating analytical method for estimating depth and range of a sperm whale using two hydrophones (Section V.4.3.b, Eqs. (V.6 -V.7)).

V.4.4 Using a ray-tracing numerical model for tracking

Unlike the analytical formulas listed above, the use of a numerical ray-tracing algorithm should be viable at all source ranges and depths, provided that an accurate sound speed profile is used, and a propagation grid size of sufficient resolution is selected. A key advantage of numerical modeling is that it accounts for variations in sound speed over depth and range, thus eliminating the systemic errors from the rectilinear assumptions and capturing additional ray paths not predicted by them (e.g. rays trapped in the sound-speed minimum channel, and rays that refract, instead of reflect, from the surface). An additional advantage of numerical modeling is that a given ray path does not need to be flagged as a direct, surface- reflected, or bottom-reflected path in the data, a task that can be difficult when multiple animals are vocalizing simultaneously.

The model-based localization algorithm requires three fundamental steps. First, the relative multipath arrival times and arrival angles must be extracted from the recorded acoustic data, as already discussed in Section V.4.2. Second, a numerical propagation model must be configured to generate simulations of the viable ray paths with a set of acoustic sources placed on a range-depth grid in a realistic propagation environment. Every candidate location generates a series of predicted relative ray path arrival times and vertical arrival angles, often dubbed "replicas" in the tracking literature. Finally, the measured and modeled arrival patterns are compared to generate an "ambiguity surface," which provides a visual representation of the most probable whale position relative to the array as a function of range and depth. These last two steps are now reviewed in detail.

V.4.4.a Replica generation

The Gaussian beam-tracing acoustic propagation model BELLHOP (Porter and Bucker, 1987) was used to simulate the relative arrival times and angles of ray paths received by a hydrophone for hypothetical sources located at various

depths and ranges. The Gaussian ray-tracing model allows for depth-dependent sound speed profiles and has been previously employed in sperm whale tracking research (Tiemann *et al.*, 2004; Tiemann *et al.*, 2006; Nosal *et al.*, 2006; Nosal *et al.*, 2007). While the model can also incorporate range-dependent effects, a single range-independent sound speed profile was used, based on the sound speed profile measured during the vertical array deployment (Figure 17), as discussed in Section V.3.1. Given the lack of additional environmental data, assuming range independence is reasonable, given that the scale of variability of oceanographic features in this region is tens to hundreds of kilometers, at least in regions not adjacent to large straits of the Inside Passage (e.g. Chatham Strait).

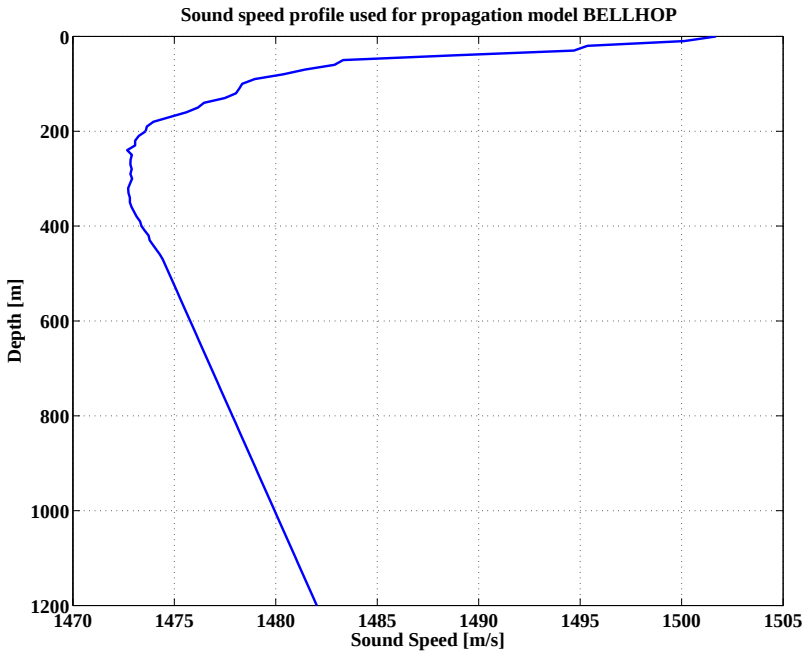

Figure V.17: Sound speed profile used in propagation model BELLHOP. The profile is derived from the sound speed profile of Figure V.3 for depths above 450 m and linearly interpolated for depths below 450m.

Simulated sources were spaced every 10 m in depth down to 1200 m and

every 10 m in range out to 40 km range from the receiver, which was modeled at 300 m depth. For each candidate location 200,000 rays were launched, since a fine angular sampling is required to solve for "eigenrays," or ray paths connecting a given source and receiver. A ray had to pass within 5 m to the receiver to be counted as an eigenray. The model assumed a source frequency of 6000 Hz, the averaged peak frequency of clicks recorded on the vertical array over the three-day experiment. A frequency is required by the ray-tracing algorithm in order to model how the effective width of the propagating Gaussian beam "diffuses" over range, but the model output is relatively insensitive to the frequency chosen. Geoacoustic properties of the sea floor were assumed to be typical of sand: density 1.9 g/cm3, compressional wave speed 1650 m/s, and compressional wave attenuation of 0.8 dB/wavelength. While required by the program to run, these values are actually of no practical importance, as ray paths that interact with the bottom in this model are rejected. Figure V.18 displays an example of propagation paths that dont reflect off the bottom modeled up to a 6 km range, and illustrates the transition from reflected to refracted paths.

The model outputs the travel times of all eigenrays that connect a candidate source position, including any paths reflecting from the surface and bottom. For every eigenray the model also provides the transmission loss and vertical launch and arrival angles. Figure V.19 displays an example of the predicted direct and surface-refracted acoustic ray paths between a whale at 500m depth and a recorder at 300m depth, along with the associated travel times and arrival angles at the receiver.

Bottom-reflected paths were excluded from the output since the bottom depth is only known precisely at the vertical array location, and the bottom bathymetry is highly variable in the area. Besides, bottom-reflected paths quickly disappear at larger ranges (Section V.5.1) so any long-range tracking method needs to exclude bottom-interacting multipaths from consideration.

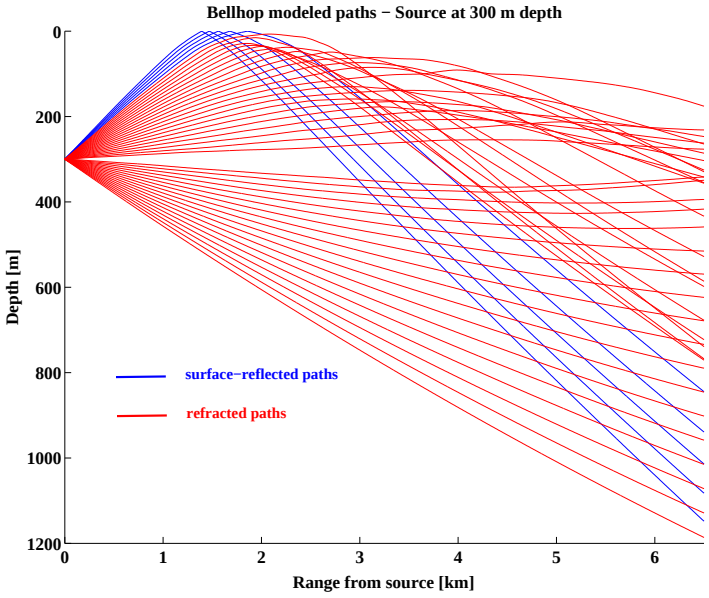

Figure V.18: Propagation paths modeled with BELLHOP up to a 6 km range with a source at 300 m depth, using the sound speed profile of Figure V.17.

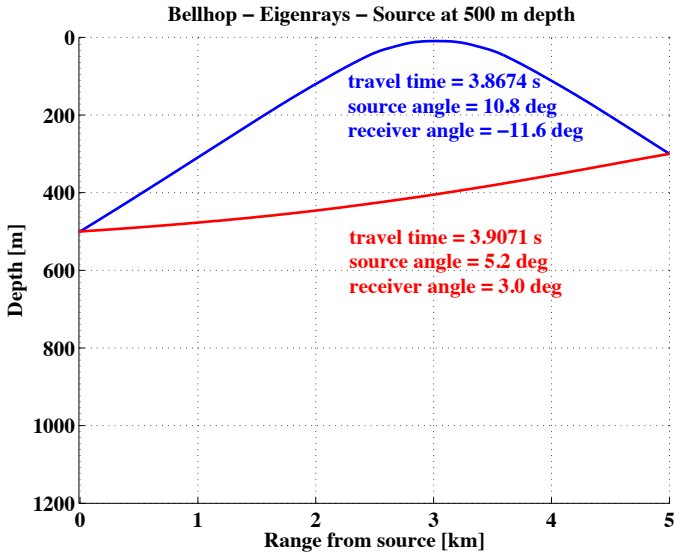

Figure V.19: Predicted direct and surface-refracted eigenrays between a whale at 500 m depth and a recorder at 300 m depth.

V.4.4.b Producing an ambiguity surface using scoring

The ambiguity surface is a two-dimensional function that displays some metric of similarity between the modeled and measured ray paths, as a function of range and depth locations along a vertical grid extending from the array location, which defines the origin of the range axis. The scoring method discussed here for producing the ambiguity surfaces was inspired by Tiemann *et al.* (2006), but has been extended to incorporate elevation angle information along with relative arrival time.

The score for each candidate source position was obtained by counting the number of modeled eigenrays from that position that share the following characteristics with the measured data: the same relative arrival time, to within 5 ms; and the same vertical elevation angle, to within 1 deg. These tolerances were derived from the average standard deviation of the measured arrival times and arrival angles of 10 sets of 10 consecutive clicks, selected from times spanning the entire deployment. Excess arrival ray paths in the modeled data are not penalized. The maximum possible score is $2M - 1$, where M is the number of ray paths per click in the measured data. This scoring process was repeated for all candidate source positions and the scores were assembled into ambiguity surfaces. High scores, indicating likely source positions, are represented by red regions.

For example, on 15 August 2010 at 13:49 an arrival pattern consisting of two ray paths was extracted from the vertical array acoustic data. The arrival angles of the two paths were -11 and 5 deg (recall that a positive sign means that the ray path is arriving from above the array), with a measured relative arrival time of 0.046 s. For a source at 400 m depth and 5800 m range, the model predicts two ray paths with arrival angles of -7.4 and 1.4 deg, and a relative arrival time of 0.013 s. Thus, the score for this location is zero. By contrast, the model predicts that a source at 580 m depth and 5800 m range will generate two ray paths with arrival angles of -10.5 and 5.8 deg, and a relative arrival time of 0.043 s. Thus,

this modeled source location gets a score of 3, the highest possible for data with two ray paths per click event.

V.4.4.c Producing an ambiguity surface using weighted mean-square error

Another approach for creating an ambiguity surface is to compute the mean-square error (MSE) between the measured and modeled relative arrival times (Nosal *et al.*, 2007). The present case also requires the inclusion of the measured and modeled arrival angles, which requires a more complex unit normalization.

Two different MSE strategies were studied. First the weighted mean-square error L_{WMS} at each point of the grid (r, z) was computed for each combination of 2 modeled ray paths:

$$L(r,z)_{WMS} = L_1 \ + \ L_2 \ + \ L_3 \ , \tag{V.8}$$

with:

$$L_1(r,z) \ = \ \frac{[dT_{mod}(r,z) \ - \ dT_{meas}]^2}{{\sigma_{time}}^2} \ ,$$

$$L_2(r,z) \ = \ \frac{[\alpha 1_{mod}(r,z) \ - \ \alpha 1_{meas}]^2}{{\sigma_{angle}}^2} \ ,$$

$$L_3(r,z) \ = \ \frac{[\alpha 2_{mod}(r,z) \ - \ \alpha 2_{meas}]^2}{{\sigma_{angle}}^2} \ ,$$

where $dT_{mod}(r,z)$ is the modeled arrival time difference between two ray arrivals on the top hydrophone at location (r,z), $dT_{meas}(r,z)$ is the measured arrival time difference between two multipath arrivals on the top hydrophone at location (r,z), $\alpha 1_{mod}(r,z)$ is the modeled elevation angle of the first,second multipath arrival at location (r,z), $\alpha 1_{meas}(r,z)$ is the measured elevation angle of the first,second

multipath arrival at location (r, z), σ_{time} is the estimated standard deviation of the measured arrival time differences, and σ_{angle} is the estimated standard deviation of measured elevation angles. $\sigma_{time}$was set to 5 ms and σ_{angle} was set to 1 deg.

The total error L_{tot_WMS} at each point of the grid is then the minimum value of L_{WMS} among all the possible combinations of 2 modeled paths:

$$L_{tot_WMS}(r, z) = min\ [L_{WMS}(r, z)]\ . \tag{V.9}$$

Dividing each individual error term by its standard deviation lowers the weight of components with a high variance relative to the mean. The relative standard deviation of the measured arrival angles σ_{angle} is larger than the relative standard deviation of the measured arrival time differences σ_{time} , so the arrival time measurements dominate the final error L_{tot_WMS}.

An alternative normalization achieves more equal weighting between angles and arrival times by dividing the normalized errors by the maximum error encountered in the simulation for that term. The error L_{NMS} at each point of the grid then becomes:

$$L_{NMS}(r, z) = \left[\frac{L_1(r, z)}{\max_{r,z}(L_1)} + \frac{L_2(r, z)}{\max_{r,z}(L_2)} + \frac{L_3(r, z)}{\max_{r,z}(L_3)} \right] \tag{V.10}$$

where $\max_{r,z}(L_i)$is the maximum value of L_i encountered when modeling all candidate source ranges and depths. Eq. (V.10) might thereby change depending on the range and depth intervals modeled; as a practical matter, the maximum values of a given term L_i are relatively insensitive to the span of the model parameter space. The total error L_{tot_NMS} is then the minimum value of L_{tot_NMS} among all the possible combinations of 2 modeled paths:

$$L_{tot_NMS}(r, z) = min\ [L_{NMS}(r, z)]\ . \tag{V.11}$$

Blue regions in the resulting ambiguity surface indicate low values, and thus likely source positions.

V.5 Localization results

This section presents localization results from the analytical and model-based techniques described above. Even though several whales were present in the area, the particular results shown here only concern the one whale that had been tagged with satellite and bioacoustic units within 300 m of the vertical array, thereby providing independent estimates of the whale's position and indicating the accuracy of each passive acoustic technique as the whale moves away from the vertical array.

V.5.1 Depth and range tracking at ranges less than 2 km using analytical methods

The first set of depth and range localizations were computed immediately after the whale was tagged with the B-probe tag on 15 August 2010 at 19:00. Figure 20 compares the depth estimates from the two analytical methods with the depth recorded by the B-probe, while Figure V.21 compares the range estimates from the two analytical methods with the satellite tag range data. The two analytical methods provide accurate range estimates at the start of the first B-probe dive. Both methods indicate that the whale came very close to the vertical array (within 50 m at 19:05) and then started to steadily swim away. The received level of the tagged whale clicks around 19:05 indicates that the whale was indeed very close to the acoustic recorders. The signal was clipped, indicating a minimum received level of 152 dB re 1uPa. By the end of the first B-probe dive the whale had swum approximately 1.6 km away from the array.

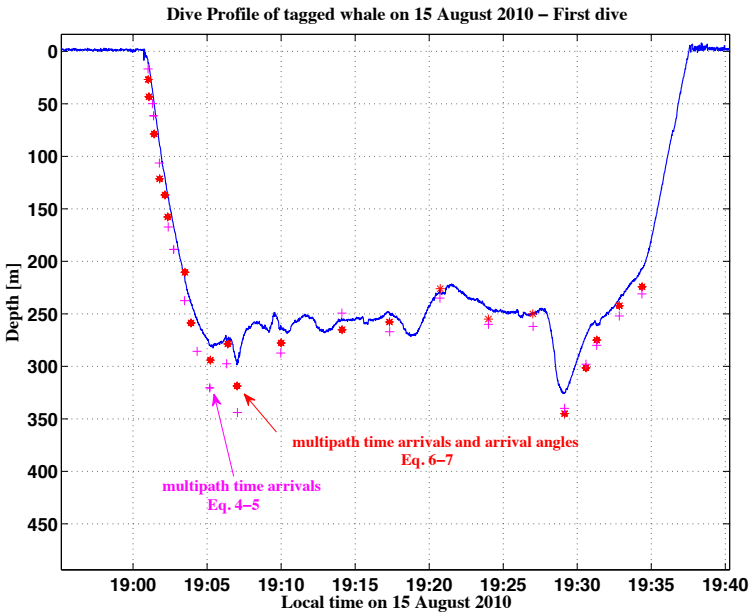

Figure V.20: First dive profile of the tagged whale recorded by the B-probe tag on 15 August 2010 (blue solid line). Depth estimates using the single hydrophone method (Section V.4.3.a, Eqs. (V.4-V.5)) are marked with magenta crosses. Depth estimates using the two-hydrophone method (Section V.4.3.b, Eqs. (V.6 -V.7)) are marked with red stars.

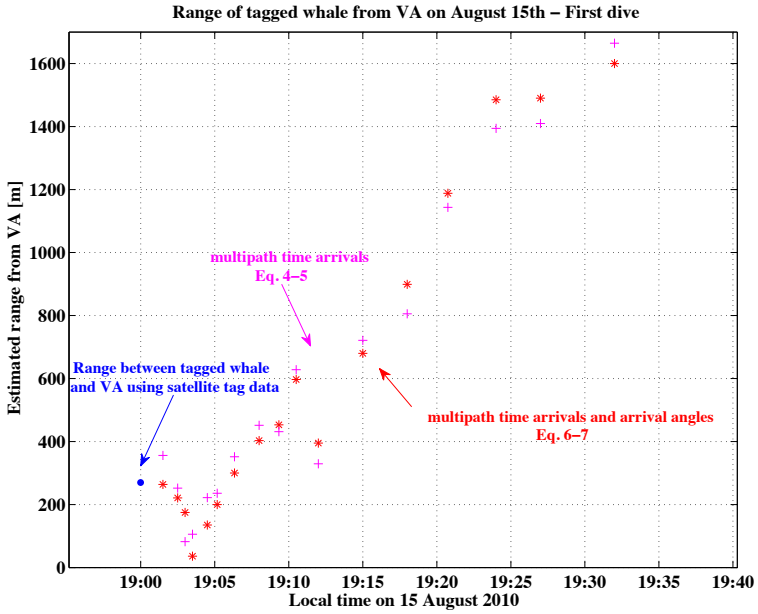

Figure V.21: Range of the tagged whale from the vertical array (VA) during the first dive recorded by the B-probe tag on 15 August 2010. Range estimates using the single hydrophone method (Section V.4.3.a, Eqs. (V.4-V.5)) are marked with magenta crosses. Depth estimates using the two-hydrophone method (Section V.4.3.b, Eqs. (V.6 -V.7)) are marked with red stars. The blue dot indicates the range of the whale from the vertical array at 19:00 computed from the satellite tag data.

V.5.2 Depth and range tracking at ranges greater than 2 km

The whale was at about 2 km range at the start of the second B-probe dive at 19:49. By this point, the bottom-reflected path had disappeared from the vertical array acoustic data, so the first analytical method couldnt be used. The depth estimates provided by the second analytical method (which doesnt require the bottom-reflected path) became inaccurate: the depth error was 40 m for a 230 m whale depth.

Thus rectilinear propagation assumptions became invalid for ranges greater than 2 km in this environment, and effects of ray refraction need to be treated with a sound propagation model at these ranges and beyond.

The B-probe released from the whale after only 2.5 hours, so detailed depth data is unavailable after 15 August 2010 at 21:00. The next reported satellite position of the tagged whale was 400 m from the array at 7:17 the following morning, and this range then increased over the next two days. Figure V.22 shows spectrograms of signal samples at ranges of 2, 5, 8, 22, and 35 km from the vertical array, in units of power spectral density. Figures V.23a -V.27a then show the ambiguity surfaces created using the scoring method described in Section V.4.4.b, using these data samples. The red areas correspond to the best estimates of whale position as predicted by this model-based technique. The horizontal and vertical dashed lines indicate the maximum depth and range recorded by the satellite tag during this dive, respectively. Figures V.23b,c-V.27b,c show the corresponding ambiguity surfaces created using the normalized (NMS) and weighted (WMS) mean square error methods described in Section V.4.4.c.

For both methods, the location uncertainty grows with range, as discussed in Section V.6.3.e and V.6.4 Ways to reduce these uncertainties are discussed in the Conclusion.

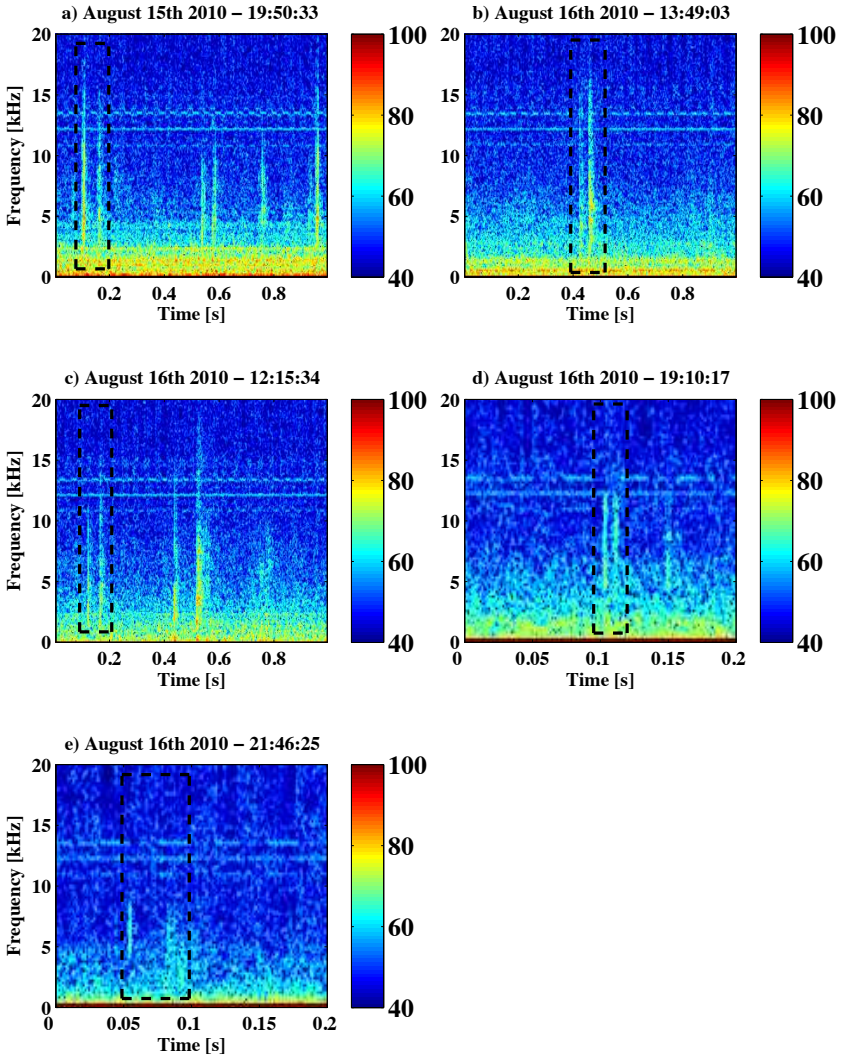

Figure V.22: Spectrogram of the ray path arrivals (dashed box) used for localization when the whale range was (a) 2 km away, (b) 5 km away, (c) 8 km away, (d) 22 km away, and (e) 35 km away from the vertical array. The color-scale corresponds to the power spectral density in units of dB re 1 uPa^2/Hz.

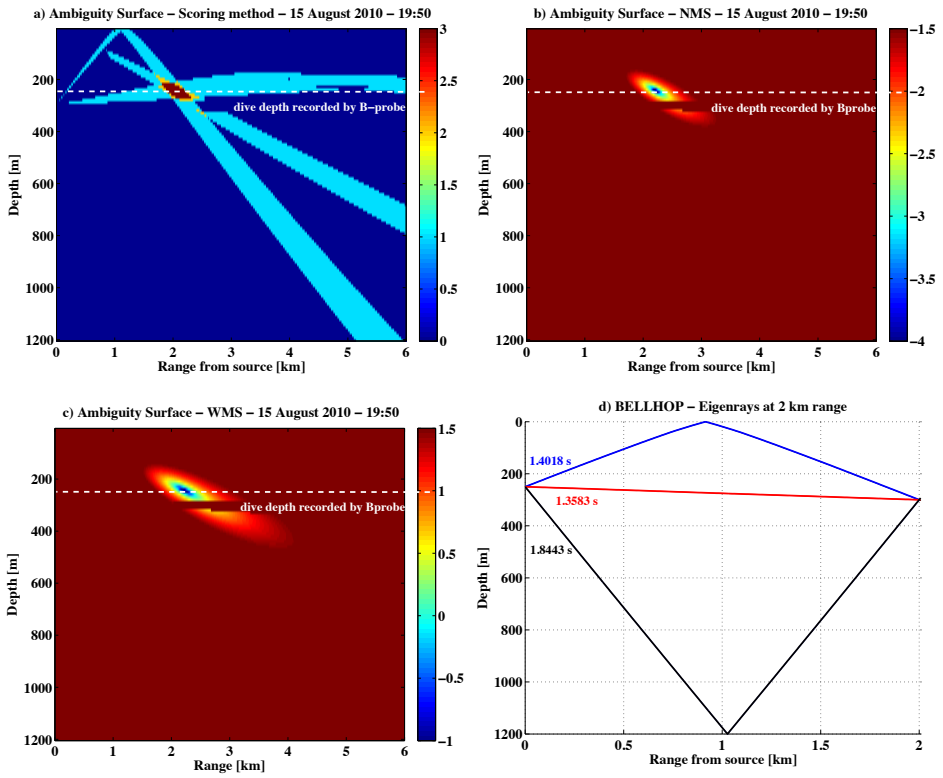

Figure V.23: Localization estimates of whale at 2 km range. The horizontal and vertical dashed lines indicate the maximum depth and range recorded by the satellite tag during this dive.

(a) Ambiguity surfaces using scoring method (Section V.4.4.b for multipath arrivals recorded on the vertical array on 15 August 2010 at 19:50. Red regions indicate likely source positions.

(b) Ambiguity surfaces using normalized mean-square (NMS) error method for multipath arrivals recorded on the vertical array on 15 August 2010 at 19:50. The error term for each measurement variable is weighted equally (Section V.4.4.c), and a logarithmic scale is used. Blue regions indicate likely source positions.

(c) Ambiguity surfaces using weighted mean-square (WMS) error method for multipath arrivals recorded on the vertical array on 15 August 2010 at 19:50. The error term for each measurement variable is weighted using the variance of the measurement (Section V.4.4.c), and a logarithmic scale is used. Blue regions indicate likely source positions.

d) Eigenrays and travel times modeled between a sperm whale at 250 m depth and a hydrophone at 300 m depth and 2 km range. Blue solid lines represent surface-reflected paths, red solid lines represent direct and refracted paths, and black solid lines represent bottom-reflected paths. Dashed lines indicate paths that are predicted in the model but were not found in the vertical array data. Travel times (in seconds) are indicated for most of the paths using the color code described above.

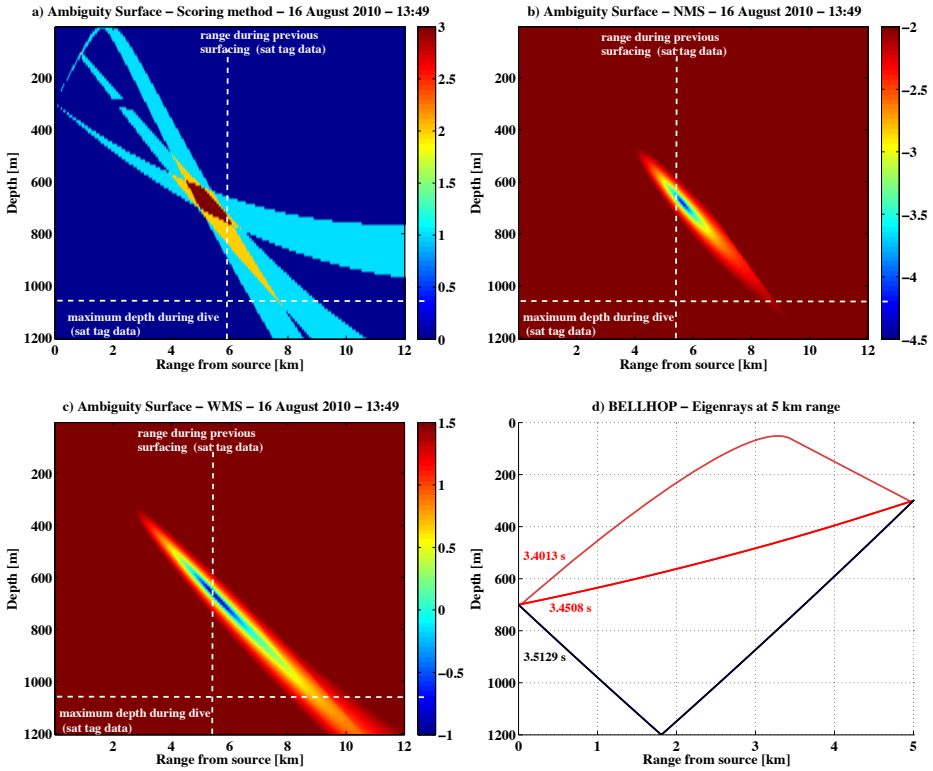

Figure V.24: Similar to Fig. 23, but for multipath arrivals recorded on the vertical array on 16 August 2010 at 13:49. Source depth in subplot d) was modeled at 700 m depth.

V.5.3 Click received level as a function of range

In this section the received level of clicks on the vertical array are estimated using several metrics. As discussed by Madsen (2005), different metrics are commonly used in bioacoustics to report the sound pressure level of transient signals in water, leading to levels varying by as much as 15 dB for the same signal.

The received levels of clicks emitted by the tagged whale at known ranges were measured using three metrics. First, the peak-to-peak (pp) sound pressure level (SPL) (in dB re 1uPa) was selected from the click waveform, filtered between 2 and 25 kHz. Second, the root-mean-squared (rms) sound pressure level (in dB

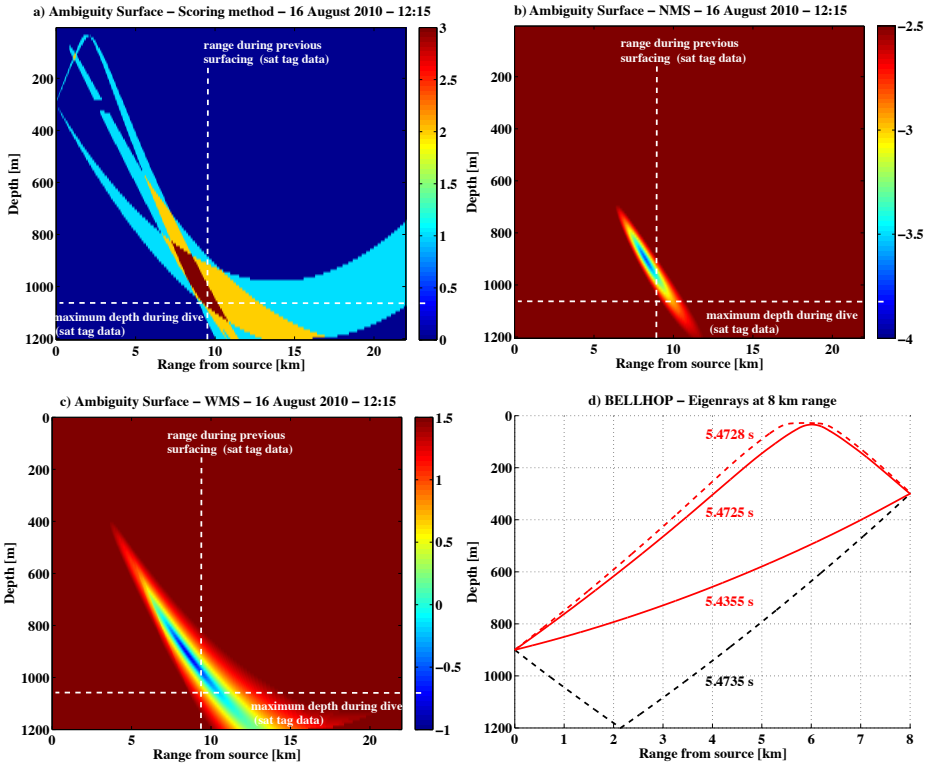

Figure V.25: Similar to Fig. 23, but for multipath arrivals recorded on the vertical array on 16 August 2010 at 12:15. Source depth in subplot d) was modeled at 900 m depth.

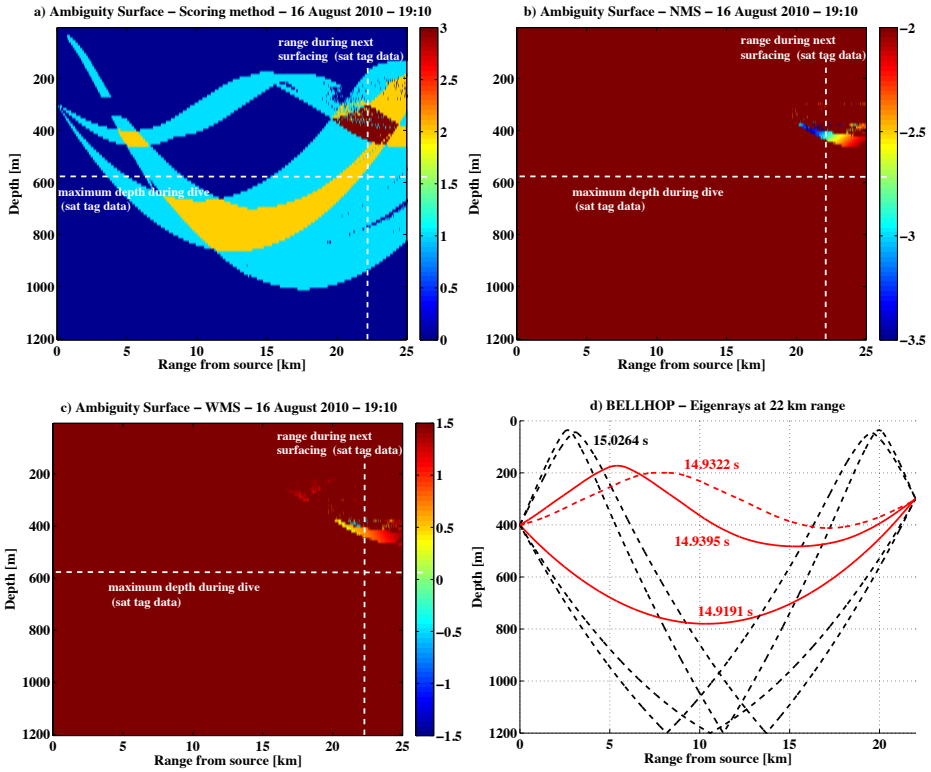

Figure V.26: Similar to Fig. 23, but for multipath arrivals recorded on the vertical array on 16 August 2010 at 19:10. Source depth in subplot d) was modeled at 400 m depth.

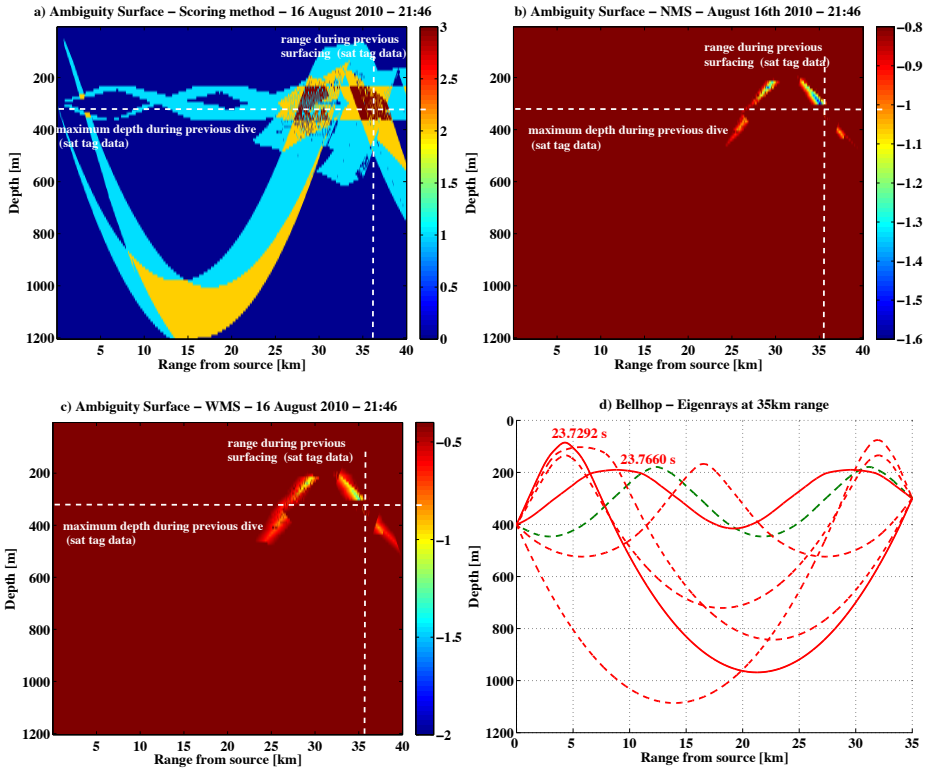

Figure V.27: Figure 27. Similar to Fig. 23, but for multipath arrivals recorded on the vertical array on 16 August 2010 at 21:46. In subplot d) the source depth was modeled at 400 m depth. The green dashed line indicates a path that is predicted in the model, not present in the data, and but generates a sidelobe in the ambiguity surface.

re 1uPa) was estimated using the following formula (Urick, 1983):

$$SPL_{rms} = 10\ log\ (\frac{1}{T}\ \int_0^T\ p^2(t)\ dt)\ , \tag{V.12}$$

where $p(t)$ is the instantaneous pressure and T is the time series duration.

Finally, the energy flux density or the sound exposure level (SEL) of the transient was computed:

$$SPL_{rms} = 10\ log\ (\int_0^T\ p^2(t)\ dt)\ , \tag{V.13}$$

$$SPL_{rms} = SPL_{rms}\ +\ 10\ log\ (T)\ .$$

The value of T was estimated by measuring the portion of the waveform that comprised 90% of the cumulative equalized sound exposure level ($CESEL$) values in the time series incorporating the click (Malme *et al.*, 1986; Madsen, 2005).

$$CESEL = 10\ log\ \int_0^{T_{tot}}\ (p^2(t) - {p_{rms,0}}^2)\ dt\ , \tag{V.14}$$

where $p(t)$ is the instantaneous pressure, $p_{rms,0}$ is the root-mean-square ambient pressure over the filtered data, and T_{tot} is the time series duration. The time series included 0.1 s of background noise before the click, and this data snippet was used to estimate $p_{rms,0}$.

T is defined as the range of the time series where the $CESEL$ meets the following criteria:

$$0.05\ <\ \frac{CESEL}{max(CESEL)}\ <\ 0.95\ . \tag{V.15}$$

Figure V.28 displays the received sound pressure levels RL (pp), $RL_{90\%}$ (rms) and SEL ($SEL_{90\%}$) of clicks received on the vertical array top hydrophone at various ranges. In the Discussion these data will be combined with modeled transmission losses to estimate sperm whale source levels.

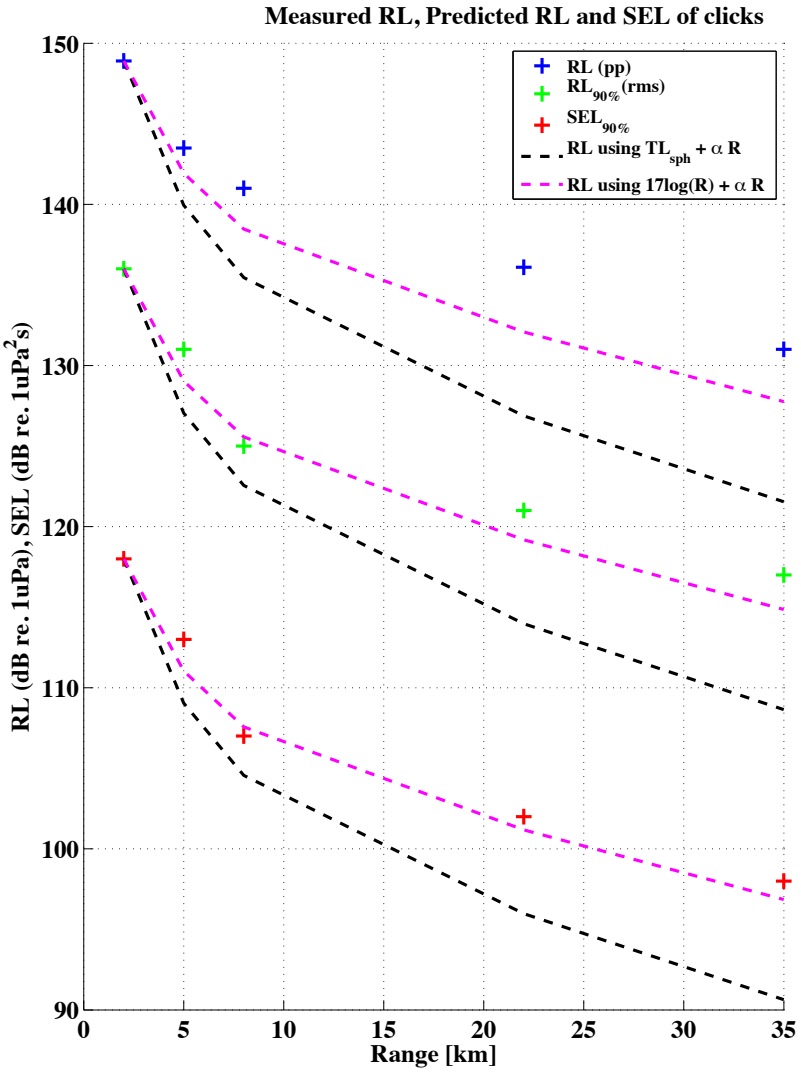

Figure V.28: Measured peak-to-peak (pp) received levels (blue crosses), rms received levels (green crosses) and sound exposure levels (SEL) (red crosses) of clicks measured on the vertical array top hydrophone when the whale range was 2 km, 5 km, 8 km, 22 km, and 35 km. The predicted received levels are estimated by adding the spherical and BELLHOP-derived transmission loss models to the first received level, and are plotted for all three estimates (black and magenta dotted lines).

V.6 Discussion

V.6.1 Limits of the analytical approach

As stated previously, Eqs. (V.4 -V.7) assume that ray paths are straight lines. Equations (V.4) and (V.5) also require the presence of a bottom-reflected path. These assumptions are expected to be valid at short range only (Thode *et al.*, 2002). Indeed, Section showed that the depth estimates provided by the analytical method became inaccurate at 2 km range. A manual review of the data recorded on the vertical array revealed that bottom-reflected paths couldn't be identified past 2 km range. Figure V.18 also demonstrates how no surface-reflected paths reach a 300 m receiver past 5 km range; instead the surface-reflected path becomes a refracted path that never reaches the surface.

A second weakness of analytical methods is that human judgment is also required to classify a given measured arrival as a direct path, surface reflection or bottom reflection. This task can be difficult, especially when multiple animals are vocalizing simultaneously. Thus a model-based localization approach is necessary for estimating the whale depth and range past 2 km.

V.6.2 Nature of the acoustic propagation environment

Here we discuss how acoustic propagation characteristics of the study area enable the long range tracking of sperm whales. The acoustic propagation model BELLHOP was used to predict the acoustic ray path travel times, arrival angles and transmission loss between a hypothesized sperm whale at 400 m depth and a hydrophone at 300 m depth, a various ranges. The model environmental inputs (grid size, sound speed profile, bottom properties) are described in Section V.4.4.a.

Figures V.23d -V.27d display the eigenrays modeled between a hypothesized sperm whale and an hydrophone at 300 m depth and 2 km, 5 km, 8 km, 22

km and 35 km range, along with their associated travel times. Only paths with one interface reflection or less are shown. Up to 2 km range, the eigenrays between the source and the receiver can be easily labeled as direct, surface-reflected and bottom-reflected paths. At 2 km range, the assumption of straight ray propagation seems valid (Figure V.23d), which explains why the analytic formulas worked well up to 2km range.

By 5 km range the surface-reflected path has transformed into a refracted path that does not contact the surface (Figure V.24d). Now the surface-reflected path arrives before the direct-path, as the sound speed is greater close to the surface. This situation illustrates the importance of using a propagation model to eliminate the need to manually identify propagation paths. Indeed, when reviewing the acoustic data in Figure V.22b, a manual analyst would probably make the assumption that first arrival is the direct path.

Starting at 8 km range, additional refracted paths start to appear (Figure V.25d). By 22 km range, the modeled bottom-reflected paths disappear (Figure V.26d). However this path couldn't be identified on the vertical array data past a 2 km range anyway (Section V.6.1), probably due to either a low SNR or a complex bottom bathymetry that bears no relationship to the flat bottom assumed in the model.

By 35 km range the model produces no eigenrays with a bottom reflection (Figure V.27d). However, seven distinct refracted eigenrays appear, all arising from being trapped in the minimum sound speed channel. Interestingly, only two ray arrivals were confidently extracted at long ranges (Figure V.22e). Our initial explanation for this discrepancy is that many of the modeled eigenrays have arrival times within 20 msec of each other, so additional ray paths might have been recorded by the vertical array, but couldnt be separated in time, as sperm whale click durations are on the order of 10 msec. To investigate this hypothesis, Figure V.29 displays the duration, maximum frequency and bandwidth of the two ray paths used for localization between 2 km and 35 km range (as seen in the

spectrograms in Figure V.22). The duration of each pulse was computed according to the cumulative SEL method described in Section 5.5.3. The plots show that the ray arrivals' duration lengthens with increasing source range, with the second ray path (associated with the path trapped in the sound speed minimum channel) displaying a longer duration than the first path at higher ranges.

One might argue that this pulse lengthening arises primarily from the reduction in signal bandwidth, which in turn arises from the disappearance of the high frequency components at higher ranges, as indicated by the bottom subplot in Figure V.29. However, the duration of the first path's pulse is similar at 22 and 35 km range, but over the same range interval the second path's pulse duration nearly doubles, even though the bandwidths of both pulses decrease significantly over the same range interval. This difference in duration suggests that a simple volume attenuation of higher frequency components with range is insufficient for explaining the increase in pulse duration for the trapped refracted ray path, and thus the presence of several closely-arriving ray paths cannot be discounted.

In terms of mitigation and population density modeling, a simple formula for transmission loss is often desired. Thus, three simple analytic transmission loss models were compared up to 25 km range against the computed transmission loss generated by BELLHOP, which is accepted as the accurate transmission loss. The three analytical models were the spherical ($20log(R)$) and cylindrical ($10log(R)$) transmission loss models, along with a $17log(R)$ model. All the simple models also incorporated Thorp (1967) volume attenuation, which was calculated using the following formula:

$$\alpha = 0.10936 \ \frac{f^2}{1+f^2} \ + \ 50 \ \frac{f^2}{5000+f^2} \ , \tag{V.16}$$

where α (in dB/km) is the Thorp frequency dependant attenuation, and f is the frequency in kHz. A frequency of 6 kHz was used for ranges less than 10 km, and a frequency of 3 kHz was used at higher ranges, to reflect the change in frequency content in the detected pulses with range. Thus the bulk attenuation is 0.5 dB/km

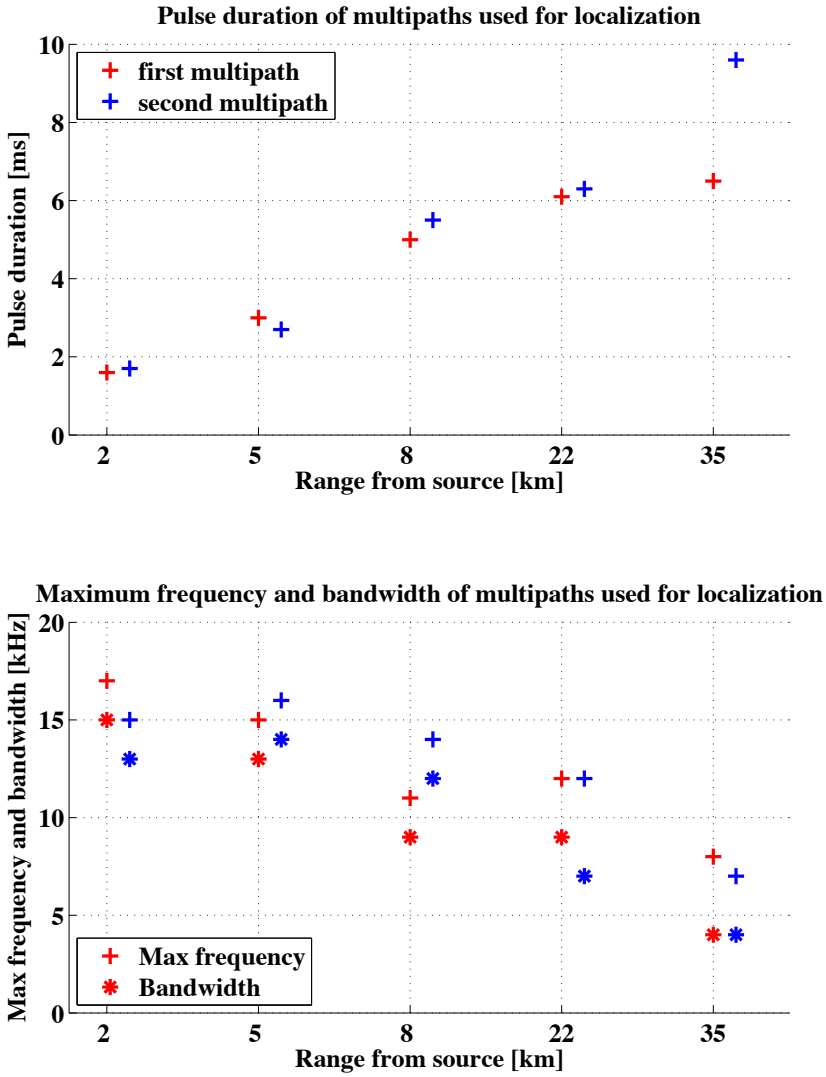

Figure V.29: Top panel: Duration in ms of the ray path arrivals used for localization (Figure V.22) when the whale range was 2 km, 5 km, 8 km, 22 km and 35 km away. The duration was computed by taking the part of the waveform that made up 90% of the cumulative equalized SEL values in the time series (Section V.6.1). Bottom panel: Maximum frequency (cross) and bandwidth (star) in kHz of the multipath arrivals used for localization (Figure V.22) when the whale range was 2 km, 5 km, 8 km, 22 km and 35 km away.

The red symbols indicate the first multipath arrival and the blue symbols indicate the second multipath arrival

at 6 kHz and 0.2 dB/km at 3 kHz.

The final analytical spherical and cylindrical transmission loss models then become:

$$TL_{sph} = 20\ log(1000\ R)\ +\ \alpha\ R\ , \tag{V.17}$$

$$TL_{cyl} = 10\ log(1000\ R)\ +\ \alpha\ R\ , \tag{V.18}$$

where R is the distance in kilometers between the source (sperm whale) and the receiver (vertical array).

Figure V.30 displays the four transmission loss curves at ranges between 0.5 and 25 km. Spherical spreading loss (Eq. (V.17)) models transmission loss in free space from an omnidirectional source; all of the acoustic energy propagates out evenly in all directions. This model is often used in deep-water environments, and Figure 30 shows that the detailed numerical model closely matches spherical spreading out to 1 km range. But sound cannot propagate uniformly in all directions from a source in the ocean forever; beyond some range the sound will contact the sea surface or sea floor. In the extreme case where sound is assumed perfectly-reflected (with no absorption or scattering) from the ocean surface or sea floor, the acoustic energy becomes trapped in the water column and the transmission loss becomes cylindrical, with transmission loss decreasing much more slowly with range when compared with spherical spreading. In general, realistic ocean environments would be expected to display transmission losses between these two extreme values, and in fact, Figure V.30 shows that the best fit to the BELLHOP transmission loss curve at longer ranges is an analytical transmission model of $17log(R)$, plus bulk attenuation.

Figure V.28 also provides some insight into the validity of the analytical transmission loss models, assuming a constant source level (a topic to be addressed shortly). Here predicted received levels using both a spherical and a $17log(R)$

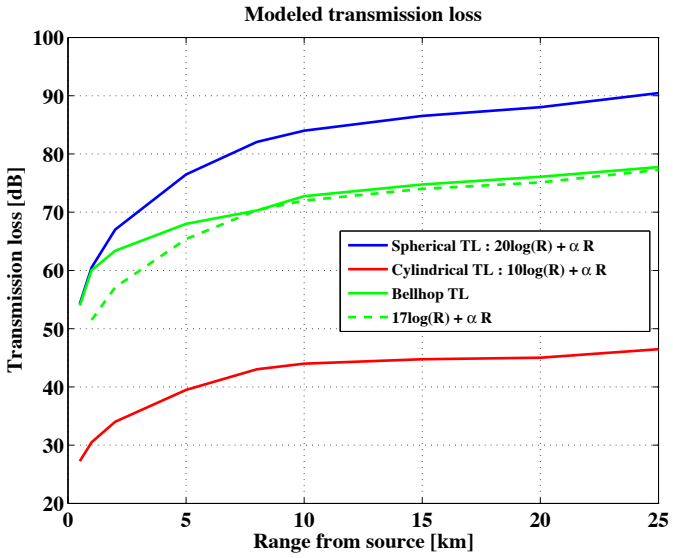

Figure V.30: Transmission loss (TL) estimated up to 25 km range using a simple spherical transmission loss model (solid blue line), a simple cylindrical transmission loss model (red line), the Bellhop transmission loss (green line) and a simple transmission loss model of 17log(R) (dotted green line). The Thorp volume attenuation at 3 and 6 kHz (Section V.6.2) is incorporated into the three analytical transmission loss models and Bellhop computations.

transmission loss models are compared with measured received levels, using the received levels at 2 km as a starting point. As expected, the spherical transmission loss model overestimates the transmission loss at ranges above 2km. The received levels predicted using $17log(R)$ (and thus the BELLHOP-predicted transmission loss) provide a better estimate of the measured received levels at all ranges.

Sections V.6.5 and V.6.6 will use the results of this section extensively, when estimating sperm whale source levels and maximum detection range.

V.6.3 Sources of localization error

Two sources of measurement bias and two sources of measurement uncertainty affect the accuracy and resolution of the localization techniques. Quick sensitivity analyses were conducted for all the factors.

V.6.3.a Inclination precision

The first source of error arises from potential measurement bias in the array inclination, which was measured using inclinometers taped inside each acoustic unit. The standard deviation of the measured array tilt was 0.3 deg. An inaccurate estimate of array inclination will bias the elevation angle estimates, and thus shift the location estimate.

To evaluate the impact of inclination bias, the arrival pattern from a source at 400 m depth and 10 km range (the true source location) was simulated using a 0 deg array inclination and the standard model environmental inputs (grid size, sound speed profile, bottom properties) described in Section V.4.4.a. The results were saved as true data. Next, a set of replicas were generated using a 1 deg inclination (or three times that of the inclinometer uncertainty), and a localization was attempted on the true data using the scoring method described in Section V.4.4.b. The resulting location estimate was 550 m away from the true source location, a 5.5% underestimate in range. In general, the addition of a 20 kg lead

sphere underneath the vertical array seemed successful in keep the array inclination nearly vertical.

V.6.3.b Environmental model

The second source of error arises from measurement bias in the sound speed profile. To assess the effects of bias the sound-speed structure on the localization, the same simulated true data were used as in the previous section. Next, a set of replicas were generated by adding 5 m/s to the sound speed profile of Figure V.17, and a localization was attempted on the true data using the scoring method described in Section V.4.4.b. The resulting location estimate was 150 m away from the true source location, a 1.5% underestimate in range. By contrast, the sound speed profile at the deployment site, changed by only 0.1 m/s during the deployment.

V.6.3.c Time of arrival measurement precision

A third source of error arises from imprecise measurements of the relative arrival times. As stated before, each click ray path arrival has a duration of about 10 ms, and the estimated standard deviation of the relative arrival time estimates was found to be 5 ms. To estimate the error in measurement of click arrival times, an bias of 5 ms was added to the true data. A replica was generated using an array tilt of 0 deg and a localization was attempted on the true data. The resulting location estimate was 350 m away from the true source location, a 3.5% reduction in range.

V.6.3.d Angular measurement precision

The final source of error is due to imprecise measurements of arrival angle, which can also be a cross-product of imprecise measurements of the relative arrival times. The standard variation of the measured arrival angles was found to be 1

deg and translates into a 5.5% underestimate in range for a source at 400 m depth and 10 km range, as discussed in Section V.6.3.a.

The expected localization error arising from measured array tilt and arrival angles are greater than an error arising the measurement of click arrival times and sound speed using expected biases and uncertainties from the data. However, all location errors are within 5% of the true range, and lie within the intrinsic uncertainty of the localization method itself.

V.6.3.e Sidelobes at long range

At ranges greater than 25 km, two disjoint regions emerge as possible whale locations in Figure V.27a-c; one at roughly 28 km, and one at 35 km. The emergence of this "sidelobe" is explained by the eigenray travel times and arrival angles shown in Figure V.27d. This happens because at this range two trapped ray paths arrive at 35 km with similar vertical elevation angles and slightly different travel times (the green dashed line shows the "sidelobe" eigenray path. It is this difference in travel time that splits the candidate locations into two distinct patches. The NMS method and WMS methods (Figures V.27b-c) seem to be able to break the ambiguity, while the scoring method does not (Figure V.27a). As discussed in Section 5.6.2, at large ranges several eigenrays have similar travel times and would thus appear to be merged together in the data, thus making it difficult to identify the two distinct ray paths in the data in Figure V.22e.

V.6.4 Comparison of ambiguity surface construction methods

Section V.4.4 describes the two approaches used to construct ambiguity surfaces, and Section V.6.1 contains the corresponding localization results. The scoring method described in Section V.4.4.b is robust when using both time difference of arrival and arrival angle values, as it doesnt require any unit normalization.

However, the scoring method has a poor precision. Indeed the range uncertainty is already 1.8 km for a source at 5 km range (Figure V.24a), and the scoring method cannot distinguish between the sidelobes at 35 km range (Figure V.27a).

The advantage of the weighted mean-square error (WMS) and normalized mean-square error (NMS) approaches over the scoring method is the localization precision: the range uncertainty is 0.5 km for a source at 5 km range (Figure V.24b-c), which is even smaller than the ARGOS location 1 km uncertainty. At 8 km and 22 km range the range uncertainty is 2 km for the WMS method and 1 km for the NMS error (Figures V.25b-c and V.26b-c). Both the WMS and NMS methods also resolve the sidelobe ambiguity at 35 km (Figure V.27b-c), but the NMS method provides a more precise localization with a range uncertainty of only 1 km, similar to the ARGOS location uncertainty.

The NMS method described in Section V.4.4.c requires a complex unit normalization to ensure that arrival times and arrival angles have an equal weight on the localization results. One weakness of this method is that the choice of the normalization value can change, depending on the ranges and depths modeled, and thus the choice of range or depth span may impact the localization estimate. However, the resulting precision and accuracy of the NMS results seems higher than the WMS approach. Thus the NMS method is currently the preferred approach for future tracking studies.

For all methods the location uncertainty grows with range as shown in Figures V.23 -V.27. One explanation is that the uncertainty in the sound speed profile used increases uncertainty with increasing source range. The second, more likely explanation is that the uncertainties in the arrival angle and arrival time measurements map into larger potential source regions with increasing range. For example, in the simple case of an infinite homogenous environment, a 1 degree uncertainty in a horizontal (0 degree) vertical arrival angle corresponds to a 17 m depth uncertainty at 1 km range, but a 174 m uncertainty at 10 km range. Similar effects are clearly visible in the scoring ambiguity plots of Figures V.23a -V.27a.

The conclusion will discuss how these localization uncertainties might be reduced at long ranges.

V.6.5 Source level estimates

V.6.5.a Click source levels

The combined acoustic and tagging data, along with the BELLHOP-derived transmission loss, were used to estimate the tagged sperm whale's click source levels over the detected bandwidth. Figure V.28 provides estimates of received levels (RL) for clicks emitted at known ranges, using the three different metrics defined in Section V.5.3.

The acoustic source levels were derived by adding the estimated transmission loss to the received levels out to 35 km range using the sonar equation (Urick, 1983):

$$SL = RL \ + \ TL \ , \tag{V.19}$$

where SL is source level, RL is received level, TL is transmission loss, all in dB units. The TL includes the Thorp volume attenuation (Eq. (V.16)) and uses (Eqs.(V.17 -V.18)) defined in Section V.6.2.

Equation (V.19) was evaluated using the three received level metrics (peak-to-peak, rms and SEL) and the three transmission loss models (spherical spreading, cylindrical spreading, and $17log(R)$ approximation from the BELLHOP model), thus leading to nine source level estimates as a function of range (Figure V.31). As discussed in Section V.6.2, only the BELLHOP-derived transmission loss model should be considered the appropriate transmission model for this environment. The use of the BELLHOP-derived analytical transmission loss model yields an interesting conclusion: the sperm whale's source level remains very steady over time, for both the rms received level and SEL (Figures V.31f,i) metrics. The BELLHOP-derived model estimates a consistent source level of 186

dB re 1uPa (rms) (Figure V.31f), 170 dB re 1 uPa2-s (SEL), (Figure V.31i) and a source level between 200 and 205 dB re 1uPa (pp) (Figures V.31c). The peak-to-peak source level is less consistent with range than the other two metrics, but this is expected, as a peak-to-peak level measurement is not a very reliable sound level measurement method, in that it is extremely sensitive to the relative phases of the frequency components of the signal. The one exception to the consistent apparent source level of the rms and SEL estimates is that at 2 km range the perceived source level is a few dB less than those estimated at longer ranges. This result arises from the fact that the $17log(R)$ model underestimates the transmission loss at short ranges, where the spherical spreading model actually provides a better fit to the BELLHOP computations.

The fact that the source level remains so steady over days is somewhat surprising at first, because sperm whale clicks have been demonstrated to be highly directional (Mohl *et al.*, 2003; Zimmer *et al.*, 2005b) so one might expect to see some source level variation with range, since it is unlikely that the sperm whale remains at the same relative orientation to the hydrophone at the start of every dive. Zimmer *et al.* (2005b) provides one possible explanation, in that the paper showed that sperm whale clicks are composed of three components: an omnidirectional low-frequency (LF) component with energy below 3 kHz and maximum levels ranging from 170-190 dB re 1 uPa (pp); a highly directional and forward-directed component P1 with energy above 3 kHz and maximum measured level of 210 dB re 1 uPa (pp); and a low directionality component P0 pointing backwards with energy above 3 kHz and maximum levels of 200 dB re 1 uPa (pp).

Thus the P0 and LF components of the sperm whale click have low directionality, and span the same frequency range observed in the vertical array data at long ranges. Indeed the LF component would be expected to dominate at long range, as the peak frequency of the detected clicks decreases with increasing range (Figure V.29). The fact that only the P0 and LF portions of the click are being detected could also explain why the apparent source level estimates in this study

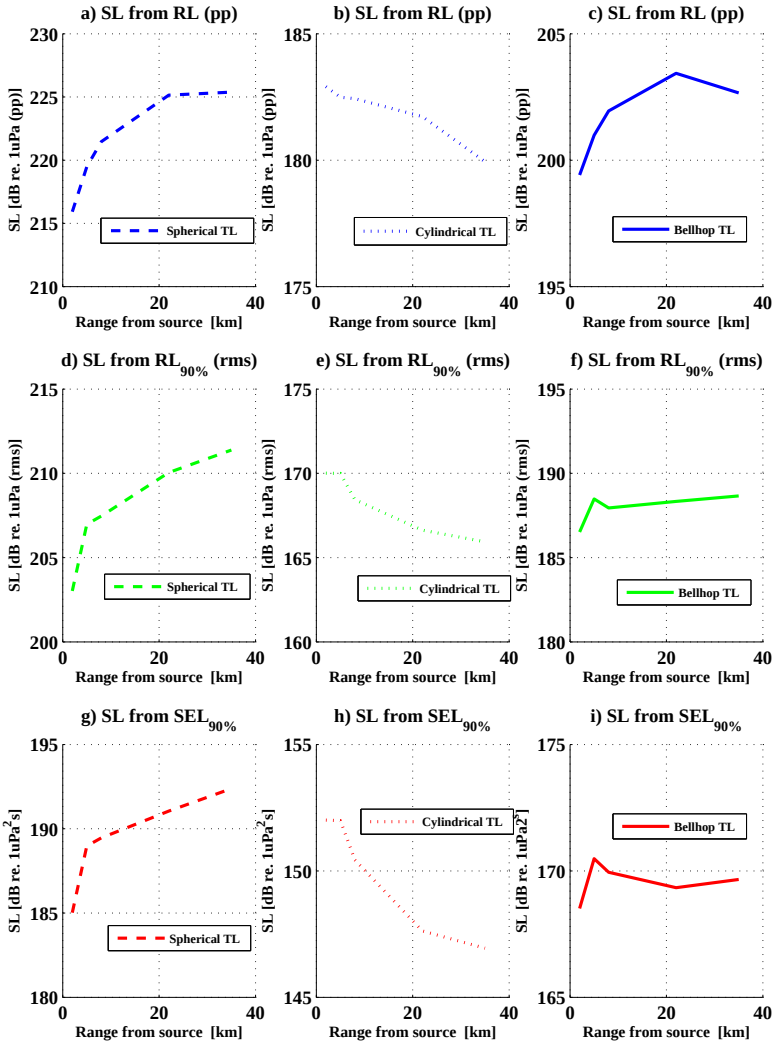

Figure V.31: Estimated source levels using the pp RL, rms RL and SEL estimates and the three different transmission loss estimates (spherical spreading TL , cylindrical spreading TL, and Bellhop-derived 17log(R) TL). All models incorporate bulk attenuation at 3 and 6 kHz.

are lower than the 235 dB re 1uPa (pp) source level reported by Mohl *et al.* (2000). He also reported a centroid frequency of 15 kHz, suggesting that he was measuring the P1 source level. Another interesting difference from previously-reported estimates is that the estimated peak-to-peak source level of 200-205 dB re 1 uPa (Figure V.31c) is higher than the Zimmer *et al.* (2005b) peak-to-peak source level estimate of the LF component, but are similar to the P0 source level component. Most likely, the discrepancy in LF source level estimates arises from the intrinsic high variability implied in a peak-to-peak source level measurement, although one must also consider that Zimmer *et al.* (2005b) measurements are from a 12 m whale in the Ligurian sea and may have a smaller source level than what is likely a 16 m Alaskan whale (Mathias *et al.*, 2009). Unfortunately, the measurements of Zimmer *et al.* (2005b) do not provide results in terms of rms or SEL.

At very close ranges, the fact that the received level of the tagged whale clicks were clipped when the whale was less than 1 km from the vertical array places a lower bound on the source level. Knowing that the signal will clip at 152 dB re 1uPa, the peak-to-peak source level is at least 200 dB re 1uPa using the BELLHOP transmission loss estimate at 1 km range. The low sampling rate on the bioacoustic tag, along with the fact that source level measurements made in close vicinity to the source violate the assumption that acoustic particle velocity and pressure are in-phase, make the bioacoustic tag data inadequate for estimating source level.

V.6.5.b Creak click source levels

Sperm whales occasionally produce creak sounds, a sequence of clicks produced at a rate of 10 per second or faster (Gordon *et al.*, 1987; Madsen *et al.*, 2002a), and often characterized by a decrease in the amplitude over the five-to-thirty second duration of the sound (Whitehead and Weilgart, 1991; Whitehead, 2003). The shift between usual clicks and creak clicks is characterized by sudden decreases in the inter-click interval. Most studies suggest that regular clicks during

foraging dives represent a search phase of echolocation, and that creaks are produced as sperm whale whales close in on prey items (Gordon *et al.*, 1987; Goold and Jones, 1995; Jaquet *et al.*, 2001; Madsen *et al.*, 2002a). Madsen *et al.* (2002a) reported creak source levels (using 5 recorded creaks) between 179 and 205 dB re 1 uPa (rms), levels that are about 20 dB smaller than usual click source levels. A reduced source level has also been seen observed in buzzes of harbor porpoises (DeRuiter *et al.*, 2009).

Here creak source levels were estimated using one creak produced by the tagged whale and detected on the vertical array data. The acoustic data from the B-probe were first manually reviewed to detect creak events, and a total of 20 creaks were found during the three dives recorded by the B-probe. The vertical array data were then manually reviewed to find the creaks produced by the tagged whale. Ten of the tagged whale's creaks were possibly identified in the vertical array data, demonstrating that creaks could be detected up to at least 1.6 km range under sea state 3 conditions.

The first creak produced by the tagged occurred when the whale was 200 m from the vertical array and when no other whale was clicking. Other creaks happened when other whales were vocalizing, making it more difficult to extract creak clicks. Received levels of clicks within that first creak were between 130 and 138 dB re 1uPa (pp) and between 121 and 130 dB re 1uPa (rms). The high directionality of creak clicks may explain the large dynamic range in received level (Madsen *et al.*, 2002a), as the received levels would fade in and out as the whale changes its orientation relative to the vertical array. Corresponding source levels were estimated using the spherical transmission loss model, since the whale was very close to the vertical array (Section V.6.2) Source levels of 176-184 dB re 1uPa (pp) and 167-176 dB re 1uPa (rms) were found. These source levels are about 20 dB lower than usual click source levels measured in the previous subsection, consistent with the pattern observed by Madsen *et al.* (2002a).

Information about usual click and creak click source levels is a key com-

ponent in terms of estimating the detection range limit of passive acoustics, the subject of the next section.

V.6.6 Limits of detection and tracking range

In previous sections the source levels of sperm whales have been estimated and the transmission loss characteristics of the environment have been obtained as a byproduct of the localization procedure. This information will now be used to estimate the ultimate detection and tracking ranges of the vertical array system as a function of sea state, in order to help provide guidelines for designing future experiments for passive acoustic monitoring of sperm whales in similar environments. In particular, results like these are essential in assisting future estimates of sperm whale density estimation using acoustics (Barlow *et al.*, 2005). In the following discussion the "detection range" of a sperm whale is defined as a range where at least one ray path would be predicted to have a 2 dB signal-to-noise ratio in terms of power spectral density (PSD). The "tracking range" is defined as a range where at least two distinct ray paths would have more than 2 dB SNR. A difference of as much as 5 dB can exist between the received levels of two ray arrivals (Figure V.22), and thus the tracking range would be expected to be less than the detection range.

The sonar equation states that a sperm whale click will be detected if the signal-to-noise ratio (SNR) exceeds a detection threshold (DT). In this study, the DT is assumed to be 2 dB, and the SNR at the receiver becomes:

$$SNR = SL \; - \; TL \; - \; ANR \; , \tag{V.20}$$

where SL is the click source level: 186 dB re 1uPa (rms) (Section V.6.5.a), TL is the BELLHOP-modeled transmission loss: $TL = 17log(R) + \alpha R$ (Section V.6.2), and ANL is the rms ambient noise level measured over the same bandwidth of the click.

Wind speed (sea state) is the dominant factor in ambient noise levels above 500 Hz (Wenz, 1962). The so-called "Wenz" curves (1962) provide pressure spectral density levels (units of dB re 1 uPa^2/Hz) of ambient noise as a function of sea state and frequency band.

The ambient noise levels measured during the two-day experiment were estimated as follows. First, a set of pressure spectral density (PSD) spectra (Figure V.32) was computed over the 0.2-24kHz frequency range using a 1024 point FFT size with 50% overlap, then all PSD spectra over a 0.5 s interval were averaged. This relatively short time interval was chosen in order to increase the odds that a sperm whale click would not be incorporated into the average, since the click interval of a single sperm whale is generally greater than 0.5 sec. The ambient noise level was then calculated by taking the minimum value of the summed pressure spectral density over the 2-10 kHz frequency band every 4 seconds (Figure V.33) (Guerra *et al.*, 2011). By taking the minimum, PSD samples contaminated by sperm whale click spectra could be rejected. The occasional increase in noise level arises from vessel noise from the F/V Northwest Explorer, but the ambient noise level over the sperm whale click bandwidth holds relatively consistent at 95 dB re 1 uPa (rms).

The Sea state was estimated to be 3 during the 2-day experiment, with wind speeds of 3 to 6 m/s logged by the NOAA Fairweather buoy (http://www.ndbc.noaa.gov/). The average value of the pressure spectral density at 2 kHz is 58 dB re 1 uPa^2/Hz, which matches well the 60dB re 1 uPa^2/Hz noise level predicted by the Wenz curves at the same frequency and sea state.

Ambient noise levels were then modeled for Beaufort sea states ranging from 0 to 5, and Equation (V.20) was used to derive sperm whale detection and tracking ranges as a function of sea state, using a detection threshold of 2 dB. Figure V.34 displays the results for sea states ranging between 0 to 5. The detection range is predicted to be up to 90 km in calm sea conditions and up to 35 km in high wind conditions of 12 m/s. The tracking range is predicted to be up to 75

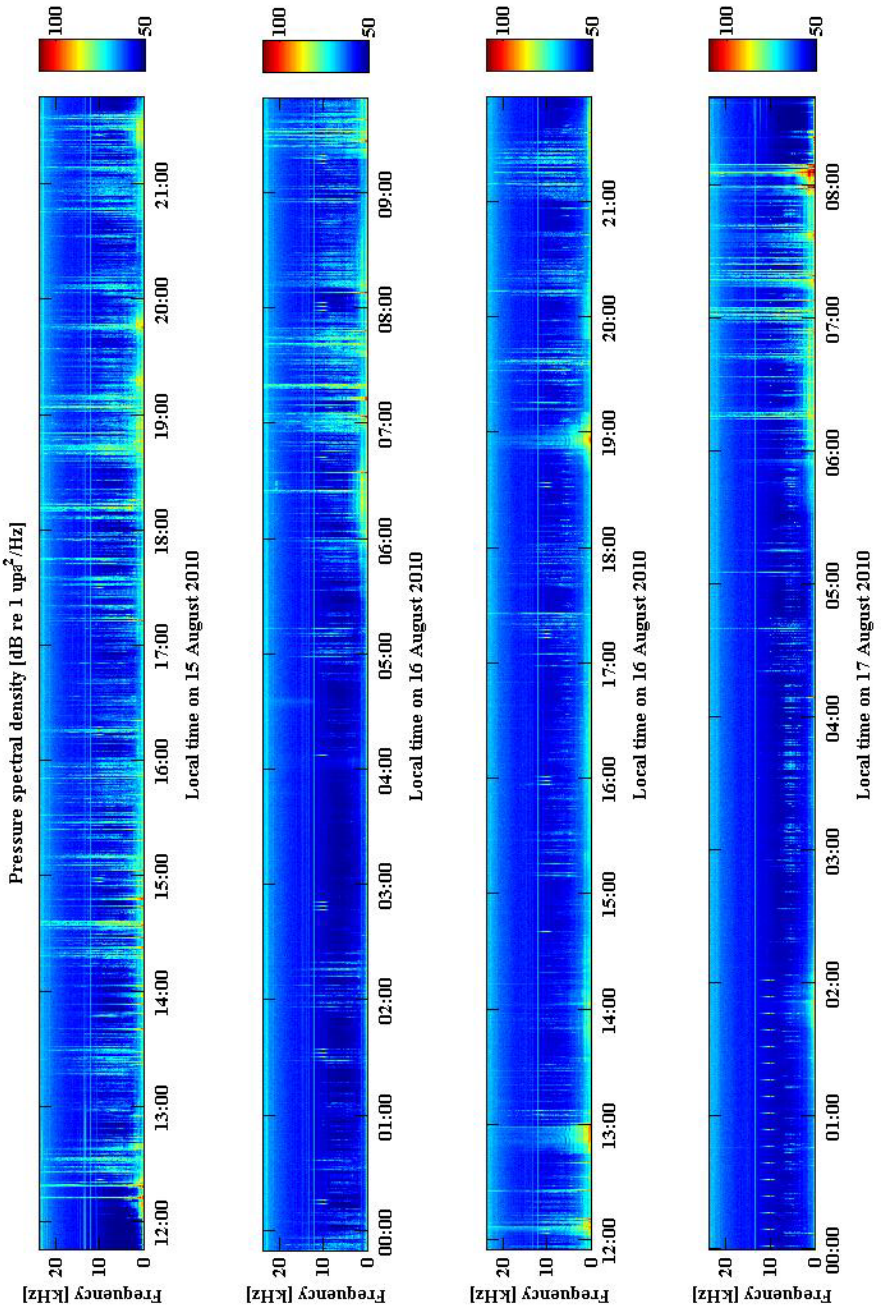

Figure V.32: Power spectral density during the 2-day experiment calculated using a 1024 point FFT size with 512 point overlap, and an averaging time of 0.5 sec. Each panel displays 9 hours of data, and incorporates contributions from sperm whales and ships. Intensity scale is in terms of power spectral density (dB re 1uPa^2/Hz).

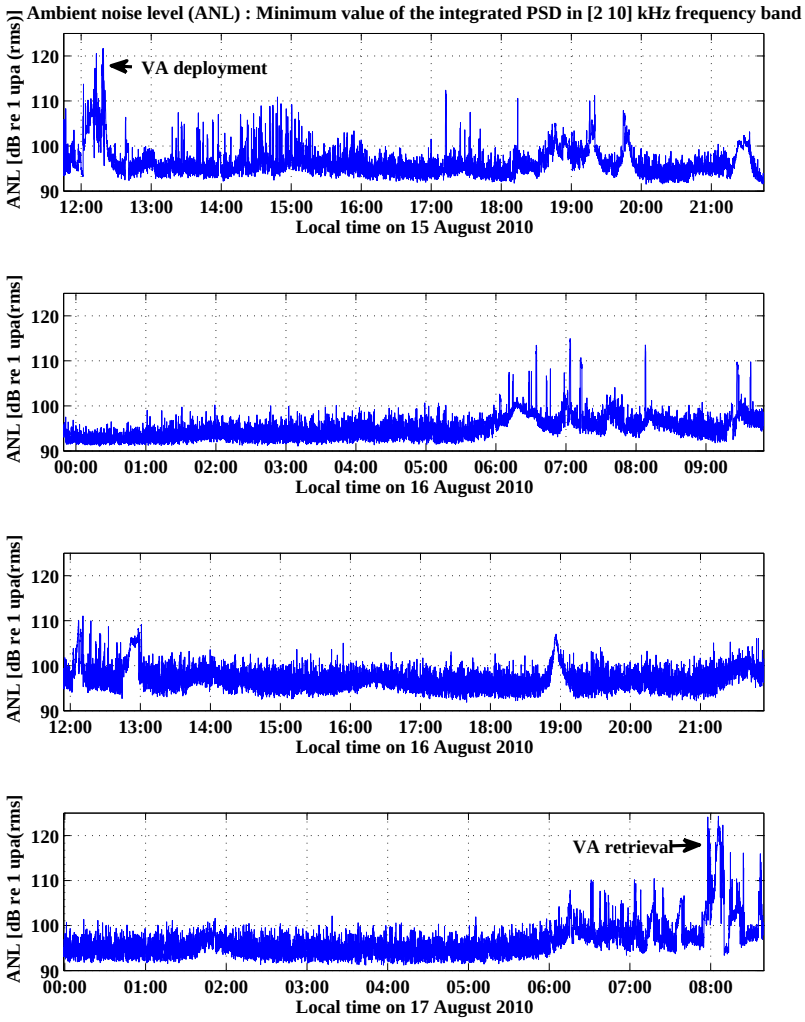

Figure V.33: Ambient noise levels (rms) estimated by taking the minimum value of the integrated power spectral density over the 2-10 kHz frequency band every 4 seconds. Each panel displays 9 hours of data.

km in calm sea conditions and up to 19 km in high wind conditions. The sonar equation predicts that for a sea state of 3, the tracking range would be 42 km, and indeed in this study we were able to track a sperm whale up to 35 km range (Section V.6.1).

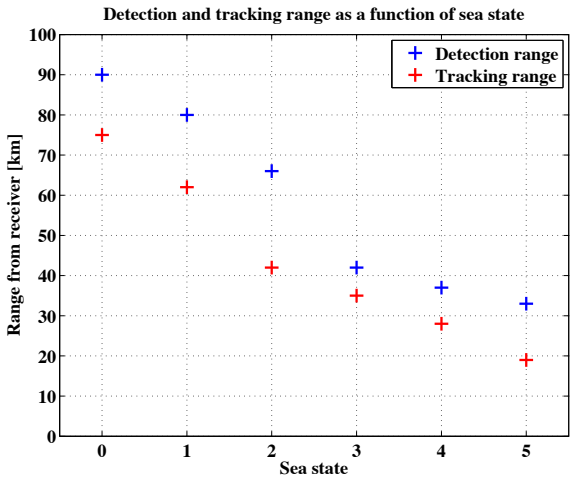

Figure V.34: Detection and tracking range of vertical array system as a function of sea state, using a detection threshold of 2 dB.

V.7 Conclusion

The main purpose of this work was to introduce techniques to track the depth and range of sperm whales using a single deployment of a two-element vertical array placed at the sound speed minimum. Tagging data was used to validate the accuracy of passive acoustic tracking techniques that used both analytic and numeric sound propagation models. The results show that the analytical method (which assumes a constant sound speed and neglects ray-refraction) provided accurate depth and range estimates up to 2 km range. At longer ranges, it is thus necessary to use an accurate sound speed profile and a propagation model to account for ray-refraction effects. After modeling arrival times and arrival angles of ray paths with BELLHOP, several methods were used to construct ambiguity

surfaces. The normalized mean-square error (NMS) resulted in a better accuracy than the weighted mean-square error (WMS) and the scoring methods. However, one potential disadvantage of the NMS method is that the weighting terms are influenced by the set of source locations chosen for modeling, a disadvantage that seems to have little practical effect. Using the NMS method the tagged whale was tracked up to 35 km range, with a ± 1 km range uncertainty.

The data collected during the 2-day vertical array deployment also permitted modeling of the propagation environment, and the best simple analytical fit to the BELLHOP transmission loss curve was found to be$17log(R)$, plus bulk attenuation. These transmission losses were used to estimate the sperm whale's click source level at 186 dB re 1uPa (rms), a value that varied little over time and source range. All this information, combined with the ambient noise statistics gathered from the deployment, suggest that even under sea state 5 conditions, sperm whale detection ranges are possible up to 35 km, with tracking ranges up to 19 km.

However, as discussed in Sections V.6.3.e andV.6.4, localization uncertainty increases with range, and an ambiguity surface can even display multiple possible whale locations several kilometers apart from each other. Further work is thus required to improve the uncertainty at longer ranges.

For now, only clicks emitted during the initial descent of the whale were used for localization. Using clicks from the entire dive profile could improve the localization estimates, by exploiting the depth diversity of all the ray paths, and using the fact that the range estimate should change relatively little during the entire dive. This approach would require the ability to extract clicks from the "target whale" when other whales are vocalizing simultaneously.

Additional future work could also investigate whether the change in pulse duration and frequency bandwidth (Section V.6.2) with range is consistent over larger sample sizes of individual sperm whales. If so, these measurements could be used to obtain range information during single-hydrophone deployments, simply

by measuring the pulse characteristics.

Finally, the ultimate goal is to apply the localization techniques presented here to track other whales present in the area during the experiment. Figure V.35 displays preliminary results of range localization on several whales detected on the vertical array data during the two-day experiment. The number of whales detected on the acoustic data and their corresponding range estimate (using the NMS method described in Section 5.4.4 is given every six hours. A manual review of the spectrogram was conducted on a 20-minute window every six hours to ensure that a whale resting at the surface would not be missed, and two multipath arrival times were extracted on both acoustic units for each whale. Whales were detected on the vertical array throughout the whole deployment. Their range to the vertical array varied between a few hundred meters to tens of km. Individual acoustic identification of whales would provide more insight into their behavior around this decoy buoy, but the figure suggests that the mean range of the group from the decoy gradually increases over time until 17 August. Visual observations were made during the two-day experiment, so we know that the only whale remaining in the area by 17 August (Figure V.35) was a new whale that had not been present during the previous two days. It would thus be interesting to see if one can find distinctive features in the acoustic behavior of this whale. This plot shows the potential utility of the method in testing decoys and other depredation countermeasures in the area, as well as its use in density estimation and other less applied applications.

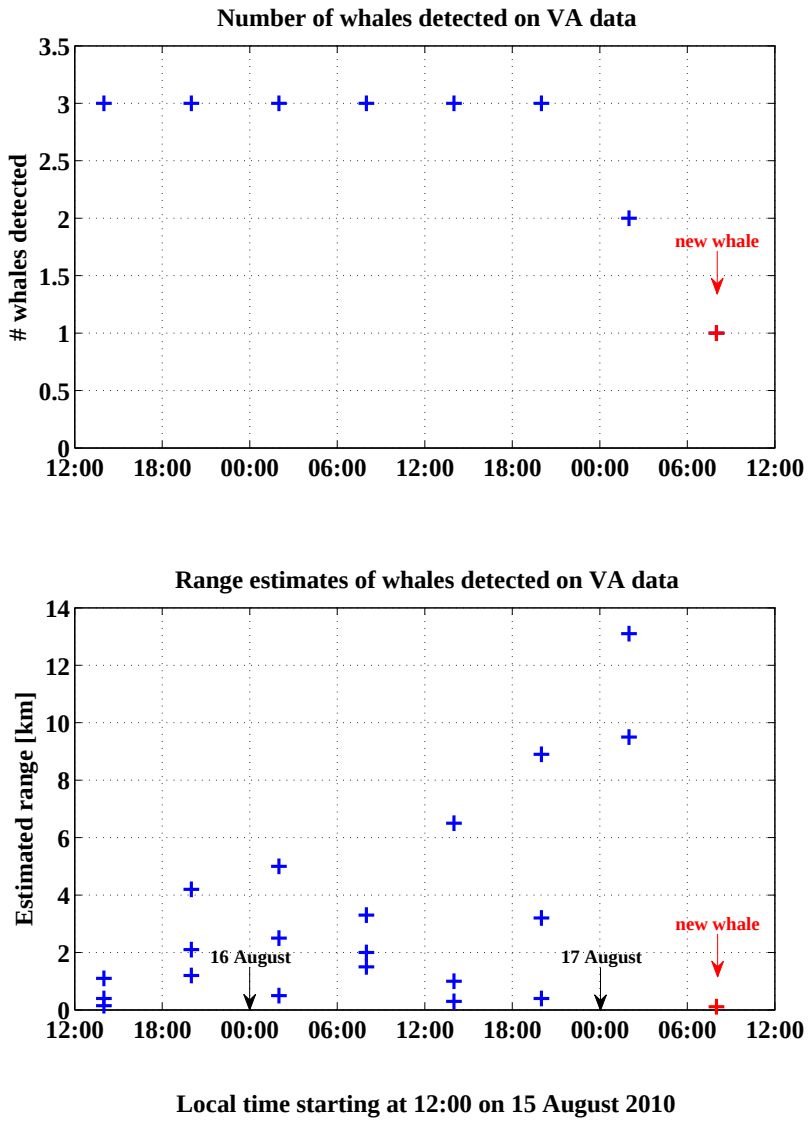

Figure V.35: Top panel: Number of whales detected on the vertical array acoustic data during the two-day deployment. A manual review of the data's spectrogram was conducted on a 20-minute window every six hours to ensure that a whale resting at the surface wouldnt be missed. Bottom panel: Range estimate for each whale detected on the vertical array. Visual observations confirmed that the one whale present on the morning of the vertical array recovery was different than those observed days earlier.

V.8 Acknowledgments

The authors thank the captain and crew of the F/V Northwest Explorer for the use of their vessel. We also thank John Moran of Auke Bay Laboratories in Juneau for allowing us to conduct our fieldwork on the F/V Northwest Explorer and Russ Andrews for sharing the satellite tag data. Visual identification of sperm whales was possible thanks to Jen Cedarleaf and Lauren Wild of the University of Alaska Southeast and the Sitka Sound Science Center. Michael Porter provided useful guidance on running BELLHOP over large ranges. This work was supported by the North Pacific Research Board Graduate Student Research Award, NOAA, and the Central Bering Sea Fishermen's Association.

Chapter 5, in part, has been submitted for publication to J. Acoust. Soc. Am.: Delphine Mathias, Aaron Thode, Jan Straley, and Russel Andrews, "Acoustic tracking of sperm whales in the Gulf of Alaska using a two-element vertical array and tags". The dissertation author was the primary researcher and author of this material.

Chapter VI: Conclusion

Sperm whale depredation provides the opportunity to observe sperm whales at close range as they approach fishing vessels. The work reported in this thesis dissertation exploited this opportunity no only to conduct applied research on the details of depredation behavior, but also to study sperm whale sound production mechanisms and natural foraging behavior. In addition, sperm whale depredation provided unique opportunities to develop and independently test passive acoustic tracking methods useful for investigating not only sperm whale depredation , but potentially other deep water cetacean behavior. The general research topics of this thesis can be summarized as follows:

1. Studying the sperm whale sound production mechanism at close range;

2. Investigating sperm whale diving and acoustic behavior during natural foraging and depredation states, in order to derive acoustic metrics for estimating depredation activity;

3. Evaluating the potential of low intensity acoustic playbacks for reducing depredation rates;

4. Developing passive acoustic tracking techniques using a single two-element short-aperture vertical array deployment, and using the resulting data to conduct initial evaluations of a passive visual decoy.

Each topic is summarized in more detail below.

VI.1 Sperm whale sound production mechanism

In Chapter II, simultaneous acoustic and visual recordings of a depredation attempt were used to compare visual estimates of the size of a sperm whale's head with acoustic estimates of its total length, spermaceti organ length, and junk length. The results suggest that the inter-pulse-interval (IPI) of the sperm whale can be related to the total length of the animal, as has been demonstrated empirically in previous literature. However, the video observations are inconsistent with standard interpretations of the propagation paths through the animals head; namely, that the P1-P2 interval is a direct measure of the size of the spermaceti organ. Furthermore, the size of the junk derived from the acoustic data is smaller than the estimated size of the spermaceti organ, which is inconsistent with anatomical fact.

This study also provided close-range measurements of the acoustic structure of the terminal creak of a sperm whale, but additional data would needed to extend these observations further.

On a more applied note, the video also gave insight into sperm whale depredation behavior. First, it showed that sperm whales use echolocation sounds when depredating the longline and produce creaks as they approached individual fish, even under excellent visual conditions. Second, the video showed that sperm whales are able to remove fish from a longline without leaving any visual evidence, such as shredded fish or damaging hooks.

The combined significance of these discoveries is that they demonstrated that visual counts of damaged fish during a haul are inadequate measures of depredation rates, and that passive acoustic monitoring might provide a viable remote measuring stick of depredation effort and possibly success. Acoustic monitoring may also help quantify the number of individuals present at a haul.

VI.2 Diving and acoustic behavior of depredating sperm whales

In Chapter III bioacoustic tagging data deployed on naturally foraging and depredating whales were used to address two of the main goals of SEASWAP: understanding sperm whale depredation strategies, and developing acoustic metrics to quantify sperm whale depredation rates.

Analyses of dive, acoustic, and orientation metrics from naturally foraging tagged whales showed that their foraging depths and durations were consistent with previous observations worldwide, but that their "creak-pause fraction" seems to be lower in the Gulf of Alaska (48%) when compared to feeding whales in the Gulf of Mexico (89%). Our interpretation of the biological relevance of this fraction is that it measures the fraction of prey capture attempts that result in successful prey acquisitions. Whales generating creak sounds had significantly greater roll rates when the creak was followed by a pause, providing support for our interpretation. Our results can then be interpreted as showing that depredating whales have many more opportunities to acquire prey when compared with natural foraging situations (high overall creak rates), but have to expend more effort per successful capture.

Two rough categories, or strategies, of depredation were identified using the bioacoustic tagging data: "deep" and "shallow". Acoustic creak rates were significantly greater during both depredation strategies than during natural foraging. We speculate fish that naturally "spin-off the line may be associated with deep depredation.

Additional data are needed to determine exactly what sperm whales are doing during this apparent deep-depredation behavior and whether differences in depredation strategy arise from conspecific competition and/or individual preference based on experience.

VI.3 Effect of acoustic playbacks on sperm whale behavior

In chapter IV bioacoustic tags were deployed on sperm whales during sound playback experiments to investigate their potential of reducing depredation rates. Two-sided Kolmogorov tests were used to test for statistically significant differences in dive and acoustic behavior during "haul-only" and "haul-playback" situations, where the latter term refers to a situation where acoustic playbacks were conducted during the latter half of a haul. Statistically significant differences in acoustic behavior were found during playback situations, with lower click and creak rates during playbacks. The sample sizes were not large enough to determine which particular acoustic signal type was responsible for the observed differences.

In contrast with the acoustic behavior, the dive characteristics of the animal showed no difference between haul-only and haul-playback situations, and no behavioral changes due to low-intensity sound playbacks was observed. The use of sound to drive away depredators has a poor record of success in the scientific literature, often due to habituation to the acoustic signals by the animals. Given the relatively poor results of this study record of playback studies in reducing depredation in the literature, SEASWAP has decided not to pursue this approach further. Alternative and much more promising approaches are the deployment of passive and "active" decoys to prevent animals from converging on a true haul, as discussed in Section VI.5.

VI.4 Passive acoustic tracking techniques

A final objective of this thesis was to exploit sperm whale depredation behavior to develop passive acoustic methods for long-range tracking of whales as they approach and leave fishing vessels.

In Chapter V a two-element vertical array deployed at the sound speed

minimum was used to track a tagged sperm whale up to 35 km range under Beaufort 3 conditions, using satellite tag data to independently verify tracking estimates. The vertical arrival angles and relative arrival times of multiple refracted and surface-reflected ray paths contain enough information for range-depth tracking without knowledge of the bottom bathymetry. A ray-tracing program was used to model the acoustic travel times from each candidate source location, using a measured sound speed profile. By comparing modeled and measured time lags and vertical angles, an ambiguity surface was created, displaying the best-fit whale position.

The tagged whale's source level was estimated using the whale location and modeled transmission loss, and yielded interesting observations. First, the source levels were significantly lower than previously reported in the literature and remained steady over days, suggesting that at long ranges (more than 5 km), only the omnidirectional low-frequency part of the whale click remains.

Thus, caution is warranted whenever estimating sperm whale detection ranges using short-range source level measurements, as has been commonly done for population density estimation. The variation of source levels between individuals and the relationship between ICI and source level are topics that can be investigated further using these data. These analyses may be useful for estimating whale ranges when only one recorder is deployed.

Ambient noise predictions were also used to model detection and tracking range in various sea state conditions, providing potentially valuable guidance when designing future experiments. For instance, possible future work includes deploying four vertical arrays separated by 40 km along the continental shelf of Sitka, which would cover the entire Sitka fishing region and would answer questions about sperm whale migration behavior and seasonal presence. Indeed, all of our current studies have occurred during the summer, and information about sperm whale presence during the winter would be valuable. It would also be interesting to know if relative sperm whale presence in the area is correlated with human fishing effort.

The deployment of several vertical arrays in the area would also permit sperm whale population density estimation. Right now, density estimates rely on photo-identification around fishing vessels, but it is possible that some local individuals are not involved in depredation. If this is the case, it would be interesting to know what fraction of the local population performs depredation.

Next, the tracking methods developed in this thesis can be applied to sperm whales in other regions and might also be modied to track other deep-water species such as beaked whales.

Finally, this two-element tracking method will be useful for testing the effect of decoys and other depredation countermeasures, as discussed below.

VI.5 Insight into depredation countermeasures

The combined results of this thesis provide some insights into how the fishing industry could counter depredation activity, which is the ultimate goal of SEASWAP.

The tagging analysis identified two categories of depredation: shallow and deep depredation. All the characteristics of shallow depredation indicate that whales attack the line directly under this behavior, as revealed by the underwater video. Our best explanation of deep depredation is that sperm whales feed on fish that naturally spin-off the line during the haul. However, additional data is needed to understand better this apparent deep-depredation behavior.

If spin-off fish provide a convenient entry for whales to learn depredation, as suggested by the apparent deep-depredation behavior, then one of the simplest long-term ways to discourage sperm whale depredation would be to discover gear modications that reduce the odds of accidentally spinning off a fish, once it is caught.

Results from videocamera and bioacoustic data showed that sperm whales use echolocation sound extensively during depredation. Thus, in 2009, sound play-

back studies were conducted to determine whether nearby tagged sperm whales demonstrated any changes in dive profile, orientation, or acoustic behavior in response to a variety of sounds, and to explore whether acoustic deterrents can practically reduce longline depredation by sperm whales. No significant changes in dive depths or durations were found; however, a two-sided Kolmogorov-Smirnov test found statistically significant differences between haul-only and haul-playback situations, in terms of the acoustic behavior of the animals. Unfortunately, the sample size for playbacks was not large enough to determine which particular signal category was responsible for the observed differences.

Upcoming fieldwork will test a whale echolocation jammer that would interfere with a sperm whales predatory behavior and reduce its ability to locate and remove sablefish caught on longline gear.

Another insight involves using creak rates to predict the distances whales are willing to swim to depredate vessels. Energetic calculations estimated that a three-hour fishing haul would provide the equivalent of nine to 12 hours of natural foraging effort by a whale. Our results predict that whales should be willing to swim up to six hours, or up to 30 nautical miles, toward a location where gear is being set. However, once a haul begins, it only makes energetic sense for a whale to swim up to two hours in order to depredate for one hour; observations from the SEASWAP tagging crew do indicate that whales are willing to swim from several miles away for at least one hour when they detect a haul in progress. Thus fishing vessels that can acoustically mask setting their gear, or do not loiter around a deployed set, will gain a significant advantage over situations where whales arrive on the gear during deployment. Finally, if vessels can deploy some sort of decoy that can delay the response of a whale to a true haul by a couple of hours, over the long term the currently large inducement to depredate could be reduced.

In August 2010 a vertical array (with no fishing gear) served as a passive decoy during three days, attracting at least seven sperm whales to the area. A few of them stayed closed to the array for at least 24 hours, suggesting that whales are

willing to wait a long time for a longline to be hauled. This passive decoy approach, which consists of surface buoys with no fishing gear attached, will be tested further in 2012 and 2013. In the past decoys have worked to a limited extent on orcas in the Aleutian Islands, where they have been effective for dumping whales following a fishing vessel (Dalheim, 1988).

In August 2011 a trial acoustic active decoy deployment was performed, which consisted of two sets spaced 5 to 10 km apart. Each set consisted of two buoylines separated by 3-4 km, mimicking the length of a typical longline deployment. One set, the true set, connected the buoylines with a bottom ground line with baited hooked gear, while the other decoy set had no ground line, but the buoy line contained an autonomous playback device. After a certain time delay, the device broadcasted vessel hauling sounds that had been previously determined to attract sperm whales. While the decoy broadcasted these sounds a true haul began. Visual observations documented that one whale, known as an experienced depredator, surfaced next to the true haul. The timing of the arrival, combined with estimates of swimming speed of sperm whales, suggested that the whale departed the decoy about 15 minutes after the playback decoy started to fail. Non-parametric hypothesis testing found significant differences between raw sperm whale acoustic detection rates and received intensities during the 110-minute playback vs. non-playback situations when the vessel was absent.

Finally SEASWAP and the Alaska Longlining Fishing Association are currently conducting eld trials of passive deterrent gear using small acrylic Lucite spheres attached to each gangion on a set. Dr. Whitlow Au of University of Hawaii, found that a single Lucite sphere has a similar target strength to a black cod, which in turn is significantly different from longline gear, supporting their use for testing as a deterrent strategy. An experiment has been designed to test this hypothesis, and autonomous acoustic recorders will be used to document creak rates with and without the Lucite spheres present. A total sample size of 24 longline sets would provide a statistical power of at least 0.90. The deterrent treatment will be

randomized to the skate quads within the 24 longline sets. This passive deterrent gear will target animals that attack the line directly but probably wont effect depredation on spin-off fishing.

This dissertation focused on the study of sperm whale depredation behavior in the Gulf of Alaska and yielded insights into depredation countermeasures. This applied research also provided unique opportunities to observe male sperm whales at very close ranges and conduct basic acoustic research on sperm whale sound production mechanisms. Another by-product of this work has been the development of a compact acoustic tracking system that has applications beyond depredation studies, including potentially the density estimation of sperm whales and other species.

VI.6 Conclusion summary

This dissertation focused on the study of sperm whale depredation behavior in the Gulf of Alaska and yielded insights into depredation countermeasures. This applied research also provided unique opportunities to observe male sperm whales at very close ranges and conduct basic acoustic research on sperm whale sound production mechanisms. Another by-product of this work has been the development of a compact acoustic tracking system that has applications beyond depredation studies, including potentially the density estimation of sperm whales and other species.

Bibliography

[1] M. Amano, and M. Yoshioka, "Sperm whale diving behavior monitored using a suction cup-attached TDR tag," Mar. Ecol. Prog. Ser. **258**, 291-295 (2003).

[2] L. Acharya, and M.B. Fenton, "Echolocation behaviour of vespertilionid bats (*Lasiurus cinereus* and *Lasiurus borealis*) attacking airborne targets including arctiid moths," Can. J. Zool. **70**,1292-1298 (1992).

[3] M. Amundin, "Sound production in odontecetes with emphasis on the harbour porpoise *Pbocoena pbocoena*," Ph.D Dissertation *, University of Stocklom. Stocklom, Sweden*, 128pp (1991).

[4] R.D. Andrews, R.L. Pitman, L.T. Balance, "Satellite tracking reveals distinct movement patterns for Type B and Type C killer whales in the southern Ross Sea", Polar Biol. **31**,1461-1468 (2008).

[5] J.I Antonov, D. Seidov, T.P. Boyer, R.A. Locarnini,A.V. Mishonov, H.E. Garcia, O.K Baranova, M.M Zweng, and D. R. Johnson, "World Ocean Atlas 2009, Volume 2: Salinity," in NOAA Atlas NESDIS 69, edited by S. Levitus (U.S. Government Printing Office, Washington, D.C.) (2010).

[6] J. R. Ashford, P. S. Rubilar, and A. R. Martin, "Interactions between cetaceans and longline fishery operations around South Georgia," Marine Mammal Sci. **12**(3), 452-457 (1996).

[7] J. Barlow, and B.L. Taylor, "Estimates of sperm whale abundance in the northeastern temperate Pacific from a combined acoustic and visual survey," Mar. Mamm. Sci. **21**, 429-445 (2005).

[8] J. Barlow, M. Kahru, and B. G. Mitchell, "Cetacean biomass, prey consumption, and primary production requirements in the California Current ecosystem", Mar. Ecol. Prog. Ser. **371**, 285-295 (2008).

[9] A. Berzin, "The sperm whale", In Yablokov AV (ed) Pischevaya Prornyshlennost, Moscow (translation by Israel Program for Scientific translations, Jerusalem) (1971).

[10] B.P. Bogert, M.J.R Healy, and J.W. Tukey,"The frequency analysis of time series for echoes; cepstrum pseud-autocovariance cross-cepstrum and shape-cracking", Proc. Symposium on Time Series Analysis, Ed Rosenblatt, Wiley NY **15**, 209-243 (1963).

[11] C.E. Bonferroni, "Teoria statistica delle classi e calcolo delle probability [Statistical theory of classes and calculating the probability]," Pubblicazioni del R Istituto Superiore di Scienze Economiche e Commerciali di Firenze **8**, 3-62 (1936).

[12] A.R.C.Britton, and G. Jones, "Echolocation behaviour and prey-capture success in foraging bats: laboratory and field experiments on *Myotis daubentonii*," J. Exp. Biol. **202**, 1793-1801 (1999).

[13] W.C. Burgess, P.L. Tyack, B.J. Le Boeuf, and D.P. Costa, "A programmable acoustic recording tag and first results from free-ranging northern elephant seals," Deep-Sea Research II **45**(7), 1327-1351 (1998).

[14] D. Capdeville, "Interaction of marine mammals with the longline fishery around the Kerguelen Island Division during the 1995/96 cruise," Ccamlr Sci. **4**, 171-174 (1997).

[15] J. Carlstrom,P. Berggren,F. Dinnetz, and P. Borjesson, "A field experiment using acoustic alarms (pingers) to reduce harbour porpoise by-catch in bottom-set gillnets," Ices J. Mar. Sci. **59**, 816-824 (2002).

[16] S. J. Childerhouse, S. M. Dawson, and E. Slooten, "Abundance and seasonal residence of sperm whales at Kaikoura, New Zealand", Can. J. Biol. **734**, 723-732 (1995).

[17] M.R. Clarke, and N. Macleod, "Cephalopod remains from sperm whales caught off Iceland," J. Mar. Biol. Assoc. U.K. **56**, 733-750 (1976).

[18] M.R.Clarke, "Structure and proportions of spermaceti organ in sperm whale", J. Mar. Biol. Ass. UK **58**, 1213-1222 (1978).

[19] M.R. Clarke, "Cephalopoda in the diet of sperm whales of the southern hemisphere and their bearing on sperm whale biology", 'Discovery' Rep. **37**, 1-324 (1980).

[20] C.W. Clark, W.T. Ellison, K. Beeman, "Acoustic tracking of migrating bowhead whales," in Proceedings of IEEE Oceans 1986, 341-346 (1986).

[21] T. Cranford, "The sperm whale's nose: sexual selection on a grand scale?," Mar. Mamm. Sci. **15**, 1133-1157 (1999).

[22] W.C. Cummings, and T.O. Thompson, "Gray Whales, *Eschrichtius robustus*, avoid underwater sounds of killer whales," Fishery Bulletin of the National Oceanic and Atmospheric Administration **69**, 525-531(1971) .

[23] M.E. Dalheim, "Killer whale (*Orcinus orca*) depredation on longline catches of sablefish (*Anoplopoma fimbria*) in Alaskan waters," NWAFC Processed Rep. 88-114 (1988).

[24] V.B. Deecke, P.J.B. Slater, and J.K.B. Ford, "Selective habituation shapes acoustic predator recognition in harbour seals," Nature **420**, 171-173 (2002).

[25] V.B. Deecke, J.K.B. Ford, and P.J.B. Slater, "The vocal behaviour of mammal-eating killer whales: communicating with costly calls," Animal Behaviour **69**, 395-405 (2005).

[26] V.B. Deecke, "Studying marine mammal cognition in the wild: a review of four decades of playback experiments," Aquatic Mammals **32**, 461-482 (2006).

[27] S.L. DeRuiter, A. Bahr, M.-A. Blanchet, S.F. Hansen, J.H Kristensen, P.T. Madsen, P.L.Tyack, and M. Wahlberg, "Acoustic behaviour of echolocating porpoises during prey capture," J. Exp. Biol. **212**, 3100-3107 (2009).

[28] L.A Douglas, S. M. Dawson, and N. Jaquet, "Click rates and silences of sperm whales at Kaikoura," J. Acoust. Soc. Am. **118**, 523-529 (2005).

[29] V. Drouot, A.Gannier, and J. C. Goold, "Diving and Feeding Behaviour of Sperm Whales (textitPhyseter macrocephalus) in the Northwestern Mediterranean Sea," Aquatic Mammals **30**(3), 419-426 (2004).

[30] K. Evans, and M.A. Hindell, "The diet of sperm whales (*Physeter macrocephalus*) in southern Australian waters," ICES J. Mar. Sci. **61** 1313-1329 (2004).

[31] G. Fant, "Acoustic Theory of Speech Production," Mouton, The Hague (1960).

[32] J.F. Fish, and J.S. Vania, "Killer Whale, *Orcinus-Orca*, sounds repel whale Whales," Fishery Bulletin of the National Oceanic and Atmospheric Administration **69**, 531-6 (1971).

[33] W.T. Fitch, "Vocal tract length and formant frequency dispersion correlate with body size in rhesus macaques," J. Acoust. Soc. Am. **102**(2), 1213-1222 (1997).

[34] J. A. Goldbogen, J. Calambokidis, R.E Shadwick, E. Oleson, M. McDonald, and J. A. Hildebrand, "Kinematics of foraging dives and lunge-feeding in fin whales," J. Exp. Biol. **209**, 1231-1244 (2006).

[35] E.F. Gonzalez, *presented at the XXI Congreso de Ciencias del Mar, Chile*, (2001).

[36] J.C. Goold, and S.E. Jones, "Time and frequency domain characteristics of sperm whale clicks," J. Acoust. Soc. Am. **98**, 1279-1291 (1995).

[37] J.C. Goold, and S.E Jones, "Sound velocity measurements in spermaceti oil under the combined influences of temperature and pressure," Deep-Sea Res. **43**, 961-969 (1996).

[38] J.C.D Gordon, "Behavior and ecology of sperm whales off Sri Lanka," PhD dissertation, University of Cambridge, Cambridge, UK: 347 pp (1987).

[39] J.C.D. Gordon, "Evaluation of a method for determining the length of sperm whales, (*Physeter catodon*), from their vocalisations," J. Zool., London **224**, 301-314 (1991).

[40] J .C.D Gordon, R. Leaper, F. G. Hartley, and O. Chappell, "Effects of whale-watching vessels on the surface and underwater acoustic behaviour of sperm whales off Kaikoura, New Zealand," Scientific and Research Series No. 52, Department of Conservation, Wellington, New Zealand 64 pp. (1992).

[41] M.E.D. Gosho, W. Rice, and J. M. Breiwick, "The sperm whale *Physeter macrocephalus*," Mar. Fish. Rev. **46**(4), 54-64 (1984).

[42] M. Guerra, A. Thode, S. Blackwell,, and M. Macrander, "Quantifying seismic survey reverberation off the Alaskan North Slope," J. Acoust. Soc. Am. **130**(5), 3046-3058 (2011).

[43] D.H. Hanselman, J.T. Fujioka, C.R. Lunsford, C.J. Rodgveller, "Assessment of Sable Fish Stock in Alaska," in Alaska Fisheries Science Center National Marine Fisheries Service, Stock Assessment and Fishery Evaluation Report for Ground Fish Resources of the Gulf of Alaska, p.353-464 (2009).

[44] P.S. Hill, J.L. Laake, and E. Mitchell, "Results of a pilot program to document interactions between sperm whales and longline vessels in Alaska waters," U.S Department of Commerce, Report No. NOAA TM-NMFS-AFSC-108, (1999).

[45] R. Hucke-Gaete, C.A. Moreno, J. Arata, and Blue Whale Center, "Operational interactions of sperm whales and killer whales with the Patagonian toothfish industrial fishery off Southern Chile," Ccamlr Sci. **11**, 127-40 (2004).

[46] V.M. Janik, S.M. VanParijs, and P.M.Thompson, "A two-dimensional acoustic localization system for marine mammals," Mar. Mamm. Sci. **16**, 437-447 (2000).

[47] N. Jaquet, "How spatial and temporal scales influence understanding of Sperm Whale distribution: a review," Mammal Rev. **26**(1), 51-65 (1996).

[48] N. Jaquet, S. Dawson, and E. Slooten, "Seasonal distribution and diving behaviour of male sperm whales off Kaikoura: Foraging implications," Can. J. Zool. **78**, 407-419 (2000).

[49] N. Jaquet, S. Dawson, and L. Douglas, "Vocal behavior of male sperm whales: Why do they click?," J. Acoust. Soc. Am. **109**, 2254-2259 (2001).

[50] D.H. Johnson, and D.E Dudgeon, "Array Signal Processing," published by Prentice Hall, Englewood Cliffs, NJ (1993).

[51] , D.W. Johnston, "The effect of acoustic harassment devices on harbour porpoises (Phocoena phocoena) in the Bay of Fundy, Canada," Biological Conservation **108**, 113-118 (2002).

[52] M. Johnson, P. Tyack, "A digital acoustic recording tag for measuring the response of wild marine mammals to sound," IEEE J. Ocean. Engng. **28**, 3-12. (2003).

[53] M. Johnson, N. Aguilar Soto, P. T. Madsen, "Studying the behaviour and sensory ecology of marine mammals using acoustic recording tags: a review," Marine Ecology Progress Series **395**, 55-73 (2009).

[54] R.A. Kastelein, D. de Haan, N. Vaughan,C. Staal, and N.M. Schooneman, "The influence of three acoustic alarms on the behaviour of harbour porpoises (*Phocoena phocoena*) in a floating pen," Marine Environmental Research **52**, 351-371 (2001).

[55] R.A. Kastelein, N. Jennings, W.C. Verboom, D. de Haan, and N.M. Schooneman, "Differences in the response of a striped dolphin (*Stenella coeruleoalba*) and a harbour porpoise (*Phocoena phocoena*) to an acoustic alarm," Marine Environmental Research **61**, 363-378 (2006a).

[56] R.A. Kastelein, S. Van der Heul, J.M. Terhune, W.C. Verboom, and R.J.V. Triesscheijn, "Deterring effects of 8-45 kHz tone pulses on harbour seals (*Phoca vitulina*) in a large pool," Marine Environmental Research **62**, 356-373 (2006b).

[57] T. Kasuya, "Density dependant growth in north pacific sperm whales," Marine Mammal Science, **7**, 230-257 (1991).

[58] T. Kawakami, "A review of sperm whale food," Sci. Rep. Whales Res. Inst. **32**, 199-218 (1980).

[59] M. Kleibe, "The fire of life: an introduction to animal energetics," R.E. Krieger Publishing, Huntington, NY (1975).

[60] D.E. Kroodsma, "Using appropriate experimental-designs for intended hypotheses in song playbacks, with examples for testing effects on song repertoire sizes," Animal Behaviour **40**, 1138-1150 (1990).

[61] D.M. Lavigne, S. Innes, G.A.J. Worthy, K.M. Kovacs, O.J. Schmitz, J.P. Hickie, "Metabolic rates of seals and whales," Can. J. Zool. **64** 279-284 (1986).

[62] R. Leaper, O. Chappell, and J. Gordon, "The development of practical techniques or surveying sperm whale populations acoustically, Rept. Int. Whal. Commn. **42**, 549-560 (1992).

[63] P. Lieberman, "The Biology and Evolution of Language," Harvard University Press, Cambridge, Massachusetts (1984).

[64] C. Lockyer, "Body weights of some species of large whales," Journal du conseil **36**(3), 259-273 (1976).

[65] C. Lockyer, "Estimates of growth and energy budget for the sperm whale, Physeter catadon," FAO Fish. Ser. (5) Mammals in the Sea **3**, 489-504 (1981).

[66] C. Lockyer, "Body composition of the sperm whale, Physeter catodon, with special reference to the possible function of fat depots," Rit Fiskideildar **12**(12), 1-24 (1991).

[67] K.V. Mackenzie, "Nine-term equation for the sound speed in the oceans," J. Acoust. Soc. Am. **70**(3), 807-812 (1981).

[68] P.T. Madsen, M. Wahlberg, and B. Mohl, "Male sperm whale (*Physeter macrocephalus*) acoustics in a high latitude habitat: implications for echolocation and communication," Behav. Ecol. Sociobiol. **53**, 31-41 (2002a).

[69] P.T. Madsen, M. Wahlberg, and B. Mohl, "Sperm whale sound production studied with ultrasound time/depth-recording tags," J. Exp. Biol. **205**, 1899-1906 (2002).

[70] P.T. Madsen, "Marine mammals and noise: Problems with root mean square sound pressure levels for transients," J. Acoust. Soc. Am. **117**(6), 3952-3957.

[71] C.I. Malme, P.W. Smith, and P.R. Miles, "Characterisation of geophysical acoustic survey sounds," OCS Study. Prepared by BBN Laboratories Inc., Cambridge, for Battelle Memorial Institute to the Department of the Interior-Mineral Management Service, Pacific Outer Continental Shelf Region, Los Angeles, CA (1986).

[72] D. Mathias, A. Thode,J. Straley, and K. Folkert, "Relationship between sperm whale (*Physeter macrocephalus*) click structure and size derived from videocamera images of a depredating whale (sperm whale prey acquisition)," J. Acoust. Soc. Am. **125**(5), 3444-3453 (2009).

[73] D. Mathias, A. Thode, J. Straley, V. O'Connell, J. Calambokidis, and G.S. Schorr, "Acoustic and foraging behavior of tagged sperm whales (*Physeter macrocephalus*) under natural and depredation foraging conditions in the Gulf of Alaska," Accepted by J. Acoust. Soc. Am (2012).

[74] D.K. Mellinger, and C.W. Clark, "Blue whale (Balaenoptera musculus) sounds from the North Atlantic," J. Acoust. Soc. Am. **114**(2), 1108-1119 (2003).

[75] D.K. Mellinger, K.M. Stafford, and C.G. Fox, "Seasonal occurrence of sperm whale (*Physeter macrocephalus*) sounds in the gulf of Alaska," Mar. Mamm. Sci. **20**(1), 48-62 (2004).

[76] P.J.O. Miller,M.P. Johnson, and P.L Tyack, "Sperm Whale Behaviour Indicates the Use of Echolocation Click Buzzes 'Creaks' in Prey," Proceedings: Biological Sciences **271**, 2239-2247 (2004a).

[77] P.J.O. Miller, M.P. Johnson, P.L Tyack, and E.A. Terray, "Swimming gaits, passive drag and buoyancy of diving sperm whales *Physeter macrocephalus*," J. Exp. Biol. **207**, 1953-1967 (2004b).

[78] P.J.O. Miller, K. Aoki, L. E. Rendell, and M. Amano, "Stereotypical resting behavior of the sperm whale," Current Biology **18**(1), 21-23(2008).

[79] P.J.O. Miller, M.P. Johnson, P. T. Madsen, N.Biassoni, M.Quero, and P.L.Tyack, "Using at-sea experiments to study the effects of airguns on the foraging behavior of sperm whales in the Gulf of Mexico," Deep-Sea Research I **56**, 1168-1181 (2009).

[80] S. Mitchell, and J. Bower, "Localization of animal calls via hyperbolic methods," J. Acoust. Soc. Am. **97**, 3352-3353 (1995).

[81] B. Mohl, E. Larsen, and M. Amundin, "Sperm whale size determination: outlines of an acoustic approach," In Fisheries series, FAO Rome, 327:332 (1981).

[82] B. Mohl, "Sound transmission in the nose of the sperm whale, *Physeter Catodon*. A post mortem study," J.Comp. Physiol. **187**, 335-340 (2001).

[83] B. Mohl, M. Wahlberg, P.T. Madsen, A. Heerfordt, and A. Lund, "Sperm whale clicks: Directionality and source level revisited," J. Acoust. Soc. Am. **114**, 1143-1154 (2000).

[84] B. Mohl, M. Wahlberg, P.T. Madsen, A. Heerfordt, and A. Lund, "The monopulsed nature of sperm whale clicks," J. Acoust. Soc. Am. **114**, 1143-1154 (2003).

[85] A. B. Morton, and H.K. Symonds, "Displacement of *Orcinus orca* by high amplitude sound in British Columbia, Canada," Ices J. Mar. Sci. **59** (2002).

[86] X. Mouy, D. Hannay, M. Zykov, and B. Martin, "Tracking of Pacific Walruses in the Chukchi Sea using a single hydrophone," J. Acoust. Soc. Am. **131**(2), 1349-1358 (2011).

[87] J. Mullins, H. Whitehead, L. S. Weilgart, "Behaviour and vocalizations of two single sperm whales, Physeter macrocephalus, off Nova Scotia," Can. J. Fish. Aquat. Sci. **45**, 1736-1743 (1988).

[88] T. Nearey, "Phonetic Features for Vowels," Indiana University Linguistics Club, Bloomington (1979).

[89] K. Nielsen, and B. Mhl, "Hull-mounted hydrophones for passive acoustic detection and tracking of sperm whales (Physeter macrocephalus)," Appl. Acoust. **67**, 1175-1186 (2006).

[90] N. Nishiwaki, S. Oshumi, and Y. Maeda, "Changes in form of the sperm whale accompanied with growth," Sci. Rep. Whale Res. Inst. Tokyo **17**, 1-13 (1963).

[91] C.P. Nolan, and G.M. Liddle, "Interactions between killer whales (*Orcinus orca*) and sperm whales (*Physeter macrocephalus*) with a longline fishing vessel," Marine mammal Sci. **16**(3), 658-664 (2000).

[92] K.S. Norris, and G.W. Harvey, "A theory for the function of the spermaceti organ of the sperm whale (*Physeter catodon L.*)" in Animal Orientation and Navigation, edited by S. R. Galler, K. Schmidt-Koenig, G. J. Jacobs, and R. E. Belleville, Washington D.C., 397-417 (1972).

[93] J.C. Norris, W.E. Evans, R. Benson, and T.D. Sparks, "Acoustic surveys," in R.W. Davis and G.S. Fargion (eds). Distribution and Abundance of Cetaceans in the North-central and Western Gulf of Mexico. OCS Study MMS 96-0027. Minerals Management Service, New Orleans, Louisiana, 133-187 (1996).

[94] E.M. Nosal , and L.N. Frazer, "Track of a sperm whale from delays between direct and surface-reflected clicks," Appl. Acoust. 67, 1187-1201 (2006).

[95] E.M. Nosal , and L.N. Frazer, "Sperm whale three-dimensional track, swim orientation, beam patter, and click levels observed on bottom-mounted hydrophones," J. Acoust. Soc. Am. **122**(4), 1969-1978 (2007).

[96] A.M. Thode, J. Straley, D. Mathias, K. Folkert, T. OConnell, L. Behnken, J. Calambokidis, C. Lunsford,"Testing low-cost methods to reduce sperm whale depredation in the Gulf of Alaska," North Pacific Research Board Final Report F626, 85 p. (2008).

[97] D.P. Nowacek, M.P. Johnson, and P.L. Tyack, "North Atlantic right whales (*Eubalaena glacialis*) ignore ships but respond to alerting stimuli," Proceedings of the Royal Society of London Series B-Biological Sciences **271**, 227-231(2004).

[98] T. Okutani, and T. Nemoto, "Squids as the food of sperm whales in the Bering Sea and Alaska Gulf," Tokai Regional Fisheries Laboratory, Tokyo Scientific Reports of the Whales Research Institute, Tokyo **18** (1964)

[99] E.M. Oleson, J. Calambokidis, W.C. Burgess, M.A. McDonald, C.A. LeDuc, and J.A. Hildebrand, "Behavioral context of call production by eastern North Pacific blue whales," Mar. Ecol. Prog. Ser. **330**, 269-284 (2007).

[100] H. Omura, "On the body weight of Sperm and Sci Whales located in the adjacent water of Japan," Sci. Rep. Whales Res. Inst. Tokyo **4**, 1-13 (1950)

[101] S. Ohsumi, and Y. Masak, "Stocks and trends of abundance of the sperm whale in the north Pacific," Reports of the International Whaling Commission **21**, 167-175 (1977).

[102] V. Papastavrou, S.C. Smith, and H. Whitehead, "Diving behavior of the sperm whale, Physeter macrocephalus, off the Galpagos Islands," Can. J. Zool. **67**, 839-846 (1989).

[103] M.A. Perez, "Analysis of marine mammal bycatch data from the trawl, longline, and pot groundfish fisheries of Alaska, 1998-2004, defined by geographic area, gear type, and target groundfish catch species," U.S. Dep. Commer., NOAA Tech. Memo. NMFS-AFSC-167 (2006).

[104] G.E. Peterson and H.L. Barney, "Vocal tract length and formant frequency dispersion correlate with body size in rhesus macaques," J. Acoust. Soc. Am. **24**, 175-184 (1952).

[105] M. Porter, and H. Bucker, "Gaussian beam tracing for computing ocean acoustic fields," J. Acoust. Soc. Am. **82**, 1349-1359 (1987)

[106] M. G. Purves, D. J. Agnew, E. Balguerias, C. A. Moreno, and B. Watkins, "Killer whale *Orcinus orca* and sperm whale *Physeter macrocephalus* interactions with longline vessels in the patagonian toothfish fishery at South Georgia, South Atlantic," Ccamlir Sci. **11**, 111-126 (2004).

[107] M.Q. Rhinelander, and S.M. Dawson, "Measuring sperm whales from their clicks: Stability of interpulse intervals and validation that they indicate whale length," J. Acoust. Soc. Am. **4**, 1826-1831 (2004).

[108] D. W. Rice, "Sperm Whales," In *Handbook of Marine Mammals*, edited by S.H. Ridgway and R. Harrison, (Academic, London, 1989) Vol. **4**, pp. 177-233 (1989).

[109] H.S.J. Roe, "The food and feeding habits of the sperm whales (*Physeter catadon L.*) taken off the west coast of Iceland," Journal of the Council for International Exploration of the Sea **33**(1), 93-102 (1969).

[110] M.B. Santos, M.R. Clarke, G.J. Pierce, "Assessing the importance of cephalopods in the diets of marine mammals and other top predators: problems and solutions," Fisheries Research **52**(1-2), 121-139 (2001).

[111] M.B. Santos, G.J. Pierce, M. Garca Hartmann, C. Smeenk, M.J. Addink, T. Kuiken, R.J. Reid, A.P. Patterson, C. Lordan, E. Rogan, E. Mente, "Additional notes on stomach contents of sperm whales Physeter macrocephalus stranded in the north-east Atlantic," J. Mar. Biol. Assoc. UK. **82**, 501-507 (2002).

[112] D.E. Sergeant, "Feeding rates of Cetacea," Fisk. Dir. Skr. Serie Havundersok. **15** 246-58 (1969).

[113] M.F. Sigler,C.R. Lunsford, J.M Straley, and J.B. Liddle, "Sperm whale depredation of sablefish longline gear in the northeast Pacific Ocean," Mar. Mamm. Sci. **24**(1), 16-27 (2008).

[114] P.D. Shaughnessy, A. Semmelink, J. Cooper, and P.G.H. Frost, "Attempts to develop acoustic methods of keeping cape-fur-seals from fishing nets," Biological Conservation **21**, 141-158 (1981).

[115] J.L. Spiesberger, "Hyperbolic location errors due to insufficient numbers of receivers," J. Acoust. Soc. Am. **109**(6), 3076-3079 (2001).

[116] J.L. Spiesberger, "Geometry of locating sounds from differences in travel time: Isodiachrons," J. Acoust. Soc. Am. **116**, 3168-3177(2001).

[117] K.M. Stafford, C.G. Fox, and D.S. Clark, "Long-range acoustic detection and localization of blue whale calls in the northeast Pacific Ocean." J. Acoust. Soc. Am. **104**, 3616-3625 (1998).

[118] J. Straley, J. Lidde, A. Thode, K. Folkert, V. OConnell, L. Behnken, and D. Mathias, "Testing low-costs methods to reduce sperm whale depredation in the Gulf of Alaska: Is avoidance a viable strategy ?" presented at the Marine Mammal Conference, Quebec city (2009).

[119] A. Surlykke, V. Futtrup, V., and J. Tougaard, "Prey-capture success revealed by echolocation signals in pipistrelle bats (*Pipistrellus pygmaeus*)," J. Exp. Biol. **206**, 93-104 (2003).

[120] V. Teloni, W.M.X. Zimmer, M. Wahlberg, and P.T Madsen, "Consistent acoustic size estimation of sperm whales using clicks recorded from unknown aspects". Journal of Cetacean Research and Management **9** 127-136 (2007).

[121] V. Teloni, M.P Johnson, P.J.O. Miller, and P.T Madsen, "Shallow food for deep divers: Dynamic foraging behavior of male sperms whales in a high latitude habitat.," J. Exp. Mar. Biol. Ecol. **354**, 119-131 (2008).

[122] A. Thode, D.K. Mellinger, S. Stienessen, A. Martinez, and K. Mullin, "Depth-dependant features of diving sperm whales (*Physeter macrocephalus*) in the Gulf of Mexico," J. Acoust. Soc. Am. **116**, 245-253 (2002).

[123] A. Thode, "Tracking sperm whale (Physeter macrocephalus) dive profiles using a towed passive acoustic array, " J. Acoust. Soc. Am **116**(1), 245-253 (2004).

[124] A. Thode, J.M. Straley, C.O. Tiemann, V. Teloni,K. Folkert, V. OConnell, and L. Behnken, "Sperm Whale and Longline Fisheries Interactions in the Gulf of Alaska," in North Pacic Research Board Final Report F412, 56 pp (2006).

[125] A. Thode, J. Straley, C.O. Tiemann, K. Folkert, V. O'Connell, "Observations of potential acoustic cues that attract sperm whales to longline fishing in the Gulf of Alaska," J. Acoust. Soc. Am. **122**(2), 1265-1277 (2007).

[126] A. Thode, J. Straley, D. Mathias, K. Folkert, T. OConnell, L. Behnken, J. Calambokidis, C. Lunsford,"Testing low-cost methods to reduce sperm whale depredation in the Gulf of Alaska," North Pacific Research Board Final Report F626, 85 p. (2008).

[127] A. Thode, J. Skinner, P. Scott, J. Roswell, J.M. Straley, and K. Folkert, K., "Tracking sperm whales with a towed acoustic vector sensor using physics-based noise analysis," J. Acoust. Soc. Am. **128**(5), 2681-2694 (2010).

[128] W.H. Thorp, W.H., "Analytic Description of the Low?Frequency Attenuation Coefficient," J. Acoust. Soc. Am. **42**(1), 270 (1967).

[129] C.O. Tiemann, M.B. Porter, and L.N. Frazer, "Localization of marine mammals near Hawaii using an acoustic propagation model," J. Acoust. Soc. Am. **115**(6), 2834-1843 (2004).

[130] C.O. Tiemann, A. Thode, J. Straley, K. Folkert, and V.O'Connell. "Three-dimensional localization of sperm whales using a single hydrophone," J. Acoust. Soc. Am. **120**(4), 2355-2365 (2006).

[131] , P.Tyack, "Acoustic playback experiments to study behavioral responses of free ranging marine animals to anthropogenic sound," Mar. Ecol. Progr. Ser. **395**, 187-200 (2009).

[132] R.J. Urick, "Principles of Underwater Sound," 3rd ed. (McGraw-Hill, New York) (1983).

[133] M. Wahlberg, "The acoustic behaviour of diving sperm whales observed with a hydrophone array," J. Exp. Mar. Biol. Ecol. **281**, 53-62 (2002).

[134] W.A. Watkins, and W. E. Schevill, "Sperm whale codas," J. Acoust. Soc. Am. **62**, 1485-1490 (1977).

[135] W.A.Watkins, M.A. Daher, K.M. Fristrup, T.J. Howald, and G. Notarbartolo di Sciara, "Sperm whales tagged with transponders and tracked underwater by sonar," Mar. Mammal Sci. **9**(1), 55-67 (1993).

[136] W.A. Watkins, M.A. Daher, N.A. DiMarzio, A. Samules, D. Wartzok, K.M. Fristrup, P.W. Howey, and R.R. Maiefski, "Sperm whale dives tracked by radio tag telemetry, Mar. Mamm. Sci. **18**, 55-78 (2002).

[137] S.L. Watwood, ,P.J.O. Miller,M.P Johnson,P.T Madsen, and P.L Tyack, "Deep-diving foraging behaviour of sperm whales (*Physeter macrocephalus*)," Journal of animal ecology **75**(3), 814-825 (2006).

[138] G.M. Wenz, "Acoustic ambient noise in the ocean: Spectra and sources," J. Acoust. Soc. Am. **34**, 1936-1956 (1962).

[139] P.R. White, T.G. Leighton, D.C. Finfer, C. Prowles, and O. Baumann, "Localisation of sperm whales using bottom-mounted sensors," Appl. Acoust. **67**, 1074-1090.

[140] H. Whitehead, and L. Weilgart, "Click rates from sperm whales," J. Acoust. Soc. Am. **87**, 1798-1806 (1990).

[141] H. Whitehead, and L. Weilgart, "Patterns of visually observable behavior and vocalizations in groups of female sperm whales," Behavior **118**, 275-296 (1991).

[142] H. Whitehead, S. Brennan, and D. Grover, "Distribution and behaviour of male sperm whales on the Scotian Shelf, Canada," Can. J. Zool. **70**, 912-918 (1992).

[143] H. Whitehead, "Sperm whales: Social evolution in the ocean," University of Chicago Press, Chicago, IL (2003).

[144] W. Whitney, "Observations of sperm whale sounds from great depths," Marine Physical Laboratory, Scripps Institution of Oceanography Report MPL-U 11/68 (1968).

[145] L.V. Worthington, and W.E. Schevill, "Underwater Sounds heard from Sperm Whales," Nature, **Vol. 180, Issue 4580**, pp. 291 (1957).

[146] W.M.X Zimmer, M.P Johnson, A. D'Amico, and P. L. Tyack, "Combining Data From a Multisensor Tag and Passive Sonar to Determine the Diving Behavior of a Sperm Whale (*Physeter macrocephalus*)," IEEE J. Oceanic Eng., **28**, 13-28 (2003).

[147] W.M.X Zimmer, P.L. Tyack, M.P. Johnson, and P.T. Madsen, "Three- dimensional beam pattern of regular sperm whale clicks confirms bent-horn hypothesis," J. Acoust. Soc. Am. **118** 3337-3345 (2005).

[148] W.M.X Zimmer, P.T. Madsen, V. Teloni, M.P. Johnson, and P.L. Tyack, "Off-axis effects on the multi-pulse structure of sperm whale usual clicks with implications for the sound production," J. Acoust. Soc. Am. **118** 3337-3345 (2005).